Scaffold-diverse synthesis via Petasis–sequence reactions and the discovery of IRE1α modulators

Dissertation

For the achievement of the academic degree of the

Doctor in Natural Sciences

(Dr. rer. Nat.)

Submitted to

The Department of Chemistry and Chemical Biology

Technical University of Dortmund

By

Amrutha Krishnan Avathan Veettil, M.S.

From Kerala, India

Dortmund, 2025

The work presented in this dissertation was carried out from January 2021 to December 2024 under the supervision of V-Prof. Dr. Peng Wu at the Chemical Genomics Centre of the Max Planck Institute for Molecular Physiology, Dortmund, and the Department of Chemistry and Chemical Biology at the Technical University of Dortmund.

Dean: Prof. Dr. Stefan M. Kast

1st Examiner: Prof. Dr. Dr. h.c. Herbert Waldmann

2nd Examiner: V-Prof. Dr. Peng Wu

Results presented in this thesis contributed to the following publications:

(#: These authors contributed equally to this work)

Liu, Y.; [#] Avathan Veettil, A. K.; [#] Gasper, R.; Jiang, M.; Hastürk, O.; Wu, P., Harnessing Indole Scaffolds to Identify Small-molecule IRE1α Inhibitors Modulating *XBP1* mRNA Splicing. *Nat. Commun*., **2025**, *Accepted in principle.*

Avathan Veettil, A. K.; [#] Liu, Y.; [#] Wagner, L.; Hastürk, O.; Huynh, N. S. T.; Wu, P., Pyrazolylpyrimidinamines decorated via Petasis reaction as small-molecule activators of the RNA-degrading ribonuclease IRE1α. **2025**, *submitted manuscript in revision.*

Avathan Veettil, A. K.; Kirchhoff, J.-L.; Brieger, L.; Strohmann, C.; Wu, P., Petasis Sequence Reactions for the Scaffold-Diverse Synthesis of Bioactive Polycyclic Small Molecules. *ACS Omega*, **2023**, *8* (1), 1168-1181.

The author also contributed to the following publication during the PhD studies:

Azam, U.; Humayun, W.; Avathan Veettil, A. K.; Liu, Y.; Hastürk, O.; Jiang, M.; Sievers, S.; Wu, P.; Naseer, M. M., Identification of 5-Amino-1,3,4-thiadiazole Appended Isatins as Bioactive Small Molecules with Polypharmacological Activities. *RSC Med. Chem.*, **2025**, *16*, 2004-2018.

Results displayed in this dissertation can also be found in the following master's thesis:

O. Hastürk, "Evaluation of small-molecule modulators targeting the RNA-cleaving protein IRE1α", Master's thesis, **2023**

Dedicated to my family

Acknowledgements

The completion of my PhD journey over the past four years has been made possible through the guidance, support, and encouragement of many people. I am deeply grateful to all those who have contributed to this endeavor.

First of all, I would like to express my sincere gratitude to V-Prof. Dr. Peng Wu for giving me the opportunity to join his research group and for his invaluable guidance and support throughout my PhD journey. I am incredibly fortunate to have been part of projects that not only contributed to my research but also played a significant role in shaping my academic growth. I would also like to thank him for serving as my second examiner and for his insightful feedback during the thesis writing process, which greatly helped refine this work.

I am immensely thankful to Prof. Dr. Dr. h.c. Herbert Waldmann for his willingness to be the first examiner of my thesis and for establishing the Chemical Genomics Centre (CGC), which provided an excellent platform for conducting my research.

I extend my heartfelt thanks to Prof. Dr. Andreas Brunschweiger and Prof. Dr. Markus Kaiser for their valuable insights and suggestions during my Thesis Advisory Committee (TAC) meetings, which greatly enriched my work.

My gratitude extends to the International Max Planck Research School (IMPRS) coordinators, Dr. Lucia Sironi and Christa Hornemann, for their continuous support and guidance. I am also grateful to Dr. Debora Bruzzese and Birgit Apprecht for coordinating and supporting the CGC in many ways.

I am thankful to the analytical team, especially Christiane Heitbrink, Svetlana Gerdt, Jens Warmers, and the TU Dortmund NMR and HRMS facility for their valuable assistance. I would also like to express my appreciation to Prof. Dr. Carsten Strohmann, Dr. Lukas Brieger, and Dr. Jan-Lukas Kirchhoff for their collaboration on X-ray crystallography measurements, which were instrumental in my research. I am also grateful to Dr. Sonja Sievers and the Compound Management and Screening Center (COMAS), Dortmund team, for testing my compounds and for providing crucial biological results that contributed to my research.

Special thanks go to my colleagues, particularly Yang Liu, Mao Jiang, Xiaqiu Qiu, and Dr. Fubao Huang, for their scientific inputs and collaboration. Yang Liu, Oguz. Hastürk, Xiaqiu Qiu, and Leon Wagner are acknowledged for kindly performing biological experiments for this

thesis work. I would also like to extend my heartfelt thanks to my former colleagues and friends, namely Dr. Mahesh Puthanveedu, Dr. Joseph Openy, Dr. Sukdev Bag, and Dr. Devika C. Namboodiri, for their guidance during my initial days at the graduate school, as well as to all my current and former colleagues at CGC for their unwavering support and encouragement. I am also grateful to V-Prof. Dr. Peng Wu, Yang Liu, Dr. Georg Goebel, Dr. Jeffrey Schloßhauer, and Dr. Aarya Prabhakaran for proofreading my thesis and providing valuable feedback.

I am deeply indebted to my Master's project guides, the late Dr. Abhijit Hazra and Dr. Yogesh Bharitkar, whose mentorship set the foundation for my scientific career.

Lastly, I wish to express my profound gratitude to my family–my mom, dad, and sisters–for their unconditional love and support. To my partner, Abhiram K.R., thank you for your patience, understanding, and encouragement throughout this journey. I also take a moment to appreciate all the wonderful friends I made along the way, without whom this journey would not have been as meaningful or fulfilling. My friends Vivek Vijayan, Arjun Radha Krishnan, and Malavika Kalarikkal, with whom I had lunch almost every single day of my PhD, thank you for the countless lunchtime discussions and for bringing laughter to an otherwise demanding experience. I wish you the best for your respective PhD journeys at TU Dortmund.

To everyone who directly or indirectly supported me during this academic journey, thank you. This would not have been possible without you!

Table of Contents

Abstract

Once considered undruggable, RNAs are now emerging as attractive therapeutic targets, with various strategies actively being explored to modulate the functional transcriptome using small molecules. Among several RNA-binding and RNA-cleaving proteins, ribonucleases play a central role in regulating RNA metabolism and transcriptome dynamics, making them promising targets for therapeutic intervention. This doctoral thesis focuses on inositol requiring enzyme 1 alpha (IRE1α), a key ribonuclease involved in endoplasmic reticulum (ER) stress response and a critical regulator of RNA metabolism. IRE1α is a transmembrane ER protein with dual serine/threonine kinase and ribonuclease activities, acting as the primary sensor of the unfolded protein response (UPR). Upon ER stress, IRE1α catalyzes the splicing of *X-box binding protein 1* (*XBP1*) mRNA, a process essential for maintaining proteostasis. Dysregulation of the IRE1α–XBP1 axis of UPR has been implicated in the pathogenesis of multiple diseases, making IRE1α an attractive therapeutic target. Although several IRE1α modulators have been developed to date, the mechanisms of action for certain classes of these compounds remain only partially understood. Moreover, how the intensity and duration of ER stress influence IRE1α signaling and the balance between its pro-survival and pro-apoptotic outputs is yet to be fully understood. Given its central role in RNA processing during ER stress and emerging links to disease pathogenesis, this thesis presents a small-molecule screening approach to identify novel IRE1α modulators.

Traditional screening collections often exhibit limited exploration of chemical space, and many of the current commercial libraries are heavily centered around established criteria dictated by the limitations of traditional medicinal chemistry lead optimization approaches. Therefore, diversity-driven approaches for library generation are highly desirable, and novel chemistry strategies to generate diverse, structurally complex small molecules are highly in demand. Among these, the Petasis reaction (PR)–a three-component coupling reaction–stands out as a versatile method for generating highly functionalized amines with structural diversity. Integrating the PR with subsequent ring-closing transformations offers a powerful strategy for constructing novel polycyclic scaffolds. As a complementary effort to the modulation of the IRE1–XBP1 signaling axis, the latter part of this thesis presents the synthesis of a diverse array of small molecules featuring polycyclic scaffolds with a high degree of sp^3-hybridized carbon atoms and multiple stereogenic centers. This was achieved through three-component Petasis reaction (3C-PR) followed by intramolecular Diels–Alder (IMDA) reactions, as well as a

sequential 3C-PR, ruthenium-catalyzed ring-closing metathesis (RCM), and IMDA process. Our synthetic efforts led to the formation of a collection of epoxyisoindoles and pyridazino[4,3-*c*]azepines in good yields, within 2-3 steps. The stereochemistry of the products was confirmed via single-crystal X-ray diffraction analysis. Our findings highlight the broad substrate scope and versatility of Petasis–sequence reactions in accessing previously unexplored polycyclic scaffolds with favorable predicted drug-like properties and potential biological relevance.

Subsequently, a fluorescence resonance energy transfer (FRET)-based assay was established and conducted screening of an in-house collection of ~10,000 structurally diverse, complex, biologically relevant small molecules based on simplified natural product scaffolds. This screening effort led to the identification of promising hit series, including indole-based inhibitors (compound **10**) and aminopyrimidine-based activators (compound **78**). Further optimization of the indole scaffold via solid-phase and liquid-phase Fischer indole synthesis, as well as Suzuki-Miyaura coupling reactions, resulted in the most potent inhibitor **54** (IRE1α, IC_{50} 16 nM; p-IRE1α, IC_{50} = 9 nM), exhibiting a 20-fold improvement in potency. In parallel, systematic modifications of the aminopyrimidine scaffold led to the discovery of compound **91**, the most potent activator with sub-micromolar activity (IRE1α, EC_{50} 0.48 μM; p-IRE1α, EC_{50} 0.18 μM). These efforts introduced novel indole-based inhibitors that allosterically inhibited IRE1α RNase activity by targeting its ATP-binding pocket and the aminopyrimidine-based activators that enhanced IRE1α RNase function. Furthermore, through biophysical binding assays, cellular evaluations, and mechanistic studies, the potential mechanism of RNase activity modulation was elucidated. The resulting compounds can serve as valuable chemical tools for probing the IRE1α function and provide insights into IRE1α's role in UPR signaling, offering a foundation for developing therapeutically relevant IRE1α-targeting small molecules.

Collectively, this work showcased the capability of Petasis–sequence reactions as an efficient, complexity-generating synthetic strategy in constructing polycyclic bioactive small molecules and highlighted the potential of scaffold-diverse IRE1α modulators as useful chemical probes and starting points for drug development. The optimized derivatives provided critical insights into IRE1α function and its role in ER stress response, paving the way for further studies aimed at targeting this pathway therapeutically, such as in cancer.

Kurzzusammenfassung

Lange Zeit als unheilbar geltend, erweisen sich RNAs nun als attraktive therapeutische Ziele, wobei verschiedene Strategien aktiv erforscht werden, um das funktionale Transkriptom mithilfe small molecules zu modulieren. Unter mehreren RNA-bindenden und RNA-spaltenden Proteinen spielen Ribonukleasen eine zentrale Rolle bei der Regulierung des RNA-Metabolismus und der Transkriptomdynamik, was sie zu vielversprechenden Zielen für therapeutische Interventionen macht. In dieser Doktorarbeit liegt der Fokus auf dem Inositol-abhängigen Enzym 1 Alpha (IRE1α), eine Schlüssel-Ribonuklease, die an der Stressreaktion des endoplasmatischen Retikulums (ER) beteiligt ist und den RNA-Metabolismus entscheidend reguliert. IRE1α ist ein Transmembranprotein des ER mit Serin/Threonin-Kinase- und Ribonuklease-Aktivität, das als primärer Sensor der ungefalteten Protein-Antwort (UPR) fungiert. Bei ER-Stress katalysiert IRE1α das Spleißen der mRNA des *X-Box-Bindungsproteins 1* (*XBP1*), ein Prozess, der für die Aufrechterhaltung der Proteostase unerlässlich ist. Eine Fehlregulation der IRE1α–XBP1-Achse der UPR wurde mit der Pathogenese mehrerer Krankheiten in Verbindung gebracht, was IRE1α zu einem attraktiven therapeutischen Ziel macht. Obwohl bisher mehrere IRE1α-Modulatoren entwickelt wurden, sind die Wirkmechanismen für bestimmte Klassen dieser Verbindungen nur teilweise verstanden. Darüber hinaus ist noch nicht vollständig geklärt, wie die Intensität und Dauer von ER-Stress die IRE1α-Signalübertragung und das Gleichgewicht zwischen ihren überlebensfördernden und ihren apoptotischen Auswirkungen beeinflussen. Angesichts seiner zentralen Rolle bei der RNA-Verarbeitung während ER-Stress und seiner neu entdeckten Verbindungen zur Pathogenese von Krankheiten präsentiert diese Arbeit einen Screening-Ansatz für small-molecule Verbindungen zur Identifizierung neuer IRE1α-Modulatoren.

Die traditionellen Screening-Sammlungen weisen oft eine begrenzte Erkundung des chemischen Raums auf, und viele der aktuellen kommerziellen Bibliotheken sind stark auf etablierte Kriterien ausgerichtet, die durch die Einschränkungen der traditionellen Ansätze zur Optimierung von Leitstrukturen in der medizinischen Chemie vorgegeben sind. Daher sind diversitätsorientierte Ansätze für die Erstellung von Bibliotheken sehr wünschenswert und neuartige chemische Strategien zur Erzeugung vielfältiger, strukturell komplexer small molecules sind sehr gefragt. Unter diesen sticht die Petasis-Reaktion (PR)–eine Dreikomponenten-Kupplungsreaktion–als vielseitige Methode zur Erzeugung hochfunktionalisierter Amine mit struktureller Vielfalt hervor. Die Integration der PR mit

nachfolgenden Ringschlussreaktionen bietet eine leistungsstarke Strategie zur Konstruktion neuartiger polycyclischer Gerüste. Als ergänzende Maßnahme zur Modulation der IRE1–XBP1-Signalachse wird im letzten Teil dieser Arbeit die Synthese einer Vielzahl small-moleules mit polycyclischen Gerüsten mit einem hohen Grad an sp^3-hybridisierten Kohlenstoffatomen und mehreren stereogenen Zentren vorgestellt. Dies wurde durch eine Dreikomponenten-Petasis-Reaktion (3C-PR) mit anschließenden intramolekularen Diels-Alder-Reaktionen (IMDA) sowie durch einen sequenziellen 3C-PR-, Ruthenium-katalysierten Ringschlussmetathese- (RCM) und IMDA-Prozess erreicht. Unsere synthetischen Bemühungen führten zur Bildung einer Sammlung von Epoxyisoindolen und Pyridazino[4,3-*c*]azepinen in guten Ausbeuten innerhalb von 2–3 Schritten. Die Stereochemie der Produkte wurde durch eine Einkristall-Röntgenstrukturanalyse bestätigt. Unsere Ergebnisse unterstreichen die breite Substratpalette und Vielseitigkeit der Petasis–Sequenzreaktionen beim Zugang zu bisher unerforschten polyzyklischen Gerüsten mit vielversprechenden arzneimittelähnlichen Eigenschaften und potenzieller biologischer Relevanz.

Anschließend wurde ein auf Fluoreszenz-Resonanzenergietransfer (FRET) basierender Assay entwickelt und ein Screening einer internen Sammlung von ca. 10.000 strukturell unterschiedlichen, komplexen, biologisch relevanten small molecules durchgeführt, die auf vereinfachten Naturstoffgerüsten basieren. Diese Screening-Bemühungen führten zur Identifizierung vielversprechender Hit-Serien, darunter Indol-basierte Inhibitoren (Verbindung **10**) und Aminopyrimidin-basierte Aktivatoren (Verbindung **78**). Die weitere Optimierung des Indolgerüsts durch Festphasen- und Flüssigphasen-Fischer-Indolsynthese sowie Suzuki-Miyaura-Kupplungsreaktionen führte zum stärksten Inhibitor **54** (IRE1α, IC_{50} 16 nM; p-IRE1α, IC_{50} 9 nM), der eine 20-fache Verbesserung der Wirksamkeit aufweist. Parallel dazu führten systematische Modifikationen des Aminopyrimidin-Gerüsts zur Entdeckung der Verbindung **91**, dem stärksten Aktivator mit submikromolarer Aktivität (IRE1α, EC_{50} 0.48 μM; p-IRE1α, EC_{50} 0.18 μM). Diese Bemühungen führten zu neuartigen Indol-basierten Inhibitoren, die die IRE1α-RNase-Aktivität allosterisch hemmten, indem sie auf ihre ATP-Bindungstasche abzielten, und zu Aminopyrimidin-basierten Aktivatoren, die die IRE1α-Funktion verstärkten. Darüber hinaus wurde durch biophysikalische Bindungsassays, zelluläre Bewertungen und mechanistische Studien der potenzielle Mechanismus der Modulation der RNase-Aktivität aufgeklärt. Die resultierenden Verbindungen können als wertvolle chemische Werkzeuge zur Untersuchung der IRE1α-Funktion dienen und Einblicke in die Rolle von IRE1α bei der UPR-

Signalübertragung geben. Sie bieten eine Grundlage für die Entwicklung therapeutisch relevanter Moleküle die auf IRE1α abzielen.

Insgesamt zeigte diese Arbeit die Fähigkeit von Petasis–Sequenzreaktionen als effiziente, komplexitätserzeugende synthetische Strategie bei der Konstruktion polyzyklischer bioaktiver small molecules und hob das Potenzial von gerüstdiversen IRE1α-Modulatoren als wertvolle chemische Sonden und Ausgangspunkte für die Arzneimittelentwicklung hervor. Die optimierten Derivate lieferten entscheidende Erkenntnisse über die Funktion von IRE1α und seine Rolle bei der Stressreaktion des ER und ebneten den Weg für weitere Studien, die darauf abzielen, diesen Signalweg therapeutisch zu beeinflussen, beispielsweise bei Krebserkrankungen.

1 Introduction

1.1 Scaffold-diverse synthesis

Small molecules have been at the center of attention in the pharmaceutical industry for decades. They play a crucial role as therapeutic agents for treating diseases and also as effective agents for investigating the biological functions of proteins, human physiology, and cellular activities. When the protein target and a native ligand are known, structure- or mechanism-based rational design is employed to identify new therapeutic compounds or probes. Alternatively, high-throughput screening (HTS) in which researchers explore small-molecule libraries is employed in cases of less-characterized ligands or systems involving multiple ligands. One of the key challenges in small-molecule research is the restricted exploration of "chemical space," as synthetic compounds and commercially available screening libraries cover only a limited portion of the vast potential structural diversity. There is widespread agreement that many of the current compound collections are lacking and are largely dominated by flat, sp^2-rich compounds. Therefore, chemistry strategies that enable the development of higher-performing small molecules are in great need (Figure 1).[1-2] Additionally, with the advancement in genomics and proteomics approaches in drug discovery, there is a significant growth in potential therapeutic targets, driving an ever-increasing demand for access to diverse chemical libraries.[3]

Figure 1. The decline in drug discovery successes and the presence of undruggable targets are often attributed to low-performing screening collections.

The immense scope of vast unexplored chemical space has driven researchers to develop innovative strategies for expanding current collections of small molecules and compound libraries, with a particular focus on areas associated with bioactive chemical space.[4-6] Thus, there is considerable unmet need in accessing compound collections with high structural diversity covering unexplored chemical space that are biologically relevant. Although the term

"diversity" is subjective, there are three major levels of molecular diversity that have been consistently identified in the literature reports (Figure 2),[7] including "Appendage diversity"–variation in structural moieties around a common skeleton; "Stereochemical diversity"–variation in the orientation of potential macromolecule interacting elements; and "Skeletal /scaffold diversity"–presence of many distinct molecular skeletons.

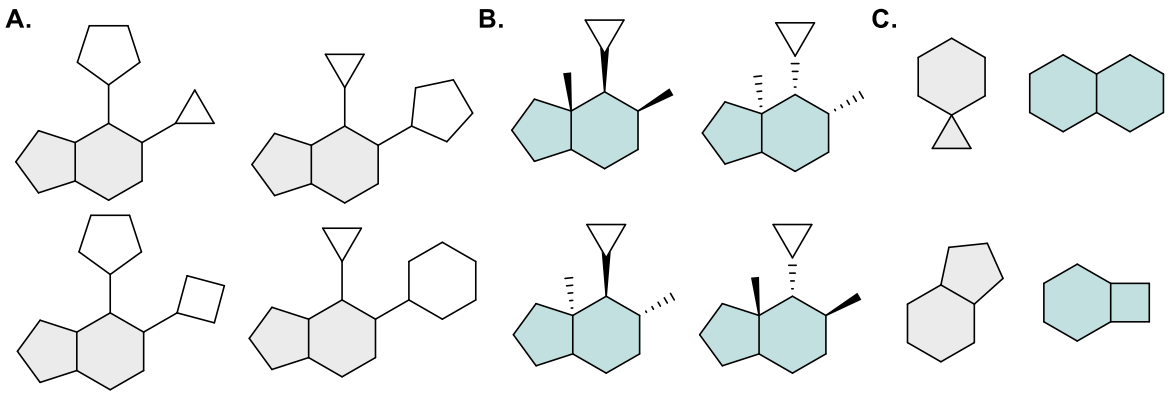

Figure 2. Major components of molecular diversity. (A) Appendage, (B) Stereochemical, and (C) Skeletal/scaffold diversity

Increasing structural complexity in a series of compounds inherently leads to higher diversity; examples of such efforts among many include (i) "libraries-from-libraries"- chemical transformation of combinatorial libraries using solid-phase synthetic approaches to expand their range and collection of chemical diversity. The chemical libraries built by this process have very different physical, chemical, and biological properties compared to the original libraries from which they were derived.[8-9] (ii) "biology-oriented synthesis" (BIOS) is a strategy that takes inspiration from natural products to guide the creation of biologically relevant compound collections based on simplified natural product scaffolds. Such compound libraries inspired by natural products and synthesized following BIOS principles are often enriched in biological activity.[10] (iii) "diversity-oriented synthesis" (DOS)- this approach follow the build/couple/pair strategy, in which chiral building blocks are coupled to induce stereochemical diversity, followed by intramolecular pairing of complementary functional groups, resulting in skeletal diversity.[1]

The scaffold-diverse synthesis of compound libraries greatly depends upon sequences of complexity-generating reactions, like multicomponent reactions, cycloadditions, and ring-opening or ring-closing metathesis reaction.[11] Such cascade-type reactions are of great interest from a medicinal chemistry perspective, as the structurally diverse heterocycles developed contain multiple stereogenic centers, can be readily obtained through single or few subsequent synthetic transformations, and exhibit natural-product-like properties.[12] All these factors

encouraged us to develop novel synthetic pathways involving multicomponent Petasis–sequence reactions to access small molecule libraries, covering unexplored chemical space, exhibiting improved potency and selectivity, and potentially targeting biological macromolecules.

1.1.1 Multicomponent Petasis reaction

Multicomponent reactions (MCRs) are relevant to medicinal chemistry and drug discovery as they allow for the efficient synthesis of diverse heterocyclic scaffolds with high complexity and stereoselectivity.[13-14] These are one-pot reactions in which three or more starting materials combine in a single reaction to form a single product that incorporates essentially all of the atoms of the starting materials.[15-16]

Petasis reaction (PR) is one of the significant multicomponent reactions that facilitates the synthesis of highly functionalized amines from a primary or secondary amine, a carbonyl component, and a boronic acid derivative via the *in-situ* formation of an iminium boronate complex (Scheme 1).[17-19] It was first coined in 1993 by Petasis and coworker with the synthesis of *(E)*-allylamines from secondary amines, paraformaldehyde, and *(E)*-vinylboronic acids.[17] Density functional theory (DFT) and NMR studies revealed that the possible mechanism involves the formation of an "iminium boronate complex," which aids an irreversible transfer of the boron substituent in a *cis*-diastereoselective way, forming a new carbon-carbon bond.[20-22]

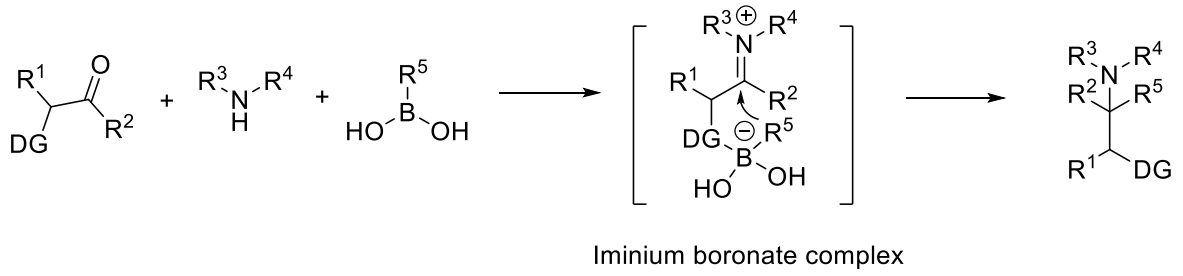

Scheme 1. General scheme of a three-component PR of an aldehyde, secondary amine, and a boronic acid. DG: directing group

Over the years, the scope of the PR has been rapidly expanded, and it has emerged as a powerful and reliable multicomponent transformation. Its key advantages include the wide substrate scope, easily available starting materials, mild reaction conditions, short duration, atom-economical nature, and importantly, the high stereoselectivity for the formation of substituted amine products. It also provides straightforward access to structurally diverse and biologically relevant amine products.[19] Three decades have passed since the discovery of the PR, during

which numerous variants have been developed, and the topic has been thoroughly reviewed.[12, 18-19, 23] Some of the very recent developments include covalent organic frameworks (COFs) prepared via the photoredox-catalyzed multicomponent PR reported by Wang *et al*. in 2023,[24] PR catalyzed by nanoparticles under solvent free conditions,[25] in 2019 Rivera and coworkers introduced PR for the late stage multicomponent diversification, labelling and stapling of peptides.[26] These findings highlighted the potential of the PR in peptide drug discovery and chemical biology, showcasing its effectiveness and versatility. In 2022, Vytla *et al*. reported an efficient three-component photoredox-catalyzed PR using $[Ir_2(dtbpy)]PF_6$ as the photocatalyst. They showed that a range of amine components like sulphonamides, amides, and hydrazines can readily undergo imine formation, followed by radical α-alkylation with alkyltrifluoroborates in the presence of sodium hydrogen sulfate, giving rise to structurally diverse α-substituted secondary sulfonamides, amides, and hydrazides.[27] Additionally, the asymmetric versions of PRs are of particular interest from a medicinal chemistry perspective and have also undergone several improvements over the years.[23]

1.1.2 Diversity syntheses using Petasis–sequence reactions

The products of multicomponent PRs are versatile precursors for sequential reactions and are compatible with various secondary transformations. Such cascade-type reactions yield structurally diverse polycyclic scaffolds, many of which display resemblance to natural products and contain multiple chiral centers in a single or few subsequent synthetic transformations. The build/couple/pair strategy proposed by Schreiber and coworkers is applied in Petasis-sequence reactions to synthesize such densely factionalized, biologically relevant scaffolds. A few representative examples of sequential strategies combining PR with Ruthenium catalyzed ring-closing reactions, intramolecular Diels–Alder (IMDA) reaction, and other cyclization reactions are illustrated in Figure 3.[28]

Nielsen and coworkers reported successfully combining 3C-PR (couple) with Ru-catalyzed ring closing metathesis (RCM) and isomerization reactions (pair). Olefin-containing components used for 3C-PR were aligned in such a way as to undergo ring-closing metathesis, forming ring moieties. The *anti*- amino alcohols formed in the "build" stage underwent ring-closing metathesis reaction in the presence of a ruthenium alkylidene catalyst to form 5- and 7-membered ring systems (Figure 3A). The different combinations of olefin-containing building blocks aid easy access to structural diversity within a few steps.[29] Flagstad *et al*. reported the synthesis of highly functionalized *anti*-hydrazido alcohols via the 3C-PR of diverse hydrazides, α-hydroxy aldehydes, and boronic acids. The resulting Petasis products

underwent regio and stereoselective cyclization reactions, including ring-closing metathesis and intramolecular Diels−Alder reactions to afford ten structurally unique scaffolds (Figure 3B).[30] Ishoey *et al*. reported rapid access to complex sp^3-rich heterocyclic scaffolds by using an interesting ROM–RCM (ring opening–closing metathesis) reaction when 3C-PR/IMDA products were subjected to the Grubbs II catalyst. The products were formed as a single diastereomer (Figure 3C).[31] Flagstad *et al*. reported another 3C-PR/IMDA–oxidative cleavage/reductive cyclization strategy (Figure 3D) and the same group reported Petasis/Diels–Alder/cyclization sequence for the generation of scaffolds with multiple stereogenic centers and suitable functionalities for potential diversification. This work resulted in a library of compounds with highly complex tricyclic and tetracyclic scaffolds with a high fraction of sp^3 carbon atoms (Figure 3E).[32]

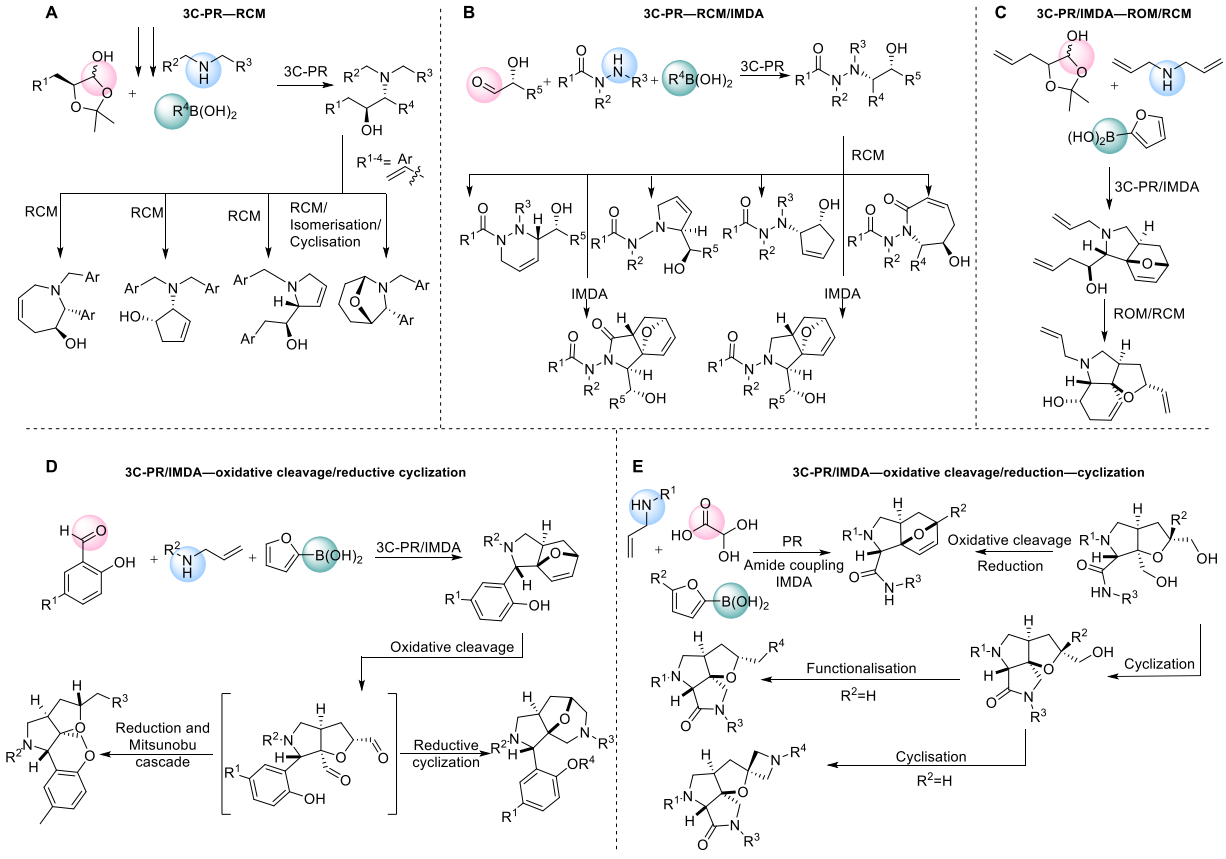

Figure 3. Selected literature reports of multicomponent Petasis sequence reactions to generate structurally diverse small molecules. *Figure adapted from "Petasis sequence reactions for the scaffold-diverse synthesis of bioactive polycyclic small molecules".*[28]

Examples reported in the literature showed the great value of Petasis sequence reactions to readily synthesize highly complex, polycyclic scaffolds with a high fraction of sp^3 carbons and several stereocenters. The presence of "undruggable" targets and "demanding" targets whose structural requirements are not completely met by current compound collections makes it relevant to develop short synthetic strategies to effectively develop such privileged scaffolds. In this context, we are advancing our exploration of novel chemical spaces accessible through small molecules by developing efficient synthetic strategies for creating small molecules with polycyclic frameworks. Specifically, this study highlighted synthetic approaches using multicomponent PR to generate structurally diverse and synthetically accessible small molecules, which were further assessed for their potential as bioactive compounds in the early stages of drug discovery.

Building on this foundation, we extended our approach towards the discovery of small molecule modulators of IRE1α. We adopted an activity-based screening strategy and screened an in-house library of ~10000 compounds containing natural product-inspired, scaffold-diverse small molecules. The following part of this introduction explores the discovery and evaluation of such small molecules as modulators of protein–RNA interactions.

1.2 RNA: The conduit of central dogma

Ribonucleic acid (RNA) is the key player in genetic information transfer, as explained by the central dogma of molecular biology. The genetic information stored in deoxyribonucleic acid (DNA) is transcribed into RNA, and then it is translated into proteins.[33] Apart from its central role in protein translation, it also participates in RNA processing, modification, and the regulation of gene expression.[34] RNAs with their broad range of biological functions have captured significant attention in recent times. It is revealed that about 70-90% of the human genome is transcribed to RNAs, while only ~1-2% of which codes for proteins.[35-37] Protein-coding RNA transcripts, known as messenger RNAs (mRNAs), contain genetic information and direct protein synthesis. Non-coding RNA (ncRNA) transcripts, by definition, are not translated to proteins but play critical regulatory and structural roles in cells, thereby providing a vast druggable space.[38] But the current protein-targeted therapeutics, such as small molecules and biologics, only cover a small fraction of the human genome, as most DNA sequences are transcribed into ncRNAs. Hence, RNA-based therapeutics have immense potential as they expand the range of druggable targets.[39]

The field of RNA therapeutics has been on the rise for many years, and this growth was further accelerated by the success of mRNA-based COVID-19 vaccines. Various RNA-targeted approaches are used in drug discovery, namely antisense oligonucleotides (ASOs), RNA interference (RNAi), CRISPR-based genome editing, aptamers, mRNA and mRNA vaccines, and RNA related small- molecules.[39-40] Antisense oligonucleotides (ASOs) and small interfering RNAs (siRNAs) act via Watson–Crick–Franklin base-pairing with the specific RNA target of interest. So far, eight ASO-based drugs and three siRNA-based drugs approved by the FDA and are in the market (e.g., ASO exon skipping oligonucleotide Nusinersen (Spinraza) approved in 2016 for spinal muscular atrophy; siRNA- Givosiran (Givlaari) approved in 2019 targeting liver mRNAs for acute hepatic porphyria).[39-41] Several disease targets are being addressed with CRISPR-based gene editing and are in clinical trials. But so far, none of them are in the market.[42] Aptamers are single-stranded oligonucleotides with well-defined 3D structures that specifically bind to and inhibit proteins.[43] The aptamer-based therapeutics include (i) antagonist aptamers, which disrupt interaction between disease-associated targets, and (ii) cell type-specific aptamers serving as carriers in delivering other therapeutic agents to the target cells or tissues.[39, 44] Anti-vascular endothelial growth factor (VEGF) aptamer pegaptanib (Macugen) is the only FDA-approved aptamer-based drug.[44] Vaccines designed to target infectious diseases are the most advanced and widely adopted

application of mRNA therapeutics. The most famous examples of mRNA technology in therapeutics are the mRNA vaccines developed against the severe acute respiratory syndrome coronavirus 2 (SARS-CoV-2), the Pfizer-BioNTech vaccine Comirnaty and the Moderna vaccine mRNA-1273.[45-46] However, RNA-targeted small molecules have certain merits over oligonucleotides owing to their favorable pharmacokinetic and pharmacodynamic properties, ease of biodelivery, tunability through medicinal chemistry approaches, lower production costs and most importantly, the years of experience in developing small molecules for protein targets.[47-50] The burgeoning interest in RNA as a therapeutic target and subsequent high-throughput screening campaigns have led to the identification of a number of compounds that can regulate disease-associated RNAs.[48] One class of initial RNA ligands discovered were antibiotics that targeted bacterial ribosomal RNA, such as aminoglycosides, tetracyclines, macrolides, and oxazolidinones.[51-52] The 2020s marked a significant shift with the discovery of FDA-approved mRNA splicing modulator Risdiplam for spinal muscular atrophy, indicating the growing potential of small molecule RNA therapeutics.[53] Besides, RNA-focused ligand datasets were also curated to provide insights into the rational design of chemical probes and potential drugs.[54-55] These datasets revealed some commonalities among RNA binding small molecules, such as the presence of positively charged groups to approach the highly negatively charged backbone, heteroaromatic moieties to form π-stacking interactions with nucleobases, and nitrogen-containing groups that act as both H-bond donors and acceptors. However, targeting more complex tertiary structures of RNA with protein-like binding pockets requires a more sp^3 nature than planar geometry.[48] With the expanding understanding of RNA binders, innovative strategies like ribonuclease targeting chimeras (RIBOTACs)-which modulate RNA function by facilitating its degradation have emerged. RIBOTACs involve covalently linking specific RNA-binding ligands to RNase L-recruiting modules that selectively mediate RNA decay.[56] Once considered undruggable, RNAs are now seen as attractive therapeutic targets, though much remains to be discovered about the rational design of ligands for specific RNA targets and their biological outcomes.

1.2.1 Ribonucleases as regulators of RNA and emerging drug targets

Ribonucleases are enzymes with a pivotal function in RNA biology. They regulate RNA processing, maturation, degradation, and quality control.[57] Analysis of the human proteome has unraveled 122 ribonucleases.[58] Ribonuclease (RNase) acts by cleaving specific RNA sequences at internucleotide phosphodiester bonds. They are broadly classified as endoribonucleases and exonucleases based on their RNA processing mechanisms.

Endoribonucleases cleave RNA internally, breaking the phosphodiester bonds within the RNA molecule (e.g. RNase A, RNase E, RNase H) and exoribonucleases degrade RNA from either the 5' or 3' end (e.g. RNase II, RNase R).[59] Studies on vertebrate proteome identified enzyme group exclusive to vertebrates which are homologous to RNase A, called the "RNase A superfamily" or vertebrate-secreted RNases. So far, up to eight secretory variants of RNase have been characterized in humans. They include pancreatic ribonuclease or RNase 1, eosinophil-derived neurotoxin or RNase 2, eosinophil-cationic protein or RNase 3, RNase 4, angiogenin or RNase 5, k6 or RNase 6, RNase 7, and RNase 8.[60] Zhang *et al*. in 2002 reported the complete identification of human RNase 1-8 genes, located on chromosome 14q11.2.[60-61]

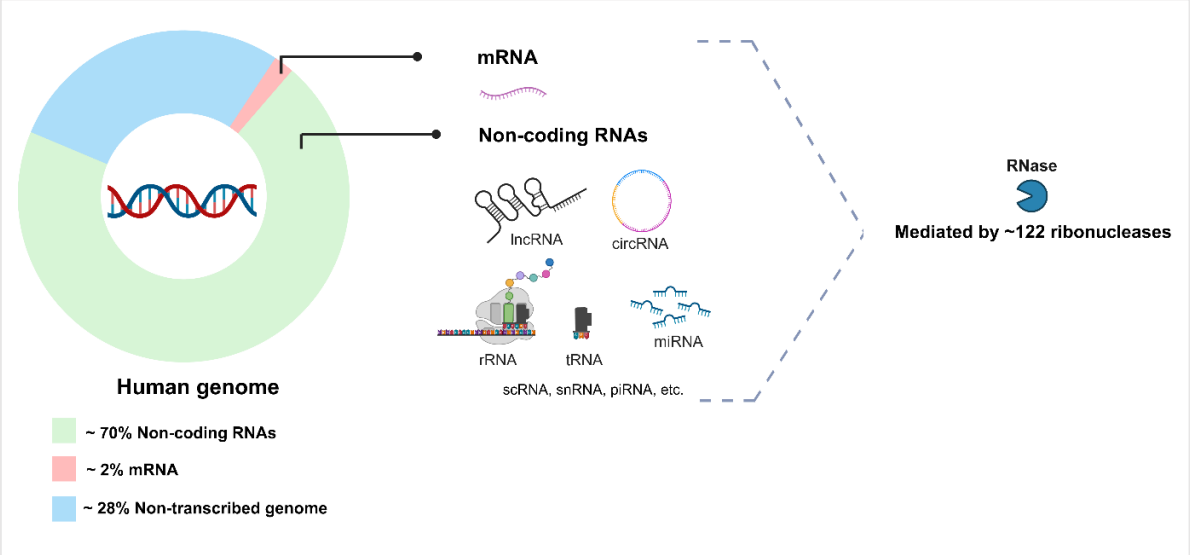

Figure 4. About 70-90% of the human genome is transcribed into non-coding RNAs and mRNAs. This vast fraction of the transcriptome is mediated by a comparatively smaller fraction of 122 ribonucleases.[58]

Targeting enzymes and RNA-binding proteins that regulate RNA biology and metabolism is an emerging approach in targeting RNA. As approximately three-fourths of the human genome is transcribed to RNA, while only 1-2% of which codes for proteins, leading to a major fraction of non-coding RNA transcripts. This vast size of transcriptome contains tens of thousands of mRNAs and non-coding RNAs that are regulated by a comparatively smaller group of ribonucleases (Figure 4).[58] In the case of the biogenesis of small non-coding mircoRNA (miRNA), it follows a distinct two-step pathway which is conserved for most miRNAs. The biogenesis of thousands of miRNA is majorly mediated by two ribonucleases, Drosha and Dicer, which belong to the RNase III class of enzymes.[62] The primary mRNA transcripts (pri-miRNA) are cleaved by Drosha to precursor miRNA (pre-mRNA) with ~70 nucleotides length. Pre-miRNA is then recognized by the endonuclease Dicer, which processes it to mature

miRNA with ~22 nucleotides. Mature miRNA is loaded into a ribonucleoprotein complex, known as the RNA-induced silencing complex (RISC). This complex directs the miRNA to the target mRNA, which leads either to translational repression or degradation of the target mRNA.[62] Therefore, small molecules targeting ribonuclease could address multiple RNA transcripts involved in a disease pathway. Being central controllers in the RNA metabolism network, ribonucleases are positioned as promising targets for RNA therapy.

Table 1. Selected list of mammalian RNases implicated in cancers [63]

Class	RNase	Cancer implications	Alterations in function
Conventional mRNA decay	PARN	Malignant glioma	Inaccessibility to mRNA
	XRN1	Osteosarcoma	Downregulation/depletion
Stress induced	RNase L	Prostate adenocarcinoma	Higher frequencies of variants with reduced activity (R462Q and E265X)
	IRE1	Breast carcinoma	Enhanced activity
		Breast carcinoma-derived cell lines	Overexpression
		Hepatocellular carcinoma	HCC Enhanced activity
miRNA maturation	Drosha	Esophageal squamous cell carcinoma	Overexpression
		Cervical squamous cell carcinoma	Amplification
			Overexpression
	Dicer	Leukemic cell lines	Enhanced accessibility to pri-miRNA
		Mucoepidermoid carcinoma	Abnormal expression
		Lung adenocarcinoma	Overexpression
		Prostate adenocarcinoma	Overexpression
		Ovarian serous carcinoma	Overexpression
		Burkitt's Lymphoma	Overexpression
		Non-small cell lung cancer	Downregulation
		Breast carcinoma	Downregulation
Others	Angiogenin	Prostate adenocarcinoma	Overexpression
		Gastric carcinoma	Overexpression
		Melanoma	Overexpression
	FEN1	Prostate adenocarcinoma	Overexpression
		Non-small cell lung cancer	Overexpression
		Small cell lung cancer	Overexpression

As discussed, RNases, along with ncRNAs and RNA-binding proteins (RBPs), regulate gene expression at the mRNA level. Disruption of this process is linked to tumorigenesis and cancer progression, and hence several of these RNases have implications in human cancers (Table 1).[63] Some RNases contribute to tumorigenesis (Drosha),[64-65] others act as potential tumor suppressor candidates (PARN, RNase L),[66-69] and some of them exhibit dual roles (IRE1α).[70-72] IRE1α with its dual tumor-suppressing and promoting role, makes it an intriguing target in cancer biology.

1.2.2 The endoribonuclease IRE1α and its activation as a stress sensor

IRE1α belongs to the class of RNases that require a specific signal to become active and is activated in response to stress signals from the endoplasmic reticulum (ER). Housekeeping ribonucleases actively contribute to the maturation, quality control, and turnover of cellular RNAs. In contrast, stress-induced ribonucleases become active only under specific stress conditions. Activation or inactivation of such RNases can rapidly alter RNA levels within the cells, thereby altering cellular physiology to protect cells from the deleterious effects of stress.[73]

ER serves as the main hub for synthesizing, folding, modifying, and transporting approximately one-third of the cellular proteins.[74] IRE1α is an ER-resident protein with bifunctional Kinase and RNase activity and serves as a primary sensor of the accumulation of unfolded proteins and monitors the protein folding quality (β isoform is only expressed in the lung and intestine). The accumulation of misfolded proteins within the lumen of the ER induces stress, which subsequently activates the evolutionarily conserved, adaptive or anticipatory response called unfolded protein response, [75-77] a concept which was introduced by Kozutsumi *et al*. in 1988.[78] IRE1α ribonuclease is a central component of the UPR activated by ER stress (Figure 5) and is the most evolutionarily conserved and well-studied arm of the UPR. UPR mediates ER function through three different pathways defined by three distinct ER transmembrane sensors: IRE1α, protein kinase R–like endoplasmic reticulum kinase (PERK), and activating transcription factor 6 (ATF6).[77, 79-80] Impaired UPR signaling is associated with several diseases and specifically the IRE1α-XBP1 branch has implications in cancers,[81-83] metabolic disorders,[74] and neurodegeneration.[84] Hence, modulating the UPR pathway by targeting the key effector proteins of the UPR signaling cascade presents a promising strategy for the treatment of these human diseases.

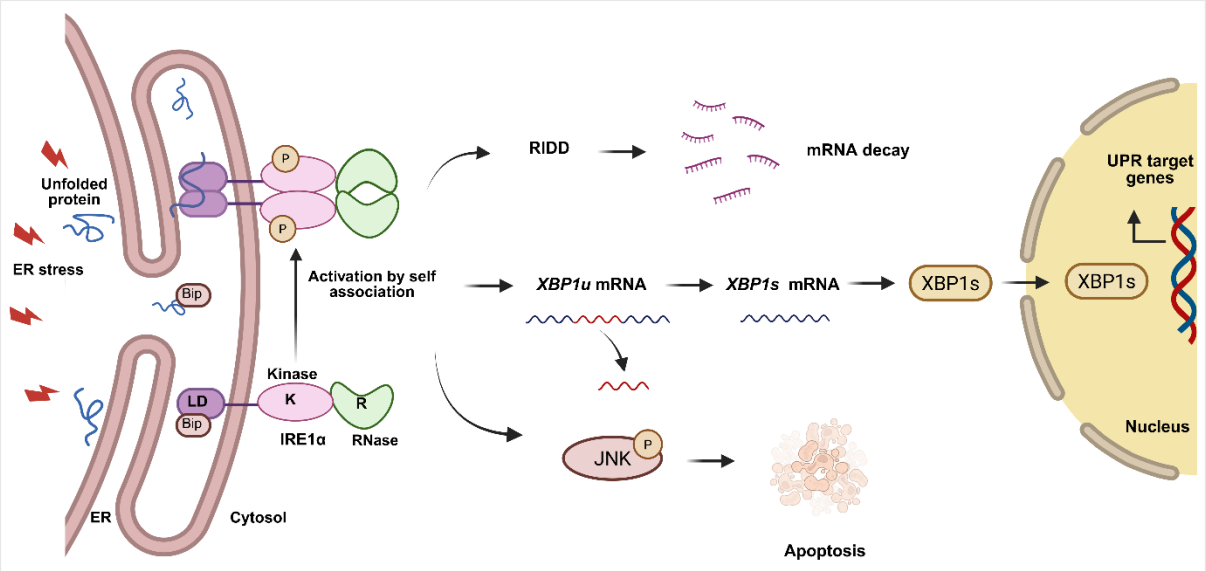

Figure 5. Brief illustration of the activation of IRE1α and the subsequent unfolded protein response.

The bifunctional protein IRE1α consists of two domains: The N-terminal luminal domain (LD) and the C-terminal cytoplasmic region, which incorporates two functional domains, the serine/threonine kinase and RNase domains.[79] The LD of IRE1α senses the presence of unfolded proteins in the ER lumen, triggering dimerization/oligomerization and auto-transphosphorylation, which in turn, leads to the activation of C-terminal RNase activity in the cytosolic domain.[85] This leads to IRE1α-RNase catalyzed excision of a 26-nucleotide intron from the mRNA, *unspliced XBP1* (*XBP1u*) followed by ligation mediated by RNA ligase RtcB to yield spliced form of *XBP1* (*XBP1s*) mRNA that encodes the potent transcription factor (spliced X-box-binding protein 1) XBP1s (Figure 5).[86] XBP1s protein combat the stress by up-regulation genes involved in protein folding and quality-control mechanisms, as well as by activating the ER-associated degradation (ERAD) components.[87] In addition, activated IRE1α-RNase targets ER-bound RNAs (mRNA, miRNA, and rRNA) and degrades them through a process known as regulated IRE1α-dependent decay (RIDD), resulting in reduced mRNA levels and a subsequent decrease in the protein-folding burden within the endoplasmic reticulum.[88] The activity of XBP1s is pro-survival and supports proteostasis; however, under severe ER stress conditions, UPR can also execute apoptosis via activation of the c-Jun N-terminal kinase (JNK) pathway. Therefore, IRE1α responds to ER stress via XBP1s, RIDD, and induction of apoptosis and acts as a critical regulator in balancing ER homeostasis as well as in determining cell fate.

1.2.3 Structure of IRE1α

Two IRE1 genes have been identified in the mammalian genome: ERN1 (endoplasmic reticulum to nucleus signaling 1) and ERN2, which encode for IRE1α and IRE1β, respectively. The former is ubiquitously expressed[79] and serves as a UPR stress sensor in most cells, while the latter is expressed only in the gastrointestinal and bronchial epithelium.[89-90] Both isoforms of IRE1 share structural similarities with TGF-β serine/threonine protein kinase receptors and functionally resemble receptor tyrosine kinases, depending on ligand binding-induced dimerization as the activation mechanism for the cytoplasmic domains.[85] To elucidate the molecular mechanism of the IRE1α-XBP1 signalling event, a detailed insight into the structure of IRE1α is necessary (Figure 6).

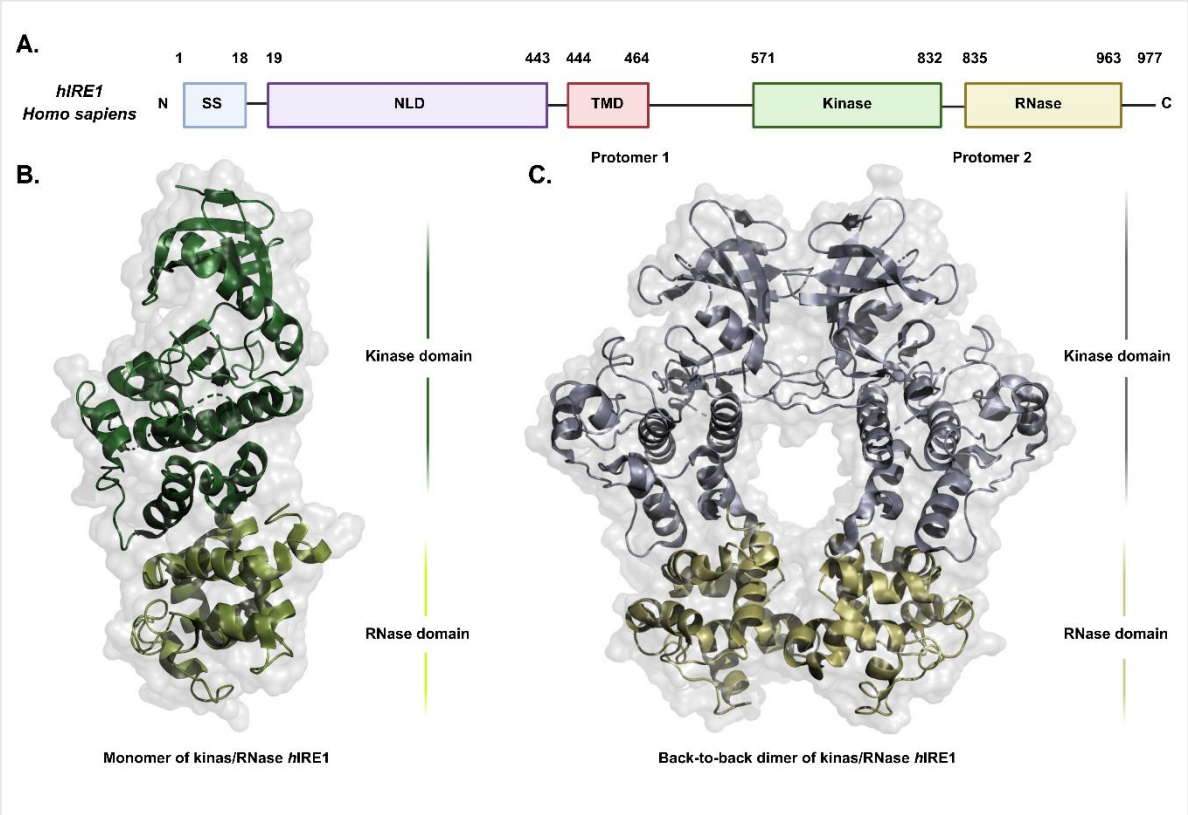

Figure 6. The structure of IRE1. (A) Schematic visualization of the domain architecture of IRE1, showing the signal sequence (SS), the N- terminal luminal domain (LD), transmembrane domain (TM), and the cytosolic kinase and RNase domains; (B) The crystal structure of the monomer of hIRE1 Kinase/RNase-apo (PDB: 4Z7G), (C) The back-to-back dimer of hIRE1 (PDB: 4YZC, ligand removed for clarity).

Zhou *et al*. reported the crystal structure of the monomer of the LD of human IRE1α,[85], which included a LD of 367 amino acid residues (24-390). It adopts a unique structural arrangement described as a triangular β-sheet cluster with each side occupied by β-structural motifs referred to as N, C, and M. These β-structural motifs are interconnected by several α-helices inserted

between them. The N, C, M motifs pack tightly together without any visible gaps, forming a compact triangular shape. Additionally, an 18-amino-acid signal sequence (SS) is located at the N-terminus of the protein.[91] The transmembrane domain of IRE1α consists of a single continuous amino acid chain with a juxta-membrane amphipathic helix and transmembrane helix.[92] The cytosolic region of IRE1α is subdivided into a serine/threonine protein kinase domain and a C-terminal endoribonuclease domain. Kinase domain of *h*IRE1α (571-832) consists of a bilobal protein kinase fold with the ATP-binding site in the cleft between the N-terminal β-sheet lobe and the α-helical C-terminal lobe.[93] Additionally, there is a helical domain fused to and structurally continuous with the C-terminal lobe of the kinase, which is responsible for the sequence-specific RNase activity by which IRE1α is able to initiate splicing of *XBP1* mRNA.[93-95] The kinase activation segment (711-741) is disordered, and the central ~10 residues 720-729 of the activation segment are proposed to contain the S724 phosphorylation site. Residues 746-748 are similarly disordered and carry an APE motif and the conserved DFG motif at residues 711-713.[93] C-terminal RNase domain (residues 835–963) has an α-helical conformation with a fully ordered connection between helices 3 and 4 and is directly fused to the kinase domain through the kinase C-lobe.[91, 96]

1.2.4 Small molecules targeting of IRE1α in cancer

IRE1α plays a significant role as the key player of the UPR in maintaining ER homeostasis and determining cell fate, while also contributing to the progression of various diseases.[97-98] Cancer cells are exposed to higher levels of stress, and they often exploit the pro-survival UPR signals to overcome such physiological, metabolic, or therapeutic stresses. IRE1α activity has been reported to promote tumor development and aggressiveness across various cancers, including leukemia, glioblastoma, myeloma, renal, and breast cancers.[99-102] The IRE1α-XBP1 branch has also been reported to exhibit resistance against chemotherapy in cancer.[103-104] In prostate cancer, the IRE1α-XBP1 pathway regulates c-Myc expression, further contributing to oncogenicity.[99-100] Similarly, the IRE1α-XBP1 pathway promotes melanoma progression by regulating IL-6/STAT3 signaling.[105] In contrast to the IRE1-XBP1 signaling arm that exhibits pro-tumorigenic effects, RIDD may counteract the tumor invasion and angiogenesis.[102] Because of the indications of the tumorigenic role, IRE1α has been evaluated as an appealing target for several anticancer drug development strategies. These efforts can be classified as (i) inhibiting IRE1α activity to disrupt the adaptive response that allows tumor cells to survive, which can be achieved by IRE1α inhibitors; (ii) hyperactivating IRE1α to initiate its pro-death RIDD that ultimately leads to apoptosis, which may be achieved by IRE1α activators.

1.2.4.1 IRE1α RNase inhibitors

Over the years, several small molecules have been identified that bind directly either to the catalytic site of the IRE1α RNase domain or to the ATP-binding pocket of its kinase domain, ultimately leading to inhibition of the IRE1α–XBP1 signaling axis (Figure 7). Most competitive inhibitors of the endoribonuclease activity of IRE1α share a common hydroxy-aryl-aldehyde residue (HAA). (4μ8c, MCK series, B-109 and STF-083010).[106-110] B-109 and STF-083010 undergo hydrolysis in physiological conditions to form HAA residue *in situ*. HAA residue reacts specifically with K907 in the active site of the RNase domain, thus forming a stable imine via Schiff base formation and inhibiting the ER stress-induced *XBP1* mRNA splicing.[111] HAA derivative, 4μ8C, is also reported to inhibit RIDD-mediated mRNA degradation in mouse embryonic fibroblast cultures treated with tunicamycin.[112] STF-083010 shows inhibitory effects in multiple myeloma xenografts.[113] B-I09 suppresses the growth of human chronic lymphocytic leukemia (CLL) cells in vitro and induces regression in a murine CLL model.[109] MKC-3946, when used as an adjuvant therapy along with the proteasome inhibitor bortezomib, increased the ER stress by blocking *XBP1* mRNA splicing.[107] All these reports from the literature proved the therapeutic potential of IRE1α inhibitors in cancer.

In search of more specific inhibitors of IRE1α RNase, a type of ATP-competitive kinase (type II) inhibitors that inhibit IRE1α RNase through the kinase domain by stabilizing monomeric IRE1α were identified.[114-115] Compound 3 is a type II kinase inhibitor that attenuates IRE1α RNase activity.[115] Accordingly, a series of Kinase-inhibiting RNase-attenuators (KIRAs) were developed based on compound 3, sharing a similar allosteric mode of action.[116-117] Successively, GSK2850163 is a type III inhibitor of IRE1α that has been described to occupy a binding site adjacent to the hinge region of the kinase was identified.[117] An imidazo[1,2-*b*]pyridazin-8-amine based kinase inhibitor (compound 31) with allosteric RNase inhibition was discovered through small molecule screening followed by structural optimization.[118] Additionally, compound 18 was reported as a selective inhibitor of IRE1α kinase, and it inhibited its RNase activity towards *XBP1* and showed efficacy in pre-clinical myeloma models.[119-120]

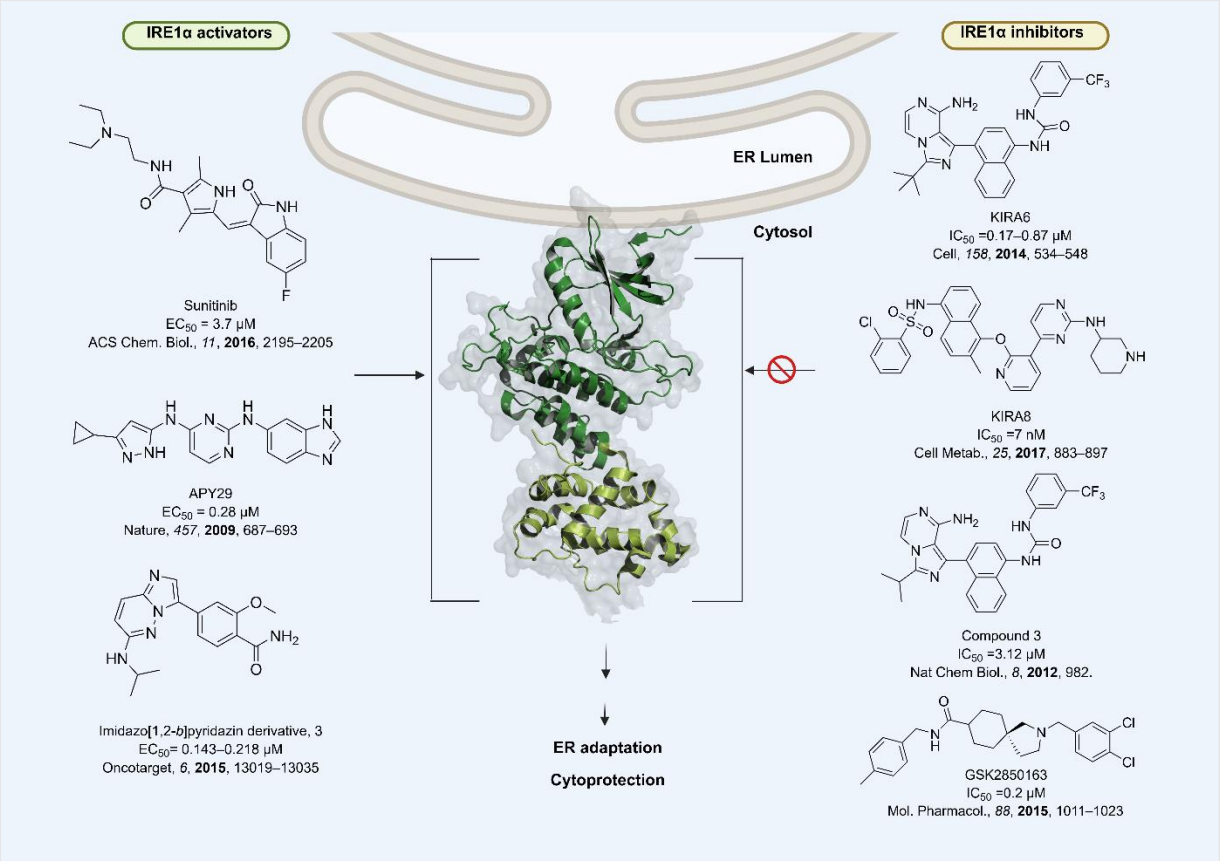

Figure 7. Different classes of reported small molecule inhibitors and activators of IRE1α RNase.

1.2.4.2 IRE1α RNase activators

Hyperactivating IRE1α to initiate its pro-death RIDD that ultimately leads to apoptosis is an alternate strategy to harness IRE1α as a therapeutic target in cancer. Sunitinib, APY 29, and Imidazo[1,2-*b*]pyridazin derivative (Compound 3) are type I kinase inhibitors - a type of ATP-competitive inhibitors of IRE1α which interact with the ATP binding site, block kinase trans autophosphorylation but promote dimerization and activation of RNase activity.[114, 121-122] Sunitinib is a FDA-approved anti-cancer small-molecule kinase inhibitor.[83] CXC195 is another reported activator that induced ER stress and apoptosis by inhibiting the PI3K/Akt/mTOR signaling pathway in hepatocarcinoma.[123] Even though a number of studies showed the tumorigenic as well as tumor-suppressing roles of the IRE1α-XBP1 branch of UPR, there are remaining questions to be addressed regarding the switch between those dual roles. Therefore, there is a pressing need to develop specific and selective chemical tools to explore IRE1α functions. Furthermore, among the reported IRE1α modulators, many exhibit poor pharmacokinetic properties, limiting their utility as clinically useful agents (e.g., 4μ8c). The discovery of novel modulators of IRE1α, along with gaining insight into IRE1α mediated signaling pathways, is of relevance for the development of new therapeutics.

2 Objective of the thesis

Small molecules have long been central to pharmaceutical research, serving as therapeutic agents and tools for investigating biological functions. While structure-based and high-throughput screening approaches aid in drug discovery, the key challenge remains the limited exploration of chemical space, as most available small molecule libraries are dominated by flat, sp^2-rich compounds. The growing number of potential therapeutic targets, driven by advances in genomics and proteomics, underscores the urgent need for novel chemistry strategies to generate diverse, structurally complex small molecules. The first part of this thesis aims to develop novel and efficient synthetic strategies for the construction of polycyclic scaffolds covering the underrepresented area of chemical space. A sequence of complexity generating Petasis and secondary cyclization reactions is designed for library production of complex tricyclic and tetracyclic scaffolds. The resulting complex scaffolds with high content of sp^3-hybridized carbon atoms are tested for their drug-like properties and biological relevance.

The latter part of this thesis aims to expand the RNA-targeting drug discovery by focusing on a regulator of RNA metabolism, the ribonuclease IRE1α. As a dual kinase/RNase, IRE1α controls the splicing of *XBP1* mRNA and mediates RNA degradation via downstream pathways like RIDD, making it a crucial player in RNA processing and cellular stress responses. Given its dual role in cancer progression and stress adaptation, modulating IRE1α activity with small molecules offers a powerful approach to influencing RNA-driven disease pathways. We search for new IRE1α-targeting small molecules from an in-house library with structurally diverse compounds for novel classes of modulators of endoribonuclease IRE1α. This work focuses on identifying and optimizing small-molecule IRE1α modulators through an RNase activity-based screening, following a pipeline of extensive structure modifications, leading to the discovery of indole-based inhibitors that allosterically inhibit the RNase activity by targeting its ATP-binding pocket and aminopyrimidine-based activators that enhance RNase function and downstream UPR signaling while inhibiting the kinase function. Through biophysical binding assays, mechanistic studies, and cellular evaluations, the study aims to elucidate the mechanism of action of the identified modulators, offering insights into IRE1α function and its role in disease-related unfolded protein response signaling. Collectively, this research work demonstrates the potential of Petasis-based methodologies in generating complex bioactive small molecules and highlights the significance of scaffold-diverse IRE1α modulators as promising candidates for RNA-targeted therapeutic development.

3 Results and discussion

3.1 Bioactive polycyclic small molecules via Petasis–sequence reactions

Results from this section were published as "Petasis sequence reactions for the scaffold-diverse synthesis of bioactive polycyclic small molecules."[28] Figures were adapted from the publication. MTT assay was performed by X. Qiu.

3C-PR serves as a highly adaptable approach for synthesizing amines with diverse functional groups. Numerous studies from the literature have highlighted its value in the construction of structurally diverse small molecules, natural products, and compound libraries.[12, 29, 31-32, 124-126] Integrating the PR with subsequent cyclization steps provides a concise and efficient route to increase molecular complexity and generate novel polycyclic scaffolds. In this chapter, various small molecules bearing polycyclic scaffolds, enriched with sp^3-hybridized carbon atoms and multiple stereocenters, were synthesized using 3C-PR in tandem with intramolecular Diels–Alder (IMDA) cyclizations or through a sequence involving 3C-PR, ring-closing metathesis (RCM), and IMDA reactions (Figure 8).

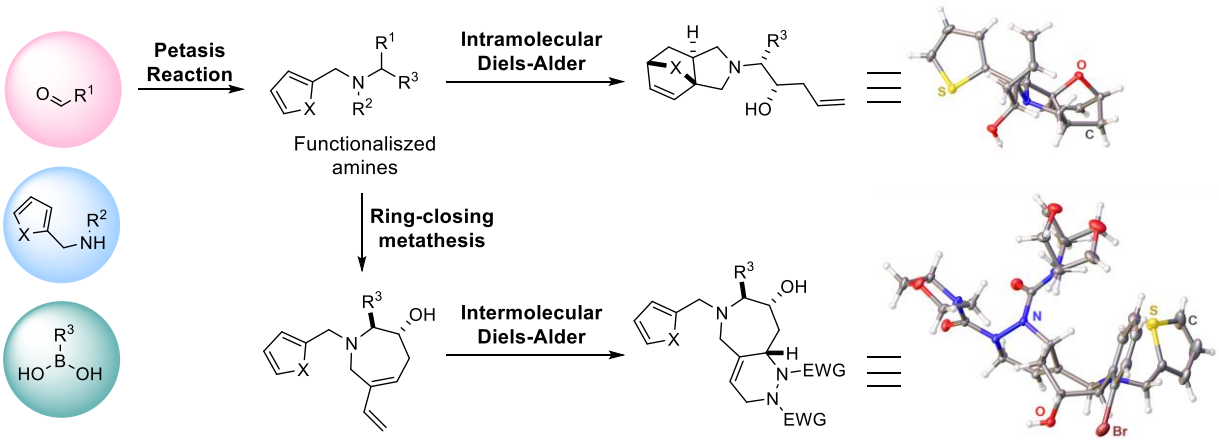

Figure 8. Summary of 3C-PR/ (IMDA) and 3C-PR/ RCM/ IMDA sequence strategy used in this thesis for library generation. Figure adapted from publication Petasis- sequence reactions for the scaffold-diverse synthesis of bioactive polycyclic small molecules [28]

3.1.1 Synthesis of allylated tertiary amines by Petasis reaction

This work began with the preparation of Petasis products designed to undergo further transformations leading to polycyclic scaffold formation. The initial reactions utilized primary amines such as furfurylamine (**1a**) and 2-thiophenemethylamine (**1b**), along with an α-hydroxy

aldehyde protected in the form of its corresponding lactol, specifically 5-allyl-2,2-dimethyl-1,3-dioxolan-4-ol (**2**), which was synthesized based on a reported procedure[31] and various arylboronic acids **3,** which were commercially supplied. Hexafluoroisopropanol (HFIP) was used as the solvent[127] because of its reported evidence in enhancing the reactivity in PR.[128] The reaction was carried out in the presence of 3Å molecular sieves (MS) at room temperature (Scheme 2). Interestingly, primary aromatic amines (**1**), which are typically less reactive in PR reactions, successfully produced the corresponding PR products with yields varied from 13% to 87% depending on the boronic acid derivative used. As expected, boronic acids containing electron-withdrawing groups, such as (4-nitrophenyl)boronic acid and (4-(trifluoromethyl)phenyl)boronic acid, did not afford Petasis products.

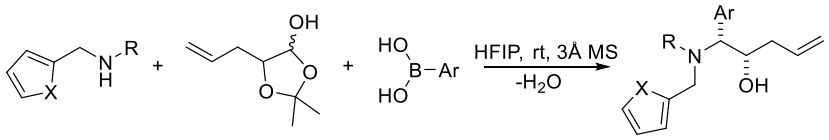

1 **2** **3** **4**

Entry	R	Ar	X	Time (h)	Yield (%)	Product
1	H		O	5	87	**4a**
2	H		S	3	83	**4b***
3	H	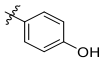	S	1	50	**4c**
4	H	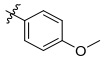	O	3	13	**4d**
5	Allyl		O	2	80	**4e**
6	Allyl		O	3	70	**4f**
7*	Allyl		S	24	45	**4g**
8	Allyl		O	3	62	**4h**
9	Allyl		O	2.5	43	**4i**

Scheme 2. The 3C-PR synthetic route to obtain allylated tertiary amines **4**. Reagents and conditions: primary aromatic amine (1 equiv.), 5-allyl-2,2-dimethyl-1,3-dioxolan-4-ol (1.2 equiv.), boronic acid (1.2 equiv.). **N*-allylation of **4b**

Subsequent *N*-alkylation with allyl bromide successfully yielded the corresponding allylated compounds. Alternatively, using secondary amines, *N*-allyl-furfurylamine and *N*-allyl-thiophenemethylamine as the amine components, resulted in Petasis products **4e**–**4i** with moderate to good yields (43–83%). The synthesis resulted in the formation of only one diastereomer for all products with strategically positioned appendages for secondary transformations.

3.1.2 Intramolecular Diels–Alder Reaction of Petasis-Derived Compounds (3-C PR/IMDA)

Initial cyclization of Petasis products **4e**–**4i**, containing olefinic groups, was attempted for an intramolecular Diels-Alder (IMDA) reaction. The goal was to form two types of cyclic scaffolds, epoxyisoindole and epoxybenzoazepine. Despite exploring multiple cyclization conditions, only the epoxyisoindole scaffold was successfully formed. The furan-2-ylmethyl-substituted Petasis products (**4f**, **4h**, **4i)** underwent cyclization to afford epoxyisoindoles (**5a**–**5c)** with yields ranging from 50% to 59%. (Scheme 3). In contrast, the thiophen-2-ylmethyl-substituted product **4g** failed to cyclize even under prolonged reflux at 120 ˚C in toluene. All final compounds were isolated as single diastereomer, and the *exo*-configuration was confirmed via single-crystal X-ray diffraction analysis of one of the representative compounds, **5a,** and deposited in the Cambridge Crystallographic Data Centre (CCDC) under deposition number 2191710.

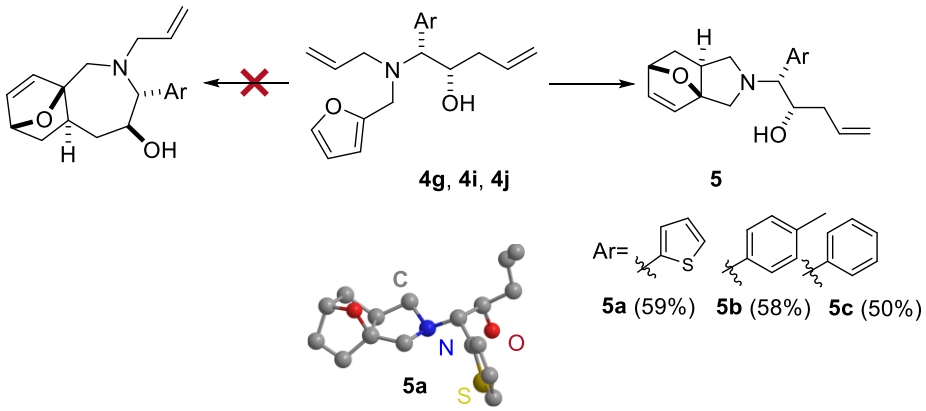

Scheme 3. Intramolecular Diels-Alder products **5** from Petasis products **4g,4j,4i**. Reaction conditions: toluene (0.5–0.4 M), reflux at 110 °C, 6 h.

3.1.3 *N*-propargylated tertiary amines by Petasis reaction

Motivated by the results of the efficient 3-C PR/IMDA sequence, I continued the synthesis of Petasis products with propargyl appendages to couple them via IMDA or RCM. The amine

component *N*-propargyl-thiophenemethylamine **6** was synthesized by the reported literature procedure.[129] Using 5-allyl-2,2-dimethyl-1,3-dioxolan-4-ol (**2**) and arylboronic acids, the corresponding Petasis products (**7a-d)** were yielded as a single diastereomer in yields up to 91% in 2-3 h reaction time (Scheme 4).

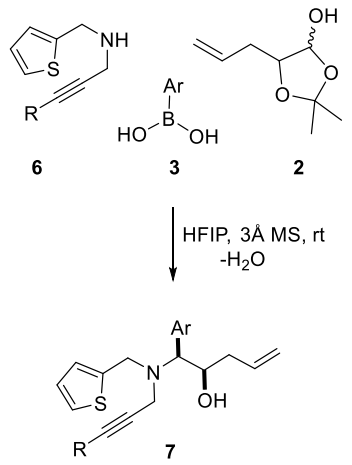

Entry	R	Ar	Time (h)	Yield (%)	Product
1	H		2	82	**7a**
2	H		2	80	**7b**
3	H		3	74	**7c**
4	CH_3		2.5	91	**7d**

Scheme 4. Synthetic route to access tertiary amines with allyl and propargyl functionalities. Reaction condition: *N*-propargyl-thiophenemethylamine (1 equiv.), boronic acid (1.2 equiv.), 5-allyl-2,2-dimethyl-1,3-dioxolan-4-ol (1.2 equiv.).

3.1.4 Ring closing metathesis–intermolecular Diels Alder reaction of Petasis products (3-C PR/RCM/IMDA)

Having confirmed the viability of allylated 3-C PR products as IMDA precursors, it was decided to use **7a**–**7d** as substrates under refluxing conditions, but it did not result in the formation of any IMDA cyclized products. Therefore, I tried to employ ring closing metathesis reaction to bring about cyclization. Various ruthenium catalysts were screened to obtain maximum conversion. Using the Grubbs second-generation catalyst to perform the eneyne metathesis reaction primarily resulted in the dimerization of the Petasis product **7**, with only minimal formation of the desired cyclized product **8**. In contrast, the use of Grubbs first-generation catalyst resulted in the formation of cyclized products **8a**-**8d,** however, in low yields (Scheme 5).

The products obtained from the 3C-PR/RCM reaction sequence were subsequently employed in an intermolecular Diels-Alder reaction, thereby providing a more divergent approach. Cyclized intermediates **8a**-**8d** were reacted with activated dienophiles to form bicyclic compounds **9** featuring a pyridazino[4,3-*c*]azepine core (Scheme 6). Activated dienophiles such as azodicarboxylic dimorpholide and 1,1′-(azodicarbonyl)dipiperidine provided the expected products in 55–77% yields as diastereomeric mixtures, predominantly favoring the

endo-product. The stereochemistry of final compounds **9a** (CCDC number: 2191711) and **9j** (CCDC number**:** 2191712) was assigned via X-ray crystallography, which provided unambiguous confirmation of the *endo* diastereomer being the major product. Further functionalization of pyridazino[4,3-*c*]azepines can be achieved by Boc-deprotection and subsequent modification of hydrazine amines (e.g., **9e** and **9f**), opening the possibility for further diversification. The *in-silico* study of pharmacokinetic parameters is an essential tool for the development of bioactive compounds and hence assessed the molecular (Table 1) and absorption-distribution-metabolism-excretion (ADME) profiles (Table 3) of synthesized compounds **5** and **9**. The analysis indicated that several of these compounds exhibited promising predicted drug-likeness attributes.

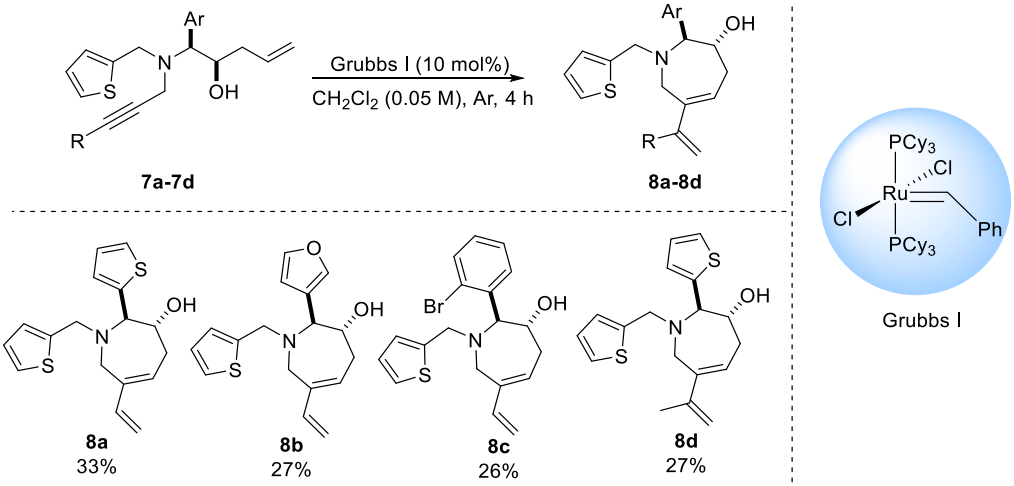

Scheme 5. Enyne metathesis reaction of Petasis Products **7a-d,** forming cyclized products **8a-d**.

Table 2. Predicted molecular properties*:

ID	5a	5b	5c	9a	9c	9g	9h	9j	9l
Molecular Weight	303.42	311.43	297.47	569.78	573.73	519.68	492.61	646.60	551.67
LogP	2.87	3.42	2.97	4.55	2.43	4.13	2.76	3.29	2.69
Rotatable bonds	5	5	5	3	3	7	1	3	11
tPSA	32.70	32.70	32.70	70.56	89.03	82.55	72.41	89.03	101.02

*The Molecular properties were predicted using pkCSM tool https://biosig.lab.uq.edu.au/pkcsm/prediction[130] and the molinspiration cheminformatics free web services were used. *Figure adapted from publication Petasi- sequence reactions for the scaffold-diverse synthesis of bioactive polycyclic small molecules.* [28]

Table 3. Predicted ADME properties*:

ID	5a	5b	5c	9a	9c	9g	9h	9j	9l
Absorption									
Water solubility log mol/L	-2.305	-2.365	-2.406	-4.984	-4.462	-5.473	-4.107	-4.666	-4.784
Caco2 permeability log Papp in 10^{-6} cm/s	1.522	1.358	1.517	0.986	0.905	0.566	0.834	1.029	0.836
Intestinal absorption (human) % Absorbed	89.378	90.642	90.532	88.04	91.233	87.246	92.584	91.768	85.498
Skin Permeability log Kp	-2.793	-2.779	-2.755	-2.857	-2.859	-2.858	-2.752	-2.824	-2.814
P-glycoprotein substrate	No	No	No	Yes	Yes	Yes	Yes	Yes	Yes
P-glycoprotein I inhibitor	No	Yes	No	Yes	Yes	Yes	Yes	Yes	Yes
P-glycoprotein II inhibitor	No	No	No	Yes	Yes	Yes	Yes	Yes	Yes
Distribution									
VDss (human)	0.876	1.101	1.076	0.862	0.358	0.322	0.571	0.483	0.227
Fraction unbound (human)	0.62	0.593	0.597	0.082	0.191	0.026	0.103	0.15	0.183
BBB permeability	0.167	0.177	0.207	-1.09	-1.22	-0.618	-0.447	-1.26	-1.244
CNS permeability	-2.86	-2.8	-2.767	-1.859	-2.491	-1.86	-2.05	-2.303	-3.223
Metabolism									
CYP2D6 substrate	No	No	No	Yes	Yes	No	No	Yes	No
CYP3A4 substrate	Yes	Yes	Yes	Yes	Yes	Yes	Yes	Yes	Yes
CYP1A2 inhibitior	No	Yes	Yes	No	No	No	Yes	No	No
CYP2C19 inhibitior	No	No	No	No	No	No	No	No	No
CYP2C9 inhibitior	No	No	No	No	No	Yes	No	No	No

CYP2D6 inhibitior	Yes	Yes	Yes	No	No	No	Yes	No	No
CYP3A4 inhibitior	No	No	No	Yes	No	Yes	Yes	No	Yes
Excretion									
Total Clearance log ml/min/kg	1.179	1.055	1.053	0.477	0.449	0.506	0.688	0.218	0.629
Renal OCT2 substrate	No	Yes	No	Yes	Yes	Yes	No	Yes	Yes

P-glycoprotein substrate- (Yes): Compound is effluxed out of cells causing reduced bioavailability: P-glycoprotein inhibitor-(Yes): Compound can inhibit drug efflux, possibly affecting other drugs' systemic absorption; CYP inhibitors-(Yes): Compound may alter metabolism of co-administered drugs; CYP substrates-(Yes): Compound is metabolized by the enzyme; Renal OCT2 substrate (Yes): Compound may be excreted through the kidney via OCT2 transporter. *The ADME properties were predicted using pkCSM tool https://biosig.lab.uq.edu.au/pkcsm/prediction[130] and the molinspiration cheminformatics free web services were used. *Figure adapted from publication Petasis- sequence reactions for the scaffold-diverse synthesis of bioactive polycyclic small molecules*.[28]

3.1.5 Antiproliferative effect evaluation

Finally, the biological significance of the synthesized polycyclic compounds was demonstrated using an MTT assay, a colorimetric method employed to assess cell viability and proliferation. In this assay, cell growth inhibition was evaluated using 3-(4,5-dimethylthiazol-2-yl)-2,5-diphenyltetrazolium bromide (MTT). The principle of the assay is based on the reduction of MTT, a yellow tetrazolium dye, into insoluble purple formazan crystals by NAD(P)H-dependent oxidoreductases in metabolically active cells. Since this reduction occurs only in living cells, the assay provides a reliable measure of cell number and growth. At a test concentration of 10 μM, pyridazino[4,3-*c*]azepine derivatives (**9**) displayed 40–90% inhibition against human acute myeloid leukemia (MOLM-13) and choriocarcinoma (JAR) cell lines. From the tested series, compounds that achieved at least 50% inhibition were selected for further evaluation of their IC_{50} values. Among these, several analogs–including **9a**, **9b**, **9e**, and **9f**–exhibited potent activity in the low micromolar range. Notably, compound **9e** demonstrated IC_{50} values of 5.3 μM against MOLM-13 and 9.0 μM against JAR cells (Figure 9).

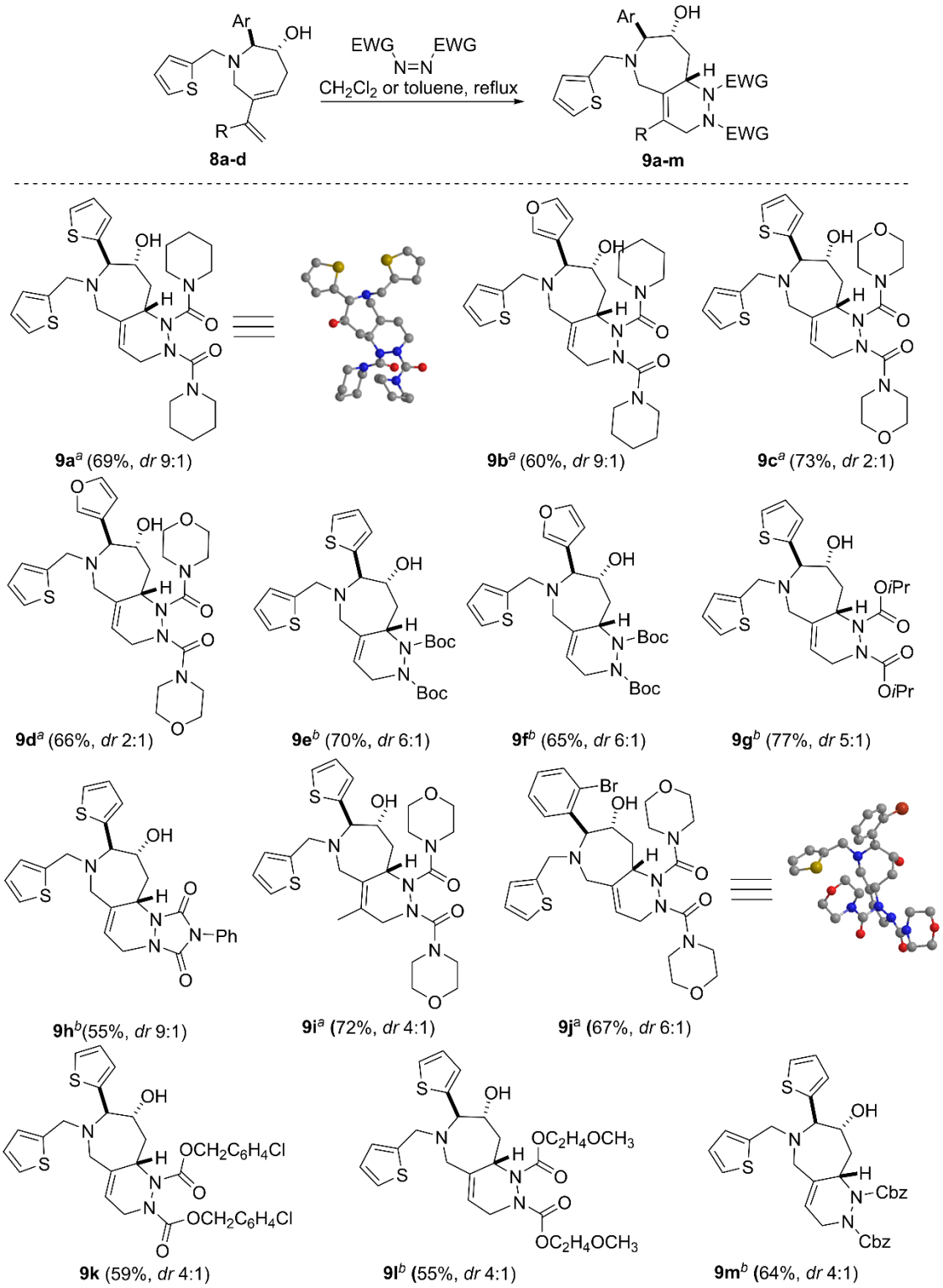

Scheme 6: Scheme for the secondary cyclization of 3C-PR/RCM products via an intermolecular Diels-Alder reaction. Reaction conditions: [a] Toluene reflux. [b] DCM reflux. *dr* determined by LC-MS.

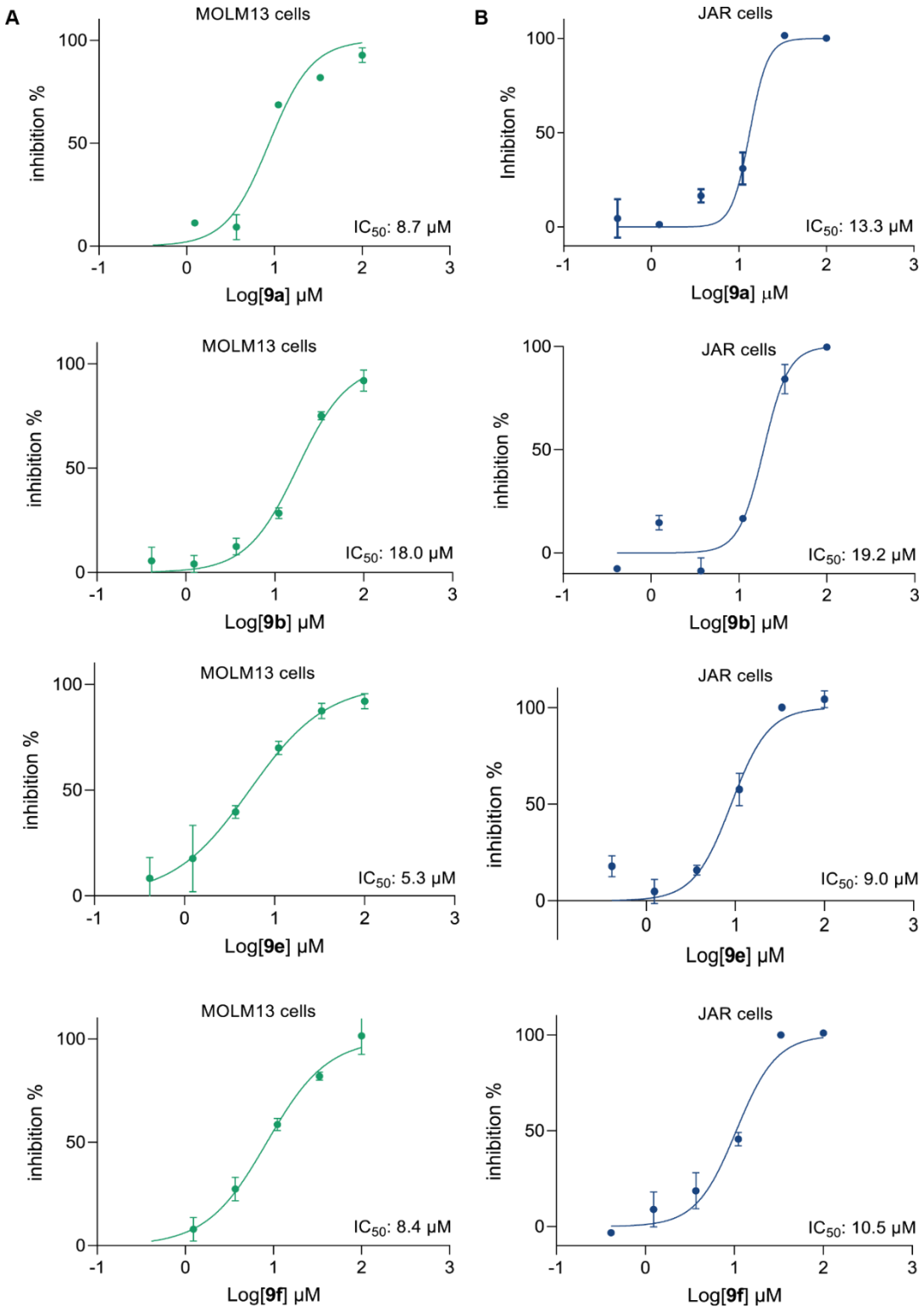

Figure 9. Antiproliferation activity of the pyridazinoazepines **9a**, **9b**, **9e**, and **9f**. Dose-dependent response and the IC_{50} against two human cancer cells lines, (A) MOLM13 and (B) JAR. Experiments were conducted in duplicate. MTT assay was performed by X. Qiu.

3.1.6 Summary

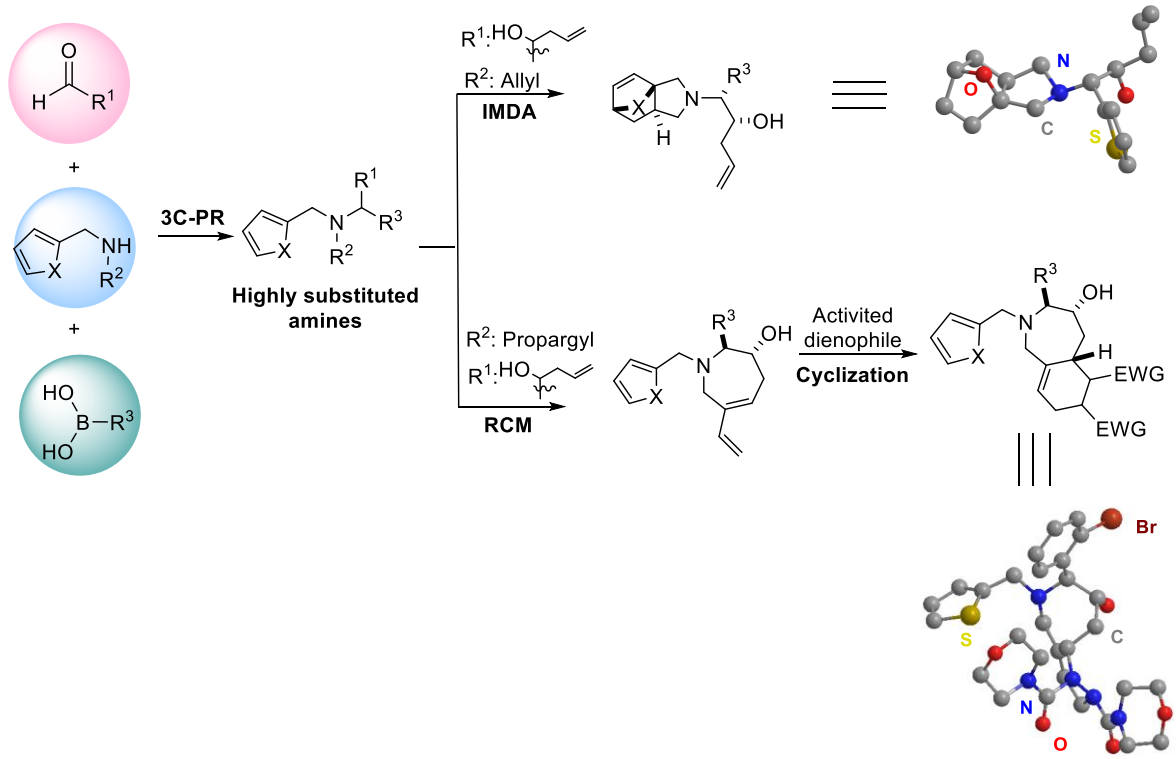

Figure 10. Summary of the 3C-PR/IMDA and 3C-PR/RCM/IMDA reaction sequences for generating complex polycyclic small molecules.

I utilized 3C-PR/IMDA and 3C-PR/RCM/IMDA reaction sequences, known for their robustness and ability to build molecular complexity, to synthesize novel small molecules bearing epoxyisoindole and pyridazinoazepine scaffolds (Figure 10). These sequential reactions were conducted under facile and mild reaction conditions using readily available substrates. The resulting Petasis products and polycyclic compounds exhibited a high fraction of sp^3-hybridized carbon atoms and suitable substitutions, which offered opportunities for further functionalization.

The biological significance of the synthesized compounds was evaluated in an antiproliferation assay against human cancer cell lines. This study highlights the broad applicability of 3C-PR-based sequence reactions in accessing previously unexplored polycyclic scaffolds with potential biological relevance.

3.2 Identification and evaluation of ribonuclease IRE1α-modulators

"Harnessing indole scaffolds to identify small-molecule IRE1α inhibitors modulating XBP1 mRNA splicing, 2025" [Manuscript in revision]. Y. Liu performed small-molecule screening, validations, and mechanism studies.

This chapter outlines the discovery of new classes of IRE1α modulators via a screening-based approach. Subsequent ligand optimization by using medicinal chemistry-driven optimization yielded potent inhibitors (nanomolar range) and activators (submicromolar range).

3.2.1 IRE1α ribonuclease inhibition

3.2.1.1 FRET-based screening for IRE1α inhibitors and hit validation

A FRET-based assay was established for IRE1α small-molecule inhibitor screening by using unphosphorylated IRE1α protein and *XBP1* hairpin substrate dually-labeled with FAM (Fluorescein amidites) and Black Hole Quencher (BHQ). Upon cleavage of the dual-labeled RNA substrate by IRE1α, the FAM will be switched on, and the resultant fluorescence is monitored by a fluorescent spectrometer (Figure 11A). To identify IRE1α inhibitors, a screening approach was performed against a chemical library of about ~10,000 compounds from the Compound Management and Screening Center (COMAS, MPI Dortmund, Germany).

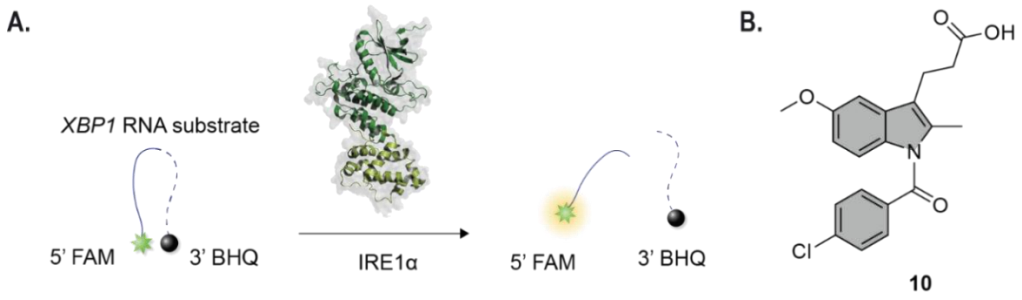

Figure 11. The screening-based approach resulted in the discovery of **10** as a potential IRE1α inhibitor. (A) Schematic diagram of FRET-based screening assay; (B) The hit compound **10** based on an indole scaffold.

The FRET-based screening assay used 40 nM unphosphorylated IRE1α (Kinase and RNase) sequence 547-977 and 100 nM FAM and BHQ-labeled *XBP1* hairpin RNA, and the compound collection was screened at a test concentration (5 μM). The assay revealed indole-based compounds as potential IRE1α inhibitors showing micromolar potency. The most promising hit compound **102793** was resynthesized as **10** (Figure 11B), and it showed inhibitory potency of 0.30 μM against unphosphorylated IRE1α and 0.32 μM against phosphorylated IRE1α (p-IRE1α) in primary FRET assay. This indicated that compound **10** (Figure 12A) displays comparable potency against both the phosphorylated and unphosphorylated forms of IRE1α

(Figure 12C). Gel-based cleavage assay using phosphorylated IRE1α showed a dose-dependent inhibition of the cleavage of RNA substrate (Figure 12B). In order to evaluate the interaction between IRE1α and compound **10**, *in vitro* biochemical assays were performed. The differential scanning fluorimetry (DSF) assay revealed that **10** dose-dependently stabilized both unphosphorylated and phosphorylated IRE1α upon binding (Figure 12D). To quantify the binding affinity between IRE1α and **10**, an isothermal titration calorimetry (ITC) assay was performed to determine the dissociation constant (K_D) of 12 μM (Figure 12E).

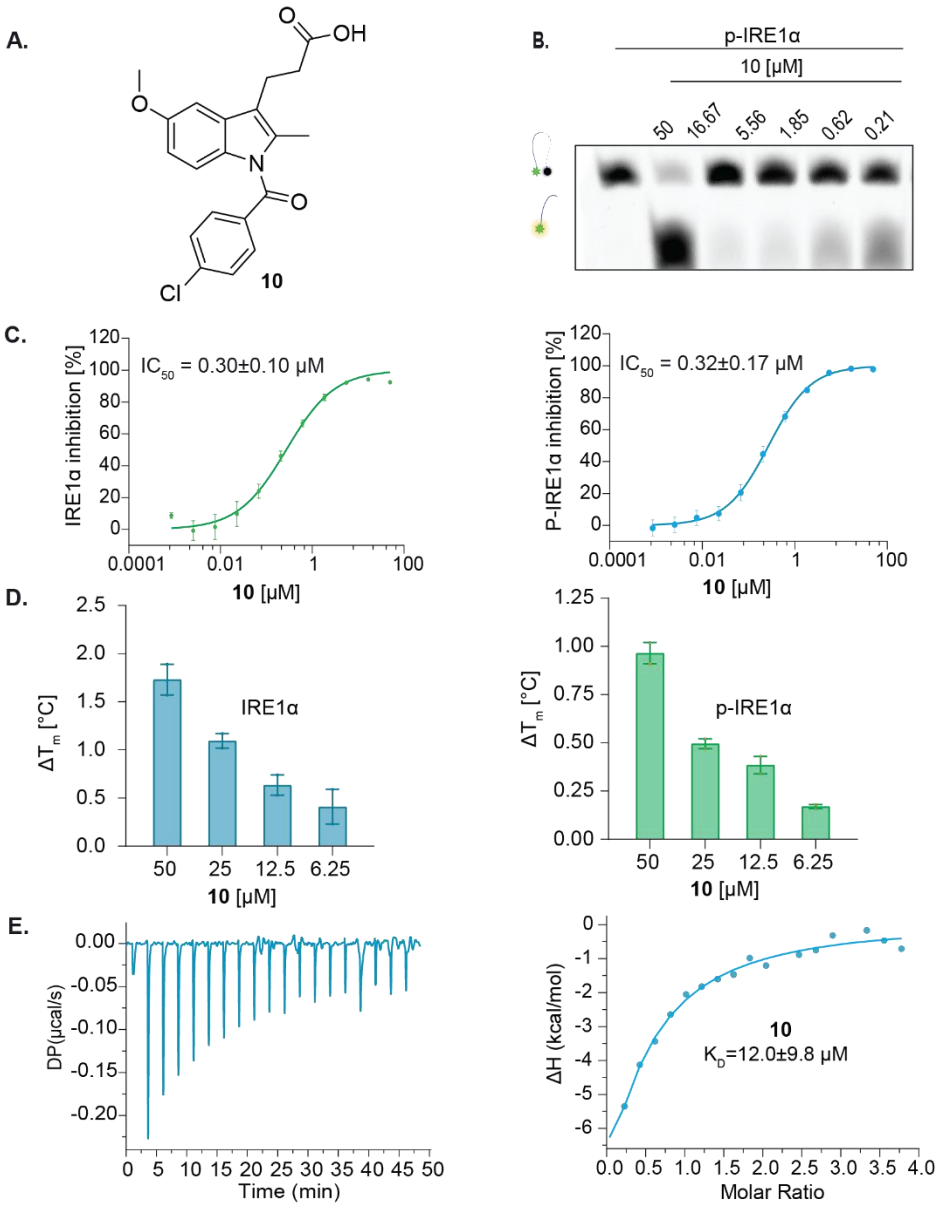

Figure 12. (A) The structure of **10**; (B) Gel-based cleavage assay showed **10** dose-dependently inhibited RNase activity of p-IRE1α; (C) FRET results showed that **10** has inhibitory activity against IRE1α (0.30 μM) and p-IRE1α (0.32 μM). Data are reported as mean±SEM, (n=4); (D) DSF assay demonstrates dose-dependent stabilization of IRE1α. Data are reported as mean±SD, n=2; (E) Compound **10** exhibited binding to IRE1α (K_D =12.0 ± 9.81 μM) in ITC.

Collectively, we identified a new IRE1α inhibitor **10**, 3-(1-(4-chlorobenzoyl)-5-methoxy-2-methyl-1*H*-indol-3-yl)propanoic acid, which formed the foundation for the following structural modifications to explore the structure-activity, based on the initial scaffold.

3.2.1.2 Structural optimization to improve inhibitory efficiency

Intrigued by the structural resemblance of compound **10**, to a well-known a non-steroidal anti-inflammatory drug (NSAID)–indomethacin (**11)** and indole-3-acetic acid (auxin)-a plant hormone **(12)**, we began by screening a selection of indomethacin and auxin analogues from our compound library for their ability to inhibit IRE1α RNase activity. These similarities did not translate into functional activity, and none of the tested compounds or their analogues demonstrated more than 50% inhibition at a concentration of 50 μM (Table 4 and Table 5). To further explore the structure-activity relationships (SAR) of **10**, we systematically modified the indole scaffold at various substituent positions (R^1, R^2, and R^3) (Table 6 ,Table 7, Table 8, Table 9) to identify pharmacophoric features critical for enhancing IRE1α inhibitory activity. The *in vitro* endoribonuclease activity was evaluated in a FRET assay to investigate the improvement in potency of the new derivatives.

Table 4. The IRE1α RNase inhibitory activities of indomethacin and its analogues at a single tested concentration (50 μM) in the FRET assay

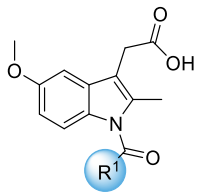

Indomethacin analogues, **11**

Entry	R^1	IRE1α Inhibition (%)	p-IRE1α Inhibition (%)	Entry	R^1	IRE1α Inhibition (%)	p-IRE1α Inhibition (%)
Indomethacin, **11**		< 30	< 30	**11e**		< 30	< 30
11a		< 30	< 30	**11f**	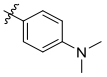	35.3±4.4	32.5±5.3
11b		< 30	< 30	**11g**	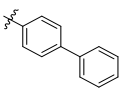	< 30	< 30
11c		< 30	< 30	**11h**		< 30	< 30
11d		< 30	< 30				

Compounds from the in-house screening collection, Data reported as mean±SEM, n=4. FRET assay performed by Y.Liu

Table 5. The IRE1α RNase inhibitory activities of auxin and its analogues at a single tested concentration (50 μM) in the FRET assay

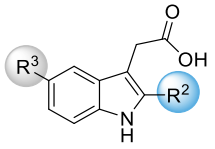

Auxin analogues, **12**

Entry	R^2	R^3	IRE1α Inhibition (%)	p-IRE1α Inhibition (%)
Auxin, **12**	-H	-H	< 30	< 30
12a		-H	< 30	< 30
12b	-CH_3		< 30	< 30

Compounds from the in-house screening collection. Data are reported as mean±SEM, n=4. FRET assay performed by Y.Liu

Table 6. Structural optimization based on the hit compound **10** with varying C3/R^1 substituents

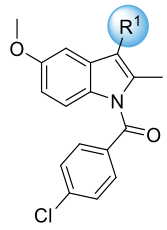

Modification around R^1

Entry	R^1	IRE1α Inhibition (%)	p-IRE1α Inhibition (%)	Entry	R^1	IRE1α Inhibition (%)	p-IRE1α Inhibition (%)
10	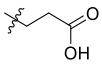	**97.1±16.9**	**99.3±4.2**	**18**	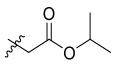	< 30	< 30
13	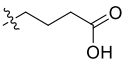	40.3±26.1	42.5±22.5	**19**		< 30	< 30
14	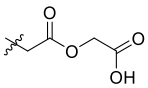	< 30	< 30	**20**		< 30	< 30
15	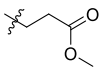	< 30	< 30	**21**		< 30	< 30
16	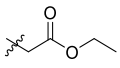	< 30	< 30	**22**	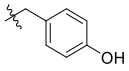	< 30	< 30
17	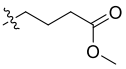	< 30	< 30	**23**	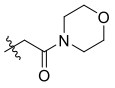	< 30	< 30

Data are reported as mean±SEM, n=4. Blue colour label for the most active compound in the collection

Table 7. Structural optimization based on the hit compound **10** with varying R^2 substituents

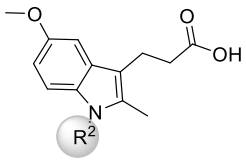

Modification around R^2

Entry	R^2	IRE1α IC_{50} (μM)	p-IRE1α IC_{50} (μM)	Entry	R^2	IRE1α IC_{50} (μM)	p-IRE1α IC_{50} (μM)
10	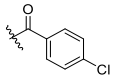	0.30±0.10	0.32±0.17	**35**	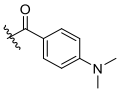	0.32±0.14	0.73±0.59
24	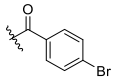	1.46±0.66	1.98±0.16	**36**	-H	>20	>20
25		0.10±0.02	0.12±0.05	**37**	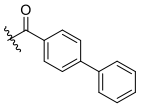	0.86±0.35	1.15±0.33
26		0.53±0.45	1.01±0.82	**38**		>20	>20
27	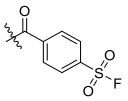	7.32±2.58	7.79±2.98	**39**		>20	>20
28	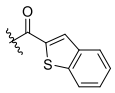	1.81±0.98	1.97±1.01	**40**		2.04±0.17	5.61±1.74
29	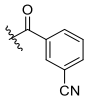	0.09±0.02	0.04±0.02	**41**		0.83±0.38	1.74±0.72
30	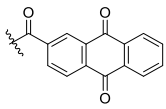	0.76±0.34	0.61±0.46	**42**		>20	>20
31	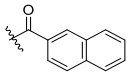	>20	>20	**43**	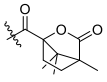	>20	>20
32	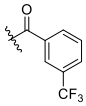	0.10±0.06	0.06±0.04	**44**		0.18±0.04	0.34±0.13
33		**0.03±0.01**	**0.03±0.02**	**45**	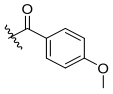	0.17±0.19	0.20±0.17
34	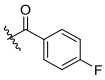	0.14±0.07	0.20±0.14				

Data are reported as mean±SEM, n=4. Blue colour label for the most active compound in the collection.

Table 8. Structural optimization based on the hit compound **10** with varying R^2 and R^3 substituents

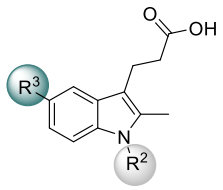

Modification around R^2 and R^3

Entry	R^2	R^3	IRE1α IC_{50} (μM)	p-IRE1α IC_{50} (μM)	Entry	R^2	R^3	IRE1α IC_{50} (μM)	p-IRE1α IC_{50} (μM)
25		OCH_3	0.10±0.02	0.12±0.05	**29**	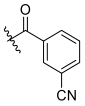	OCH_3	0.09±0.02	0.04±0.02
46		-H	2.09±1.12	2.77±2.34	**50**	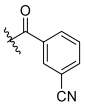	-H	2.93±1.23	2.84±2.92
47		-Br	0.08±0.02	0.10±0.09	**51**	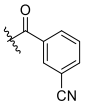	-F	2.82±1.66	5.57±2.09
48		-F	0.35±0.21	0.80±0.49	**52**	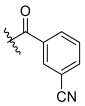	-Cl	0.09±0.01	0.23±0.16
49		-Cl	0.11±0.01	0.27±0.19					

Data are reported as mean±SEM, n=4.

The modifications at the R^1 substitution involved replacing the propionic acid moiety with different carboxylic acids with varied chain lengths, esters, aliphatic heterocycles, aromatic rings, and alkyl groups (**13**-**23**). Based on the data obtained from the FRET assay, it is revealed that compounds with R^1 groups being carboxylic acid derivatives showed the most potent activity. In contrast, all other substitutions led to a significant decline in activity (IRE1α inhibition less than 30%), indicating that the presence of a carboxylic acid at the C-3 position of the core indole scaffold is essential for the RNase activity. Consequently, propionic acid at the C-3 (R^1) position was maintained for subsequent studies, with **10** displaying an IC_{50} of 0.30±0.10 μM against IRE1α (Table 7).

We then investigated the modifications at the *N*-substituent (R^2) position of the indole core, which revealed that a diverse range of acyl groups could be tolerated well as R^2, incorporating functionalized phenyl rings, aromatic heterocycles, aliphatic rings, and fused or isolated

bicyclic/tricyclic systems without losing the inhibitory activity. Variations in the *N*-benzoyl group, including both electron-donating and electron-withdrawing substituents, resulted in only modest changes in inhibitory activity. Remarkably, the analogue bearing an unsubstituted *N*-benzoyl moiety (**33**) exhibited a substantial enhancement in potency against IRE1α (IC_{50} = 0.030 ± 0.01 μM). Building on this promising result, we expanded the structural scope to include indole derivatives incorporating benzothiophene, thiophene, and nitrogen-based heterocycles. The majority of these newly synthesized analogues maintained a similar level of inhibition to that of compound **33**. Conversely, substitution of the aromatic ring with a secondary amine (**38**) or complete elimination of the acyl group (**36**) abolished inhibitory activity entirely (IC_{50} > 20 μM). Furthermore, compounds containing thiophene-2-carbonyl (**25**) and 3-cyanobenzoyl (**29**) groups displayed strong inhibitory effects, which led us to further explore modifications at the 5-methoxy position. Several halogenated analogues at this site retained potent IRE1α inhibition, as summarized in Table 8.

Finally, guided by the potent activities of **10** and **33**, we further explored modifications at the C-5 (R^3) position while maintaining the carboxylic acid at R^1 and the benzoyl group at R^2 (Table 9). Indole derivatives featuring a *meta*-substituted phenyl group (**66** and **63**) exhibited comparable potency (IRE1α, IC_{50} 1.01±0.27 μM and 1.21±0.82 μM, respectively). However, *ortho*- and *para*-substituted aromatic rings led to a potency reduction. Substituting the methoxy group in **33** with a trifluoromethoxy group (**65**, IC_{50} 0.57±0.36 μM) resulted in an approximately 19-fold decrease in activity. Retaining an unsubstituted indole C-5 led to a 10-fold potency decrease compared to **33**. Interestingly, introducing halogen substituents at R^3 significantly enhanced inhibitory activity. Notably, **54**, featuring a bromine atom at C-5, exhibited a 20-fold potency increase (IRE1α IC_{50} 16±1 nM), establishing it as the most active compound among those synthesized.

Table 9. Structural optimization based on the hit compound **10** with a varying R^3 substituent

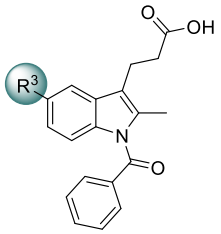

Modification around R^3

Cpd	R^3	IRE1α Inhibition IC_{50} (μM)	p-IRE1α Inhibition IC_{50} (μM)	Cpd	R^3	IRE1α Inhibition IC_{50} (μM)	p-IRE1α Inhibition IC_{50} (μM)
53	-H	0.34±0.29	0.54±0.13	**63**		1.21±0.82	6.65±1.83
54	-Br	**0.016±0.001**	**0.009±0.002**	**64**	$-CH_3$	0.066±0.023	0.133±0.12
55		0.24±0.05	0.20±0.01	**65**	$-OCF_3$	0.57±0.36	0.94±0.12
56	-F	0.42±0.25	0.72±0.44	**66**		1.01±0.27	8.81±2.49
57		1.27±1.05	2.03±1.87	**67**	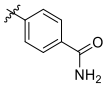	12.08±11.12	>20
58		2.97±0.77	7.56±4.85	**68**		2.16±0.64	11.59±4.27
59	-Cl	0.052±0.015	0.082±0.018	**69**		0.70±0.01	2.34±1.19
60		1.61±0.94	4.68±0.94	**70**		6.22±1.00	>20
61	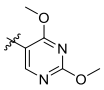	14.1±5.4	>20	**71**		4.73±2.05	15.12±0.98
62	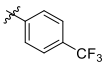	13.40±1.34	>20	**72**	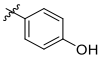	7.41±1.46	>20

Data are reported as mean±SEM (n=4). Blue colour label for the most active compound in the collection.

3.2.1.3 Chemical synthesis of the indole-based IRE1α inhibitors

Extensive structural modifications around the best hit compound **10** have been performed while retaining the indole core. The modifications resulted in a 20-fold improvement in the inhibitory potential compared to the initial hit compound. The synthesis of various indole derivatives was performed by using two synthetic approaches: (i) a solid-phase Fischer-indole synthesis utilizing a resin-capture-release strategy (scheme 7)[131] and typical liquid phase Fischer-indole synthesis (scheme 8), followed by Suzuki coupling for further functionalization.

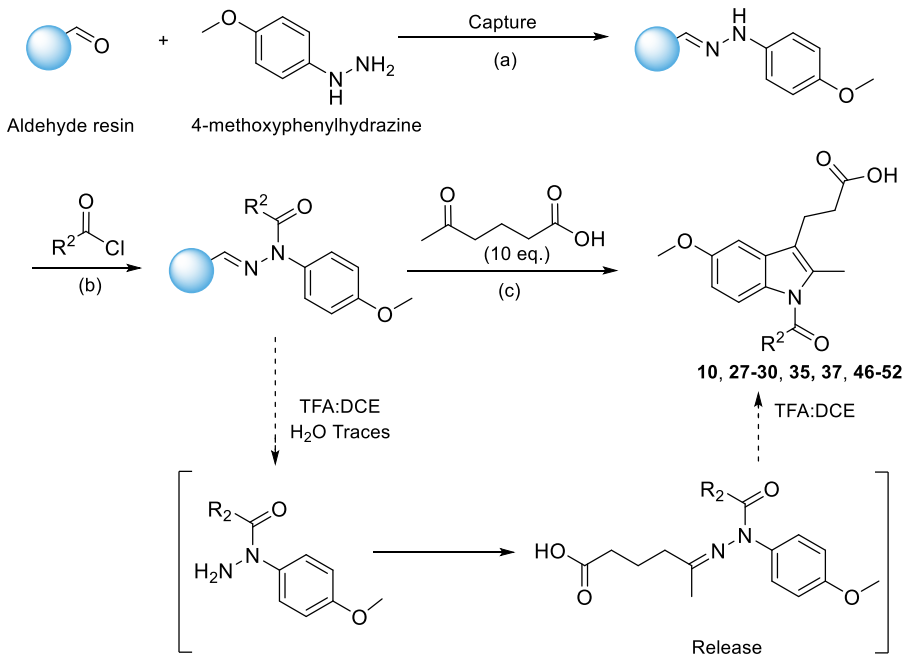

Cpd	Yield (%)	Cpd	Yield (%)
10	67	**46**	42
27	18	**47**	34
28	8	**48**	13
29	12	**49**	22
30	8	**50**	16
35	14	**51**	14
37	14	**52**	18

Scheme 7. Fischer indole-based a solid-phase synthesis with resin-capture-release strategy[131]; Reagents and conditions: (a) TEA (6 equiv.), DCM 5 mL, reflux 16 h; (b) Pyridine 5 mL, 80 °C, Ar, 16 h; (c) TFA: DCE (1:1), 70 °C, 15 min-2 h.

In the Fischer indole-based solid-phase synthesis, the aldehyde resin was condensed with 4-methoxyphenylhydrazine to form hydrazine bound to the polymer, which facilitates the regioselective *N*-acylation. The acylated hydrazine is then treated with trifluoracetic acid and the corresponding ketone (4-acetylbutyric acid), in the presence of a trace amount of water, to get the corresponding indole derivative. During this process, water hydrolyzes the hydrazones,

selectively releasing acylated hydrazines into the solution. These subsequently condense with ketones to generate hydrazone intermediates, which undergo a [3,3]-sigmatropic rearrangement under the reaction conditions (Scheme 7). This strategy yields a diverse set of indole derivatives efficiently within a very short span of time. Alternatively, liquid phase Fischer indole synthesis followed by Suzuki coupling reaction was also used to generate more complex indole derivatives needed for the study (Scheme 8). Indole derivatives formed by both the synthetic routes were all isolated in >99% purity.

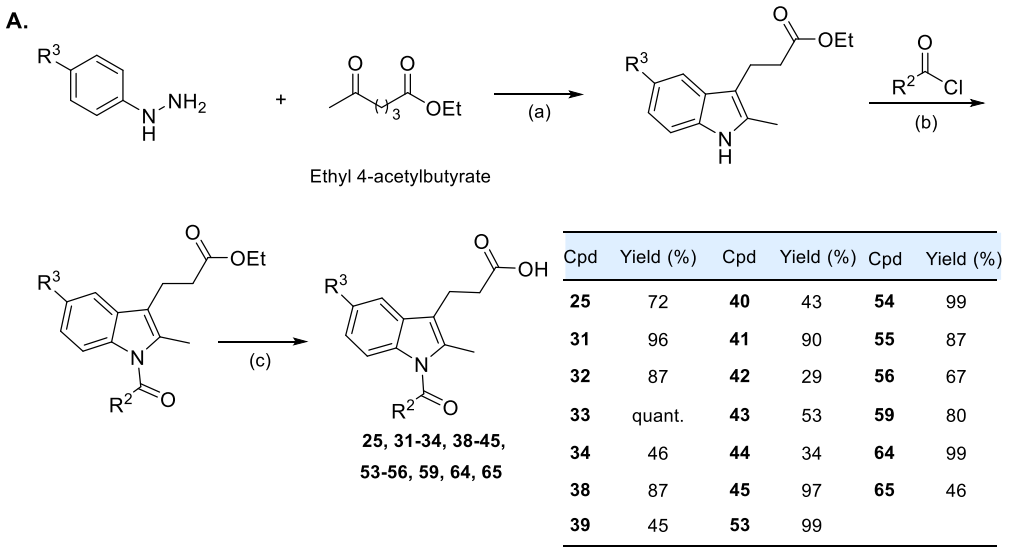

Cpd	Yield (%)	Cpd	Yield (%)	Cpd	Yield (%)
25	72	**40**	43	**54**	99
31	96	**41**	90	**55**	87
32	87	**42**	29	**56**	67
33	quant.	**43**	53	**59**	80
34	46	**44**	34	**64**	99
38	87	**45**	97	**65**	46
39	45	**53**	99		

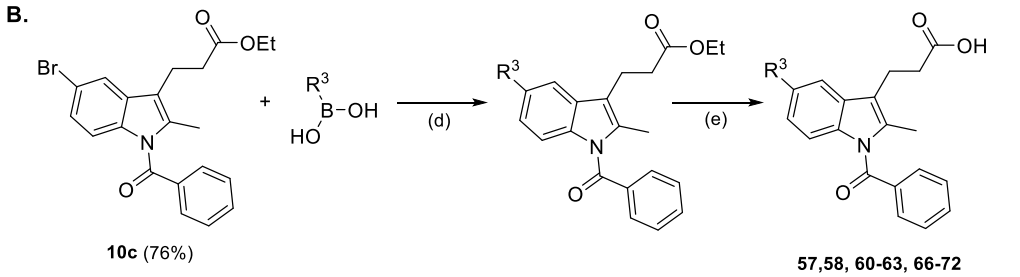

Cpd	Yield (%)	Cpd	Yield (%)
57	54	**67**	79
58	73	**68**	27
60	71	**69**	14
61	62	**70**	32
62	36	**71**	43
63	48	**72**	80
66	26		

Scheme 8. Liquid phase Fischer indole synthesis and subsequent functionalization; Reagents and conditions: (a) i. Glacial acetic acid, sodium acetate, reflux, 3 h; ii. Ethanol, 4M HCl in 1,4-dioxane, reflux, 15 h/ H_2SO_4, Ethanol, reflux, 16-24 h (b) NaH, DMF, Ar, 0 °C – rt, 12 h, (c) Trimethyltin hydroxide, DCE, 80 °C; (d) $Pd(dppf)Cl_2$ (5.0 mol%), K_3PO_4, 1,4-dioxane and water (4:1), Ar, 80°C, 14 h (e) Trimethyltin hydroxide, DCE, 80 °C.

3.2.1.4 Biochemical and biophysical validations

Compound **54**, which exhibited the highest inhibitory potency against IRE1α RNase (IC_{50} IRE1α 16±1 nM; Figure 13 A), was subsequently selected for further validation through biochemical and biophysical assays. Gel-based RNA cleavage assay showed that **54** inhibited p-IRE1α RNase activity in a dose-dependent manner (Figure 13 B). The interactions of IRE1α with the inhibitor **54** were confirmed by DSF assay, demonstrating stabilization of IRE1α in a dose-dependent manner, with changes in melting temperature (ΔTm) correlating with its inhibitory activity (Figure 13 C). Inactive indole derivative **31** (IRE1α and p-IRE1α IC_{50} > 20 μM) with an *N*-naphthoyl substitution used as a negative control did not induce detectable change in ΔT_m in the DSF assay (Figure 13 D).

Furthermore, microscale thermophoresis (MST) analysis confirmed the binding affinity of compound **54**, resulting in a dissociation constant (K_D) of 1.36 μM (Figure 13 E). Isothermal titration calorimetry revealed that **54** bound to IRE1α with a dissociation constant (K_D) of 0.94 μM (Figure 13 F).

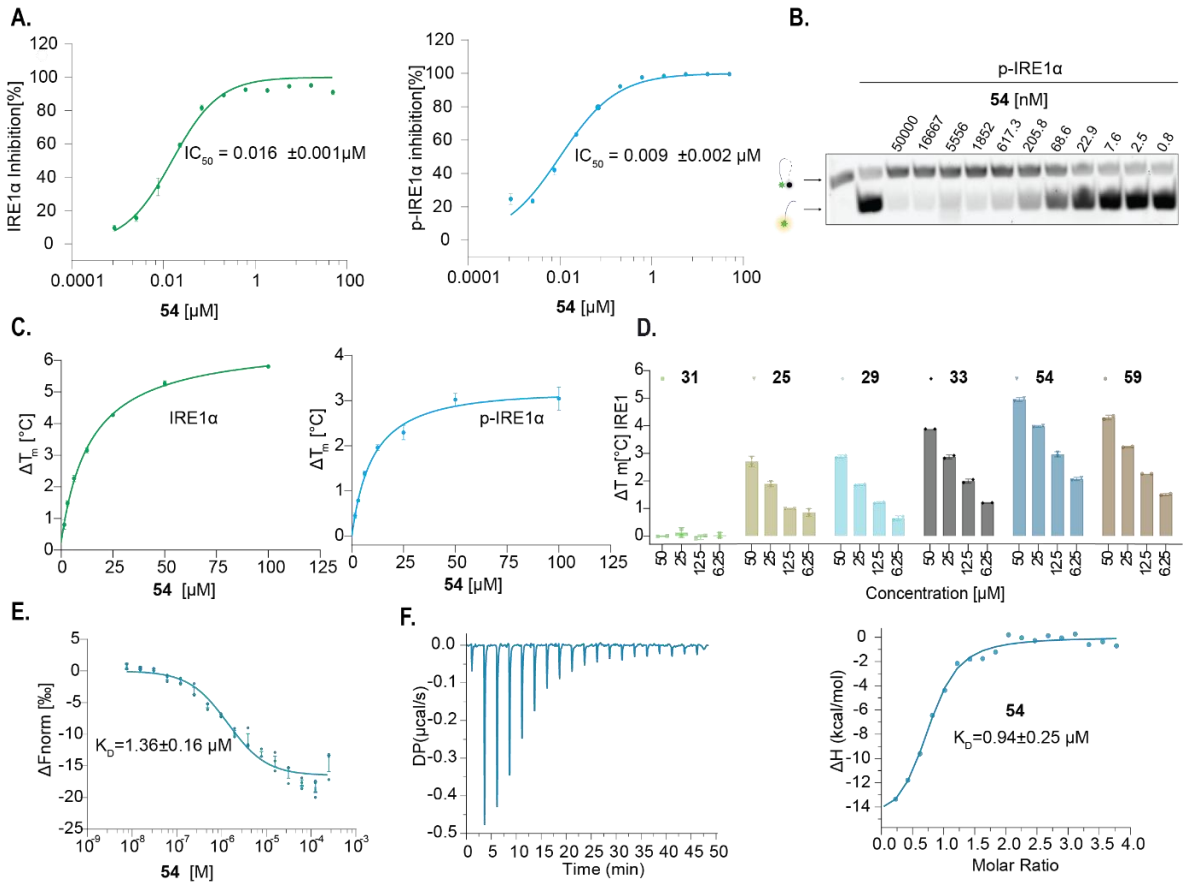

Figure 13. (A) FRET results showing **54** inhibited both IRE1α and p-IRE1α RNase activity. Data are reported as mean±SEM, (n=4); (B) Gel-based cleavage assay showing compound **54** dose-dependently inhibiting the p-IRE1α RNase activity; (C)

Stabilization of IRE1α and p-IRE1α by **54** was observed in a dose-dependent manner in the DSF.assay. Data are reported as mean±SEM, (n=4); (D) Thermal shift (ΔT_m) values of IRE1α protein measured in the DSF assay following treatment with inhibitors and negative control **31**; Data are reported as mean±SD, (n=2); (E) MST (Data are reported as mean±SEM, (n=3) and (F) ITC confirmed the interaction of **54** with IRE1α, indicating specific binding affinity.

3.2.1.5 Cellular inhibition of IRE1α RNase function

The cellular inhibition of IRE1α RNase function was measured for the most potent derivative **54** (Figure 14A). Under conditions of ER stress, IRE1α activation leads to splicing of *XBP1* mRNA.[132] To evaluate the cellular impact of compound **54**, experiments were conducted in HAP1 and A549 cell lines. As illustrated in Figure 14 B and Figure 14 C, tunicamycin treatment induced *XBP1* mRNA splicing, while pre-treatment with **54** resulted in a dose-dependent reduction of this splicing event. These results indicate that compound **54** effectively suppresses ER stress-induced *XBP1* mRNA splicing in cells.

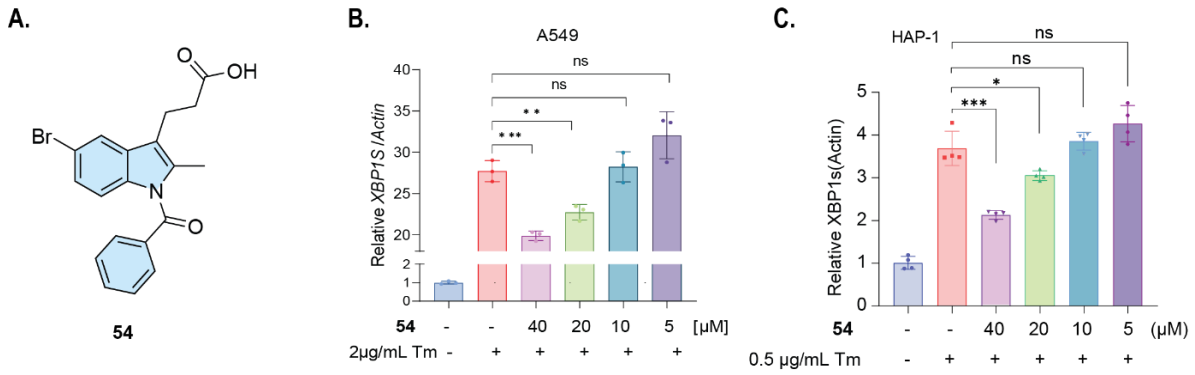

Figure 14. Dose-dependent inhibition of ER stress-mediated *XBP1* splicing by **54**; (A) Structure of the most potent indole derivative **54**; RT-qPCR to detect spliced *XBP1* transcript due to ER stress induced by tunicamycin (Tm) in (B) A549 and (C) HAP-1 cells. (The statistical significance: ns when p>0.05 * when p≤ 0.05, ** when p≤0.01, *** when p≤0.001 was calculated using one-tailed independent student's t-test).

3.2.1.6 Preliminary studies on the inhibitory mechanism of compound 54

The mode of inhibition of IRE1α by **54** was studied via Michaelis–Menten kinetic analysis. It was investigated whether there is competition between potent indole-based inhibitor and *XBP1* mRNA substrate to bind to IRE1α. The results showed minimal changes in the K_m values across different tested concentrations, such as 0.01 μM, 0.1 μM, and 1 μM of compound **54**. However, the measured values of V_{max} showed a dose-dependent decrease as summarized in the Figure 15. The relatively unchanged K_m values, along with the dose-dependent reduction in V_{max}, indicate that compound **54** likely functions as a non-competitive inhibitor of the *XBP1* mRNA.

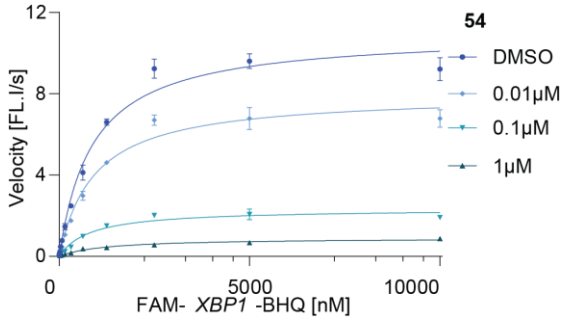

54	Km [nM]	Vmax [FL.I/s]
DMSO	876.5	10.98
0.01 μM	915.5	7.98
0.1 μM	819.2	2.33
1 μM	1210	0.90

Figure 15. Kinetic studies. Non-competitive inhibition of IRE1α by **54** revealed by Michaelis–Menten kinetic analysis.

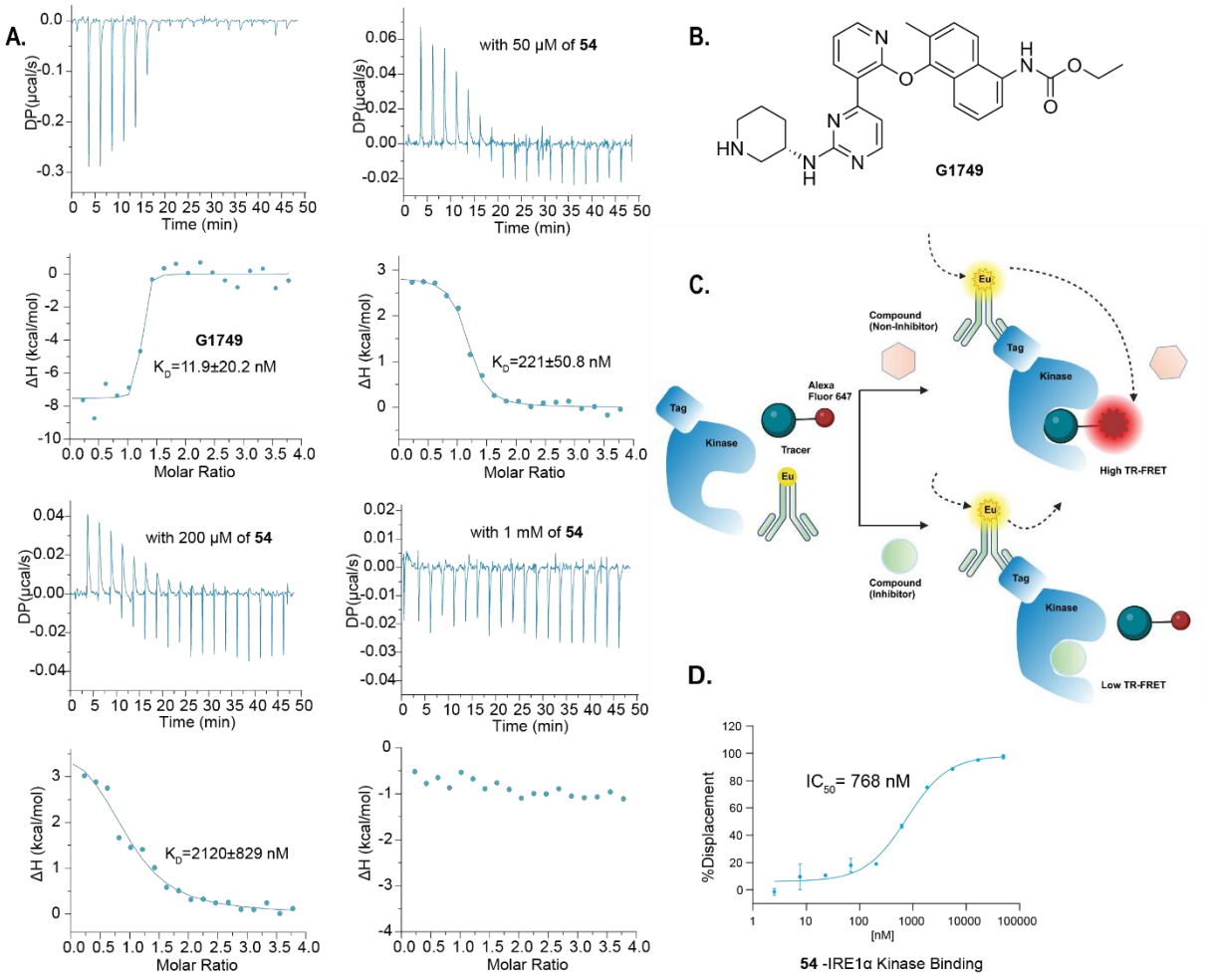

Figure 16. The inhibitory mechanism studies of 54. (A) ITC-based competition assays, 200 μM of reference compound **G1749** was titrated into 10 μM IRE1α pre-incubated with DMSO control or with compound **54** at increasing concentrations; (B) Structure of **G1749** (C) Schematic diagram of LanthaScreen® Eu kinase binding assay; (D) Compound **54** demonstrated binding to the kinase domain of IRE1α (IC_{50} 768 nM). Data are reported as mean±SD (n=2).

To explore the mechanism by which compound **54** modulates IRE1α activity, it was investigated whether it targets the ATP-binding site within the kinase domain–a region known to influence RNase function when occupied by small molecules. For comparison, we utilized

G1749, a previously characterized RNase activator that engages this same ATP-binding site (Figure 16B). **G1749** was synthesized following reported protocols.[133] Using isothermal titration calorimetry, it was observed that increasing concentrations of compound **54** progressively weakened the binding affinity of **G1749** (Figure 16A). This reduction suggested that compound **54** competes for the ATP-binding pocket in the IRE1α kinase domain. To confirm this hypothesis, we employed a LanthaScreen™ Eu kinase binding assay (Figure 16C), which verified the interaction between compound **54** and the ATP-binding site. The assay yielded an IC_{50} value of 768 nM, supporting the conclusion that compound **54** engages the ATP-binding region of the kinase domain (Figure 16D).

3.2.1.7 Evaluation of IRE1α kinase selectivity of compound 54

Once the studies on the RNase inhibitory mechanism of the most potent compound **54** confirmed that it binds to the ATP binding site of the kinase domain of IRE1α, the compound was profiled for its broad kinase selectivity (Figure 17).

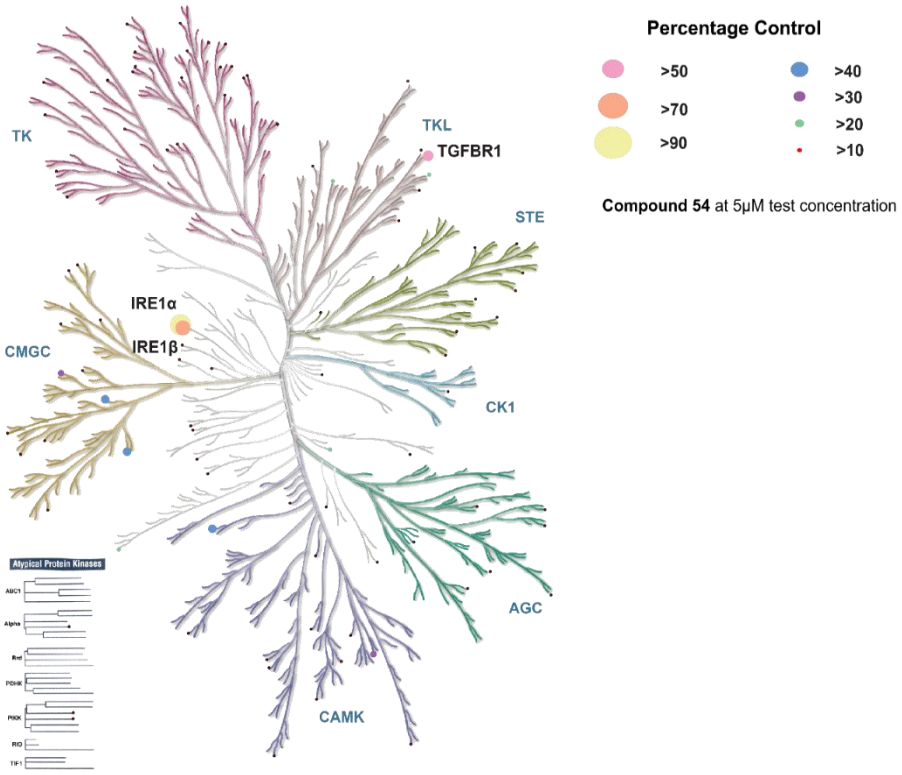

Figure 17. Kinase dendrogram of compound **54** at 5 µM test concentration. Kinases where probe binding was inhibited by >50% at 5 µM test compound concentration are marked in the kinase profiling tree from the LanthaScreen™ Eu kinase binding assay (Thermo Fisher SelectScreen).

When tested at a concentration of 5 µM in the LanthaScreen™ Eu kinase binding assay (Thermo Fisher SelectScreen), compound **54** showed very low inhibitory effects on the

majority of kinases in the screening panel, with most showing inhibition of less than 10%–30 %. As expected, a notable exception was observed in the IRE1 isoforms: compound **54** significantly suppressed kinase activity of ERN1 (IRE1α) by 91% and ERN2 (IRE1β) by 70%, indicating a roughly two-fold preference for IRE1α over IRE1β, despite the high sequence similarity (80%) shared between their kinase domain.[134] Besides IRE1α and IRE1β, **54** exhibited >50% inhibition of TGFBR1 with an inhibition rate of 54%.

3.2.1.8 Assessment of the effect of compound 54 on p-IRE1α dimerization and oligomerization

As a continued effort to understand the inhibition of IRE1α by compound **54**, a DSS (disuccinimidyl suberate) mass photometry-based cross-linking assay was performed to assess its effect on the self-association of phosphorylated IRE1α. Previously reported allosteric inhibitor of p-IRE1α, **KIRA8** (AMG-18)[133] which inhibited RNase activity by stabilizing the monomeric form of IRE1α and thereby inhibiting the dimer formation, was used as a reference compound in this assay along with test compound **54**. The comparison of the results revealed that compound **54** did not inhibit the self-association of phosphorylated IRE1α compared to **KIRA8,** suggesting that the kinase domain interactions remain stable upon binding to **54** (Figure 18).

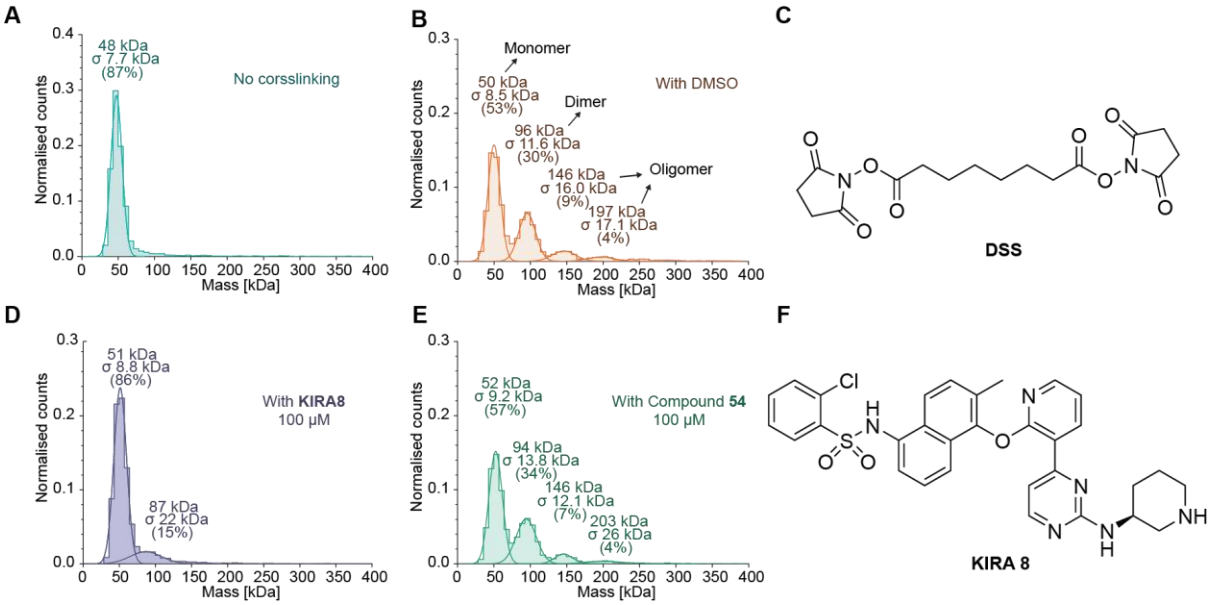

Figure 18. DSS cross-linking assay showing that compound **54** did not inhibit the self-association of p-IRE1α. (A) p-IRE1α without DSS; (B) p-IRE1α with DSS and DMSO (control); (C) Structure of DSS; (D) p-IRE1α with **KIRA8** and DSS; (E) p-IRE1α with **54** and DSS, and (F) Structure of **KIRA8**.

3.2.1.9 Summary

In summary, this chapter presented a study that identified substituted indoles as a novel class of potent as well as selective IRE1α inhibitors via a FRET-based screening assay and reported a collection of indole-based inhibitors represented by compound **10**. The hit compound showed an IC_{50} of 0.30 μM against unphosphorylated IRE1α and 0.32 μM against phosphorylated IRE1α, and effectively stabilized IRE1α dose-dependently in a DSF assay. Compound **54**, an indole analogue obtained after rigorous structural modifications based on **10**, exhibited a 20-fold potency increase with an IC_{50} value of 16 nM (IRE1α). Multiple biophysical techniques confirmed that compound **54** directly interacted with IRE1α, with binding affinities determined by MST (K_D = 1.36 μM) and ITC (K_D = 0.94 μM). Mechanistic investigations further revealed that **54** acts as a non-competitive inhibitor by targeting the ATP-binding site within the kinase domain. Consistent with this, the LanthaScreen™ Eu kinase binding assay demonstrated compound **54**'s engagement with the ATP-binding pocket of IRE1α, showing an IC_{50} of 768 nM. Subsequent cellular assays demonstrated that **54** suppressed ER stress-induced *XBP1* mRNA splicing in a dose-dependent manner. Collectively, these findings indicated that compound **54** bound to the kinase domain and allosterically inhibited RNase activity, thereby enriching the IRE1α targeting chemotypes. Compound **54** could potentially be used as a chemical tool to probe IRE1α functions and as a base for developing IRE1α-targeting small-molecule therapeutic candidates.

3.2.2 IRE1α ribonuclease activation

3.2.2.1 FRET-based screening for IRE1α activators and hit validation

Y. Liu. performed small-molecule screening. Compound validations were performed by Y.Liu and O. Hastürk. Antiproliferative assay was performed by O. Hastürk. RT-qPCR was performed by O. Hastürk and L.Wagner.

Following the successful efforts in discovering new chemotypes for IRE1α inhibition, we simultaneously pursued the identification of novel chemotypes for IRE1α RNase activation. The FRET assay was used to screen our in-house compound collection of approximately 10,000 compounds from COMAS, MPI Dortmund, Germany, by using unphosphorylated IRE1α (residues 547-977) and *XBP1* hairpin substrate mimic labelled with FAM and BHQ. Upon cleavage of the dually-labelled RNA substrate (5′FAM-CAUGUCCGCAGCGCAUG-3′BHQ1) by IRE1α, the FAM will be switched on and monitored by fluorescent spectrometer. The aminopyrimidine-based hit compound **286214**, recognized for its versatile and valuable scaffold in medicinal chemistry, was identified from the screening collection and selected for further validations. (Figure 19). The compound showed a single-digit micro-molar range of activation potency against unphosphorylated IRE1α.

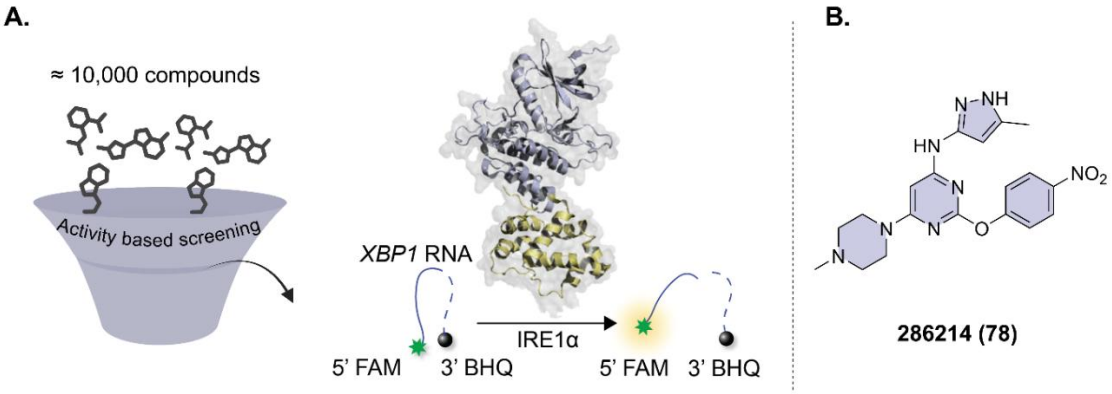

Figure 19. Discovery of potential IRE1α activators. (A) Schematic diagram of FRET-based screening assay; (B) most potent hit compound **286214,** with an aminopyrimidine scaffold resynthesised in-house as **78**.

IRE1α activator hit candidate **286214**[135] obtained in the FRET-based screening assay was synthesized in-house as compound **78** for further validations (Scheme 9). The hit compound shares scaffold with the previously reported IRE1α RNase activator compound, **APY 29**.[136] It has been utilized in structural studies on IRE1α activity and preclinical studies, but found to be toxic at low micromolar concentrations, which limits its application. However, the

established interaction of aminopyrimidine with IRE1α provided a rational starting point for further validations and structural optimisations. By optimising the hit compound, we aimed to enhance potency as well as expanding the chemical space for IRE1α-targeting therapeutics.

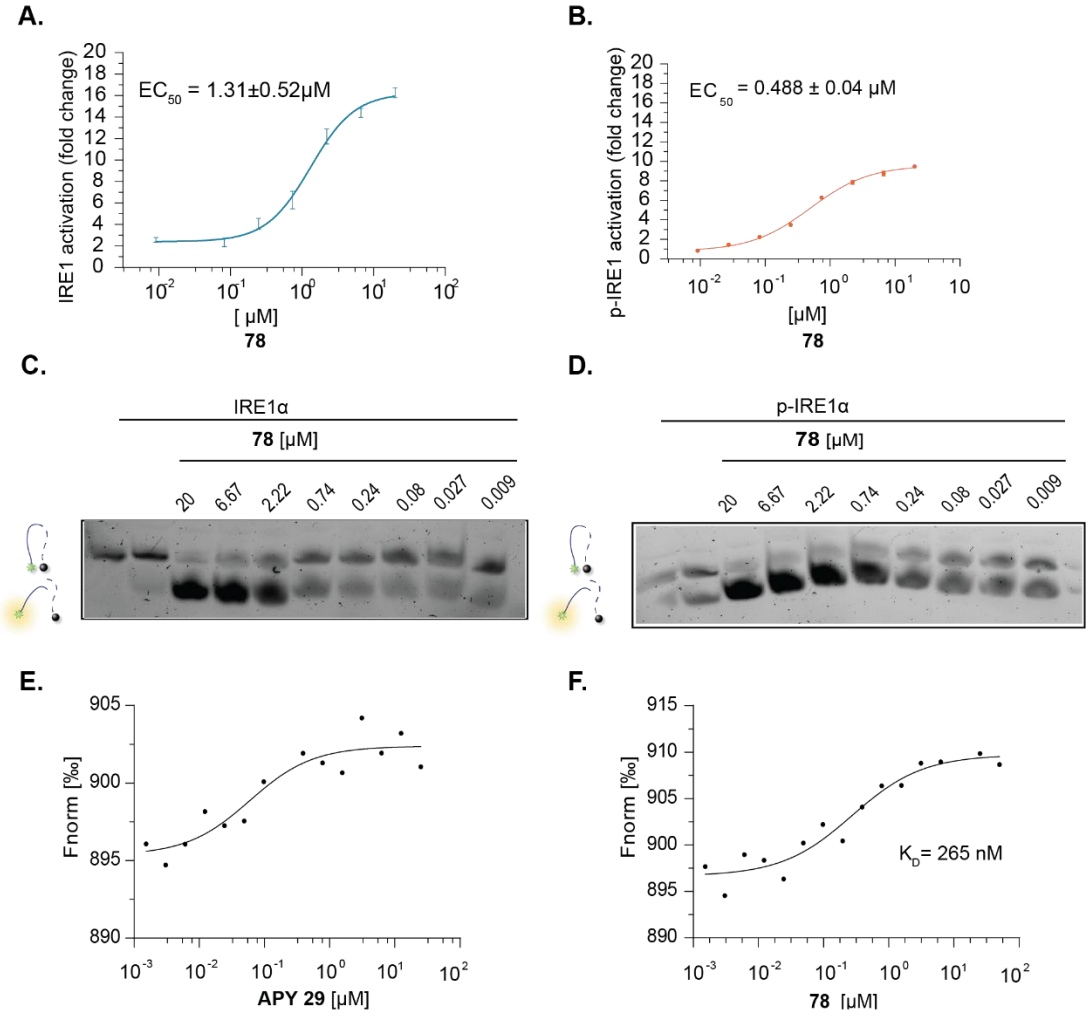

Figure 20. Validation of aminopyrimidine based hit compound from screening campaign. (A**)** FRET results showed that **78** activates IRE1α and (B) p-IRE1α; (C) Compound **78** showed dose dependant activation of IRE1α and (D) p-IRE1α in gel-based cleavage assay; (E) MST measurement showed K_D= 52 nM for reference compound (**APY 29**, N=1) and (F) K_D= 256 nM for compound **78** in MST assay.

Compound **78** was tested against IRE1α and its phosphorylated form. The resynthesized hit has an EC_{50} value of 1.31 ± 0.52 μM (IRE1α) and 0.488 ± 0.04 μM (p-IRE1α) (Figure 20A and Figure **20**B). **78** showed better activation towards phosphorylated IRE1α (p-IRE1α). The reason for the better EC_{50} value of the p-IRE1 is attributed to the oligomerisation of phosphorylated IRE1α leading to conformational changes of the RNase domain. The activation could be observed with a gel-based experiment where a dose-dependent enhanced cleavage effect could be seen (Figure **20**C and Figure **20**D) for the compound treatment compared to the control. Additionally, the binding affinity of **78** was determined by MST assay. The K_D value

of the hit compound was found to be 256 nM (Figure 20F). The reported IRE1 activator **APY 29**[136] was used as the positive control (K_D= 52 nM) (Figure 20E).

3.2.2.2 Synthetic procedure for the preparation of hit compound 78

The best hit compound from the screening campaign was synthesized using the reported procedure (Scheme 9).[135] 4,6-Dichloro-2-(methylthio)pyrimidine was oxidized using *meta*-chloroperoxybenzoic acid to generate the corresponding sulfone, **75**. The methylsulfonyl leaving group activated by the pyrimidine undergoes nucleophilic aromatic substitution reaction with phenoxide nucleophile generated from *p*-nitrophenol, giving rise to the subsequent intermediate **76.**

The chlorine at the 4-position of the pyrimidine core was substituted by 5-methyl-1*H*-pyrazol-3-amine using DIPEA and DMF as solvent, yielding intermediate **77**. Subsequently, the methylpiperazine group was introduced at position-6 of the pyrimidine core by refluxing the corresponding precursor, **77,** in 1-methylpiperazine, affording compound **78** in 79% yield.

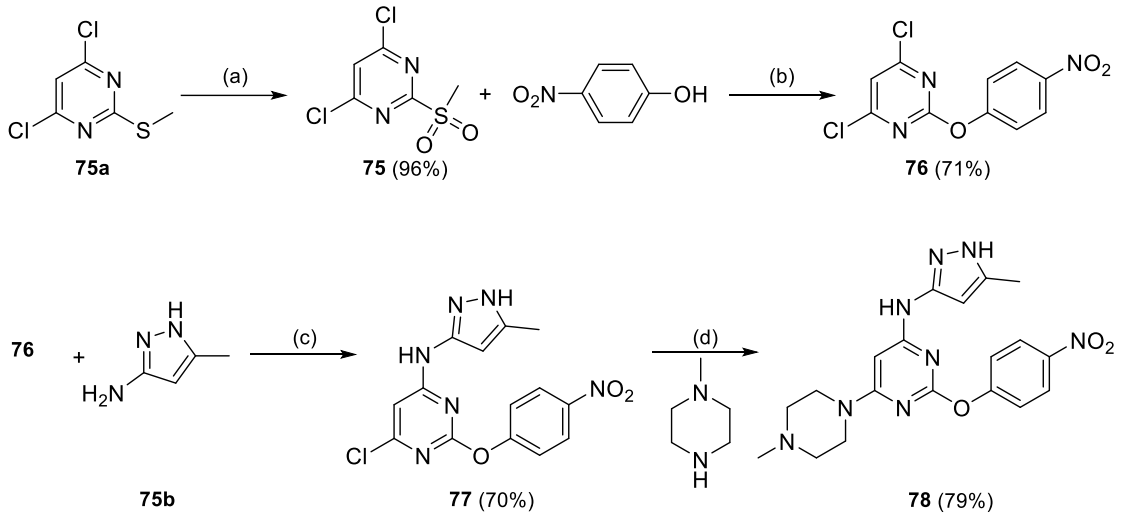

Scheme 9. Synthetic route for compound **78**. Reagents and conditions: (a) mCPBA, DCM, 0 °C-rt, 72h; (b) NaH, DMF, Ar, 0 °C-rt, 4h; DIPEA, DMF, 80 °C, 12 h; 110 °C, 30 min.

3.2.2.3 Structural activity studies to improve activation efficiency

To optimize ligand potency, a preliminary SAR study was conducted. For this study, the *N*-(5-methyl-1*H*-pyrazol-3-yl)pyrimidin-4-amine core of the hit compound **78** was retained due to its reported network of interactions with the ATP-binding pocket of the IRE1α kinase domain. The C6/R^2 position of the pyrimidine and the phenoxide moiety were altered for improved potency (Table 10).

Table 10. Series I of synthesized IRE1α activators and their potency in the FRET assay

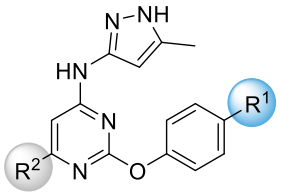

Entry	R^1	R^2	EC_{50} (IRE1α, μM)	EC_{50} (p-IRE1α, μM)
78	-NO_2	1-methylpiperazinyl	1.31	0.49
81	-$CONH_2$	-Cl	8.35	2.27
82	-SO_2CH_3	-Cl	0.65	1.10
83	-SO_2NH_2	-Cl	1.04	0.45
84	-CHO	-Cl	0.87	2.52
85	-NH_2	-Cl	10.02	5.39
86	amino-2-phenylacetic acid	-Cl	2.71	4.96
87	2-amino-2-(thiophen-2-yl)acetic acid	-Cl	2.23	4.28
88	2-amino-2-(2,4-dimethoxypyrimidin-5-yl)acetic acid	-Cl	17.66	5.49
89	2-amino-2-(3,5-dimethylisoxazol-4-yl)acetic acid	-Cl	ND	4.23
91	-SO_2NH_2	2-phenyl-2-(piperazin-1-yl)acetic acid	**0.48**	**0.18**

Blue colour label for the most active compound in the collection

Initially, the study explored the effect of different *para*-substitutions on the phenyl ring by keeping the R^2 position as chloride. Different *para*-substituted phenol derivatives were used or nucleophilic aromatic substitution reaction with intermediate **80** (Scheme 10). Derivatives with groups like sulphonamide (1.04 μM EC_{50} IRE1α, 0.45 μM EC_{50} p-IRE1α) and sulphone, **82** (0.65 μM EC_{50} IRE1α, 1.10 μM EC_{50} pIRE1α) which can potentially act as hydrogen bond donor/acceptor and hydrogen bond acceptor, respectively, at the ATP binding site, showed the best activation potential. In case of an aldehyde substitution (**84**), the compound retained the activity, but the higher EC_{50} 2.52 μM (p-IRE1α), suggests poor activation. The removal of

methyl piperazine as R^2 did not affect the activity significantly. The -NH_2 group (**85**) significantly weakens activity on both IRE1α and p-IRE1α, making it a less suitable candidate.

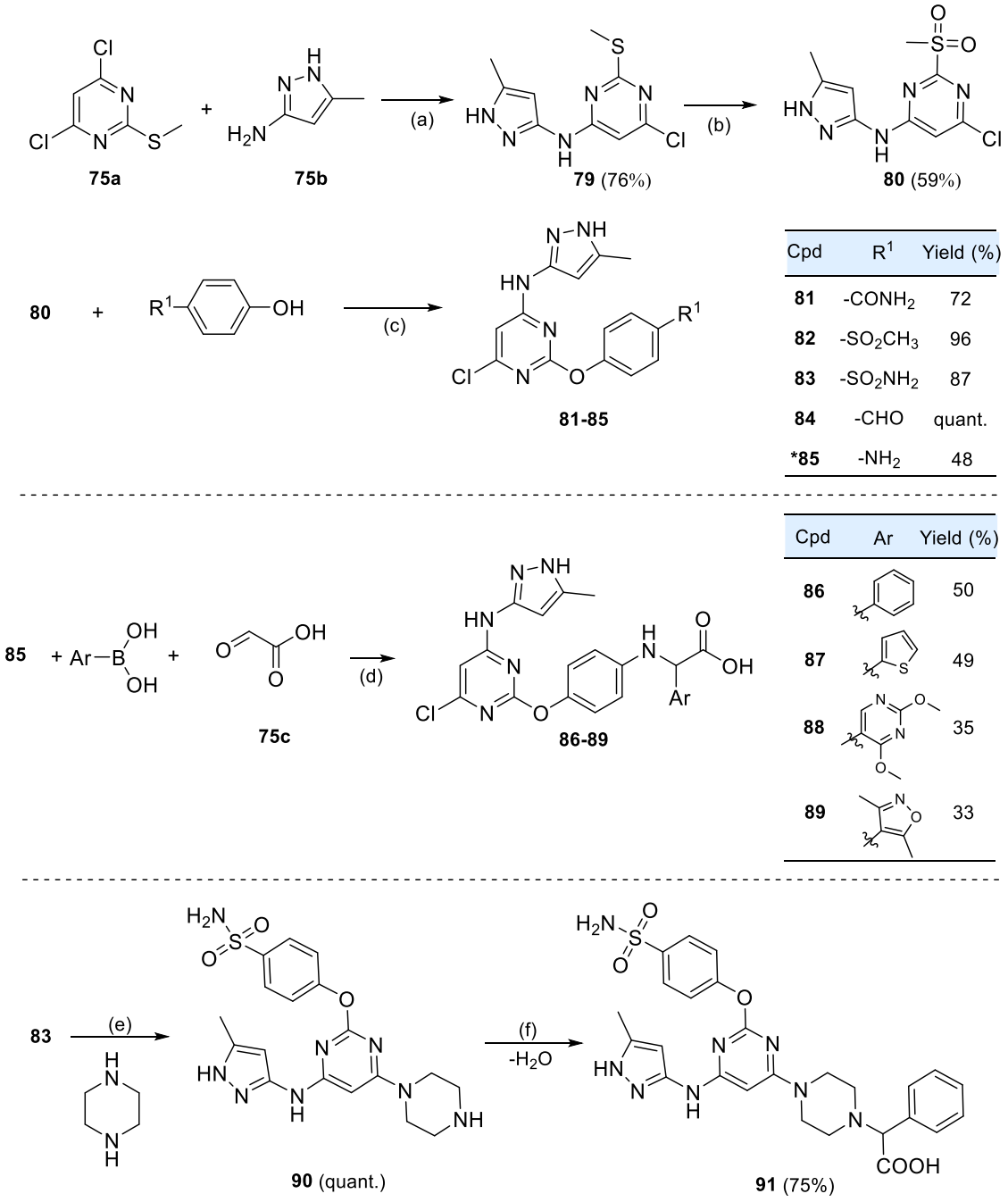

Cpd	R^1	Yield (%)
81	-$CONH_2$	72
82	-SO_2CH_3	96
83	-SO_2NH_2	87
84	-CHO	quant.
***85**	-NH_2	48

Cpd	Ar	Yield (%)
86		50
87		49
88		35
89		33

Scheme 10. Synthetic route for *N*-(5-methyl-1*H*-pyrazol-3-yl)pyrimidin-4-amine based IRE1α activators I. Reagents and conditions: (a) DIPEA, 50 °C, 16 h; (b) $2KHSO_5$. $KHSO_4$. K_2SO_4, MeOH, 0 °C 30 min, 0 °C-rt, 2 h; (c) KOtBu, *tert*-butanol, 50 °C[137] ; * (c) K_2CO_3, DMF, 100 °C, 2 h; (d) HFIP, 3 Å MS, rt, 3-4 h; (e) 1, 4-dioxane, 100 ˚C, 1 h; (f) **75c**, $PhB(OH)_2$, HFIP, 3 Å MS, rt, 3 h.

Subsequently, we tried to modify this -NH_2 group by multicomponent PR, which can also bring functional diversity in a single transformation. The primary aromatic amino group of the derivative **85** successfully reacted with heterocyclic arylboronic acids and glyoxylic acid as the carbonyl component to produce the corresponding PR products with satisfactory yields (Scheme 10). When the R^1 group was substituted by bulky groups like 2-(methylamino)-2-phenylacetic acid (**86**) and 2-(2,4-dimethoxypyrimidin-5-yl)-2-(methylamino)acetic acid (**88**), there was a sharp deterioration of activity or complete loss of activity.

The sulphonamide-based derivative, **83**, which showed the best activation potential, was further modified at the R^2 position, replacing the chloride group with a 2-(4-methylpiperazin-1-yl)-2-phenylacetic acid moiety, resulting in compound **91** with an EC_{50} value of 0.48 µM (IRE1α) and 0.18 µM (p-IRE1α). When the -OPh group at the C-2 position of aminopyrimidine scaffold was replaced by other nitrogen-containing ring systems was also proven to be detrimental to the activity (Table 11 and Scheme 11).

Table 11. Series II of synthesized IRE1α activators and their potency in the FRET assay

Entry	R^1	R^2	R^3	EC_{50} (IRE1α, µM)	EC_{50} (p-IRE1α, µM)
92	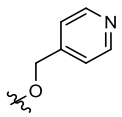	-Cl	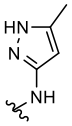	31.81	55.85
95	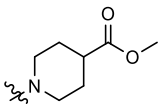	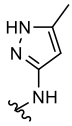	-H	22.85	8.2
97	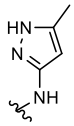	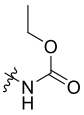	-H	19.41	16.70

From the preliminary structure activity studies performed, it is revealed that the IRE1α RNase activation by the hit is mostly structure-dependent, and there is a limited scope to explore around the scaffold to obtain better activity. However, the sulphonamide group as R^1 substituent and bulky phenyl and piperazine groups, which can potentially form hydrophobic interactions as $R^{2,}$ contributed to the IRE1α RNase activation. The structure activation studies

resulted in compound **91** with approximately 3-fold improvement in potency in activation of the phosphorylated IRE1α. The aminopyrimidine derivatives **78** and **91** with the best potency were selected for further analysis.

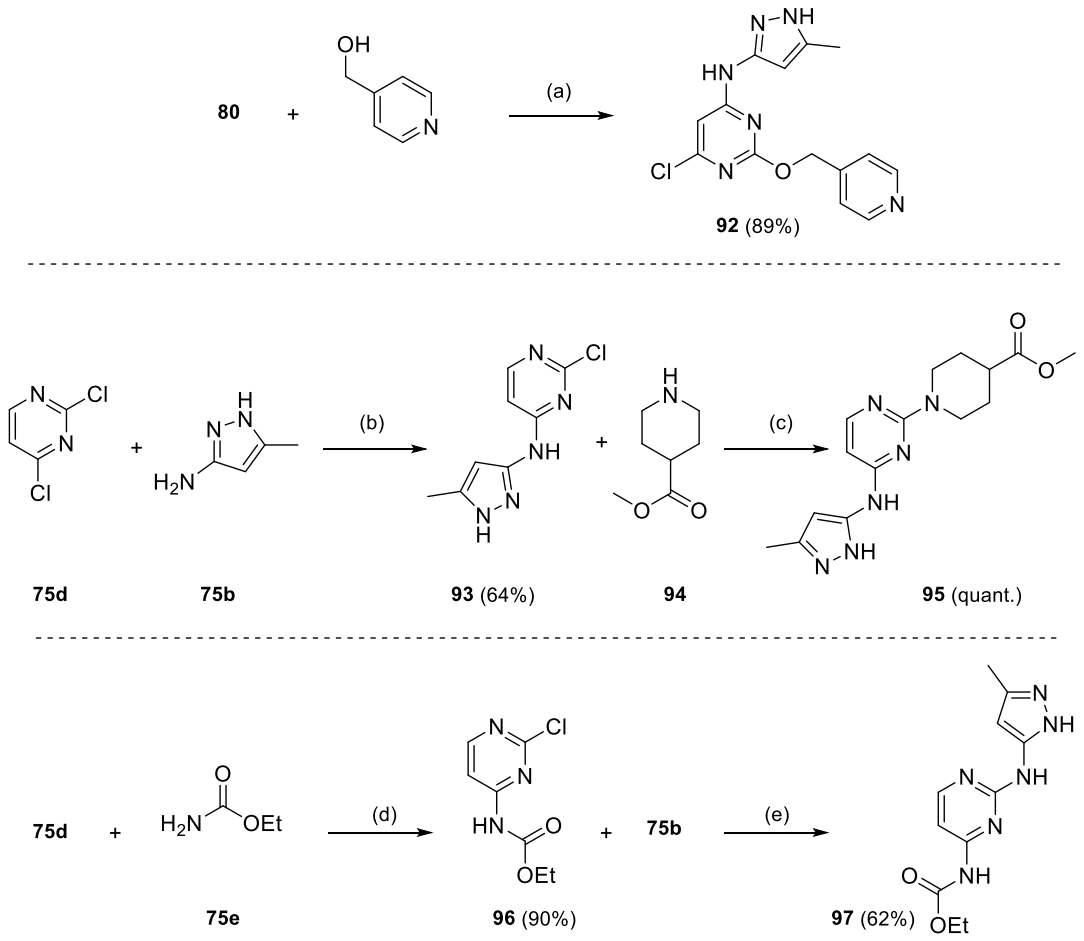

Scheme 11. Synthetic route for pyrimidine-based IRE1α activator series II**.** Reagents and conditions: (a) KOtBu, *tert*-butanol, 50 °C; (b) DIPEA, EtOH, 50 °C, 24 h, (c) 1, 4-dioxane, 80 °C, 72 h; (d) NaH, DMF, -10 °C –rt, overnight, (e) PTSA, EtOH, 100 °C, 12 h.

3.2.2.4 Evaluation of binding affinity of compound 91 to IRE1α

The interactions of IRE1α with the activator compound **91,** which showed the best potency in the FRET assay, were confirmed by DSF assay. The assay demonstrated the stabilization of IRE1α in a dose-dependent manner, with changes in melting temperature (ΔT_m) in correlation with its IRE1α RNase activity (Figure 21).

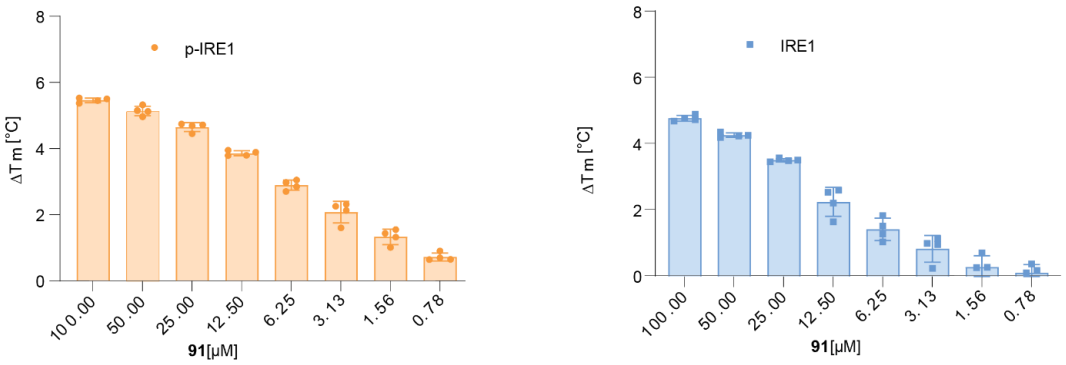

Figure 21. Stabilization of IRE1α and p-IRE1α by compound **91** was observed in a dose-dependent manner in the DSF assay.

3.2.2.5 Inhibition of IRE1α kinase

After confirming the *in vitro* binding and activation of IRE1α RNase, we moved on to identify the effect of our small collection of compounds on the IRE1α kinase activity. LanthaScreen™ Eu kinase binding assay was used to measure the inhibition of the kinase domain at 5μM test concentration. Derivatives **78**, **91** which showed maximum RNase activation potency showed maximum Kinase inhibition too. The IC_{50} values of both derivatives with particularly high inhibition (>85%) were identified as 0.13 μM (compound **78**) and 0.19 μM (compound **91**) against IRE1α (Figure 22).

A.

Entry	% Inhibition	Entry	% Inhibition
78	102±4	**89**	16±5.5
81	41±6	**91**	86±4.5
82	49±1.5	**92**	10±8
83	62±6	**93**	-13±3.5
84	40±4	**95**	6±10
85	20±4	**96**	-11±4
86	16±10.5	**97**	-7±8.5
88	-1±10.5	APY **29** [a]	81±4

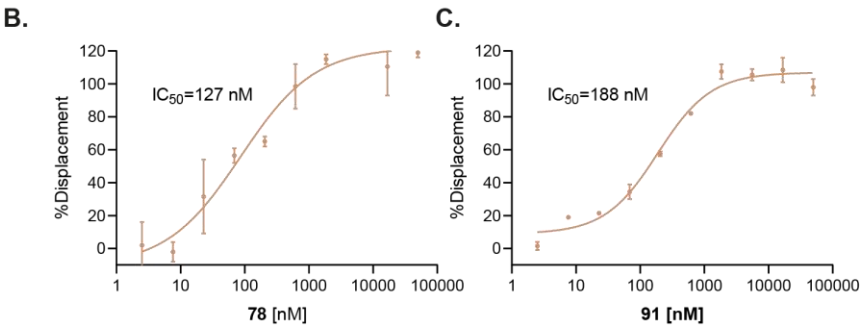

Figure 22. Inhibition of IRE1α kinase. (A) Percentage inhibition of Kinase activity by LanthaScreen™ Eu kinase binding assay at 5 μM concentration. [a] reported IRE1α RNase activator APY**29** used as a positive control; (B) IC_{50} value of compound **78** and (C) **91**.

The results from the in vitro binding, kinase inhibition, and RNase activation assays for the most potent compounds suggest that our compound is a kinase-inhibiting, RNase-activating type of derivative. Such ligands bind to the kinase domain and act by stabilizing it in its active conformation, followed by allosteric activation of the RNase domain. To better understand the kinase inhibitory and RNase activation potential for the newly synthesized compounds, their binding mode can be investigated by docking studies or by X-ray crystallography for the complex.

3.2.2.6 Evaluation of the effect of compound 78 on the dimerization and oligomerization of IRE1α

In order to study the effect of compound **78** on the self-association of IRE1α, a mass photometry-based DSS crosslinking assay was performed. The analysis was carried out in the presence of test compound **78**, DMSO (control), and reported IRE1 α RNase activator compound **G-7658**. Consistent with its ability to activate, IRE1α compound **78** induced the dimerization and oligomerization of IRE1α compared to the DMSO control (Figure 23).

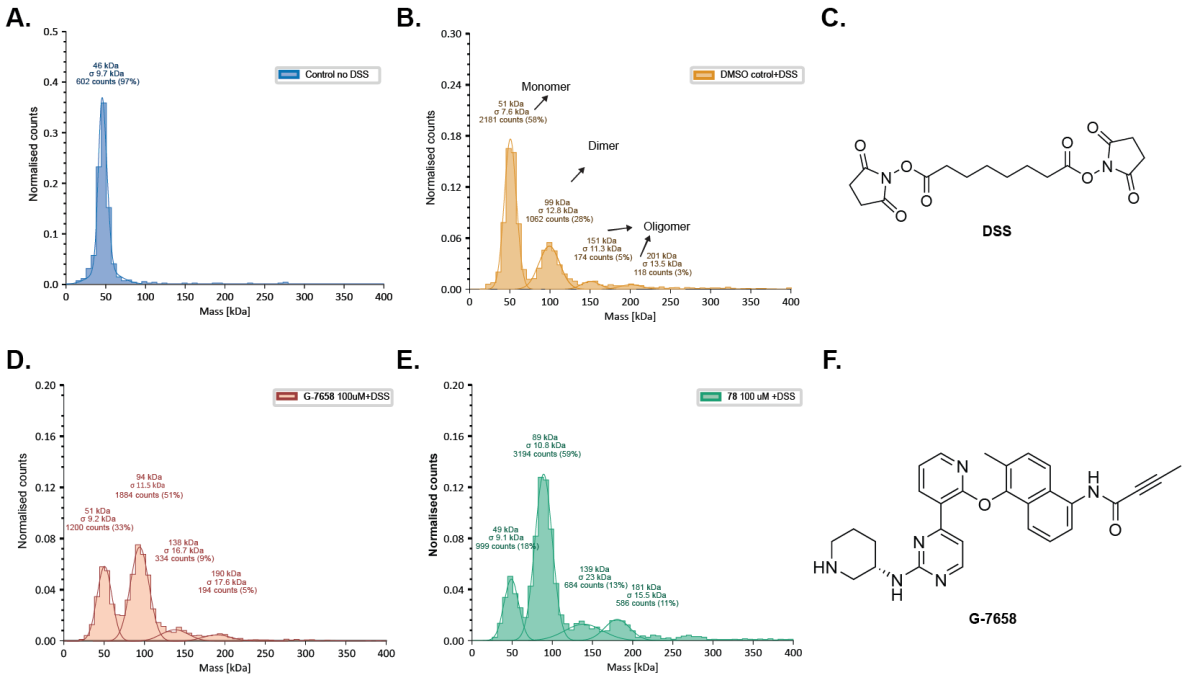

Figure 23. DSS cross-linking assay showing compound **78** promoted the self-association of p-IRE1α. (A) p-IRE1α without DSS, (B) p-IRE1α with DSS and DMSO (control), (C) Structure of DSS, (D) p-IRE1α with **G-7658** and DSS, (E) p-IRE1α with **78** and DSS, (F) Structure of **G-7658**.

3.2.2.7 Cellular effects of IRE1α activators 78 and 91

The cellular activation of IRE1α RNase function was measured for the two best-performing aminopyrimidine derivatives **78** and **91**. The activation is measured as a function of *XBP1* splicing activity tested at the cellular level by RT-qPCR measurement (reverse transcription-quantitative polymerase chain reaction) in Michigan Cancer Foundation-7 (MCF-7) breast cancer cell line. MCF-7 cells were incubated with different concentrations of **78** and **91** for a period of 24h. After treatment, the total RNA was isolated and converted to cDNA, followed by an RT qPCR measurement, and the levels of the spliced *XBP1* mRNA were measured. The results revealed that compound **78** can dose-dependently activate the *XBP1* mRNA splicing, even at submicromolar range as 0.74 µM concentration. (Figure 24 A). Compound **91** also showed a dose-dependent activation of *XBP1* mRNA splicing; however, in comparison to **78,** it exhibited weaker activation of IRE1α RNase function in MCF-7 cells (Figure 24 B). The reduced activity may be attributed to the carboxyl group present in its structure, which could hinder cellular permeability.

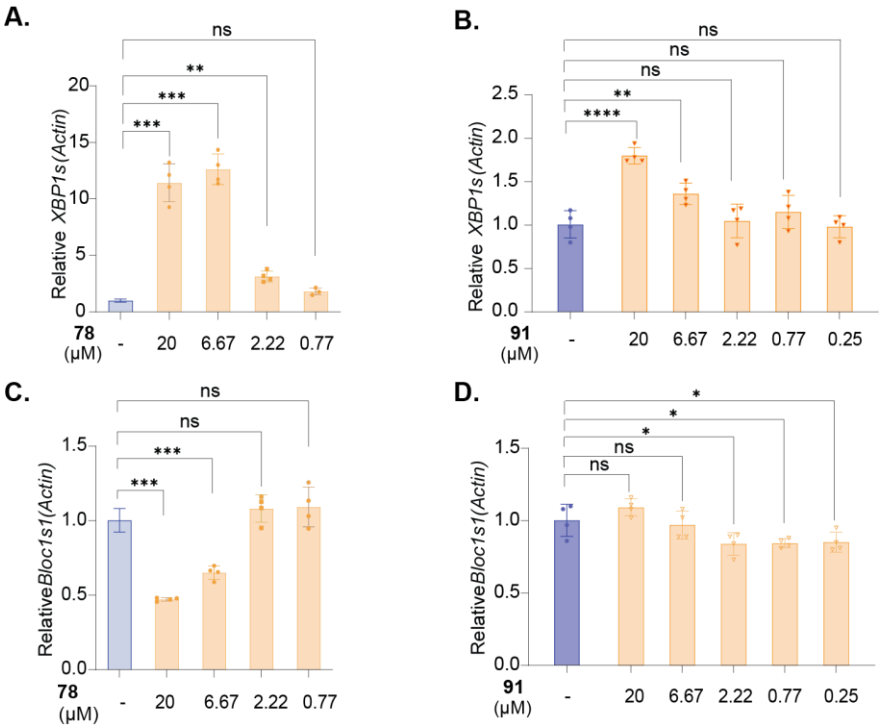

Figure 24. RT-qPCR-based evaluation of cellular effects of IRE1α activators. (A) Compound **78** and (B) compound **91** treatment dose dependently increase the splicing of *XBP1* mRNA; (C) degradation of *Bloc1s1* mRNA by compound **78** indicated activation of IRE1α downstream pathways like RIDD in the MCF-7 cell line; (D) however, there was no significant degradation of *Bloc1s1* mRNA. Statistical significance (ns when $p \geq 0.05$; * when $p \leq 0.05$, ** when $p \leq 0.01$, *** when $p \leq 0.001$, **** when $p \leq 0.0001$) calculated by Student's t-test.

Additionally, the RIDD activity was assessed using RT-qPCR by quantifying *Bloc1s1* mRNA levels, a known RNA substrate of the RIDD pathway. Since *Bloc1s1* mRNA is expected to be degraded upon RIDD activation, its levels were measured following treatment with compounds **78** and **91**. The RT-qPCR results of compound **78** demonstrated a dose-dependent decrease in *Bloc1s1* mRNA levels at concentrations of 20.00 µM and 6.67 µM, with approximately a 50% reduction compared to the control (Figure 24 C). However, no significant changes were observed in the case of compound **91** (Figure 24 D). The cell-based experiments suggest that compounds **78** and **91** successfully activate IRE1α at the cellular level.

3.2.2.8 Evaluation of anti-proliferative activity

To evaluate the effect of IRE1α activation in cancer cells, the colony formation assay was conducted using two breast cancer cell lines, MCF-7 and MDA-MB-231, as well as the human colorectal adenocarcinoma cell line HT-29. All cell lines were treated with the compound **78** and a DMSO control group for a duration of nine days. At concentrations of 20 µM and 10 µM, no colony formation was observed. The first detectable colonies appeared at 5 µM, with their numbers increasing at lower concentrations. Cell lines HT29 and MDA-MB-231 displayed a similar reduction in proliferation when compared to the DMSO control. Among the tested cell lines, MCF-7 exhibited lower proliferative capacity, as evidenced by a reduced number of colonies in its control group compared to the other cell lines (Figure 25).

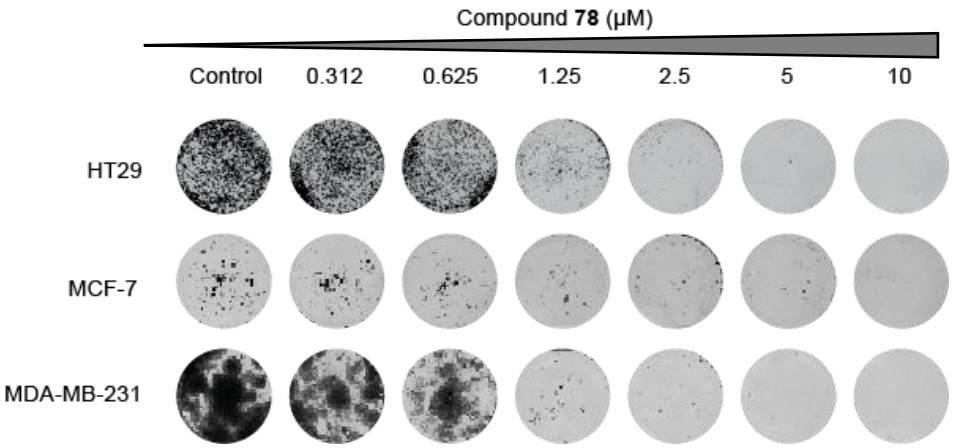

Figure 25. Antiproliferation effect of compound **78** measured by colony formation assay. Dose-dependent response exhibited by cancer cell lines HT29, MCF-7, and MDA-MB-2

3.2.2.9 Summary

In summary, we reported a new collection of aminopyrimidine-based compounds represented by the most potent derivatives **91** as IRE1α activators. The hit compound **78** was validated in our in-house assays. It showed EC_{50} value of 0.488 ± 0.04 μM for p-IRE1 and 1.31 ± 0.52 μM for IRE1α in FRET-based assay. In the attempt to improve the potency of the activators, structural modification was performed. Most of the synthesized derivatives retained the activity, and we could see a three-fold improvement in activation of p-IRE1α. The results suggested that the activity was mostly structure-dependent. The most advanced compound **91** in our collection showed a sub-micromolar potency (EC_{50} 0.48 μM IRE1α and 0.18 μM p-IRE1α) against IRE1 ribonuclease and IRE1α kinase (IC_{50} 0.19 μM). The binding between **91** and IRE1α was evaluated by a DSF assay, and it was revealed that our compound bound to and dose-dependently stabilized IRE1α. Subsequent cellular assays indicated that **91** upregulated the ER stress-induced *XBP1* splicing as well as other downstream IRE1α signaling in a concentration-dependent manner. Additionally, compound **78** exhibited good anticancer effects in colon, breast, and colorectal cancer cells at a low μM range.

Collectively, our RNase activity-based screening studies and structural optimization resulted in the identification of novel IRE1α RNase activator compounds that also inhibit the kinase activity of the protein. The optimized derivatives are anticipated to serve as useful chemical tools for deciphering IRE1α-related downstream signaling pathways and as a starting point for subsequent drug design efforts targeting the IRE1α branch of UPR.

4 Conclusion and Perspectives

In this thesis, two distinct small molecule-based approaches have been described, focusing on the scaffold-diverse synthesis of bioactive polycyclic compounds and the discovery of novel IRE1α modulators, respectively. The former centers on addressing the need for small molecule libraries covering unexplored chemical space by providing complex three-dimensional chemical structures. This work successfully leveraged the Petasis–sequence reactions to achieve the scaffold-diverse synthesis of bioactive polycyclic small molecules, leading to a collection of small molecules featuring a high content of sp^3-hybridized carbon atoms, multiple stereogenic centers, and a polycyclic core scaffold. In the latter part, such a library of scaffold-diverse small molecules containing natural product-inspired compounds was screened to identify novel chemotypes for the modulation of the dual RNase/Kinase RNA-cleaving protein IRE1α, a key regulator of the unfolded protein response signaling pathway.

The 3C-PR enabled the rapid synthesis of highly functionalized amines in a single one-pot transformation with mild reaction conditions. We designed and synthesized PR products with strategically positioned side chains suitable for undergoing secondary transformations. Preliminary cyclization was performed based on Petasis products that contained olefin side chains, which undergo an intramolecular Diels–Alder reaction with the furan ring present within the scaffold. Furthermore, Petasis products with allyl and propargyl appendages were synthesized for a subsequent ruthenium-catalyzed eneyne metathesis reaction for the generation of a diene within the molecule, which in turn was used for intermolecular Diels–Alder reaction with appropriate dienophile components. The integration of 3C-PR with intramolecular Diels–Alder and ring-closing metathesis sequences successfully enabled the rapid construction of structurally diverse polycyclic scaffolds enriched with sp^3-hybridized carbon centres and multiple stereogenic elements. The stereochemistry of the final products from the Petasis–sequence reactions was confirmed by X-ray crystallographic structures of three derivatives, **5a**, **9a,** and **9j**. The resulting library of complex small molecules not only demonstrated high chemical diversity but also exhibited favorable drug–like properties and promising antiproliferative effects against human cancer cell lines, underscoring their potential for therapeutic applications.

In parallel, an RNase activity-based screening approach was employed to identify new small-molecule modulators of IRE1α, a key player in the unfolded protein response. IRE1α activity has been reported to promote tumor development and aggressiveness across various cancers,

and hence, using small molecules to target the IRE1α-XBP1 branch of UPR poses a promising strategy for the treatment of these diseases. The screening efforts enabled the discovery of indole-based IRE1α inhibitors and aminopyrimidine-based activators, which were further structurally modified and optimized to yield small molecules with improved potency. The extensive structural modifications for the indole-based activators resulted in a collection of 61 indole-based IRE1α inhibitors. The structural activity relationship analysis guided by the inhibitory potency in the FRET assay led to the identification of highly selective inhibitors with nanomolar potency. Among them, compound **54** emerged as the most potent, exhibiting IC_{50} values of 16 nM and 9 nM towards IRE1α and pIRE1α, respectively. Its binding affinity was further validated using orthogonal biophysical techniques, including MST (K_D = 1.36 μM) and ITC (K_D = 0.94 μM). Mechanistic studies demonstrated that **54** engages the ATP-binding site within the kinase domain of IRE1α, thereby inducing allosteric inhibition of its RNase function. In cellular assays, compound **54** effectively suppressed ER stress-induced *XBP1* mRNA splicing in a dose-dependent manner and attenuated downstream UPR signaling.

In comparison, the aminopyrimidine-based activators, represented by compound **91**, demonstrated sub-micromolar potency (EC_{50} 0.48 μM IRE1α and 0.18 μM p-IRE1α) in enhancing IRE1α RNase activity. Preliminary structure-activity relationship studies identified critical functional groups responsible for the IRE1α ribonuclease activity. The binding of the novel activator compounds to IRE1α was confirmed through biophysical techniques, including MST (K_D= 256 nM for **78)** and DSF, which demonstrated a dose-dependent, ligand-induced stabilization of IRE1α. Cellular assays confirmed their ability to upregulate *XBP1* mRNA splicing and downstream UPR signalling. Additionally, antiproliferative effects of the identified IRE1α activators were evaluated using *in vitro* assays across multiple cancer cell lines. The methylpiperazinylphenylacetic acid **91** showed a significant reduction in colony formation at low micromolar concentrations. Notably, the evaluated RNase activators also inhibited IRE1α kinase function, suggesting its dual function modulating IRE1α that could be further exploited for therapeutic benefit.

Overall, this thesis work showcases the capability of Petasis–sequence reactions as efficient and complexity-generating strategies in constructing polycyclic bioactive small molecules and highlights the potential of scaffold-diverse IRE1α modulators as valuable chemical probes and starting points for drug development. The optimized derivatives provide critical insights into IRE1α function and its role in ER stress response, paving the way for further studies targeting this pathway in disease contexts such as cancer.

5 Experimental Section

5.1 General chemistry information

All reagents and solvents used in this study were obtained from commercial sources, including Sigma-Aldrich, TCI Chemicals, BLD Pharm, or Fisher Scientific and were used without additional purification. All solvents employed for chromatography were laboratory grade. Reaction progress was monitored by an LC-MS (Agilent 1260 II Infinity system) coupled with a mass detector (column: InfinityLab Poroshell 120 EC-C18, 2.1 × 150, 2.7 μm) and thin layer chromatography (TLC). Suitable gradient systems were employed for LC-MS analysis using mixtures of water and acetonitrile containing 0.1% trifluoroacetic acid. TLC analyses were conducted on Merck silica gel aluminum plates with F-254 indicator, visualized under UV light (at 254 nm or 356 nm) as well as by using iodine stain, or dipping in potassium permanganate stain (1.5 g of $KMnO_4$, 1.25 mL of 10% aqueous NaOH solution, 10 g of K_2CO_3 and 200 mL of water). Crude products were purified using flash column chromatography (FlashPure EcoFlex Silica gel cartridge, Irregular particle shape, particle size: 40-63 μm) and preparative HPLC with acetonitrile and water in appropriate gradients (Nucleodur C18 gravity column, 5 μm). The ^{1}H and ^{13}C NMR spectra were recorded on a Bruker DRX400 (400 MHz), DRX500 (500 MHz), DRX600 (600 MHz), and DRX700 (700 MHz) spectrometers in solvents $CDCl_3$, DMSO-d_6, and CD_3OD. NMR data are presented in the following sequence: chemical shift values (in ppm), followed by signal multiplicities defined as s (singlet), d (doublet), t (triplet), q (quartet), hep (heptet), dd (doublet of doublets), dt (doublet of triplets), td (triplet of doublets), tt (triplet of triplets), ddt (doublet of doublet of triplets), and m (multiplet). Coupling constants (*J*) are reported in Hertz (Hz). High-resolution mass spectrometry (HRMS) analyses were conducted using either an LTQ Orbitrap mass spectrometer interfaced with an Accela HPLC System (equipped with a Hypersyl GOLD column, 50 mm × 1 mm, 1.9 μm), or a compact QTOF (Bruker Daltonics GmbH & Co. KG, Bremen, Germany) coupled to an Agilent 1260 Infinity II platform (Agilent Technologies, Waldbronn, Germany) comprising a G7129A autosampler, G7116A column compartment, G7117C photodiode array detector, and G7111B quaternary pump, using either ESI or APCI ionization techniques. Compounds **13**–**23**, **24**, **26**, **36**, and indomethacin were sourced from the COMAS compound library at the Max Planck Institute of Molecular Physiology, Dortmund.[131] All the remaining compounds in this thesis were synthesized following the procedures detailed in the subsequent sections, with references to previously published methods provided where appropriate.

5.2 Synthetic procedures and compound characterizations

5.2.1 Petasis–sequence reactions

5.2.1.1 Building blocks with olefin substitution

***N*-Allyl-*N*-(2-furylmethyl) amine (1c)**

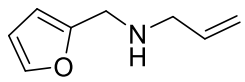

The synthesis of compound **1c** was carried out according to the reported procedure[138] using allylamine (0.98 g, 17.17 mmol), furfural (1.50 g, 15.61 mmol), and $MgSO_4$ (1.88 g) in DCM (12 mL). The crude imine formed from the reaction was used in the next step in methanol (30 mL) and $NaBH_4$ (0.42 g, 11.10 mmol). The resulting crude amine was purified by column chromatography to afford pure *N*-allyl-*N*-(2-furylmethyl) amine (**1c**), 1.65 g, 81% yield. ^{1}H NMR (600 MHz, DMSO-*d* ^{6}) δ= 7.54 (m, 1H), 6.37 (dd, *J* = 3.0, 1.8 Hz, 1H), 6.21 (d, *J* = 3.0 Hz, 1H). 5.85-5.78 (m, 1H), 5.16-5.03 (m, 2H), 3.63 (s, 2H), 3.12-3.11 (m, 2H), 2.12 (bs, 1H). Spectroscopic data were in accordance with the reported data.[138]

5-Allyl-2,2-dimethyl-1,3-dioxolan-4-ol (2)

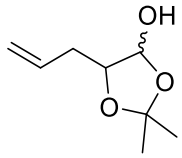

The synthesis of compound **2** was carried out according to the reported procedure.[31] At first, 2-hydroxypent-4-enoic acid was obtained from glyoxylic acid (3.00 g, 32.59 mmol), allyl bromide (6.81 g, 52.15 mmol), and fine flakes of freshly cut indium (3.78 g, 0.174 mmol) in a 2:1 mixture of THF and H_2O (60 mL). The resulting 2-hydroxypent-4-enoic acid was used in the next step without further purification (2.23 g, 59% yield). ^{1}H NMR (400 MHz, $CDCl_3$) δ= 5.87-5.77 (m, 1H), 5.23-5.17 (m, 2H), 4.36 (dd, *J* = 6.8, 4.8 Hz, 1H), 2.68-2.46 (m, 2H). Spectroscopic data were in accordance with the reported literature.[31]

Secondly, 5-allyl-2,2-dimethyl-1,3-dioxolan-4-one was synthesized from 2-hydroxypent-4-enoic acid (2.21 g, 19.07 mmol), 2,2-dimethoxypropane (15.87 g, 152.54 mmol), and pyridine p-toluenesulfonate (0.96 g, 3.8 mmol) in acetone (124 mL). The crude reaction mixture was purified by using flash column chromatography on silica gel to afford the title compound as a colorless oil that was used for the next step (2.3 g, 77% yield). ^{1}H NMR (400 MHz, $CDCl_3$) δ

5.82 (ddt, *J* = 17.1, 10.2, 6.9 Hz, 1H), 5.33-5.14 (m, 2H), 4.47 (dd, *J* = 6.7, 4.3 Hz, 1H), 2.71-2.59 (m, 1H), 2.56-2.43 (m, 1H), 1.61 (s, 3H), 1.55 (s, 3H). Spectroscopic data were in accordance with the reported literature.[31]

Finally, 5-allyl-2,2-dimethyl-1,3-dioxolan-4-ol (**2**) was synthesized from a solution of 5-allyl-2,2-dimethyl-1,3-dioxolan-4-one (2.30 g, 14.73 mmol) in toluene (60 mL) using DIBAL-H (18.59 mL, 17.52 mmol, 25% DIBAL-H in toluene). The final product (**2**) was immediately used for reactions without further purification (2.08 g, 89 % yield).

***N*-Propargyl-thiophenemethylamine (6a)**

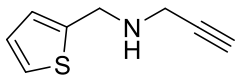

The synthesis of **6a** was carried out according to the reported procedure[139] using thiophene methylamine (2.0 g, 17.67 mmol), propargylbromide 80% (2.63 g, 17.67 mmol), and K_2CO_3 in THF. The crude amine was purified by column chromatography to afford the pure product (1.63 g, 60.91% yield). ^{1}H NMR (500 MHz, $CDCl_3$) δ= 7.24 (dd, *J* = 5.0, 1.0 Hz, 1H), 6.99-6.98 (m, 1H), 6.96 (dd, *J* = 5.0, 3.5 Hz, 1H), 4.11 (d, *J* = 0.7 Hz, 2H), 3.47 (d, *J* = 2.5 Hz, 2H), 2.27 (t, *J* = 2.5 Hz, 1H). Spectroscopic data were in accordance with the reported data.[139]

***N*-(Thiophen-2-ylmethyl)but-2-yn-1-amine (6b)**

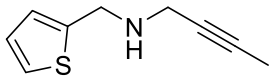

The synthesis of compound **6b** was carried out by a procedure adapted from reported literature.[139] Thiophene methylamine 0.70 g (6.18 mmol) and K_2CO_3 1.734 g (12.37 mmol) were added to THF (42 mL), cool down the mixture to zero degree. A solution of 1-bromo-2-butyne 822.487 (6.18 mmol) in THF 42 mL was added drop-wise to the mixture over a period of 2 h at 0 ˚C. Stirred the reaction mixture at room temperature for 12 h. The mixture was concentrated *in vacuo*. The crude amine was purified by column chromatography on silica gel using petroleum ether and ethyl acetate (355 mg, 35% yield). ^{1}H NMR (400 MHz, $CDCl_3$) δ= 7.22 (dd, *J* = 4.8, 1.2 Hz, 1H), 6.97-6,.94 (m, 2H), 4.07 (s, 2H), 3.41 (q, *J* = 2.3 Hz, 2H), 1.84 (t, *J* = 2.4 Hz, 3H), 1.77 (s, 1H).

5.2.1.2 General Procedure for allylated tertiary amines by Petasis reaction

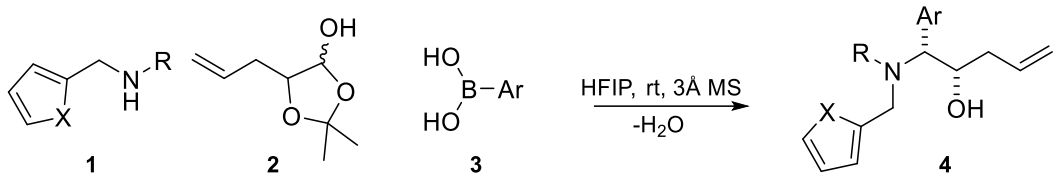

A mixture of primary or secondary amine (1 equiv.), aldehyde (1.2 equiv.), and boronic acid (1.2 equiv.) was added to HFIP (0.1 M) in the presence of 3Å molecular sieves. The reaction was stirred at ambient temperature, with progress monitored by TLC and LC-MS. Upon completion, the solvent was removed under reduced pressure. The crude product was then subjected to flash chromatography using 4–10% ethyl acetate in petroleum ether as the eluent to afford the purified compound.

(1*S*,2*R*)-1-((Furan-2-ylmethyl)amino)-1-(thiophen-2-yl)pent-4-en-2-ol (4a)

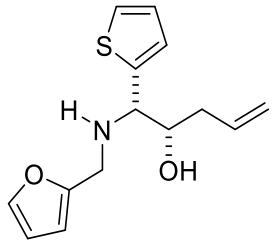

Synthesized by following the general procedure for the preparation of **4a-4j**. Compound **4a** was obtained from furfurylamine **1a** (50 mg, 0.51 mmol), 5-allyl-2,2-dimethyl-1,3-dioxolan-4-ol **2** (97.74 mg, 0.62 mmol), and 2-thienylboronic acid **3a** (79.06 mg, 0.62 mmol) in HFIP (5 mL) for 5 h. Purified as a colourless oil. (117.96 mg, 87% yield). ^{1}H NMR (500 MHz, $CDCl_3$) δ= 7.37 (dd, *J* = 1.8, 0.8 Hz, 1H), 7.31 – 7.29 (m, 1H), 7.02 – 6.99 (m, 2H), 6.31 (dd, *J* = 3.2, 1.9 Hz, 1H), 6.18 (m, 1H), 5.79 (m, 1H), 5.07 (m, 2H), 4.05 (d, *J* = 3.6 Hz, 1H), 3.96 (ddd, *J* = 8.5, 5.1, 3.7 Hz, 1H), 3.75 (dd, *J* = 73, 14.5 Hz, 2H), 2.11 (m, 2H). ^{13}C NMR (126 MHz, CDCl3) δ= 152.73, 142.29, 141.17, 134.62, 127.07, 126.49, 125.82, 118.01, 110.36, 107.93, 72.24, 61.22, 43.50, 37.88. HRMS-ESI (m/z): calculated for $[M+H]^+$ $C_{14}H_{18}NO_2S$, 264.1053; found, 264.1054.

(1*S*,2*R*)-1-(Thiophen-2-yl)-1-((thiophen-2-ylmethyl)amino)pent-4-en-2-ol (**4b**)

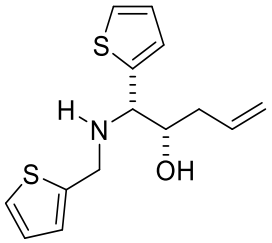

Synthesized by following the general procedure for the preparation of **4a-4j**. Compound **4b** was obtained from 2-thiophenemethylamine **1b** (50 mg, 0.44 mmol), 5-allyl-2,2-dimethyl-1,3-dioxolan-4-ol **2** (83.86 mg, 0.53 mmol), and 2-thienylboronic acid **3a** (67.83 mg, 0.53 mmol) in HFIP (4 mL) for 3 h. Purified as a colourless oil (102.46 mg, 83% yield). ^{1}H NMR (600 MHz, $CDCl_3$) δ= 7.30 (m, 1H), 7.22 (dd, *J* = 5.4, 1.2 Hz, 1H), 7.01 (dd, *J* = 5.3, 3.6 Hz, 1H), 6.99-6.98 (m, 1H), 6.95 (dd, *J* = 4.8, 3.0 Hz, 1H), 6.90-6.89 (m, 1H), 5.84-5.77 (m, 1H), 5.05-5.09 (m, 2H), 4.09 (d, J =3. 6 Hz, 1H), 4.00 (dd, *J* = 13.8, 0.6 Hz, 1H), 3.95-3.92 (m, 1H), 3.88 (dd, *J* = 13.8, 0.6 Hz, 1H), 2.199-2.15 (m, 1H), 2.12-2,07 (1H, m).^{13}C NMR (151 MHz, $CDCl_3$) δ= 143.25, 142.02, 134.75, 126.83, 126.76, 126.51, 125.56, 125.52, 124.85, 117.97, 72.70, 61.25, 45.74, 37.91. HRMS-ESI (m/z): calculated for $[M+H]^+$ $C_{14}H_{18}NOS_2$, 280.0824; found, 280.0825.

4-((1*R*,2*R*)-2-Hydroxy-1-((thiophen-2-ylmethyl)amino)pent-4-en-1-yl)phenol (**4c**)

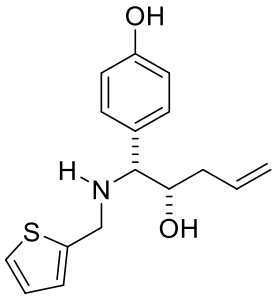

Synthesized by following the general procedure for the preparation of **4a-4j**. Compound **4c** was obtained from 2-thiophenemethylamine **1b** (50 mg, 0.44 mmol), 5-allyl-2,2-dimethyl-1,3-dioxolan-4-ol **2** (83.86 mg, 0.53 mmol), and 4-hydroxyphenylboronic acid **3b** (72.83 mg, 0.53 mmol) in HFIP (4 mL) for 1 h. Purified as a white powder (53 mg, 50% yield). ^{1}H NMR (700 MHz, DMSO-d_6) δ= 9.19 (s, 1H), 7.36 (dd, *J* = 4.9, 1.4 Hz, 1H), 7.12 – 7.09 (m, 2H), 6.93 (dd, *J* = 4.9, 2.8 Hz, 1H), 6.85 – 6.83 (m, 1H), 6.72 –6.70 (m, 2H), 5.81 – 5.75 (m, 1H), 4.96 – 4.93 (m, 2H), 4.56 (d, J = 5.4 Hz, 1H), 3.73 (d, *J* = 14 Hz, 1H), 3.65 (m, 1H), 3.58 (d, *J* = 14 Hz, 1H), 3.50 (d, *J* = 4.9 Hz, 1H), 2.55 (bs, 1H), 2.11-1.95 (m, 2H). ^{13}C NMR (176 MHz, $(CD_3)_2SO$)

δ= 156.55, 145.57, 137.11, 131.13, 129.72, 127.01, 124.86, 124.76, 116.47, 115.16, 73.84, 65.49, 45.70, 37.98. HRMS-ESI (m/z): calculated for $[M+H]^+$ $C_{16}H_{20}NO_2S$, 290.1209; found, 290.1209.

(1*R*,2*R*)-1-((Furan-2-ylmethyl)amino)-1-(4-methoxyphenyl)pent-4-en-2-ol (**4d**)

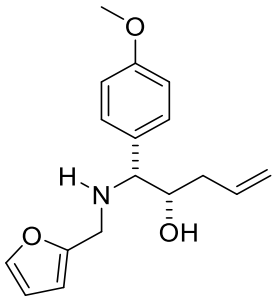

Synthesized by following general procedure for the preparation of **4a-4j**. Compound **4d** was obtained from furfurylamine **1a** (70 mg, 0.72 mmol), 5-allyl-2,2-dimethyl-1,3-dioxolan-4-ol **2** (136.83 mg, 0.86 mmol), 4-methoxyphenylboronic acid **3c** (131.43 mg, 0.86 mmol) in HFIP (5 mL) for 3 h. Purified as a light-yellow oil (27 mg, 13% yield). ^{1}H NMR (500 MHz, $CDCl_3$) δ= 7.36 (dd, *J* = 3.1, 1.9 Hz, 1H), 7.28 – 7.25 (m, 2H), 6.91 – 6.88 (m, 2H), 6.30 (dd, *J* = 3.1, 1.9 Hz, 1H), 6.12 (dd, *J* = 3.5, 0.5 Hz, 1H), 5.82-5.74 (m, 1H), 5.07-5.03 (m, 2H), 3.90-3.87 (m, 1H), 3.81 (s, 3H), 3.76 (d, *J* = 14.5 Hz, 1H), 3.69 (d, *J* = 2.5 Hz, 1H), 3.60 (d, *J* = 14.5 Hz, 1H), 2.12-1.97 (m, 2H). ^{13}C NMR (126 MHz, $CDCl_3$) δ= 159.25, 153.26, 142.12, 135.15, 130.46, 129.72, 117.74, 113.94, 110.28, 107.52, 72.78, 64.86, 55.38, 43.65, 37.66. HRMS-ESI (m/z): calculated for $[M+H]^+$ $C_{17}H_{22}NO_3$, 288.1594; found, 288.1595.

(1*R*,2*R*)-1-(Allyl(furan-2-ylmethyl)amino)-1-(furan-3-yl)pent-4-en-2-ol (**4e**)

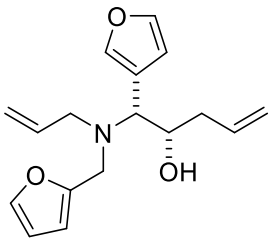

Synthesized by following general procedure for the preparation of **4a-4j**. Compound **4e** was obtained from *N*-allyl-*N*-(2-furylmethyl) amine (**1c**) (100 mg, 0.73 mmol), 5-allyl-2,2-dimethyl-1,3-dioxolan-4-ol **2** (138.38 mg, 0.87 mmol), furan-3-boronicacid **3d** (97.879 mg, 0.87 mmol) in HFIP (5 mL) for 2 h. Purified as a colourless oil (168.60 mg, 80 % yield). ^{1}H NMR (500 MHz, $CDCl_3$) δ= 7.44 (t, *J* = 1.5 Hz, 1H), 7.38-7.37 (m, 2H), 6.44 (d, *J* = 1.5 Hz, 1H), 6.32 (dd, *J* = 3.1, 1.9 Hz, 1H), 6.16 (d, *J* = 2.9 Hz, 1H), 5.86-5.77 (m, 2H), 5.22-5.15 (m,

2H), 5.11-5.07 (m, 2H), 4.11 (m, 1H), 3.82-3.76 (m, 1H), 3.60 (d, *J* = 6.1 Hz, 1H), 3.44-3.37 (m, 1H), 3.26 (m, 1H), 2.90 (dd, *J* = 14.5, 7.5 Hz, 1H), 2.39-2.34 (m, 1H), 2.16-2.10 (m, 1H). ^{13}C NMR (126 MHz, $CDCl_3$) δ= 152.86, 143.22, 142.08, 142.05, 135.98, 135.14, 119.54, 117.81, 117.69, 111.21, 110.27, 108.64, 70.31, 59.79, 53.81, 46.99, 38.67. HRMS-ESI (m/z): calculated for $[M+H]^+$ $C_{17}H_{22}NO_3$, 288.1594; found, 288.1594.

(1*S*,2*R*)-1-(Allyl(furan-2-ylmethyl)amino)-1-(thiophen-2-yl)pent-4-en-2-ol (**4f**)

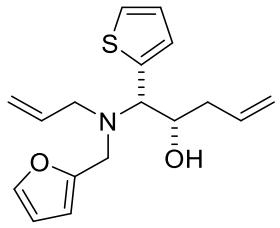

Synthesized by following general procedure for the preparation of **4a-4j**. Compound **4f** was obtained from *N*-allyl-*N*-(2-furylmethyl) amine (**1c**) (100 mg, 0.73 mmol), 5-allyl-2,2-dimethyl-1,3-dioxolan-4-ol **2** (138.38 mg, 0.87 mmol), 2-thienylboronicacid **3a** (111.934 mg, 0.87 mmol) in HFIP (5 mL) for 3 h. Purified as a colourless oil (154.8 mg, 70 % yield). ^{1}H NMR (600 MHz,$CDCl_3$) δ= 7.39 (m, 1H), 7.31 (d, *J* = 4.8 Hz, 1H), 7.04 (dd, *J* = 5.4, 3.6 Hz, 1H), 6.98-6.97 (m, 1H), 6.33 – 6.32 (m, 1H), 6.20 (m, 1H), 5.86 – 5.80 (m, 2H), 5.24 (dd, *J* = 17.2, 1.2 Hz, 1H), 5.18-5.16 (m, 1H), 5.11 – 5.08 (m, 2H), 4.20 (m, 1H), 3.96 (m, 1H), 3.82 (d, J = 14.5 Hz, 1H), 3.45 (d, *J* = 14.5 Hz, 1H), 3.28 (m, 1H), 2.93-2.89 (m, 1H), 2.45-2.43 (m, 1H), 2.19 (bs, 1H), 2.17-2.13 (m, 1H). ^{13}C NMR (151 MHz, $CDCl_3$) δ= 152.81, 142.17, 138.67, 136.01, 135.00, 127.94, 126.49, 125.60, 117.91, 117.84, 110.29, 108.81, 70.95, 63.81, 53.82, 46.95, 38.66. HRMS-ESI (m/z): calculated for $[M+H]^+$ $C_{17}H_{22}NO_2S$, 304. 1366; found, 304.1366.

(1*S*,2*R*)-1-(allyl(thiophen-2-ylmethyl)amino)-1-(thiophen-2-yl)pent-4-en-2-ol (**4g**)

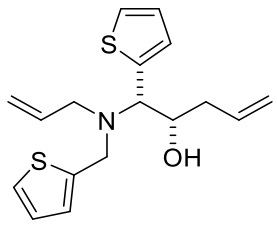

Compound **4b** (40 mg, 0.14 mmol) was dissolved in DCM (2.5 mL), followed by the addition of triethylamine (43.46 mg, 0.43 mmol) and allyl bromide (86.59 mg, 0.72 mmol). The reaction mixture was stirred at room temperature for 24 hours. Upon completion, the solvent was

removed, and the crude product was purified by flash chromatography using a mobile phase of 1% ethyl acetate in petroleum ether to yield the purified compound as a yellow oil (21 mg, 45% yield). ^{1}H NMR (700 MHz, $CDCl_3$) δ= 7.32 (d, *J* = 4.9, 1H), δ 7.23 (d, *J* = 4.9, 1H), δ 7.07 (t, *J* = 3.5, 1H), 6.97-6.90 (m, 3H), 5.92-5.82 (m, 2H), 5.26-5.18 (m, 2H), 5.16-5.11 (m, 2H), 4.16 (t, *J* = 8.4, 1H), 4.00 (d, *J* = 7.7, 1H), 3.95 (d, *J* = 14, 1H), 3.55 (d, *J* = 14, 1H), 3.34-3.32 (m,1H), 2.88 (m, 1H), 2.67-2.64 (m, 1H), 2.24-2.20 (m, 1H), 1.93 (bs, 1H). ^{13}C NMR (176 MHz, $CDCl_3$) δ= 143.83, 138.25, 136.04, 135.16, 127.90, 126.69, 126.61, 125.75, 125.50, 125.03, 118.06, 117.97, 71.59, 63.23, 53.46, 49.62, 38.90. HRMS-ESI (m/z): calculated for $[M+H]^+$ $C_{17}H_{22}NOS_2$, 320.1137; found, 320.1137.

(1*R*,2*R*)-1-(Allyl(furan-2-ylmethyl)amino)-1-(*p*-tolyl)pent-4-en-2-ol (**4h**)

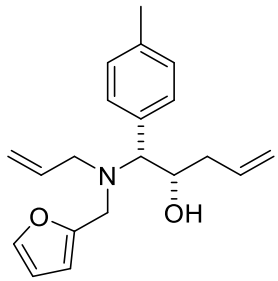

Synthesized by following general procedure for the preparation of **4a-4j**. Compound **4h** was obtained from *N*-allyl-*N*-(2-furylmethyl) amine (**1c**) (73.33 mg, 0.53 mmol), 5-allyl-2,2-dimethyl-1,3-dioxolan-4-ol **2** (101.33 mg, 0.64 mmol), tolylboronicacid **3e** (87.08 mg, 0.64 mmol) in HFIP (3 mL). Purified as a colourless oil (103.3 mg, 62% yield). ^{1}H NMR (400 MHz, $CDCl_3$) δ= 7.39 –7.38 (m, 1H), 7.20 (d, *J* = 8 Hz, 2H), 7.17 (d, *J* = 8 Hz, 2H), 6.33 (dd, *J* = 3.2, 1.6 Hz, 1H), 6.16 (d, *J* = 3.2, 1H), 5.91 – 5.78 (m, 2H), 5.23 – 5.15 (m, 2H), 5.09 – 5.06 (m, 2H), 4.31–4.26 (m, 1H), 3.81 (d, *J* = 15.0 Hz, 1H), 3.58 (d, *J* = 6.4 Hz, 1H), 3.47 (d, *J* = 15.0 Hz, 1H), 3.24 (dd, *J* = 14.5, 5.0 Hz, 1H), 2.94-2.89 (m, 1H), 2.36 (S, 3H) 2.34 – 2.31 (m, 1H) 2.04 – 1.97 (m, 1H). ^{13}C NMR (101 MHz, CDCl3) δ= 152.95, 142.02, 137.44, 135.98, 135.52, 133.23, 129.82, 129.07, 117.77, 117.42, 110.21, 108.69, 69.73, 68.07, 53.40, 46.51, 38.89, 21.26. HRMS-ESI (m/z): calculated for $[M+H]^+$ $C_{20}H_{26}NO_2$, 312.1958; found, 312.1957.

(1*R*,2*R*)-1-(Allyl(furan-2-ylmethyl)amino)-1-phenylpent-4-en-2-ol (**4i**)

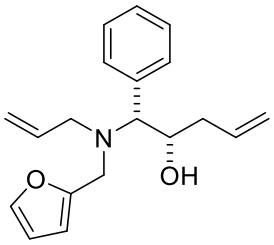

Synthesized by following general procedure for the preparation of **4a-4j**. Compound **4i** was obtained from *N*-allyl-*N*-(2-furylmethyl) amine (**1c**) (60.00 mg, 0.44 mmol), 5-allyl-2,2-dimethyl-1,3-dioxolan-4-ol **2** (83.63 mg, 0.53 mmol), phenylboronicacid **3f** (64.46 mg, 0.53 mmol) in HFIP (4 mL). Purified as a white powder (56 mg, 43 % yield). ^{1}H NMR (600 MHz, $CDCl_3$) δ= 7.39 (m, 1H), 7.38-7.30 (m, *J* = 5H), 6.33 (m, 1H), 6.17 (m, 1H), 5.84 (m, 2H), 5.22-5.17 (m, 2H), 5.08-5.05 (m, 2H), 4.32 (m, 1H), 3.82 (d, *J* =12 Hz, 1H), 3.61 (m, 1H), 3.49 (d, *J* =12.6 Hz, 1H), 3.26-3.24 (m, 1H), 2.95-2.92 (m, 1H), 2.37 (bs, 1H), 2.31-2.30 (m, 1H), 2.01-1.96 (m, 1H). ^{13}C NMR (151 MHz, $CDCl_3$) δ= 152.88, 142.11, 136.49, 135.89, 135.39, 129.98, 128.37, 127.87, 117.87, 117.55, 110.27, 108.80, 69.62, 68.46, 53.44, 46.48, 38.89. HRMS-ESI (m/z): calculated for $[M+H]^+$ $C_{19}H_{24}NO_2$; 298.1802 found, 298.1802.

5.2.1.3 General procedure for IMDA of Petasis derived products

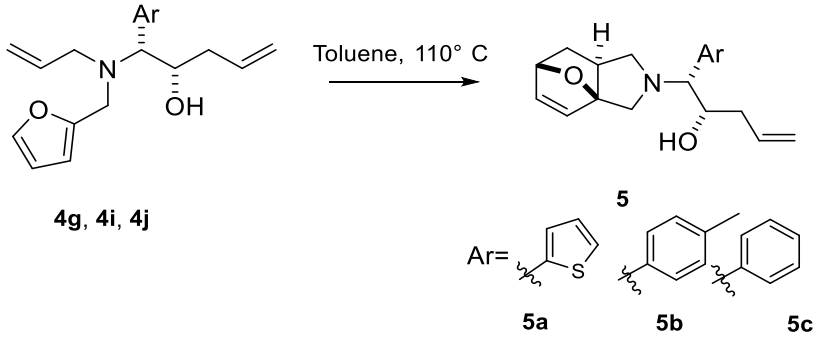

Intermediates (**4g**, **4i**, **4j**) formed from PR were individually dissolved in toluene (0.15 M) and heated to reflux at 110 °C with continuous stirring. Reaction progress was monitored using TLC and LC-MS. Upon completion, the solvent was removed under reduced pressure, and the crude material was purified by silica gel column chromatography using 2–5% methanol in dichloromethane as the eluent.

(1*S*,2*R*)-1-((3a*R*,6*R*,7a*R*)-1,6,7,7a-Tetrahydro-3a,6-epoxyisoindol-2(3*H*)-yl)-1-(thiophen-2-yl)pent-4-en-2-ol (5a)

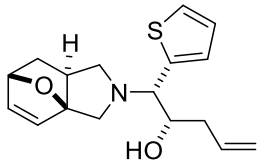

Synthesized by following the general procedure for the preparation of **5a-5c**. **5a** was obtained from **4g** (138 mg, 0.45 mmol) dissolved in toluene (3 mL) and stirred at 110 °C. Purified as colourless crystals, formed as 1:1 rotamers. (81.80 mg, 59 % yield). 1:1 rotamers: ^{1}H NMR (400 MHz, $CDCl_3$) δ= 7.29-7.28 (m,1H), 6.97-6.96 (m, 1H), 6.37 (dd, *J*= 41.2, 5.6, 1H), 6.29-6.26 (m, 1H), 5.86-5.76 (m, 1H), 5.07-5.02 (m, 2H), 4.98-4.97 (m, 1H), 4.12-4.06 (m, 1H), 3.81 (d, *J*= 2.8, 0.50 H, rotamer 1) 3.78-3.76 (m, 1H), 3.48 (t, *J*= 7.6, 0.50 H, rotamer 2), 3.31 (d, , *J* = 12.5 Hz, 0.50 H, rotamer 1), 3.14, 3.02 (two bs, total 1 H, 2 rotamers), 2.88-2.81 (m,1H), 2.75 (d, *J* = 12.5 Hz, 0.50 rotamer 2), 2.28-2.24 (m, 0.50 H, rotamer 1), 2.16-2.11 (m, 0.50H, rotamer 2), 2.09-1.92 (m, 3H), 1.74-1.71 (m, 0.50 H, rotamer 1) 1.64-1-59 (m, 0.50 H, rotamer 2), 1.37 (dd, *J* = 11.6, 7.6 Hz, 0.50 H, rotamer 1), 1.28 (dd, *J* = 11.2, 7.6 Hz, 0.50 H, rotamer 2). ^{13}C NMR (176 MHz, $CDCl_3$) δ= 140.19 (rotamer 1), 139.92 (rotamer 2), 136.26 (rotamer 1), 136.11 (rotamer 2), 135.91 (rotamer 1), 135.85 (rotamer 2), 134.76 (rotamer 1), 134.68 (rotamer 2), 127.58 (rotamer 1), 127.42 (rotamer 2), 126.11 (rotamer 1), 125.91 (rotamer 2), 125.83 (rotamer 1), 125.71 (rotamer 2), 117.62 (rotamer 1), 117.59 (rotamer 2), 95.86 (rotamer 1), 95.27 (rotamer 2), 80.21 (rotamer 1), 80.11 (rotamer 2), 70.55 (rotamer 1), 70.31 (rotamer 2), 69.19 (rotamer 1), 69.11 (rotamer 2), 57.44(rotamer 1), 57.15 (rotamer 2), 54.11 (rotamer 1), 54.03 (rotamer 2), 43.37 (rotamer 1), 42.75 (rotamer 2), 38.03 (rotamer 1), 37.92 (rotamer 2), 29.54 (rotamer 1), 29.13 (rotamer 2). HRMS-ESI (m/z): calculated for $[M+H]^+$ $C_{17}H_{22}NO_2S$, 304. 1366; found, 304.1366.

(1*R*,2*R*)-1-((3a*R*,6*R*,7a*R*)-1,6,7,7a-Tetrahydro-3a,6-epoxyisoindol-2(3*H*)-yl)-1-(p-tolyl)pent-4-en-2-ol (5b)

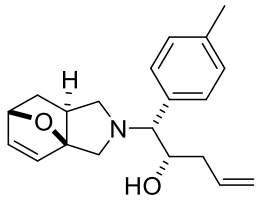

Synthesized by following the general procedure for the preparation of **5a-5c**. **5b** was obtained from **4i** (81 mg, 0.26 mmol) dissolved in toluene (1.8 mL) and stirred at 110 °C. Purified as colourless crystals, formed as 1:1 rotamers. (47.3 mg, 58 % yield). 1:1 rotamers: ^{1}H NMR (400 MHz, $CDCl_3$) δ= 7.24-7.11 (m, 4H), 6.44, 6.31 (two d, *J* = 5.6 Hz, total 1H, 2 rotamers), 6.29, 6.26 (two dd, *J* = 5.6, 1.6 Hz, total 1 H, two rotamers), 5.86 – 5.75 (m, 1H), 5.04 - 4.96 (m, 3H), 4.12-4.06 (m, 1H), 3.80 (d, *J* = 11.6 Hz, 0.50 H, rotamer 1), 3.56-3.48 (m, 0.50 H, rotamer 1), 3.37 (dd, *J* = 20, 3.2 Hz, 1H), 3.28 (d, *J* = 12.4 Hz, 0.50 H, rotamer 1), 2.91-2.87 (m, 0.50 H, rotamer 2), 2.85 (d, *J* = 11.7 Hz, 0.50 H, rotamer 2), 2.60 (d, *J* = 12.4 Hz, 0.50 H, rotamer 2), 2.34 (m, 3H), 2.30-2.25, 2.06-2.01(two m, total 1H, 2 rotamers), 2.13-2.07, 1.99-1.95 (two m, total 1 H, 2 rotamers), 1.93-1.78 (m, 2H), 1.77-1.71, 1.61-1.55 (two m, total 1H, 2 rotamers), 1.37, 1.26 (two dd, *J* = 11.6, 7.6 Hz, total 1H, two rotamers). ^{13}C NMR (101 MHz, $CDCl_3$) δ= 137.42, 136.12 (rotamer 1), 136.04 (rotamer 2), 135.99 (rotamer 1), 135.87 (rotamer 2), 135.27 (rotamer 1), 135.18 (rotamer 2), 134.80, 129.56 (rotamer 1), 129.49 (rotamer 2), 128.91 (rotamer 1), 128.86 (rotamer 2), 117.24 (rotamer 1), 117.18 (rotamer 2), 95.95 (rotamer 1), 95.34 (rotamer 2), 80.16 (rotamer 1), 80.09 (rotamer 2), 73.77 (rotamer 1), 73.67 (rotamer 2), 71.07 (rotamer 1), 70.74 (rotamer 2), 57.60 (rotamer 1), 57.32 (rotamer 2), 54.54 (rotamer 1), 54.37 (rotamer 2), 43.33 (rotamer 1), 42.89 (rotamer 2), 38.40 (rotamer 1), 38.38 (rotamer 2), 29.55 (rotamer 1), 29.09 (rotamer 2), 21.25. HRMS-ESI (m/z): calculated for $[M+H]^+$ $C_{20}H_{26}NO_2$, 312.1958; found, 312.1957.

(1*R*,2*R*)-1-Phenyl-1-((3a*R*,6*R*,7a*R*)-1,6,7,7a-tetrahydro-3a,6-epoxyisoindol-2(3*H*)-yl)pent-4-en-2-ol (5c)

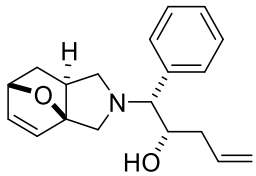

Synthesized by following the general procedure for the preparation of **5a-5c**. **5c** was obtained from **4j** (33 mg, 0.11 mmol) dissolved in toluene (1.0 mL) and stirred at 110 °C. Purified as a white powder, formed as 1:1 rotamers. (16.5 mg, 50 % yield). 1:1 rotamers: ^{1}H NMR (400 MHz, $CDCl_3$) δ= 7.35-7.31 (m, 5H), 6.46-6.26 (m, total 2H, 2 rotamers), 5.85-5.75 (m, 1H), 5.05-4.99 (m, 3H), 4.16-4.11 (m, 1H), 3.89-3.59 (two singlet, total 1H, 2 rotamers), 3.44 (dd, *J*= 18.8, 1.6, 1H), 3.32, 2.64 (two doublets , *J*= 12.4, total 1H, 2 rotamers), 2.95-2.89 (m, 1H), δ 2.36 – 2.29, 2.11 – 2.05 (two multiplets, total 1H, 2 rotamers), 2.17-2.13, 2.03-1.99 (two multiplets, total 1H, 2 rotamers) 1.93-1.80 (m, 2H) 1.78-1.73, 1.61-1.56 (two multiplets, total

1H, 2 rotamers), 1.42-1.28 (m, total 1H, 2 rotamers). ^{13}C NMR (101 MHz, $CDCl_3$) δ= 136.26 (rotamer 1), 136.18 (rotamer 2), 135.8, 135.69 (rotamer 1), 135.68 (rotamer 2), 135.11 (rotamer 1), 135.01(rotamer 2), 129.78 (rotamer 1), 129.72 (rotamer 2), 128.28 (rotamer 1), 128.23 (rotamer 2), 127.99, 117.45 (rotamer 1), 117.37 (rotamer 2), 95.83 (rotamer 1), 95.25 (rotamer 2), 80.26 (rotamer 1), 80.19 (rotamer 2), 74.29 (rotamer 1), 74.23 (rotamer 2), 70.93 (rotamer 1), 70.59 (rotamer 2), 57.78 (rotamer 1), 57.51 (rotamer 2), 54.61(rotamer 1), 54.44 (rotamer 2), 43.30 (rotamer 1), 42.89 (rotamer 2), 38.38 (rotamer 1), 38.37 (rotamer 2), 29.67 (rotamer 1), 29.22 (rotamer 2). HRMS-ESI (m/z): calculated for $[M+H]^+$ $C_{19}H_{24}NO_2$; 298.1802 found, 298.1801.

5.2.1.4 General procedure for the synthesis *N*-allylated and propargylated tertiary amines by Petasis reaction

Corresponding secondary amine (1 equiv.), masked aldehyde component (1.2 equiv.), and boronic acid (1.2 equiv.) were simultaneously added to HFIP (0.5 M) in presence of 3Å molecular sieves. The mixture was stirred at room temperature and monitored by LC-MS and TLC. The solvent then evaporated under reduced pressure. Purified the resultant residue by column chromatography (5-7% ethyl acetate in petroleum ether).

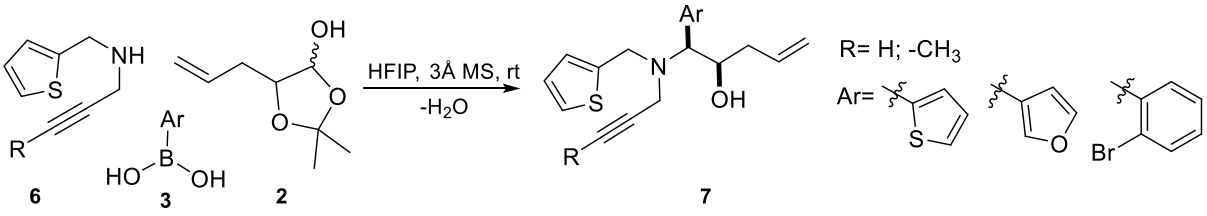

(1*R*,2*R*)-1-(Furan-3-yl)-1-(prop-2-yn-1-yl(thiophen-2-ylmethyl)amino)pent-4-en-2-ol (**7a**)

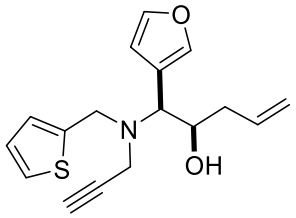

Using general procedure for the preparation of **7a-7d**. Compound **7a** was obtained from *N*-propargyl-thiophenemethylamine **6a** (223.00 mg, 1.47 mmol), 5-allyl-2,2-dimethyl-1,3-dioxolan-4-ol **2** (279.93 mg, 1.77 mmol), furan-3-boronicacid **3d** (197.99 mg, 1.77 mmol) in HFIP (6 mL). Purified as a colourless oil (365.00 mg, 82 % yield). ^{1}H NMR (500 MHz, $CDCl_3$) δ= 7.46 (s, 1H), 7.44-43 (m, 1H), 7.24 (dd, *J* = 3.5 Hz, *J* = 1.5 Hz, 1H) 6.94-6.92 (m, 2H), 6.53 (m, 1H), 5.89-5.80 (m, 1H), 5.10-5.06 (m, 2H), 4.20-4.17 (m, 1H), 3.89 (dd, *J* = 14.5 Hz, *J* =

54 Hz, 2H), 3.76 (d, *J* = 2.5 Hz, 1H), 3.51-3.25 (m, 2H), 2.72 (bs, 1H), 2.25 (t, *J* = 2.5 Hz; 1H), 2.14-2.11 (m, 2H). ^{13}C NMR (126 MHz, $CDCl_3$) δ= 143.35, 142.54, 142.28, 134.88, 126.75, 126.20, 125.30, 120.09, 117.63, 111.28, 78.71, 77.41, 77.16, 76.91, 73.75, 69.33, 60.42, 49.31, 39.32, 38.69. HRMS-ESI (m/z): calculated for $[M+H]^+$ $C_{17}H_{20}NO_2S$, 302.1209; found, 302.1211.

(1*S*,2*R*)-1-(Prop-2-yn-1-yl(thiophen-2-ylmethyl)amino)-1-(thiophen-2-yl)pent-4-en-2-ol (**7b**)

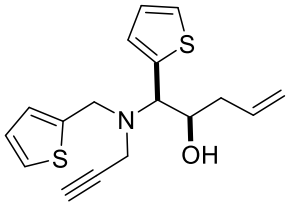

Using general procedure for the preparation of **7a-7d**. Compound **7b** was obtained from *N*-propargyl-thiophenemethylamine **6a** (400.00 mg, 2.64 mmol), 5-allyl-2,2-dimethyl-1,3-dioxolan-4-ol **2** (502.12 mg, 3.17 mmol), 2-thienylboronicacid **3a** (406.14 mg, 1.77 mmol) in HFIP (5.5 mL). Purified as a pale-yellow oil (668.00 mg, 80 % yield). ^{1}H NMR (600 MHz, $CDCl_3$) δ= 7.32 (d, *J* = 4.5 Hz, 1H), 7.23 (d, *J* = 4.5 Hz, 1H), 7.07 (d, *J* = 3, Hz, 1H), 7.02 (dd, *J* = 5.1, 3.5 Hz, 1H), 6.95 (m, 1H), 6.92 (dd, *J* = 5.0, 3.4 Hz, 1H), 5.89-5.82 (m, 1H), 5.11-5.08 (m, 2H), 4.27-4.24 (m, 1H), 4.12 (d, *J* = 1.8 Hz, 1H), 3.85 (dd, *J* = 49.2, 13.8 Hz, 1H), 3.55 (d, *J* = 17.4 Hz, 1H), 3.30 (d, *J* = 17.4 Hz, 1H), 2.52 (bs, 1H), 2.27 (s, 1H), 2.19-2.07 (m, 2H). ^{13}C NMR (151 MHz, $CDCl_3$) δ= 142.35, 138.88, 134.70, 128.38, 126.67, 126.31, 126.26, 125.38, 117.84, 78.58, 73.89, 69.52, 64.51, 49.54, 39.14, 38.73. HRMS-ESI (m/z): calculated for $[M+H]^+$ $C_{17}H_{20}NOS_2$, 318.0981; found, 318.0981.

(1*R*,2*R*)-1-(2-Bromophenyl)-1-(prop-2-yn-1-yl(thiophen-2-ylmethyl)amino)pent-4-en-2-ol (**7c**)

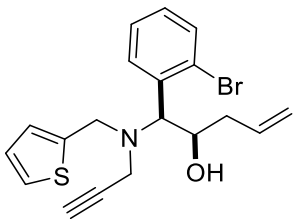

Using general procedure for the preparation of **7a-7d**. Compound **7c** was obtained from *N*-propargyl-thiophenemethylamine **6a** (300.00 mg, 1.98 mmol), 5-allyl-2,2-dimethyl-1,3-dioxolan-4-ol **2** (376.58 mg, 2.38 mmol), 2-bromophenyl boronicacid **3g** (478.06 mg, 2.38

mmol) in HFIP (4.0 mL). Purified as a pale-yellow oil. (573.60 mg, 74 % yield). ^{1}H NMR (700 MHz, $CDCl_3$) δ= 7.81 (d, *J* = 8.4 Hz, 1H), 7.58 (dd, *J* = 7.7 Hz, *J* = 1.4 Hz, 1H), 7.35 (t, *J* = 7.7 Hz, 1H), 7.21 (d, *J* = 4.9 Hz, 1H), 7.18-7.15 (m, 1H), 6.92-6.90 (m, 2H), 5.87-5.81 (m, 1H), 5.07-5.03 (m, 2H), 4.44 (m, 1H), 4.30 (d, *J*=8.4, 1H), 3.99 (d, *J*=14, 1H), 3.70 (d, *J* = 14.7 Hz, 1H), 3.63 (d, *J* = 17.9 Hz, 1H), 3.45 (d, *J* = 17.8 Hz, 1H). ^{13}C NMR (176 MHz, $CDCl_3$) δ= 142.54, 137.11, 135.20, 133.09, 131.36, 129.36, 127.70, 126.67, 126.56, 126.18, 125.24, 117.77, 78.31, 74.25, 69.67, 66.75, 49.36, 38.80, 38.28. HRMS-ESI (m/z): calculated for $[M+H]^+$ $C_{19}H_{21}BrNOS$, 390.0522; found, 390.0525.

(1*S*,2*R*)-1-(But-2-yn-1-yl(thiophen-2-ylmethyl)amino)-1-(thiophen-2-yl)pent-4-en-2-ol (7d)

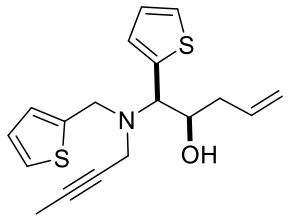

Using general procedure for the preparation of **7a-7d**. Compound **7d** was obtained from *N*-(thiophen-2-ylmethyl)but-2-yn-1-amine **6b** (324.10 mg, 1.96 mmol), 5-allyl-2,2-dimethyl-1,3-dioxolan-4-ol **2** (372.30 mg, 2.35 mmol), 2-thienylboronicacid **3a** (301.14mg, 2.35 mmol) in HFIP (4.0 mL). Purified as a colourless oil (591.62 mg, 91 % yield). ^{1}H NMR (400 MHz, $CDCl_3$) δ= 7.31 (d, *J* = 4.8 Hz, 1H), 7.21 (dd, *J* = 4.8 Hz, *J* = 1.6 Hz, 1H), 7.05 (d, *J* = 2.8 Hz, 1H), 7.02-7.00 (m, 1H), 6.93-6.91 (m, 2H), 5.92-5.82 (m, 1H), 5.12-5.08 (m, 2H), 4.25-4.24 (m, 1H), 4.12 (d, , *J* = 4.0 Hz, 1H), 3.86 (d, *J* = 14.4 Hz, 1H), 3.76 (d, *J* = 14.0 Hz, 1H), 3.48 (d, *J* = 17.2 Hz, 1H), 3.23 (d, *J* = 17.2 Hz, 1H), 2.56 (bs, 1H), 2.21-2.06 (m, 2H), 1.87 (t, 2.4) ^{13}C NMR (101 MHz, $CDCl_3$) δ= 142.87, 139.18, 134.92, 128.16, 126.60, 126.20, 126.05, 125.15, 117.61, 81.55, 73.69, 69.62, 64.37, 49.58, 39.58, 38.66, 3.73. HRMS-ESI (m/z): calculated for $[M+H]^+$ $C_{18}H_{22}NOS_2$, 332.1137; found, 332.1140.

5.2.1.5 General procedure for enyne metathesis of Petasis products

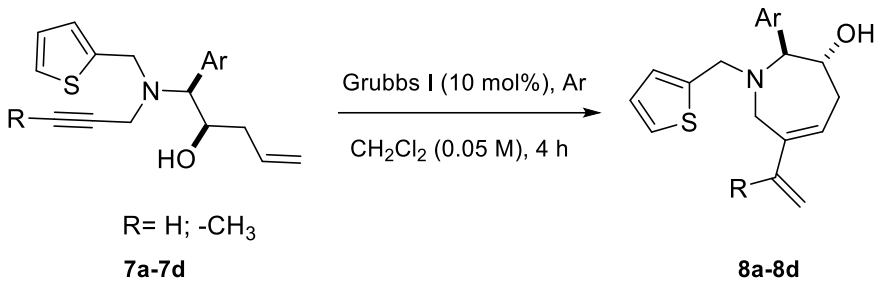

R= H; -CH_3

7a-7d **8a-8d**

Intermediates **7a-7d (**1 equiv.**)** formed after the PR were dissolved in DCM (0.05 M) were added into an oven-dried Schlenk tube followed by Grubbs first generation catalyst (10 mol%, 0.1 equiv.). The reaction was heated at 40° C for 4 h under argon atmosphere, whereupon the volatiles were removed *in vacuo.* The residue was purified by column chromatography on silica gel (10-20% EA in petroleum ether).

(2*S*,3*R*)-2-(Furan-3-yl)-1-(thiophen-2-ylmethyl)-6-vinyl-2,3,4,7-tetrahydro-1*H*-azepin-3-ol (**8a**)

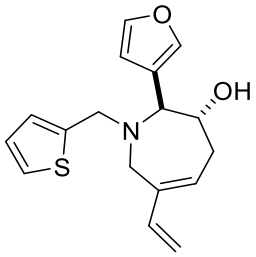

Synthesis was carried out by following the general procedure for the preparation of **8a-8d**. **8a** was obtained from **7a** (388.00 mg, 1.29 mmol), using Grubbs first generation catalyst (106.16 mg, 0.129 mmol) in DCM (25 mL, 0.05 M). Purified as a brown oil (104.76 mg, 27 % yield). ^{1}H NMR (500 MHz, $CDCl_3$) δ= 7.45 (m, 1H), 7.44 (m, 1H), 7.22 (dd, *J* = 5, 1.5 Hz, 1H), 6.92 (dd, *J* = 5.0, 3.5 Hz, 1H), 6.87-6.86 (m, 1H), 6.46 (m, 1H), 6.30 (dd, *J* = 17.6, 11.0 Hz, 1H), 5.79 (t, *J* = 5.8 Hz, 1H), 4.86-4.79 (m, 2H), 3.99-396 (m, 1H), 3.92-3.90 (m, 3H), 3.55 – 3.50 (m, 1H), 3.40 (d, *J* = 16.5 Hz, 1H), 2.88-2.77 (m, 1H), 2.58-2.54 (m, 1H), 2.36 (bs, 1H). ^{13}C NMR (126 MHz, $CDCl_3$) δ= 144.28, 143.48, 141.16, 139.79, 139.36, 128.68, 126.48, 125.44, 125.17, 123.06, 110.97, 110.86, 65.11, 54.63, 47.87, 34.34. HRMS-ESI (m/z): calculated for $[M+H]^+$ $C_{17}H_{20}NO_2S$, 302.1209; found, 302.1209.

(2*R*,3*R*)-2-(thiophen-2-yl)-1-(thiophen-2-ylmethyl)-6-vinyl-2,3,4,7-tetrahydro-1*H*-azepin-3-ol (**8b**)

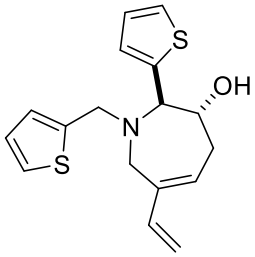

Synthesis was carried out by following the general procedure for the preparation of **8a-8d**. Compound **8b** was obtained from **7b** (600.00 mg, 1.89 mmol), using Grubbs first generation catalyst (155.53 mg, 0.189 mmol) in DCM (35 mL, 0.05 M). Purified as a brown oil (196.8 mg, 33% yield). ^{1}H NMR (500 MHz, $CDCl_3$) δ= 7.31 (m, 1H), 7.22 (dd, *J* = 5.0 Hz, *J* = 1.0 Hz, 1H), 7.05-7.04 (m, 2H), 6.92 (dd, *J* = 5.0 Hz, *J* = 3.5 Hz, 1H), 6.89-6.88 (m, 1H), 6.31 (dd, *J* = 17.5 Hz, *J* = 11 Hz, 1H) 5.81 (t, *J* = 5.5 Hz, 1H), 4.87-4.81 (m, 2H), 4.19 (d, *J* = 7.5 Hz, 1H), 4.13-4.10 (m, 1H), 3.97 (d, *J* = 14.0 Hz, 1H), 3.90 (d, *J* = 14.5 Hz, 1H), 3.68 (d, *J* = 17.0 Hz, 1H), 3.42 (d, *J* = 17.0 Hz, 1H), 2.87-2.82 (m, 1H), 2.63 (dd, *J* = 16.5, 7.5 Hz, 1H). ^{13}C NMR (126 MHz, $CDCl_3$) δ= 144.05, 143.52, 139.75, 139.20, 128.5, 126.89, 126.55, 126.42, 125.61, 125.36, 125.23, 111.02, 74.40, 68.88, 54.67, 47.28, 34.50. HRMS-ESI (m/z): calculated for $[M+H]^+$ $C_{17}H_{20}NOS_2$, 318.0981; found, 318.0980.

(2*S*,3*R*)-2-(2-bromophenyl)-1-(thiophen-2-ylmethyl)-6-vinyl-2,3,4,7-tetrahydro-1*H*-azepin-3-ol (**8c**)

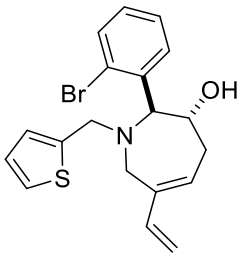

Synthesis was carried out by following the general procedure for the preparation of **8a-8d**. Compound **8c** was obtained from **7c** (546.00 mg, 1.40 mmol), using Grubbs first generation catalyst (155.21 mg, 0.140 mmol) in DCM (28 mL, 0.05 M). Purified as a brown oil (142 mg, 26% yield). ^{1}H NMR (500 MHz, $CDCl_3$) δ= 7.77-7.75 (m, 1H), 7.61 (dd, *J* = 8.0, 1 Hz, 1H), 7.35 (t, *J* = 7.0 Hz, 1H), 7.18-7.13 (m, 2H), 6.89 (dd, *J* = 5.0, 3.5 Hz, 1H), 6.81 (d, *J* = 3.0 Hz, 1H), 6.33 (dd, *J* = 17.5, 11.0 Hz, 1H), 5.73 (t, *J* = 5.2 Hz, 1H), 4.86-4.78 (m, 2H), 4.32 (d, *J* = 4.5 Hz, 1H), 4.06 (m, 1H), 3.76-3.69 (m, 3H),), 3.49 (d, *J* = 16.5 Hz, 1H), 2.82-2.78 (m, 1H),

2.54-2.48 (m, 1H), 1.89 (d, *J* = 4.5 Hz, 1H). ^{13}C NMR (126 MHz, $CDCl_3$) δ= 143.16, 140.60, 140.15, 139.11, 133.48, 129.10, 129.01, 127.95, 127.59, 126.49, 125.74, 125.65, 124.91, 111.14, 73.83, 72.22, 53.85, 48.61, 32.30. HRMS-ESI (m/z): calculated for $[M+H]^+$ $C_{19}H_{21}BrNOS$, 390.0522; found, 390.0522.

(2*R*,3*R*)-6-(Prop-1-en-2-yl)-2-(thiophen-2-yl)-1-(thiophen-2-ylmethyl)-2,3,4,7-tetrahydro-1*H*-azepin-3-ol (8d)

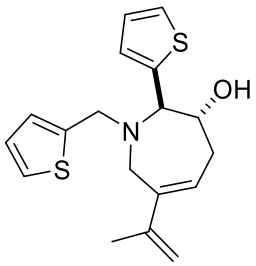

Synthesis was carried out by following the general procedure for the preparation of **8a-8d.** Compound **8d** was obtained from **7d** (540.00 mg, 1.63 mmol), using Grubbs first generation catalyst (134.1425 mg, 0.163 mmol) in DCM (32 mL, 0.05 M). Purified as a brown oil (143 mg, 27% yield). ^{1}H NMR (500 MHz, $CDCl_3$) δ= 7.31-7.30 (m, 1H), 7.21 (d, *J* = 5.0 Hz, 1H), 7.04-7.02 (m, 2H), 6.92 – 6.90 (m, 1H), 6.88 (d, *J* = 3.3 Hz, 1H), 5.91 (t, *J* = 6 Hz, 1H), 4.78 (s, 1H), 4.70 (s, 1H), 4.15 (d, *J* = 7.5 Hz, 1H), 4.12 – 4.07 (m, 1H), 3.96 (d, *J* = 14.0 Hz, 1H), 3.90 (d, *J* = 14.5 Hz, 1H), 3.77 (d, *J* = 16.5 Hz, 1H), 3.45 (d, *J* = 16.5 Hz, 1H), 2.87-2.83 (m, 1H), 2.64 (dd, *J* = 16.0, 7.5 Hz, 1H), 1.88 (s, 3H). ^{13}C NMR (126 MHz, $CDCl_3$) δ= 144.23, 144.05, 143.20, 141.47, 126.83, 126.48, 126.40, 125.53, 125.36, 125.15, 123.80, 111.13, 74.43, 69.18, 54.61, 49.15, 34.46, 21.63. HRMS-ESI (m/z): calculated for $[M+H]^+$ $C_{18}H_{22}NOS_2$, 332.1137; found, 332.1139.

5.2.1.6 Intermolecular Diels-Alder reaction of PR/RCM products

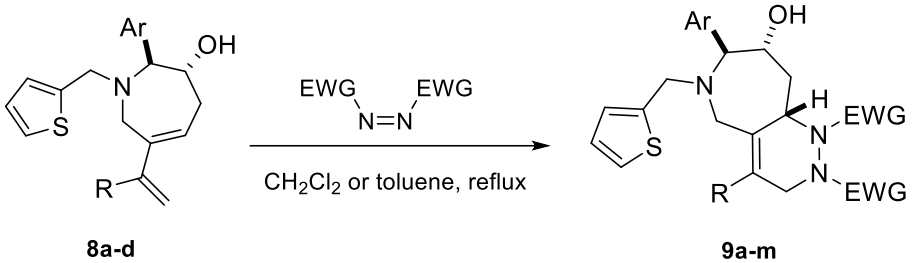

8a-d **9a-m**

((7*R*,8*R*,9a*S*)-8-Hydroxy-7-(thiophen-2-yl)-6-(thiophen-2-ylmethyl)-5,6,7,8,9,9a-hexahydro-1*H*-pyridazino[4,3-c]azepine-1,2(3*H*)-diyl)bis(piperidin-1-ylmethanone) (9a)

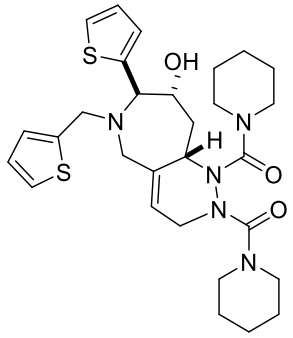

Compound **8a** (80.3 mg, 0.25 mmol, 1 equiv.), formed after the PR/RCM sequence, was dissolved in toluene (0.5 M), after which 1,1′-(azodicarbonyl)dipiperidine (70. 20 mg, 0.28 mmol, 1.1 equiv.) was added. The reaction mixture was heated to reflux and stirred overnight. Upon completion, solvent was evaporated and the crude product was purified by column chromatography using ethyl acetate in petroleum ether 20%-45% as colourless crystal in 69% yield (*dr* 9:1). The major diastereomer: ^{1}H NMR (500 MHz, $CDCl_3$) δ= 7.29-7.28 (m, 1H), 7.19 (m, 1H), 7.07 (m, 1H), 7.00 (m, 1H), 6.90-6.86 (m, 2H), 5.58 (m, 1H), 4.50 (t, *J*=8.5, 1H) , 4.20 (m, 2H), 4.11 (m, 1H), 4.04 (m, 1H), 3.91 (d, *J* = 14.0 Hz, 1H), 3.69 (d, *J* = 11.5 Hz, 1H), 3.57 (d, *J* = 15.5 Hz, 1H), 3.43-3.47 (m, 2H), 3.33-3.31 (m, 2H), 3.30-3.28 (m, 4H), 2.71-2.70 (m, 1H), 2.10 (m, 1H), 1.69-1.67 (m, 5H), 1.57-1.53 (m, 8H). ^{13}C NMR (126 MHz, $CDCl_3$) δ= 162.78, 162.47, 146.30, 143.55, 134.30, 127.07, 126.60, 125.90, 125.80, 125.13, 124.98, 119.27, 73.82, 69.80, 58.11, 53.81, 52.96, 47.28, 47.22, 43.41, 36.94, 26.05, 25.96, 24.71. HRMS-ESI (m/z): calculated for $[M+H]^+$ $C_{29}H_{40}N_5O_3S_2$, 570.2567; found, 570.2557.

((7*S*,8*R*,9a*S*)-7-(Furan-3-yl)-8-hydroxy-6-(thiophen-2-ylmethyl)-5,6,7,8,9,9a-hexahydro-1*H*-pyridazino[4,3-*c*]azepine-1,2(3*H*)-diyl)bis(piperidin-1-ylmethanone) (9b)

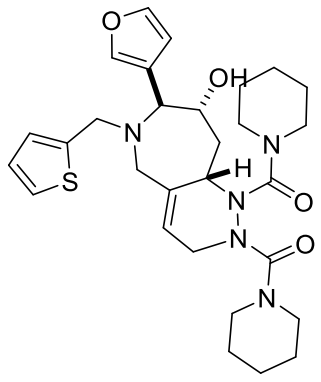

Compound **8b** (123.3 mg, 0.41 mmol, 1 equiv.), formed after the PR/RCM sequence, was dissolved in toluene (0.5 M), after which 1,1′-(azodicarbonyl)dipiperidine (113.54 mg, 0.45 mmol, 1.1 equiv.) was added. The reaction mixture was heated to reflux and stirred overnight. Upon completion, solvent was evaporated and the crude product was purified by column chromatography using acetate in petroleum ether 0%: 15% :25% then Methanol in DCM 0%: 2%: 4%, as an off-white powder in 60% yield (*dr* 1:9). The major diastereomer: ^{1}H NMR (500 MHz, $CDCl_3$) δ= 7.49 (m, 1H), 7.44 (m, 1H), 7.17 (d, *J* = 4.5 Hz, 1H), 6.89 (t, *J* = 3.5 Hz, 1H), 6.81 (m, 1H), 6.48 (m, 1H), 5.54 (m, 1H), 4.36 (t, *J* = 7.0 Hz, 1H), 4.12 (m, 2H), 4.00 (m, 1H), 3.92 (d, *J* = 14.5 Hz, 1H), 3.78 (d, *J* = 5.0 Hz, 1H), 3.67 (d, *J* = 14.0 Hz, 1H), 3.53 (d, *J* = 15.5 Hz, 1H), 3.43 – 3.35 (m, 2H), 3.31 (m, 2H), 3.28-3.25 (m, 4H), 2.59-2.56 (m, 1H), 2.48 (bs, 1H), 2.08 m (1H), 1.66 (m, 4H), 1.55-1.53 (m, 9 H). ^{13}C NMR (126 MHz, $CDCl_3$) δ= 162.50, 144.38, 143.78, 140.76, 126.72, 126.70, 125.33, 125.24, 124.60, 119.18, 109.97, 72.89, 65.38, 57.91, 54.25, 54.21, 47.23, 47.21, 37.85, 25.94, 24.70. HRMS-ESI (m/z): calculated for $[M+H]^+$ $C_{29}H_{40}N_5O_4S$, 554.2796; found, 554.2788.

((7*R*,8*R*,9a*S*)-8-Hydroxy-7-(thiophen-2-yl)-6-(thiophen-2-ylmethyl)-5,6,7,8,9,9a-hexahydro-1*H*-pyridazino[4,3-*c*]azepine-1,2(3*H*)-diyl)bis(morpholinomethanone) (9c)

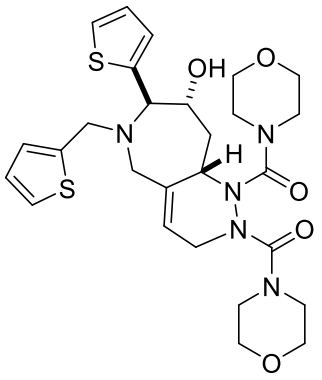

Compound **8b** (70 mg, 0.22 mmol, 1 equiv.), formed after the PR/RCM sequence, was dissolved in toluene (0.5 M), after which azodicarboxylic dimorpholide (62.15, 0.24 mmol, 1.1 equiv.) was added. The reaction mixture was heated to reflux and stirred overnight. Upon completion, solvent was evaporated and the crude product was purified by column chromatography using 70% ethyl acetate in petroleum ether (Isocratic flow), as a as an off-white powder in 73% yield (*dr* 2:1). The major diastereomer: ^{1}H NMR (700 MHz, $CDCl_3$) δ= 7.29 (m, 1H), 7.21 (m, 1H), 7.06-6.86 (m, 4H), 5.58 (m, 1H), 4.59 (m, 1H), 4.18 (m, 2H), 4.06 (m, 1H), 3.93 (d, *J* = 13.8 Hz, 1H), 3.85-3.83 (m, 2H), 3.73-3.69 (m, 3H), 3.66-3.69 (m, 5H), 3.59-3.56 (m, 3H), 3.46-3.43 (m, 1H), 3.37-3.32 (m, 6H), 2.65 (m, 1H), 2.11-2.07 (m, 1H). ^{13}C

NMR (151 MHz, $CDCl_3$) δ= 162.40, 161.89, 145.66, 143.27, 134.75, 127.21, 126.69, 125.97, 125.12, 125.10, 118.63, 73.61, 69.48, 66.84, 57.78, 53.84, 52.91, 46.65, 43.80, 36.90. HRMS-ESI (m/z): calculated for $[M+H]^+$ $C_{27}H_{36}N_5O_5S_2$, 574.2152; found, 574.2142.

((7*S*,8*R*,9a*S*)-7-(Furan-3-yl)-8-hydroxy-6-(thiophen-2-ylmethyl)-5,6,7,8,9,9a-hexahydro-1*H*-pyridazino[4,3-*c*]azepine-1,2(3*H*)-diyl)bis(morpholinomethanone) (9d)

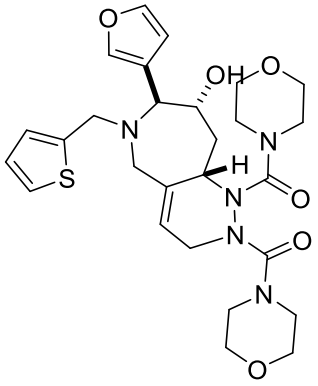

Compound **8a** (80 mg, 0.27 mmol, 1 equiv.), formed after the PR/RCM sequence, was dissolved in toluene (0.5M), after which azodicarboxylic dimorpholide (74.82 mg, 0.29 mmol, 1.1 equiv.) was added. The reaction mixture was heated to reflux and stirred overnight. Upon completion, the solvent was evaporated and the crude product was purified by column chromatography using 70% ethyl acetate in petroleum ether (Isocratic flow), as an off-white powder in 66% yield (*dr* 2:1) by The major diastereomer: ^{1}H NMR (700 MHz, $CDCl_3$) δ= 7.48 (m, 1H), 7.46 (m, 1H), 7.19 (d, *J* =4.9 Hz, 1H), 6.89 (t, *J* = 3.5 Hz, 1H), 6.81 (m, 1H), 6.45 (m, 1H), 5.55 (m, 1H), 4.38 (dd, *J* = 8.4, 4.2 Hz, 1H), 4.17 (m, 2H), 4.02 (m, 1H), 3.93 (d, *J* = 14.4 Hz, 1H), 3.80 (d, *J* = 5.8 Hz, 1H), 3.78 – 3.73 (m, 2H), 3.69 – 3.64 (m, 7H), 3.54 (d, *J* = 15.4 Hz, 1H), 3.50-3.48 (m, 2H), 3.38-3.29 (m, 7H), 2.52 (d, *J* = 13.4 Hz, 1H), 2.39 (bs, 1H), 2.07 (m, 1H). ^{13}C NMR (176 MHz, $CDCl_3$) δ= 162.32, 161.95, 144.27, 144.00, 140.80, 126.80, 125.42, 124.70, 124.53, 118.96, 111.42, 109.83, 72.36, 66.83, 66.75, 64.93, 57.72, 54.44, 53.28, 46.68, 46.57, 44.00, 38.33. HRMS-ESI (m/z): calculated for $[M+H]^+$ $C_{27}H_{36}N_5O_6S$, 558.2381; found, 558.2371.

Di-*tert*-butyl (7*R*,8*R*,9a*S*)-8-hydroxy-7-(thiophen-2-yl)-6-(thiophen-2-ylmethyl)-5,6,7,8,9,9a-hexahydro-1*H*-pyridazino[4,3-*c*]azepine-1,2(3*H*)-dicarboxylate (9e)

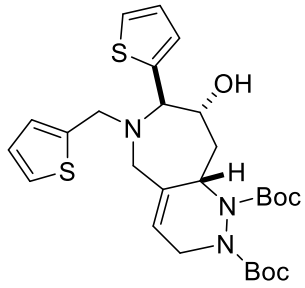

Compound **8b** (100 mg, 0.31 mmol, 1 equiv.), formed after the PR/RCM sequence, was dissolved in DCM (0.5 M), after which di-*tert*-butyl azodicarboxylate (79.78 mg, 0.35 mmol, 1.1 equiv.) was added. The reaction mixture was heated to reflux and stirred for 2.5 h. Upon completion, the solvent was evaporated, and the crude product was purified as a brown powder in 70.1% yield (6:1 *d.r*) by column chromatography using ethyl acetate in petroleum ether (25% isocratic flow). The major diastereomer: ^{1}H NMR (700 MHz, $CDCl_3$) δ= 7.29 (m, 1H), 7.21 (m, 1H), 7.05-7.00 (m, 2H), 6.90-6.87 (m, 2H), 5.50-5.46 (m, 1H), 4.78 (m, 1H), 4.49-4.29 (m, 1H), 4.09-3.98 (m, 3H), 3.87 (d, *J* = 11.2 Hz, 1H), 3.74-3.72 (m, 1H), 3.49-3.34 (m, 2H), 2.58-2.47 (m, 1H), 2.08 (bs, 1H), 2.01 (m, 1H), 1.50 (s, 9H), 1.47 (s, 9H). ^{13}C NMR (176 MHz, $CDCl_3$) δ= 154.52, 154.27, 146.32, 143.51, 135.26, 126.98, 126.49, 126.15, 125.78, 125.44, 125.34, 120.58, 81.39, 81.10, 72.50, 69.12, 54.22, 53.14, 51.85, 42.32, 39.59, 28.47. HRMS-ESI (m/z): calculated for $[M+H]^+$ $C_{27}H_{38}N_3O_5S_2$, 548.2247; found, 548.2236

Di-*tert*-butyl (7*S*,8*R*,9a*S*)-7-(Furan-3-yl)-8-hydroxy-6-(thiophen-2-ylmethyl)-5,6,7,8,9,9a-hexahydro-1*H*-pyridazino[4,3-*c*]azepine-1,2(3*H*)-dicarboxylate (9f)

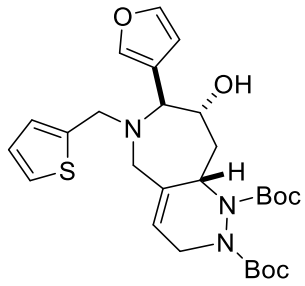

Compound **8a** (100 mg, 0.33 mmol, 1 equiv.), formed after the PR/RCM sequence, was dissolved in DCM (0.5 M), after which di-*tert*-butyl azodicarboxylate (84.04 mg, 0.36 mmol, 1.1 equiv.) was added. The reaction mixture was heated to reflux and stirred for 3 h. Upon completion, the solvent was evaporated and the crude product was purified as a brown powder in 65% yield (6:1 *d.r*) by column chromatography using ethyl acetate in petroleum ether (25%

isocratic flow). The major diastereomer: ^{1}H NMR (700 MHz, $CDCl_3$) δ= 7.53-7.42 (m, 2 H), 7.24 (m, 1H), 6.94 (m, 2H), 6.55 (m, 1H), 5.49 (m, 1H), 4.82 (m, 1H), 4.43 (d, 17 Hz, 1H), 4.30-3.96 (m, 4H), 3.83-3.71 (m, 1H), 3.61 (d, 18.5 Hz, 1H), 3.47 (m, 1H), 2.47-2.45 (m, 1H), 2.00-1.96 (m, 2H), 1.48 (s, 9H), 1.46 (s, 9H). ^{13}C NMR (126 MHz, $CDCl_3$) δ= 154.40, 154.18, 144.12, 143.90, 143.75, 134.28, 126.67, 125.50, 110.26, 81.42, 81.09, 71.79, 64.92, 53.68, 52.85, 42.21, 37.22, 31.95, 29.72, 28.32. HRMS-ESI (m/z): calculated for $[M+H]^+$ $C_{27}H_{38}N_3O_6S$, 532.2476; found, 532.2467.

Diisopropyl (7*R*,8*R*,9a*S*)-8-hydroxy-7-(thiophen-2-yl)-6-(thiophen-2-ylmethyl)-5,6,7,8,9,9a-hexahydro-1*H*-pyridazino[4,3-*c*]azepine-1,2(3*H*)-dicarboxylate (9g)

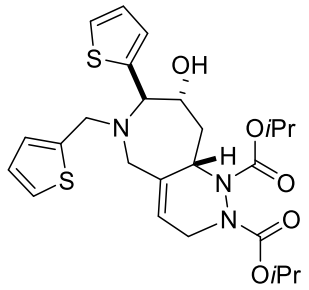

Compound **8b** (73.0 mg, 0.23 mmol, 1 equiv.), formed after the PR/RCM sequence was dissolved in DCM (0.5M), after which diisopropyl azodicarboxylate (51.15 mg, 0.25 mmol, 1.1 equiv.) was added. The reaction mixture was heated to reflux and stirred for 4h. Upon completion, the solvent was evaporated and the crude product was purified as a brown powder in 80% yield (5:1 *dr*) by column chromatography using 60% ethyl acetate in petroleum ether (isocratic flow). The major diastereomer: ^{1}H NMR (500 MHz, $CDCl_3$) δ= 7.31-7.28 (m, 1H), 7.202 (dd, *J* = 5.0 Hz, 1.0 Hz, 1H), 7.05 (d, *J* = 3.0 Hz, 1H), 6.99 (m, 1H), 6.94-6.86 (m, 2H), 5.49 (m, 1H), 4.99-4.94 (m, 2H), 4.90-4.88 (m, 1H), 4.53-4.33 (m, 1H), 4.21-4.09 (m, 1H), 3.99-3.85 (m, 2H), 3.71-3.64 (m, 1H), 3.49 (d, *J* = 15.0 Hz, 1H), 3.36-3.27 (m, 1H), 2.51-2.43 (m, 1H), 2.16-1.97 (m, 2H), 1.26 (m, 6H), 1.23-1.25 (m, 6H). ^{13}C NMR (126 MHz, CDCl3) δ= 155.22, 146.19, 143.43, 135.35, 126.95, 126.44, 126.10, 125.75, 125.41, 120.00, 116.70, 72.39, 70.19, 69.99, 69.12, 54.42, 51.75, 42.67, 39.29, 22.23, 22.07. HRMS-ESI (m/z): calculated for $[M+H]^+$ $C_{25}H_{34}N_3O_5S_2$, 520.1934; found, 520.1924

(9*R*,10*R*,11a*S*)-10-Hydroxy-2-phenyl-9-(thiophen-2-yl)-8-(thiophen-2-ylmethyl)-7,8,9,10,11,11a-hexahydro-1*H*,5*H*-[1,2,4]triazolo[1',2':1,2]pyridazino[4,3-c]azepine-1,3(2*H*)-dione (9h)

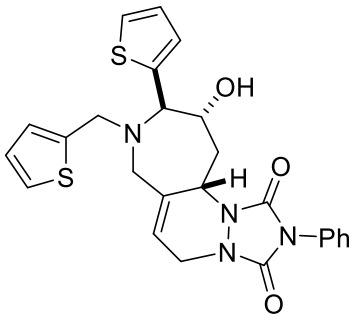

Compound **8b** (90 mg, 0.28 mmol, 1 equiv.), formed after the PR/RCM sequence, was dissolved in DCM (0.5 M), after which 4-phenyl-1,2,4-triazoline-3,5-dione (54.80 mg, 0.31 mmol, 1.1 equiv.) was added. The reaction mixture was heated to reflux and stirred for 30 min. Upon completion, the solvent was evaporated, and the crude product was purified as a white powder in 55% yield (9:1 *d.r*) using 30% ethyl acetate in petroleum ether with isocratic flow. Major diastereomer: ^{1}H NMR (500 MHz, $CDCl_3$) δ= 7.55-7.53 (m, 2H), 7.49-7.46 (m, 2H), 7.39-7.35 (m, 2H), 7.29 (d, *J* = 5.6 Hz, 1H), 7.07 (dd, *J* = 5.0, 3.5 Hz, 1H), 6.97-6.95 (m, 3H), 5.73 (m, 1H), 5.14 (m, 1H), 4.38 (d, *J* = 16.3 Hz, 1H), 4.24 – 4.23 (m, 2H), 3.95-3.92 (m, 2H), 3.71 (d, *J* = 10.5 Hz, 1H), 3.51-3.48 (m, 2H), 2.68-2.62 (m, 1H), 2.23 (bs, 1H), 2.0-1.98 (1H, m). ^{13}C NMR (126 MHz, $CDCl_3$) δ= 153.43, 151.83, 131.31, 129.26, 128.24, 127.14, 126.81, 125.97, 125.84, 125.45, 114.73, 72.57, 67.42, 54.41, 52.71, 50.96, 43.65, 37.33. HRMS-ESI (m/z): calculated for $[M+H]^+$ $C_{25}H_{25}N_4O_3S_2$, 493.1363; found, 493.1352.

((7*R*,8*R*,9a*S*)-8-Hydroxy-4-methyl-7-(thiophen-2-yl)-6-(thiophen-2-ylmethyl)-5,6,7,8,9,9a-hexahydro-1*H*-pyridazino[4,3-c]azepine-1,2(3*H*)-diyl)bis(morpholinomethanone) (9i)

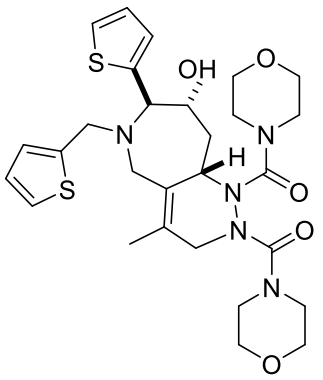

Compound **8d** (123 mg, 0.37 mmol, 1 equiv.), formed after the PR/RCM sequence was dissolved in toluene (0.5 M), after which azodicarboxylic dimorpholide (104.59 mg, 0.41 mmol, 1.1 equiv.) was added. The reaction mixture was heated to reflux and stirred overnight. Upon completion, the solvent was evaporated and the crude product was purified as a yellow powder in 72% yield (4:1 *dr*) by column chromatography using 70% ethyl acetate in petroleum ether (Isocratic flow).

NMR of 5:1 diastereomeric mixture, reporting major diastereomer. ^{1}H NMR (500 MHz, $CDCl_3$) δ= 7.27-7.26 (m, 1H), δ 7.21 (d, *J* = 4.9 Hz, 1H), 7.06 (d, *J* = 4.9 Hz, 1H), 7.02 – 6.99 (m, 1H), 6.91 (dd, *J* = 5.0, 3.0 Hz, 1H), 6.87 (m, 1H), 4.92 (t, *J* = 8.2 Hz, 1H), 4.19 (m, 1H), 4.12 (d, *J* = 16.9 Hz, 1H), 3.99-3.91 (m, 5H), 3.78-3.74 (m, 2H), 3.66-3.62 (m, 6H), 3.57 (m, 1H), 3.54-3.53 (m, 2H), 3.38-3.35 (m, 6H), 2.69 (m, 1H), 2.50 (bs, 1H), 2.01 – 1.94 (m, 1H), 1.55 (s, 3H). ^{13}C NMR (126 MHz, $CDCl_3$) δ= 162.46, 161.76, 146.19, 143.22, 128.04, 127.21, 126.75, 125.85, 125.64, 124.96, 124.71, 123.83, 74.77, 70.26, 66.86, 56.61, 54.79, 51.65, 47.28, 46.55, 34.88, 15.61. HRMS-ESI (m/z): calculated for $[M+H]^+$) $C_{28}H_{38}N_5O_5S_2$, 588.2309; found, 588.2297.

((7*S*,8*R*,9a*S*)-7-(2-Bromophenyl)-8-hydroxy-6-(thiophen-2-ylmethyl)-5,6,7,8,9,9a-hexahydro-1*H*-pyridazino[4,3-c]azepine-1,2(3*H*)-diyl)bis(morpholinomethanone) (9j)

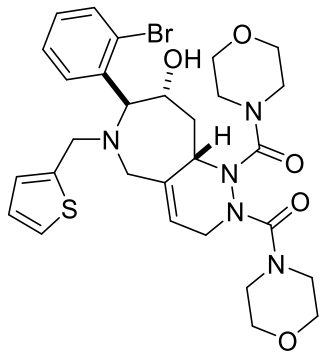

Compound **8c** (122 mg, 0.31 mmol, 1 equiv.), formed after the PR/RCM sequence was dissolved in toluene (0.5 M), after which azodicarboxylic dimorpholide (88.10 mg, 0.34 mmol, 1.1 equiv.) was added. The reaction mixture was heated to reflux and stirred overnight. The solvent was evaporated, and the crude product was purified as colourless crystals in 67% yield (*dr* 6:1) by column chromatography using 70% ethyl acetate in petroleum ether (Isocratic flow). The major diastereomer: ^{1}H NMR (500 MHz, $CDCl_3$) δ= 7.79 (d, *J* = 7.5 Hz, 1H), 7.62 (dd, *J* = 8.0 Hz, 1Hz,1H), 7.39-7.37 (m, 1H), 7.19-7.17 (m, 2H), 6.90 – 6.88 (m, 1H), 6.80 – 6.79 (m, 1H), 5.60 (m, 1H), 4.72 (t, *J* = 7.5 Hz, 1H), 4.27 (d, *J* = 4.5 Hz, 1H), 4.21 (m, 2H),

4.10-3.09 (m, 1H), 3.90- 3.86(m, 2H), 3.77-3.73 (m, 2H), 3.69-3.70 (m, 1H), 3.66-3.64 (m, 5H), 3.61 (m, 1H), 3.59-3.53 (m, 3H), 3.38-3.38 (m, 6H), 2.51-2.46 (m, 1H), 2.06-2.0 (m, 2H). ^{13}C NMR (126 MHz, $CDCl_3$) δ= 162.59, 161.96, 143.55, 139.86, 135.65, 133.87, 129.41, 128.63, 127.80, 126.92, 125.78, 125.62, 124.71, 117.40, 71.93, 71.40, 66.84, 57.30, 53.68, 53.09, 46.65, 43.73, 36.85. HRMS-ESI (m/z): calculated for $[M+H]^+$ $C_{29}H_{37}BrN_5O_5S$, 646.1693; found, 646.1689.

Bis(7-(λ^5-chloraneyl)hepta-2,4,6-triyn-1-yl) (7*R*,8*R*,9a*S*)-8-hydroxy-7-(thiophen-2-yl)-6-(thiophen-2-ylmethyl)-5,6,7,8,9,9a-hexahydro-1*H*-pyridazino[4,3-*c*]azepine-1,2(3*H*)-dicarboxylate (9k)

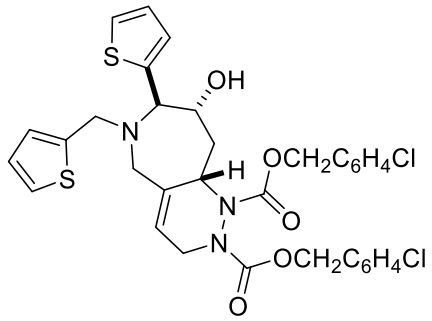

Compound **8b** (59 mg, 0.19 mmol, 1 equiv.), formed after the PR/RCM sequence was dissolved in DCM (0.5 M), after which di-(4-chlorobenzyl) azodicarboxylate (75.06 mg, 0.20 mmol, 1.1 equiv.) was added. The reaction mixture was heated to reflux and stirred for 0.5 h. The solvent was evaporated, and the crude product was purified as a brown oily liquid in 59% yield (4:1 *d.r*) by column chromatography using 30% ethyl acetate in petroleum ether (Isocratic flow). The major diastereomer: ^{1}H NMR (700 MHz, $CDCl_3$) δ= 7.32-7.10 (m, 10H), 7.14 (m, 1H), 7.03-6.93 (m, 3H), 5.50 (m, 1H), 5.20-5.04 (m, 4H), 4.92 (m, 1H), 4.54-4.41 (m, 1H), 4.12-3.80 (m, 4H), 3.71-3.43 (m, 2H), 2.49-2.64 (m, 1H), 1.90-1.68 (m, 2H). ^{13}C NMR (176 MHz, $CDCl_3$) δ= 155.14, 134.52, 134.38, 134.27, 129.64, 129.56, 129.33, 128.94, 128.89, 128.84, 127.20, 126.73, 126.53, 125.81, 69.07, 67.51, 67.30, 54.64, 53.12, 51.79, 43.28, 29.84. HRMS-ESI (m/z): calculated for $[M+H]^+$ $C_{33}H_{32}Cl_2N_3O_5S_2$, 684.1155; found, 684.1148.

Bis(2-methoxyethyl) (7*R*,8*R*,9a*S*)-8-hydroxy-7-(thiophen-2-yl)-6-(thiophen-2-ylmethyl)-5,6,7,8,9,9a-hexahydro-1*H*-pyridazino[4,3-*c*]azepine-1,2(3*H*)-dicarboxylate (9l)

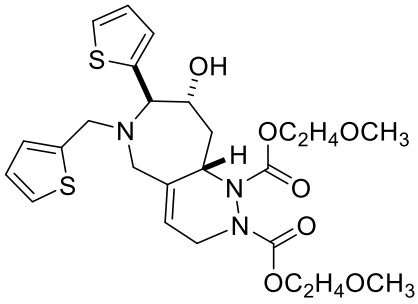

Compound **8b** (75.5 mg, 0.24 mmol, 1 equiv.), formed after the PR/RCM sequence was dissolved in DCM (0.5 M), after which di-2-methoxyethyl azodicarboxylate (61.27 mg, 0.26 mmol, 1.1 equiv.) was added. Stirred the reaction in reflux for 0.5 h. Evaporated the solvent, purified as a brown oily liquid in 50.3% yield (*dr* 4:1) by column chromatography using 60% ethyl acetate in petroleum ether (Isocratic flow). ^{1}H NMR (600 MHz, $CDCl_3$) δ= 7.28-7.27 (m, 1H), 7.21 (d, *J* = 4.8 Hz, 1H), 7.04 (m, 1H), 7.00-6.98 (m, 1H), 6.90-6.89 (m, 1H), 6.87-6.84 (m, 1H), 5.48-5.44 (m, 1H), 4.90-4.86 (m, 1H), 4.53 (d, *J* = 16.8 Hz, 1H), 4.44-4.39 (m, 1H), 4.29-4.28 (m, 4H), 4.22-4.18 (m, 1H), 4.11 (m, 1H), 4.06-4.01 (m, 1H), 3.90-3.88 (m, 1H), 3.64 (m, 1H), 3.60 – 3.58 (m, 4H), 3.49-3.46 (m, 1H), 3.40 (m, 1H), 3.37-3.35 (m, 6H), 2.59-2.52 (1H, m), 2.06-2.01 (m, 1H). ^{13}C NMR (151 MHz, $CDCl_3$) δ= 156.56, 155.43, 146.29, 143.55, 134.97, 126.96, 126.46, 125.95, 125.73, 125.33, 125.21, 119.81, 77.37, 77.16, 76.95, 72.45, 70.61, 69.00, 65.61, 65.18, 59.02, 54.70, 53.19, 51.61, 38.98. HRMS-ESI (m/z): calculated for $[M+H]^+$ $C_{25}H_{34}N_3O_7S_2$, 552.1828; found, 552.1833.

Dibenzyl (7*R*,8*R*,9a*S*)-8-hydroxy-7-(thiophen-2-yl)-6-(thiophen-2-ylmethyl)-5,6,7,8,9,9a-hexahydro-1*H*-pyridazino[4,3-c]azepine-1,2(3*H*)-dicarboxylate (9m)

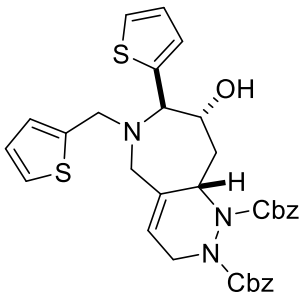

Compound **8b** (59 mg, 0.19 mmol, 1 equiv.), formed after the PR/RCM sequence was dissolved in DCM (0.5 M), after which dibenzyl azodicarboxylate (60.98 mg, 0.20 mmol, 1.1 equiv.) was added. The reaction mixture was heated to reflux and stirred for 0.5 h. Evaporated the solvent,

purified as a white powder in 64% yield (4:1 *dr*) by column chromatography using ethyl acetate in petroleum ether 30% isocratic flow). Major diastereomeric product: ^{1}H NMR (500 MHz, $CDCl_3$) δ= 7.35-7.29 (m, 10 H), 7.22 (m, 2H), 7.07 (m, 1H), 7.00 (m, 1H), 6.90 (m, 2H), 5.47 (m, 1H), 5.23-5.08 (m, 4H), 4.92 (m, 1H), 4.49 (dd, *J* = 63.9, 16.5 Hz, 1H), 4.16-4.08 (m, 2H), 3.91-3.71 (m, 3H), 3.55 – 3.34 (m, 2H), 2.50-2.47 (m, 1H), 1.95-1.93 (m, 1H). ^{13}C NMR (126 MHz, CDCl3) δ= 155.38, 155.21, 135.90, 128.71, 128.64, 128.61, 128.44, 128.36, 128.29, 128.21, 128.14, 127.83, 127.82, 127.06, 126.56, 125.63, 125.61, 125.60, 125.55, 72.04, 69.09, 68.27, 68.04, 54.65, 53.12, 51.68, 43.17. HRMS-ESI (m/z): calculated for $[M+H]^+$ $C_{33}H_{34}N_3O_5S_2$, 616.1934; found, 616.1924.

5.2.2 IRE1α inhibitors

5.2.2.1 Synthetic route A to obtain compounds 25, 31-34, 58-45:

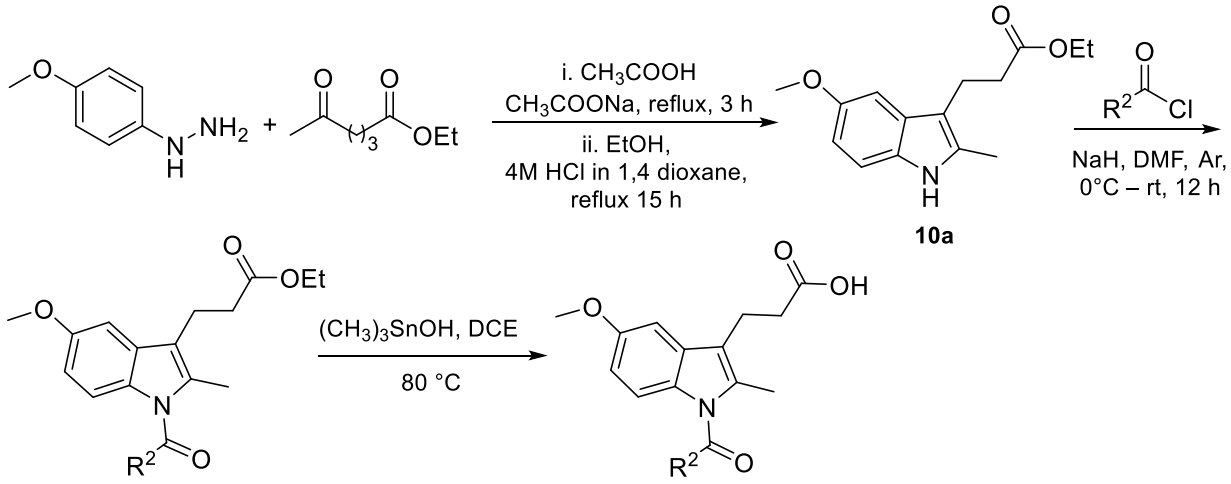

i. Ethyl 3-(5-methoxy-2-methyl-1*H*-indol-3-yl)propanoate (10a)

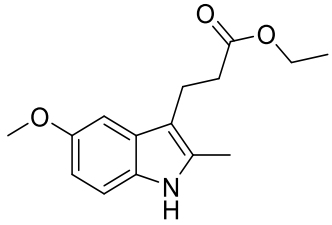

A stirred mixture containing 4-methoxyphenyl hydrazine hydrochloride (1.5 g, 8.59 mmol) and ethyl 4-acetylbutyrate (1.35 g, 8.59 mmol) was treated with sodium acetate (704.64 mg, 8.59 mmol) in glacial acetic acid (12 mL). The mixture was refluxed for 3 hours and subsequently concentrated under reduced pressure to afford a crude residue. This residue was dissolved in ethanol (7 mL), followed by the addition of 4 M HCl in 1,4-dioxane (5 mL), and the mixture was further heated under reflux for 15 hours. After evaporation under vacuum, the residue was

extracted with ethyl acetate and subjected to sequential washes with water, aqueous potassium carbonate, and brine. The combined organic extracts were dried over anhydrous magnesium sulfate, filtered, and concentrated. Final purification was achieved via flash chromatography on silica gel using 11% (v/v) ethyl acetate in petroleum ether as the mobile phase, affording ethyl 3-(5-methoxy-2-methyl-1*H*-indol-3-yl)propanoate as a pale brown oil (1.35 g, 60% yield). ^{1}H NMR (400 MHz, $CDCl_3$) δ = 7.67 (s, 1H), 7.14 (d, 1H, *J* = 8.8 Hz), 6.96-6.95 (m, 1H), 6.78-6.75 (m, 1H), 4.15-4.10 (m, 2H), 3.86 (s, 3H), 3.00 (t, 2H, *J* = 7.6 Hz), 2.60 (t, 2H, *J* = 7.6 Hz), 2.37 (s, 3H), 1.25-1.21 (m, 3H). Synthesized by using a modified literature procedure.[140]

ii. General procedure for *N*-acylated 3-(5-methoxy-2-methyl-1*H*-indol-3-yl) propanoic acid

To a round-bottom flask containing ethyl 3-(5-methoxy-2-methyl-1*H*-indol-3-yl)propanoate (130 mg, 0.50 mmol, 1.0 equiv) in 2 mL of DMF, maintained under an argon atmosphere at −20 °C. Sodium hydride (NaH, 60% dispersion in mineral oil, 30 mg, 0.75 mmol, 1.5 equiv) was added cautiously, and this suspension was stirred for 15 minutes. Subsequently, the acid chloride (2.0 equiv) was introduced to the reaction mixture. The mixture was then allowed to gradually come to room temperature and stirred overnight. Reaction progress was monitored by TLC or LC-MS. Upon completion, methanol was added dropwise to quench the reaction, and the resulting mixture was extracted with ethyl acetate. The combined organic extracts were dried over anhydrous magnesium sulfate, filtered, and concentrated under reduced pressure to yield the crude *N*-acylated product. This intermediate was dissolved in DCE, followed by the addition of trimethyltinhydroxide (2–4 equiv). The reaction mixture was heated to reflux until complete conversion, as verified by TLC or LC-MS. The solvent was then removed under vacuum, and the residue was redissolved in ethyl acetate. The organic layer was washed three times with 5% aqueous HCl, followed by a wash with 5 mL of brine. After drying over anhydrous magnesium sulfate, the solution was concentrated and subjected to flash chromatography using appropriate solvent systems, as specified for each individual.

5.2.2.2 Synthetic route B to obtain compounds 53-56, 59, 64-65:

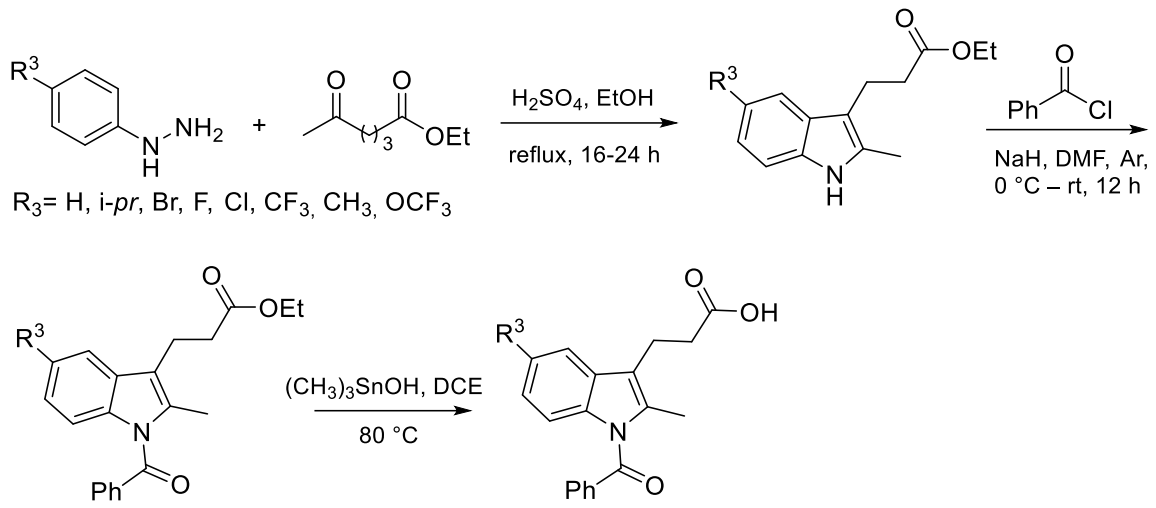

An equimolar mixture of 4-substituted phenylhydrazine hydrochloride and ethyl 4-acetylbutyrate was dissolved in ethanol (1.5 mL per mmol), followed by the addition of aqueous concentrated sulfuric acid (120 µL per mmol). The reaction mixture was heated under reflux for 16–24 hours. After cooling to ambient temperature, water (20 mL) was added, and the aqueous phase was extracted with ethyl acetate (3 × 10 mL). The combined organic layers were subsequently washed with 10% aqueous hydrochloric acid (10 mL), followed by saturated sodium bicarbonate solution (10 mL), dried over anhydrous magnesium sulfate, and concentrated under reduced pressure. The crude product was purified by flash column chromatography using 5–10% ethyl acetate in petroleum ether as the eluent, affording the corresponding indole derivative. The resulting intermediate was dissolved in DMF and cooled to −20 °C under an inert argon atmosphere. Sodium hydride (60% dispersion in mineral oil, 1.5 equivalents) was cautiously added, and the mixture was stirred for 15 minutes. Acid chloride (2 equivalents) was then introduced, and the reaction mixture was allowed to warm to room temperature and stirred overnight. Reaction progress was monitored by thin-layer chromatography (TLC) or LC-MS. Upon completion, the reaction was quenched with methanol and extracted with ethyl acetate. The combined organic extracts were dried over anhydrous magnesium sulfate and evaporated under vacuum to yield the N-acylated indole ester. This crude product was dissolved in 1,2-dichloroethane (DCE), and trimethyltinhydroxide (2–4 equivalents) was added. The mixture was heated under reflux until complete conversion was confirmed by TLC or LC-MS. After solvent removal under reduced pressure, the residue was taken up in ethyl acetate and washed three times with 5% aqueous hydrochloric acid, followed by a brine wash (5 mL). The organic phase was dried over

anhydrous magnesium sulfate, concentrated, and purified via flash chromatography using suitable solvent gradients specified under each respective final compound.

5.2.2.3 Synthetic route C to obtain 57-58, 60-63, 66-72:

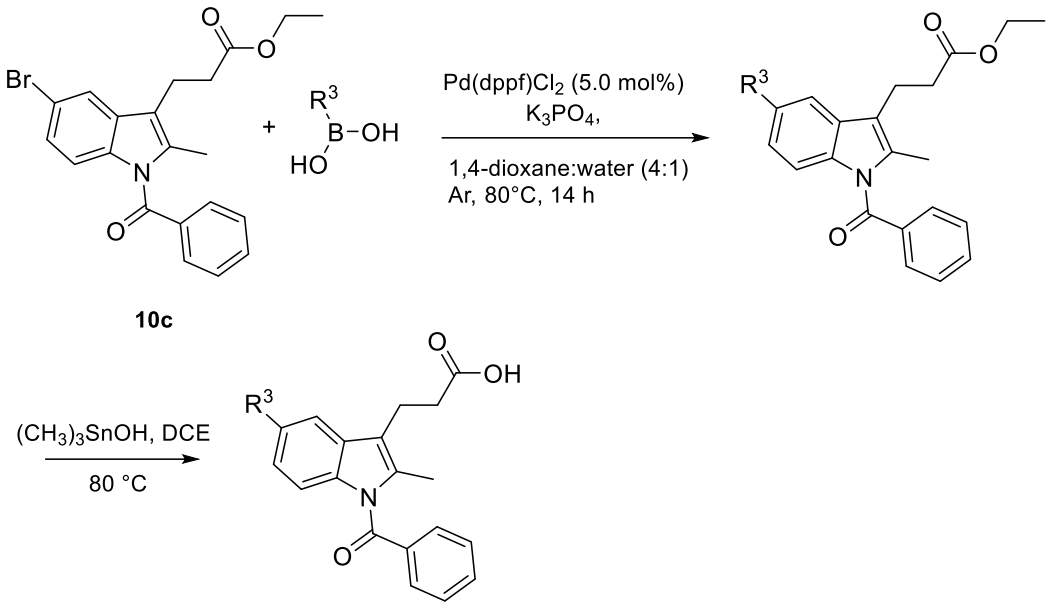

i. Ethyl 3-(5-bromo-2-methyl-1*H*-indol-3-yl) propanoate (10b)

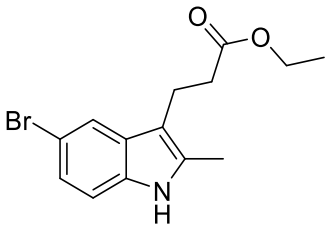

A stirred mixture containing 4-bromophenylhydrazine hydrochloride (1 equiv, 1000 mg, 4.47 mmol) and ethyl 4-acetylbutyrate (707. 814 mg, 1 equiv, 4.47 mmol, 715.69 µL) in ethanol (7 mL), conc. H_2SO_4 (aq) (0.675 mL) was added and stirred at reflux for 16 h. After allowing the reaction mixture to return to room temperature, water (20 mL) was added, and the aqueous phase was extracted with ethyl acetate (3 × 10 mL). The combined organic extracts were subsequently washed with 10% aqueous hydrochloric acid (10 mL), followed by saturated sodium bicarbonate solution (10 mL). The organic layer was dried over anhydrous magnesium sulfate and concentrated under reduced pressure. The crude residue was purified by flash column chromatography on silica gel using 8% ethyl acetate in petroleum ether as the eluent, affording ethyl 3-(5-bromo-2-methyl-1*H*-indol-3-yl)propanoate as a pale brown oil (723.30 mg, 52% yield).; ^{1}H NMR (600 MHz, $CDCl_3$) δ= 7.81 (s, 1H), 7.60 (d, 1H, *J* = 1.8 Hz), 7.18 (dd, 1H, *J*= 8.40, *J*= *J*= 8.4, 1.8 Hz), 7.11 (d, 1H, *J*= 8.4), 4.11 (q, 2H, *J* = 7.2 Hz), 2.98 (t, 2H,

J = 7.7 Hz), 2.59 (t, 2H, *J* = 7.8 Hz), 2.37 (s, 3H) 1.23 (t, 3H, *J* = 7.2 Hz). ^{13}C NMR (151 MHz, $CDCl_3$) δ= 173.41, 133.98, 132.93, 130.28, 123.83, 120.60, 112.60, 111.74, 110.24, 60.56, 35.24, 19.70, 14.33, 11.77. Prepared using modified literature procedure.[141]

ii. Ethyl 3-(1-benzoyl-5-bromo-2-methyl-1*H*-indol-3-yl) propanoate (10c)

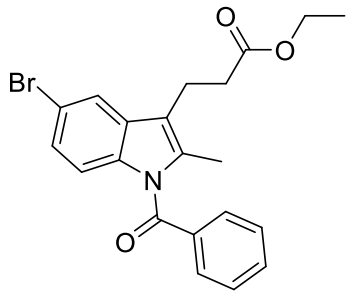

To a round-bottom flask containing ethyl 3-(5-bromo-2-methyl-1*H*-indol-3-yl)propanoate (1 equiv, 853.0 mg, 2.75 mmol) in 5 mL DMF, maintained under an argon atmosphere at -20˚C, sodium hydride (NaH) (60%, 1.5 equiv, 4.12 mmol, 164.98 mg) was carefully added. The mixture was stirred for 15 minutes. Benzoyl chloride (2.0 equivalents) was subsequently introduced, and the mixture was allowed to gradually reach room temperature and stirred overnight. Reaction progress was monitored by thin-layer chromatography (TLC) or LC-MS. Upon completion, the reaction was quenched with methanol and extracted with ethyl acetate. The combined organic extracts were dried over anhydrous magnesium sulfate, filtered, and concentrated under reduced pressure. The crude product was purified by flash column chromatography using 6% ethyl acetate in petroleum ether as the eluent, affording ethyl 3-(1-benzoyl-5-bromo-2-methyl-1H-indol-3-yl)propanoate as a bright yellow oil (865.86 mg, 76% yield).; ^{1}H NMR (700 MHz, $CDCl_3$) δ = 7.69-7.67 (m, 2H), 7.65-7.63 (m, 1H), 7.59 (d, 1H, *J* = 1.4 Hz), 7.51-7.46 (m, 2H), 7.12 (dd, 1H, *J* = 9.1, 2.1 Hz), 6.87 (d, 1H, *J* = 8.8 Hz), 4.14 (q, 2H, *J* = 7.0 Hz), 3.00-2.98 (m, 2H), 2.61 (t, 2H, *J* = 7.7 Hz), 2.34 (s, 3H), 1.25 (t, 3H, *J* = 7.0 Hz). ^{13}C NMR (176 MHz, $CDCl_3$) δ= 172.86, 169.60, 135.39, 135.37, 135.34, 133.28, 131.49, 129.89, 128.99, 125.80, 120.85, 117.14, 115.91, 115.73, 60.77, 34.42, 19.57, 14.35, 13.21. HRMS (ESI): m/z calculated for $C_{21}H_{21}BrNO_3$ $[M+H]^+$:414.0700, found: 414.0697.

iii. General procedure for 5-substituted 3-(1-benzoyl-2-methyl-1*H*-indol-3-yl) propanoic acid

Compound **10c** (1 equiv), corresponding boronic acid (1.5 equiv), [1,1'-Bis(diphenylphosphino)ferrocene]dichloropalladium(II) ($Pd(dppf)Cl_2$) (5.0 mol%), and potassium phosphate tribasic (K_3PO_4) (2.0 equiv) were charged in a Schlenk. A degassed mixture of 1,4-dioxane and water (4:1 v/v) was added, and the reaction was carried out under

an argon atmosphere at 80 °C. The progress of the reaction was monitored by thin-layer chromatography (TLC) and LC-MS. Upon completion, the reaction mixture was diluted with ethyl acetate and passed through a Celite pad. The celite was washed with additional ethyl acetate, and the combined organic filtrates were collected. The organic layer was washed sequentially with water and brine, dried over anhydrous magnesium sulfate, filtered, and concentrated under reduced pressure. The crude product was dissolved in a minimal volume of ethyl acetate and purified by passage through a short silica plug. After solvent removal, the resulting intermediate was directly employed in the subsequent step without additional purification.

The resulting intermediate (1.0 equiv) was dissolved in DCE, and trimethyltinhydroxide (2–4 equiv) was added. The mixture was refluxed until complete conversion, as determined by TLC or LC-MS analysis. After reaction completion, the solvent was removed under reduced pressure, and the residue was dissolved in ethyl acetate. The organic phase was washed three times with 5% aqueous hydrochloric acid, followed by a single wash with 5 mL of brine. The organic layer was dried over anhydrous magnesium sulfate, filtered, and concentrated. Final purification was achieved via flash chromatography using appropriate solvent gradients, as detailed for each final compound.

3-(1-(4-Chlorobenzoyl)-5-methoxy-2-methyl-1*H*-indol-3-yl)propanoic acid (10)

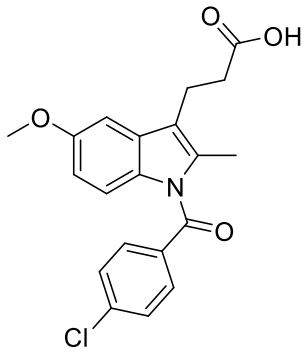

The aldehyde-functionalized resin (500 mg, 0.55 mmol, 1.0 equiv) was dried under high vacuum overnight and subsequently suspended in 5 mL of DCE. Under an argon atmosphere, (4-methoxyphenyl)hydrazine hydrochloride (384.19 mg, 2.22 mmol, 4.0 equiv) and triethylamine (162.55 mg, 2.75 mmol, 242.61 µL, 5.0 equiv) were added to the suspension. The reaction mixture was stirred at 45 °C overnight. Upon cooling to room temperature, the resin was filtered and sequentially washed three times with 5 mL each of DMF, 90:10 DMF/H_2O (v/v), DMF, dichloromethane, ethyl acetate, and methanol.

The resulting hydrazone resin (500 mg, 0.47 mmol) was again dried under high vacuum overnight and suspended in 5 mL of pyridine. To this mixture, 4-chlorobenzoyl chloride (987.06 mg, 5.64 mmol, 723.12 µL, 12.0 equiv) was added under an argon atmosphere. The reaction was allowed to proceed with shaking at 80 °C overnight. After cooling, the resin was filtered and washed as previously described using 5 mL portions of DMF, 90:10 DMF/H_2O, DMF, dichloromethane, ethyl acetate, and methanol (three times each).

Subsequently, the acylated hydrazone resin (150 mg, 0.13 mmol) was suspended in 6 mL of a 1:1 mixture of DCE and trifluoroacetic acid (TFA). 5-Oxohexanoic acid (327.20 mg, 1.26 mmol, 20.0 equiv) was added, and the reaction mixture was heated at 70 °C for 2 hours. After cooling, the resin was filtered and washed three times each with 5 mL of dichloromethane, ethyl acetate, and methanol. The combined filtrates were evaporated to dryness, and the crude product was purified by preparative HPLC using a water/acetonitrile gradient system to afford the title compound as a white solid (65 mg, 67% yield). ^{1}H NMR (DMSO-d_6, 500 MHz) δ= 12.17 (bs, 1H), 7.67-7.62 (m, 4H), 7.07 (d, 1H, *J* = 2.5 Hz), 6.94 (d, 1H, *J* = 9.0 Hz), 6.70 (dd, 1H, *J* = 9.0, 2.5 Hz), 3.78 (s, 3H), 2.89 (t, 2H, *J* = 7.5 Hz), 2.48 (m, 2H), 2.20 (s, 3H). The analytical data were consistent with those reported in the literature.[131]

3-(5-Methoxy-2-methyl-1-(thiophene-2-carbonyl)-1*H*-indol-3-yl)propanoic acid (25):

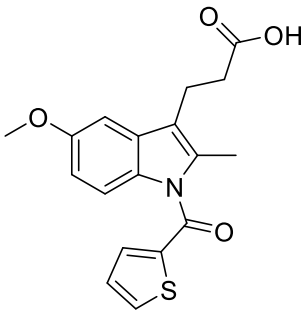

The compound **25** was synthesized following synthetic route A, employing ethyl 3-(5-methoxy-2-methyl-1-(thiophene-2-carbonyl)-1*H*-indol-3-yl)propanoate (0.29 mmol) and trimethyltinhydroxide (0.59 mmol). The crude product was purified by flash column chromatography using 5% methanol in dichloromethane (v/v) as the eluent, affording the target compound as a white powder (72 mg, 71.5% yield).; ^{1}H NMR ($CDCl_3$, 600 MHz) δ= 7.72 (1H, dd, *J* = 4.9, 0.9 Hz), 7.53 (1H, dd, *J* = 3.7, 0.9 Hz), 7.14-7.12 (m, 2H), 6.93 (1H, d, *J* = 2.5 Hz), 6.70 (1H, dd, *J* = 9.0, 2.5 Hz), 3.85 (3H, s), 3.03 (2H, t, *J* = 7.7 Hz), 2.70 (2H, t, *J* = 7.7 Hz), 2.41 (3H, s). Data were consistent with those reported in the literature.[131]

3-(1-(4-(Fluorosulfonyl)benzoyl)-5-methoxy-2-methyl-1*H*-indol-3-yl)propanoic acid (27):

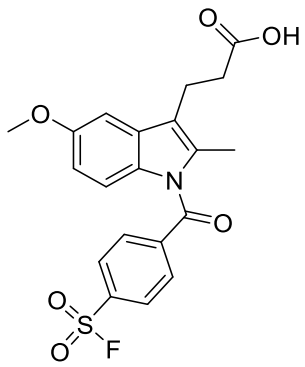

The compound **27** was synthesized following a procedure analogous to that described for compound **10** to afford pure product as a yellow powder (10.26 mg, 18% yield); ^{1}H NMR ($CDCl_3$, 500 MHz), δ= 8.06 (d, 2H, *J*= 8.5 Hz), 7.83 (d, 2H, *J*= 8.5 Hz), 6.86 (d, 1H, *J*= 2.5 Hz), 6.83 (d, 1H, *J*= 9 Hz), 6.62 (dd, 1H, *J*= 9 Hz, *J*= 2.5 Hz), 3.77 (s, 3H), 2.93 (t, 2H, *J*= 7.5 Hz), 2.62 (t, 2H, *J*= 7.5 Hz), 2.23 (s, 3H). ^{13}C NMR (126 MHz, $CDCl_3$) δ= 177.06, 167.02, 156.63, 142.65, 136.26 (d, *J*= 25.2), 134.45, 131.04, 130.88, 130.64 (d, 2C, *J*= 39.06 Hz), 129.1 (s, 2C), 119.06, 115.36, 111.75, 101.83, 55.92, 33.47, 19.39, 13.83. ^{19}F NMR (470 MHz, CDCl3) δ= -75.82. HRMS (ESI): m/z calculated for $C_{20}H_{18}FNO_6SNa$ $[M+Na]^+$: 442.0732 found: 442.0732.

3-(1-(Benzo[b]thiophene-2-carbonyl)-5-methoxy-2-methyl-1*H*-indol-3-yl)propanoic acid (28)

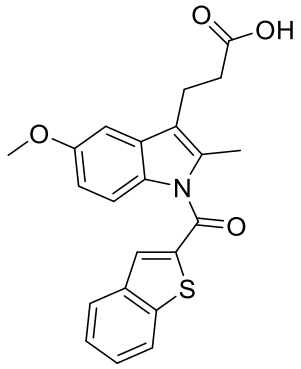

The compound **28** was synthesized following a procedure analogous to that described for compound **10** to afford pure product as a yellow powder (4 mg, 8% yield); ^{1}H NMR ($CDCl_3$, 500 MHz), δ= 7.93 (d, 1H, *J*= 8.0 Hz), 7.83 (d, 1H, *J*= 8.0 Hz), 7.77 (s, 1H), 7.50 (m,1H), 7.43 (m,1H), 7.20 (d, 1H, *J*= 9.0 Hz), 6.95 (d, 1H, *J*= 2.5 Hz), 6.69 (dd, 1H, *J*= 9 Hz, *J*= 2.5 Hz), 3.85 (s, 3H), 3.05 (t, 2H, *J*= 7.5 Hz), 2.71 (t, 2H, *J*= 7.5 Hz), 2.45 (s, 3H). ^{13}C NMR (126 MHz, $CDCl_3$) δ 177.14, 163.60, 156.07, 142.58, 138.57, 138.15, 134.78, 131.73, 131.39, 130.50,

127.57, 126.02, 125.40, 123.04, 117.53, 114.95, 111.50, 101.14, 55.93, 33.71, 19.51, 12.98. HRMS (ESI): m/z calculated for $C_{22}H_{20}NO_4S$ $[M+H]^+$: 394.1108 found: 394.1105.

3-(1-(3-Cyanobenzoyl)-5-methoxy-2-methyl-1*H*-indol-3-yl)propanoic acid (29)

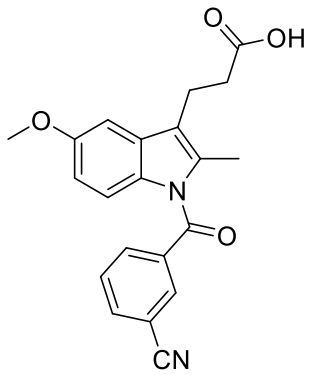

The compound **29** was synthesized following a procedure analogous to that described for compound **10** to afford pure product as a yellow powder (11.9 mg, 12.1 % yield); ^{1}H NMR ($CDCl_3$, 500 MHz), δ= 7.97 (t, 1H, *J*= 1.5 Hz), 7.92-7.88 (m, 2H) 7.65-7.62 (m, 1H), 6.94 (d, 1H, *J*= 1.5 Hz), 6.85 (d, 1H, *J*= 9.0 Hz) 6.67 (dd, 1H, *J*= 9.0 Hz, J= 2.5 Hz), 3.85 (s, 3H), 3.01 (t, 2H, *J*= 7.5 Hz), 2.69 (t, 2H, *J*= 7.5 Hz), 2.33 (s, 3H). ^{13}C NMR (126 MHz, $CDCl_3$) δ= 177.38, 167.18, 156.43, 137.27, 135.74, 134.58, 133.66, 133.15, 130.91, 129.91, 118.65, 117.72, 115.16, 113.49, 111.69, 101.64, 55.92, 33.59, 19.39, 13.61. HRMS (ESI): m/z calculated for $C_{21}H_{19}N_2O_4$ $[M+H]^+$: 363.1339 found: 363.1340.

3-(1-(9,10-Dioxo-9,10-dihydroanthracene-2-carbonyl)-5-methoxy-2-methyl-1*H*-indol-3-yl)propanoic acid (30)

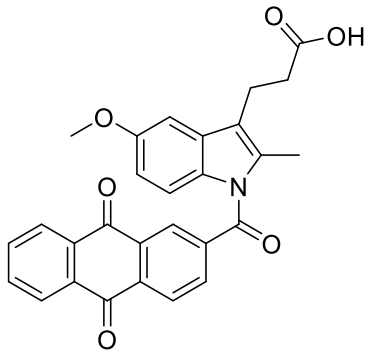

The compound **28** was synthesized following a procedure analogous to that described for compound **10** to afford pure product as a yellow powder (7.0 mg, 8% yield); ^{1}H NMR ($CDCl_3$, 600 MHz) δ= 8.47-8.46 (m, 2H), 8.37-8.33 (m, 2H), 8.16-8.14 (m, 1H), 7.88-7.83 (m, 2H), 7.16 (d, 1H, *J*= 9.0 Hz), 6.95 (d, 1H, *J*= 2.4 Hz), 6.70 (dd, 1H, *J*= 9.0 Hz, *J*= 2.4 Hz), 3.85 (s,

3H), 3.03 (t, 2H, *J*= 7.5 Hz), 2.72 (t, 2H, *J*= 7.5 Hz), 2.26 (s, 3H). ^{13}C NMR (151 MHz, $CDCl_3$) δ= 182.67, 182.44, 174.83, 167.67, 156.54, 141.17, 135.76, 134.86, 134.75, 134.51, 134.08, 133.68, 133.57, 133.50, 131.20, 130.85, 128.53, 128.25, 127.79, 127.70, 119.04, 115.30, 111.84, 101.63, 55.93, 33.31, 19.76, 14.16. HRMS (ESI): m/z calculated for $C_{28}H_{22}NO_6$ $[M+H]^+$: 468.1442, found: 468.1444.

3-(1-(2-Naphthoyl)-5-methoxy-2-methyl-1*H*-indol-3-yl)propanoic acid (31)

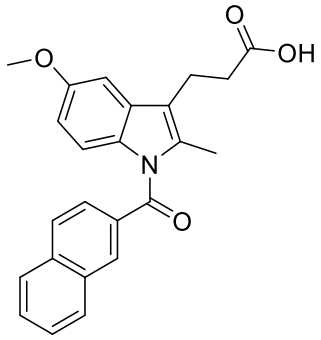

The compound **31** was synthesized following synthetic route A, employing ethyl 3-(1-(2-naphthoyl)-5-methoxy-2-methyl-1*H*-indol-3-yl)propanoate (0.15 mmol) and trimethyltin hydroxide (0.44 mmol). The crude product was purified by flash chromatography using ethyl acetate in petroleum ether (20% v/v) as the eluent, affording the target compound as a white powder (51.46 mg, 90% yield); ^{1}H NMR ($CDCl_3$, 500 MHz) δ= 8.24 (s, 1H), 7.95-7.90 (m, 3H), 7.75 (dd, 1H, *J*= 8.5 Hz, *J*= 1.7 Hz), 7.65-7.55 (m, 2H), 6.95 (d, 1H, *J* = 2.5 Hz), 6.91 (d, 1H, *J* = 9.0 Hz), 6.61 (dd, 1H, *J*= 9.0 Hz, J= 2.5 Hz), 3.84 (s, 3H), 3.05 (t, 2H, *J*= 7.7 Hz), 2.71 (t, 2H, *J*= 7.7 Hz), 2.38 (s, 3H). ^{13}C NMR ($CDCl_3$, 126 MHz) δ= 178.06, 169.69, 156.00, 135.43, 135.06, 133.07, 132.64, 131.41, 131.19, 130.57, 129.42, 128.78, 128.65, 128.08, 127.20, 125.67, 117.51, 115.33, 111.40, 101.15, 55.90, 33.90, 19.49, 13.41. HRMS (ESI): m/z calculated for $C_{24}H_{21}NO_4Na$ $[M+Na]^+$: 410.1363 found: 410.1356.

3-(5-Methoxy-2-methyl-1-(3-(trifluoromethyl)benzoyl)-1*H*-indol-3-yl)propanoic acid (32)

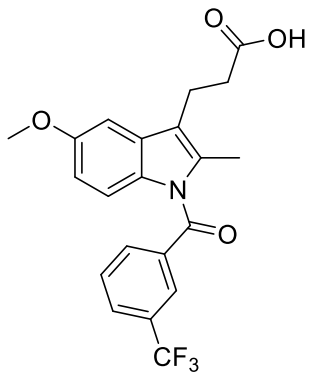

Compound **32** was synthesized by following synthetic route A, employing ethyl 3-(5-methoxy-2-methyl-1-(3-(trifluoromethyl)benzoyl)-1*H*-indol-3-yl)propanoate (0.05 mmol) and trimethyltin hydroxide (0.20 mmol). The crude product was purified by flash chromatography using ethyl acetate in petroleum ether (25% v/v) as the eluent, affording the target compound as a white powder (18 mg, 87.4% yield); ^{1}H NMR ($CDCl_3$, 600 MHz), δ= 7.98 (s, 1H), 7.86 (pseudo t, 2H, *J* = 7.8 Hz), 7.63 (t, 1H, *J* = 7.8 Hz), 6.94 (d, 1H, *J* = 2.4 Hz), 6.91 (d, 1H, *J* = 9.0 Hz), 6.68 (dd, 1H, *J* = 9.0 Hz, *J* =3.0 Hz), 3.85 (s, 3H), 3.02 (t, 2H, *J*= 7.8 Hz), 2.69 (t, 2H, *J*= 7.8 Hz), 2.32 (s, 3H). ^{13}C NMR (151 MHz, $CDCl_3$) δ= 178.65, 168.02, 156.3, 136.74, 134.61, 132.93, 131.59 (q, *J* = 33.2 Hz), 131.06, 130.80, 129.51, 129.24 (q, *J* = 3.0 Hz), 126.63 (q, *J* = 3.7 Hz), 123.62 (q, *J* = 272.6 Hz), 118.34, 115.24, 111.63, 101.42, 55.89, 33.83, 19.39, 13.58. ^{19}F NMR (565 MHz, $CDCl_3$) δ= -62.79. HRMS (ESI): m/z calculated for $C_{21}H_{18}F_3NO_4Na$ $[M+Na]^+$: 428.1081, found: 428.1076.

3-(1-Benzoyl-5-methoxy-2-methyl-1*H*-indol-3-yl)propanoic acid (33)

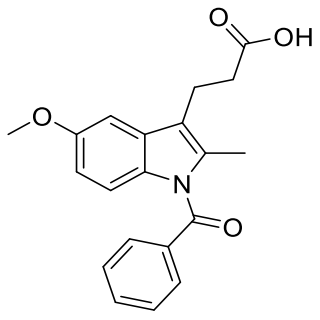

Compound **33** was synthesized by following synthetic route A, employing ethyl 3-(1-benzoyl-5-methoxy-2-methyl-1*H*-indol-3-yl)propanoate (0.33 mmol) and trimethyltin hydroxide (0.99 mmol). The crude product was purified by flash chromatography using methanol in

dichloromethane (5% v/v) as the eluent, affording the target compound as a white powder (109.68 mg, quant. yield); ^{1}H NMR ($CDCl_3$, 700 MHz), δ= 7.69-7.68 (m, 2H), 7.62-7.20 (m,1H), 7.47-7.49 (m, 2H), 6.93 (d, 1H, *J* = 2.8 Hz), 6.90 (d, 1H, *J* = 9.1 Hz), 6.65 (dd, 1H, *J*= 9.1 Hz, *J*= 2.8 Hz), 3.84 (s, 3H), 3.02 (t, 2H, *J*= 7.7 Hz), 2.68 (t, 2H, *J*= 7.7 Hz), 2.34 (s, 3H). ^{13}C NMR (176 MHz, $CDCl_3$) δ= 177.54, 169.68, 156.00, 135.94, 134.94, 132.83, 131.34, 130.57, 129.77, 128.87, 117.52, 115.34, 111.34, 101.11, 55.90, 33.77, 19.45, 13.39. HRMS (ESI): m/z calculated for $C_{20}H_{19}NO_4Na[M+Na]^+$: 360.1207, found: 360.1202.

3-(1-(4-Fluorobenzoyl)-5-methoxy-2-methyl-1*H*-indol-3-yl)propanoic acid (34)

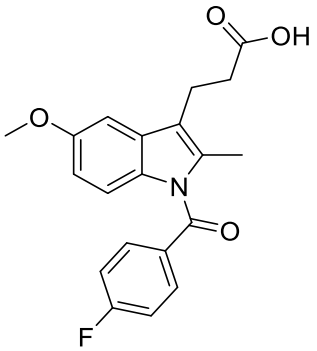

Compound **34** was synthesized by following synthetic route A, employing ethyl 3-(1-(4-fluorobenzoyl)-5-methoxy-2-methyl-1*H*-indol-3-yl)propanoate (0.25 mmol) and trimethyltin hydroxide (0.99 mmol). The crude product was purified by flash chromatography using ethyl acetate in petroleum ether (19 % v/v) as the eluent, affording the target compound as a yellow powder (40 mg, 45.49 % yield); ^{1}H NMR ($CDCl_3$, 600 MHz) δ= 7.74-7.71 (m, 2H), 7.18-7.15 (m, 2H), 6.93 (d, 1H, *J* = 2.5 Hz), 6.87 (d, 1H, *J* = 9.0 Hz), 6.66 (dd, 1H, *J* = 9.0, 2.5 Hz), 3.84 (s, 3H), 3.02 (t, 2H, *J* = 7.7 Hz), 2.69 (t, 2H, *J* = 7.7 Hz), 2.36 (s, 3H). ^{13}C NMR (151 MHz, $CDCl_3$) δ= 178.02, 168.42, 165.61 (d, *J* = 254.8 Hz), 156.05, 134.89, 132.49 (d, *J* = 9.2 Hz), 131.97 (d, 2C, *J* = 3.2 Hz), 131.25, 130.57, 117.61, 116.14 (d, 2C, *J* = 22.1 Hz), 115.13, 111.41, 101.22, 55.90, 33.83, 19.43, 13.31. HRMS (ESI): m/z calculated for $C_{20}H_{19}FNO_4$ $[M+H]^+$: 356.1293, found: 356.1294.

3-(1-(4-(Dimethylamino)benzoyl)-5-methoxy-2-methyl-1*H*-indol-3-yl)propanoic acid (35)

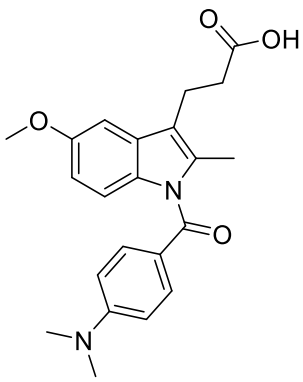

The synthesis of compound **35** was carried out according to reported procedure,[131] to afford pure product as a yellow crystalline powder (6 mg, 14% yield); ^{1}H NMR ($CDCl_3$, 700 MHz), δ= 7.63 (d, 2H, *J* = 8.9 Hz), 6.98 (d, 1H, *J* = 8.9 Hz), 6.93 (d, 1H, *J* = 2.4 Hz), 6.67-6.65 (m, 3H), 3.84 (s, 3H), 3.08 (s, 6H), 3.03 (t, 2H, *J* = 7.8 Hz), 2.69 (t, 2H, *J* = 7.8 Hz), 2.39 (s, 3H). ^{13}C NMR (176 MHz, $CDCl_3$) δ= 178.27, 169.29, 155.40, 153.73, 135.08, 132.85, 131.74, 129.92, 121.51, 115.83, 114.79, 111.07, 110.89, 100.63, 55.92, 40.20, 34.16, 19.57, 12.81. HRMS (ESI): m/z calculated for $C_{22}H_{25}N_2O_4$ $[M+H]^+$: 381.1809, found: 381.1805.

3-(1-([1,1'-Biphenyl]-4-carbonyl)-5-methoxy-2-methyl-1*H*-indol-3-yl)propanoic acid (37)

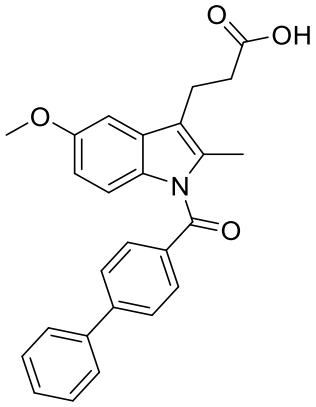

The synthesis of compound **37** was carried out according to reported procedure,[131] to afford pure product as a yellow powder (6 mg, 14% yield); ^{1}H NMR ($CDCl_3$, 700 MHz), δ= 7.78 (d, 2H, *J* = 8.4 Hz), 7.71 (d, 2H, *J* = 8.4), 7.66 (d, 2H, *J* = 7.7 Hz), 7.49 (t, 2H, *J* = 7.7 Hz), 7.42 (m, 1H), 6.98 (d, 1H, *J* = 9.1 Hz), 6.94 (d, 1H, *J* = 2.1 Hz), 6.67 (dd, 1H, *J* = 9.1, 2.1 Hz), 3.85 (s, 3H), 3.03 (t, 2H, *J* = 7.7 Hz), 2.70 (t, 2H, *J* = 7.7 Hz), 2.39 (s, 3H). ^{13}C NMR (176 MHz, $CDCl_3$) δ= 177.48, 169.40, 155.99, 145.69, 139.83, 134.98, 134.45, 131.35, 130.55, 130.52, 129.17, 128.50, 127.45, 127.43, 117.44, 115.31, 111.35, 101.13, 55.91, 33.79, 19.48, 13.39. The analytical data were consistent with those reported in the literature.[131]

3-(1-(Dimethylcarbamoyl)-5-methoxy-2-methyl-1*H*-indol-3-yl)propanoic acid (38)

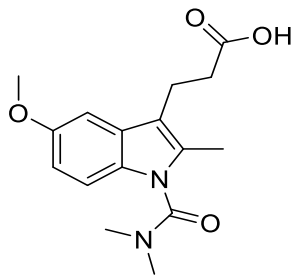

Compound **38** was synthesized by following synthetic route A, employing ethyl 3-(1-(dimethylcarbamoyl)-5-methoxy-2-methyl-1*H*-indol-3-yl)propanoate (0.15 mmol) and trimethyltin hydroxide (0.60 mmol). The crude product was purified by flash chromatography using methanol in dichloromethane (50 % v/v) as the eluent, affording the target compound as a colorless oil (40 mg, 87% yield); ^{1}H NMR ($CDCl_3$,500 MHz) δ= 7.09 (d, 1H, *J* = 9 Hz), 6.94 (d, 1H, *J* = 2.0 Hz), 6.82 (dd, 1H, *J* = 9, *J* = 2.5 Hz), 3.85 (s, 3H), 3.00 (m, 6H), 3.00-2.98 (2H, m), 2.64 (t, 2H, *J*= 8 Hz), 2.38 (s, 3H). ^{13}C NMR ($CDCl_3$, 126 MHz) δ= 178.88, 155.02, 154.77, 133.39, 129.95, 129.11, 113.54, 111.90, 111.52, 100.97, 55.98, 37.95, 37.89, 34.48, 19.53, 11.05. HRMS (ESI): m/z calculated for $C_{16}H_{21}N_2O_4$ $[M+H]^+$: 305.1496 found: 305.1498.

3-(5-Methoxy-2-methyl-1-(morpholine-4-carbonyl)-1*H*-indol-3-yl)propanoic acid (39)

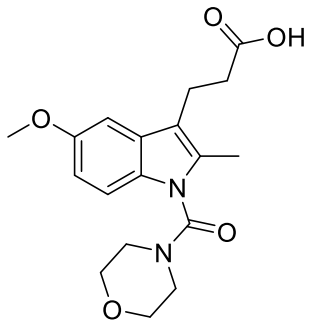

Compound **39** was synthesized by following synthetic route A, employing ethyl 3-(5-methoxy-2-methyl-1-(morpholine-4-carbonyl)-1*H*-indol-3-yl)propanoate (0.36 mmol) and trimethyltin hydroxide (1.44 mmol). The crude product was purified by flash chromatography using methanol in dichloromethane (4 % v/v) as the eluent, affording the target compound as a white powder (56 mg, 45% yield); ^{1}H NMR ($CDCl_3$,600 MHz) δ= 7.19 (d, 1H, *J* = 9 Hz), 6.94 (d, 1H, *J* = 2.4 Hz), 6.83 (dd, 1H, *J* = 9, *J* =2.4 Hz), 3.85 (s, 3H), 3.77-3.68 (m, 4H), 3.51 (bs, 4H), 2.99 (t, 2H, *J*= 7.7 Hz), 2.64 (t, 2H, *J*= 7.7 Hz), 2.34 (s, 3H). ^{13}C NMR (151 MHz, $CDCl_3$) δ= 178.69, 155.23, 153.65, 133.43, 129.77, 129.22, 114.03, 111.70, 111.63, 101.13, 66.94, 55.95,

46.54, 34.37, 19.49, 11.20. HRMS (ESI): m/z calculated for $C_{18}H_{23}N_2O_5$ $[M+H]^+$: 347.1602 found: 347.1603.

3-(5-Methoxy-2-methyl-1-(tetrahydro-2*H*-pyran-4-carbonyl)-1*H*-indol-3-yl)propanoic acid (40)

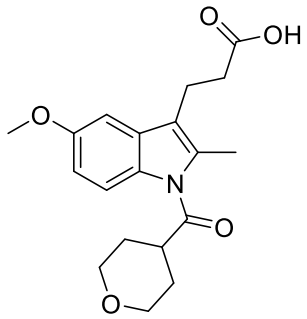

Compound **40** was synthesized by following synthetic route A, employing ethyl 3-(5-methoxy-2-methyl-1-(tetrahydro-2*H*-pyran-4-carbonyl)-1*H*-indol-3-yl)propanoate (0.30 mmol) and trimethyltin hydroxide (0.87 mmol). The crude product was purified by flash chromatography using methanol in dichloromethane (2 % v/v) as the eluent, affordingthe target compound as a white powder (44 mg, 43% yield); ^{1}H NMR ($CDCl_3$, 500 MHz) δ= 7.66 (d, 1H, *J* = 9 Hz), 6.96 (d, 1H, *J* = 2.5 Hz), 6.86 (dd, 1H, *J* = 9, *J* =2.5 Hz), 4.07 (dt, 2H, *J* = 11.5, *J* = 3.5 Hz), 3.87 (s, 3H), 3.55 (td, 2H, *J* = 11.5, *J* = 2.0 Hz), 3.49-3.45 (m, 1H), 2.98 (t, 2H, *J*= 8.0 Hz), 2.63 (t, 2H, *J*= 7.5 Hz), 2.55 (s, 3H), 2.07-1.98 (m, 2H), 1.90-1.87 (m, 2H). ^{13}C NMR (126 MHz, $CDCl_3$) δ= 178.53, 175.35, 156.12, 134.34, 131.06, 130.09, 117.90, 115.16, 111.90, 101.52, 67.17, 67.10, 55.89, 42.65, 33.96, 29.35, 28.51, 19.38, 14.24. HRMS (ESI): m/z calculated for $C_{19}H_{23}NO_4Na$ $[M+Na]^+$: 368.1469 found: 368.1486.

3-(1-(Cyclopropanecarbonyl)-5-methoxy-2-methyl-1*H*-indol-3-yl)propanoic acid (41)

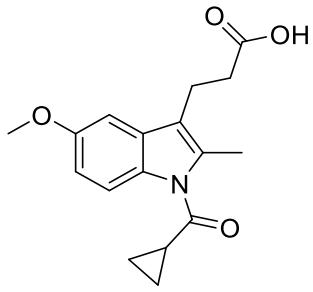

Compound **41** was synthesized by following synthetic route A, employing ethyl 3-(1-(cyclopropanecarbonyl)-5-methoxy-2-methyl-1*H*-indol-3-yl)propanoate (0.29 mmol) and trimethyltin hydroxide (1.14 mmol). The crude product was purified by flash chromatography

using ethyl acetate in petroleum ether (34 % v/v) as the eluent, affording the target compound as a white powder (77.39 mg, 90% yield); ^{1}H NMR ($CDCl_3$, 700 MHz) δ= 7.85 (d, 1H, *J* = 9 Hz), 6.94 (d, 1H, *J* = 2.5 Hz), 6.84 (dd, 1H, *J* = 9.0, *J* = 2.5 Hz), 3.87 (s, 3H), 3.00 (t, 2H, *J*= 7.7 Hz), 2.65 (t, 2H, *J*= 7.7Hz), 2.56 (s, 3H), 2.35 (tt, 1H, *J* = 7.9, 4.6 Hz), 1.40 – 1.37 (m, 2H), 1.16-1.32 (m, 2H). ^{13}C NMR (176 MHz, $CDCl_3$) δ= 178.26, 174.20, 155.99, 134.36, 130.80, 130.41, 116.87, 115.25, 111.60, 101.25, 55.92, 33.99, 19.37, 17.78, 13.73, 10.89. HRMS (ESI): m/z calculated for $C_{17}H_{19}NO_4$ $[M+Na]^+$: 324.1206 found: 324.1208.

3-(5-Methoxy-2-methyl-1-(piperidine-1-carbonyl)-1*H*-indol-3-yl)propanoic acid (42)

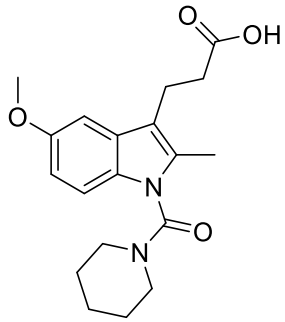

Compound **42** was synthesized by following synthetic route A, employing ethyl 3-(5-methoxy-2-methyl-1-(piperidine-1-carbonyl)-1*H*-indol-3-yl)propanoate (0.26 mmol) and trimethyltin hydroxide (1.03 mmol). The crude product was purified by flash chromatography using ethyl acetate in petroleum ether (35 % v/v) as the eluent, affording the target product as a colorless gummy solid (26 mg, 29% yield); ^{1}H NMR ($CDCl_3$, 500 MHz) δ= 7.16 (d, 1H, *J* = 8.5 Hz), 6.94 (d, 1H, *J* = 2.0 Hz), 6.81 (dd, 1H, *J* = 8.5, *J* = 2.0 Hz), 3.853 (s, 3H), 3.49-3.38 (m, 4H), 3.00 (t, 2H, *J*= 7.7 Hz), 2.65 (t, 2H, *J*= 7.7Hz), 2.39 (s, 3H), 1.68-1.56 (s, 6H). ^{13}C NMR (126 MHz, $CDCl_3$) δ= 178.74, 155.03, 153.47, 133.43, 130.11, 129.00, 113.35, 111.77, 111.44, 100.87, 55.99, 48.08, 47.26, 34.48, 26.31, 25.90, 24.47, 19.57, 11.10. HRMS (ESI): m/z calculated for $C_{19}H_{25}N_2O_4$ $[M+H]^+$: 345.1809 found: 345.1802.

3-(5-Mthoxy-2-methyl-1-(4,7,7-trimethyl-3-oxo-2-oxabicyclo[2.2.1]heptane-1-carbonyl)-1*H*-indol-3-yl)propanoic acid (43)

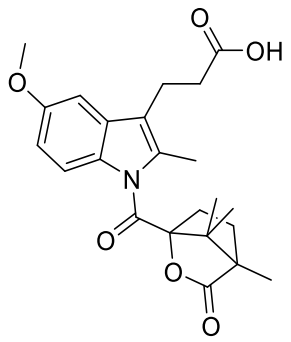

Compound **43** was synthesized by following synthetic route A, employing ethyl 3-(5-methoxy-2-methyl-1-(4,7,7-trimethyl-3-oxo-2-oxabicyclo[2.2.1]heptane-1-carbonyl)-1*H*-indol-3-yl)propanoate (0.18 mmol) and trimethyltin hydroxide (0.72 mmol). The crude product was purified by flash chromatography using methanol in dichloromethane (7 % v/v) as the eluent, affording the target product as a brown powder (40 mg, 53% yield); ^{1}H NMR (700 MHz, $CDCl_3$) δ= δ 7.55 (d, 1H, *J* = 9.0 Hz), 6.89 (d, 1H, *J* = 2.5 Hz), 6.82 (dd, 1H, *J* = 9.0, 2.5 Hz), 3.85 (s, 3H), 2.98 (t, 2H, *J* = 7.7 Hz), 2.65 (m, 2H), 2.61-2.58 and 2.10-2.06 (2m, 2H), 2.43-2.39 and 1.86-1.82 (m, 2H), 2.41 (s, 3H), 1.29 (s, 3H), 1.12 (s, 3H), 0.86 (s, 3H). ^{13}C NMR (176 MHz, $CDCl_3$) δ = 178.09, 176.45, 172.08, 156.12, 134.12, 130.67, 130.44, 117.76, 114.67, 111.72, 101.25, 93.30, 77.34, 77.16, 76.98, 58.99, 55.95, 54.81, 33.49, 31.25, 29.85, 19.65, 17.84, 16.69, 13.70, 9.87. HRMS (ESI): m/z calculated for $C_{23}H_{27}NO_6Na$ $[M+Na]^+$: 436.1731 found: 436.1727.

3-(1-Isonicotinoyl-5-methoxy-2-methyl-1*H*-indol-3-yl)propanoic acid (44):

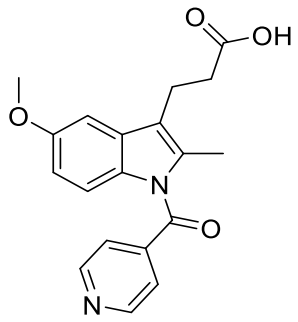

Compound **44** was synthesized by following synthetic route A, employing ethyl 3-(1-isonicotinoyl-5-methoxy-2-methyl-1*H*-indol-3-yl)propanoate (0.26 mmol) and trimethyltin hydroxide (1.06 mmol). The crude product was purified by flash chromatography using methanol in dichloromethane (2 % v/v) as the eluent, affording the target compound as a yellow

powder (30.45 mg, 34% yield); ^{1}H NMR ($CDCl_3$, 600 MHz) δ= 8.81-8.80 (m, 2H), 7.54-7.53 (m, 2H), 7.02 (d, 1H, *J* = 9.0 Hz), 6.94 (d, 1H, *J* = 3 Hz), 6.69 (dd, 1H, *J* = 9.0, *J* = 3 Hz), 3.84 (s, 3H), 3.00 (t, 2H, *J* = 7.6 Hz), 2.67 (t, 2H, *J* = 7.6 Hz), 2.29 (s, 3H). ^{13}C NMR (151 MHz, $CDCl_3$) δ= 177.20, 167.34, 156.57, 150.50, 143.80, 134.29, 131.06, 130.80, 122.89, 119.11, 115.53, 111.69, 101.67, 55.90, 33.71, 19.47, 13.89. HRMS (ESI): m/z calculated for $C_{19}H_{19}N_2O_4$ $[M+H]^+$: 339.1340 found: 339.1354.

3-(5-Methoxy-1-(4-methoxybenzoyl)-2-methyl-1*H*-indol-3-yl)propanoic acid (45):

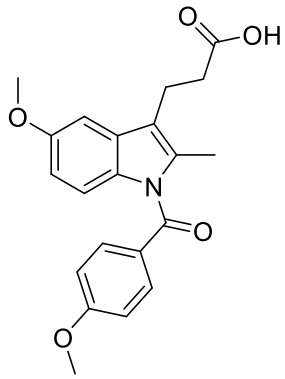

Compound **45** was synthesized by following synthetic route A, employing ethyl 3-(5-methoxy-1-(4-methoxybenzoyl)-2-methyl-1*H*-indol-3-yl)propanoate (0.33 mmol) and trimethyltin hydroxide (0.67 mmol). The crude product was purified by flash chromatography using ethyl acetate in petroleum ether (40% v/v) as the eluent, affording the target compound as an off-white powder (119.85 mg, 97% yield); ^{1}H NMR ($CDCl_3$, 500 MHz) δ= 7.70-7.68 (m, 2H), 6.97-6.96(m, 2H), 6.93 (d, 1H, *J*= 2.5), 6.91 (d, 1H, *J*= 9.0), 6.65 (dd, 1H, *J* = 9.0, 2.5 Hz), 3.90 (s, 3H), 3.84 (s, 3H), 3.02 (t, 2H, *J* = 7.5 Hz), 2.69 (m, 2H), 2.37 (s, 3H). ^{13}C NMR (126 MHz, $CDCl_3$) δ= 178.07, 169.07, 163.61, 155.77, 135.02, 132.44, 131.48, 130.31, 127.81, 116.87, 115.04, 114.12, 111.26, 100.95, 55.91, 55.69, 33.95, 19.48, 13.11. HRMS (ESI): m/z calculated for $C_{21}H_{22}NO_5$ $[M+H]^+$: 368.1493 found: 368.1493.

5.2.2.4 Synthetic route D to obtain 46-52

The synthesis was performed using a previously established resin-capture-release methodology.[131] Aldehyde-functionalized resin (500 mg, 0.55 mmol; loading capacity: 0.9 mmol/g) was dried under high vacuum overnight and suspended in 5 mL of dichloroethane (DCE). Under an inert argon atmosphere, hydrazine hydrochloride (2.75 mmol, 5.0 equiv) and triethylamine (194 µL, 6.0 equiv) were added. The reaction mixture was stirred at 45 °C overnight. Upon cooling to room temperature, the resin was filtered and washed three times

sequentially with 5 mL each of DMF, 90:10 DMF/H_2O (v/v), DMF, dichloromethane, ethyl acetate, and methanol to obtain the hydrazone-bound resin.

The hydrazone resin (500 mg) was dried under high vacuum overnight and suspended in 5 mL of pyridine. The appropriate acid chloride (3.0 equivalents) was added under argon, and the mixture was stirred at 80 °C overnight. After cooling to room temperature, the resin was filtered and washed three times each with 5 mL of DMF, 90:10 DMF/H_2O, DMF, dichloromethane, ethyl acetate, and methanol to remove residual reagents and byproducts.

The acylated hydrazone resin (150 mg) was suspended in a 1:1 mixture of DCE and trifluoroacetic acid (total volume 6 mL). The desired ketone (10.0 equiv.) was added to the suspension, and the reaction mixture was heated at 70 °C for a period ranging from 15 minutes to 2 hours. After cooling, the resin was quenched with methanol, filtered, and washed sequentially with dichloromethane, methanol, ethyl acetate, and an additional methanol wash (each in 5 mL portions). The combined filtrates were concentrated under reduced pressure, and the crude product was purified by preparative HPLC using a gradient of water and acetonitrile as the mobile phase to yield the final compound.

3-(2-Methyl-1-(thiophene-2-carbonyl)-1*H*-indol-3-yl)propanoic acid (46)

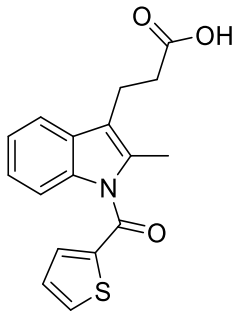

Compound **46** was prepared in accordance with general procedure D, affording the purified product as a white powder (17.39 mg, 42% yield); ^{1}H NMR ($CDCl_3$, 700 MHz) δ= 7.74 (1H, dd, *J* = 4.9, 1.4 Hz), 7.54-7.53 (m, 1H), 7.49 (1H, d, *J* = 7.8 Hz), 7.24 (1H, d, *J* = 8.3 Hz), 7.20 – 7.17 (m, 1H), 7.13 (1H, dd, *J* = 4.9, 3.5 Hz), 7.10-7.08 (1H, m), 3.06 (t, 2H, *J* = 7.7 Hz), 2.71 (t, 2H, *J* = 7.7 Hz), 2.43 (3H, s). ^{13}C NMR (176 MHz, $CDCl_3$) δ= 177.13, 163.06, 138.72, 136.72, 135.11, 134.34, 133.91, 129.40, 127.98, 122.93, 122.42, 118.08, 117.05, 113.82, 33.86, 19.51, 12.67. HRMS (APCI): m/z calculated for $C_{17}H_{15}NO_3S$ $[M+H]^+$: 314.0846 , found: 314.0837.

3-(5-Bromo-2-methyl-1-(thiophene-2-carbonyl)-1*H*-indol-3-yl)propanoic acid (47)

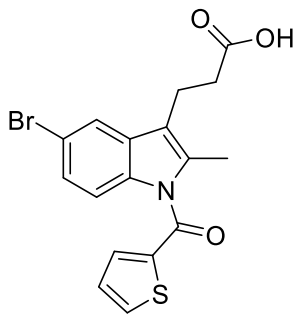

Compound **47** was prepared in accordance with general procedure D, affording the purified product as a white powder (16 mg, 34 % yield); ^{1}H NMR ($CDCl_3$, 500 MHz) δ= 7.77 (1H, dd, *J* = 5.0, 1.0 Hz), 7.61 (1H, d, *J* = 1.5 Hz), 7.50 (1H, dd, *J* = 3.5, 1.0 Hz), 7.17 1H, (dd, *J* = 9.0, 2.0 Hz), 7.14 (1H, dd, *J* = 5.0, 3.5 Hz), 7.09 (1H, d, *J* = 9.0 Hz), 3.02 (2H, t, *J* = 7.8 Hz, 2H), 2.69 (2H, t, *J* = 7.8 Hz), 2.42 (s, 3H). ^{13}C NMR (126 MHz, $CDCl_3$) δ= 176.50, 162.72, 138.28, 135.38, 135.34, 134.87, 131.14, 128.12, 125.67, 120.82, 116.30, 115.73, 115.15, 33.70, 19.37, 12.69. HRMS (APCI): m/z calculated for $C_{17}H_{14}BrNO_3S$ $[M+H]^+$: 391.9951, found: 391.9947.

3-(5-Fluoro-2-methyl-1-(thiophene-2-carbonyl)-1*H*-indol-3-yl)propanoic acid (48)

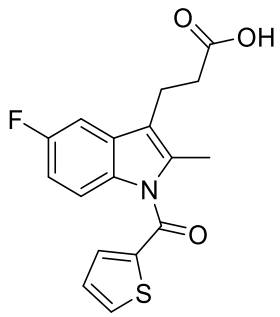

Compound **48** was prepared in accordance with general procedure D, affording the purified product as a white powder (13 mg, 30% yield); ^{1}H NMR ($CDCl_3$, 600 MHz) δ= 7.75 (1H, d, *J*= 4.8 Hz), 7.52 (1H, d, *J*= 4.2 Hz), 7.18 (1H, dd, *J*= 9, 4.2 Hz), 7.144-7.125 (2H, m), 6.81 (1H, td, *J* = 9.0, 2.4 Hz, 1H) 3.02 (t, 2H, *J* = 7.8 Hz), 2.68 (t, 2H, *J* = 7.8 Hz), 2.41 (3H, s). ^{13}C NMR (151 MHz, $CDCl_3$) δ= 177.04, 162.83, 159.27 (d, *J* = 239.2 Hz), 138.43, 135.67, 135.14, 134.56, 133.0, 130.36 (d, *J* = 9.4 Hz), 128.04, 116.95 (d, *J* = 3.9 Hz), 114.69 (d, *J* = 9.2 Hz), 110.73 (d, *J* = 23.8 Hz), 103.70 (d, *J* = 23.8 Hz), 33.72, 19.47, 12.87. HRMS (APCI): m/z calculated for $C_{17}H_{14}FNO_3S$ $[M+H]^+$:332.0752, found:332.0740.

3-(5-Chloro-2-methyl-1-(thiophene-2-carbonyl)-1*H*-indol-3-yl)propanoic acid (49)

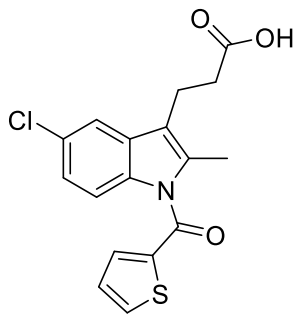

Compound **49** was prepared in accordance with general procedure D, affording the purified product as a white powder (10.25, 22% yield); ^{1}H NMR ($CDCl_3$, 600 MHz) δ= 7.76 (dd, 1H, *J* = 4.9, 1.2 Hz), 7.51 (dd, 1H, *J* = 3.6, 1.2 Hz), 7.45 (d, 1H, *J* = 2.0 Hz), 7.15-7.13 (m, 2H), 7.04 (dd, 1H, *J* = 8.8, 2.1 Hz), 3.02 (t, 2H, *J* = 7.7 Hz), 2.69 (t, 2H, *J* = 7.7 Hz), 2.42 (s, 3H). ^{13}C NMR (151 MHz, $CDCl_3$) δ= 177.04, 162.74, 138.30, 135.47, 135.30, 135.03, 134.81, 130.63, 128.12, 128.10, 123.01, 117.76, 116.43, 114.76, 33.79, 19.39, 12.74. HRMS (APCI): m/z calculated for $C_{17}H_{15}ClNO_3S$ $[M+H]^+$:348.0456, found: 348.0451.

3-(1-(3-Cyanobenzoyl)-2-methyl-1*H*-indol-3-yl)propanoic acid (50)

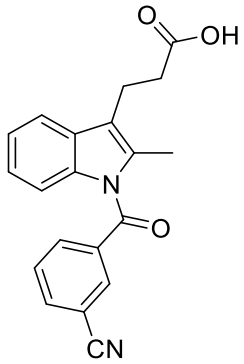

Compound **50** was prepared in accordance with general procedure D, affording the purified product as a white powder (7 mg, 16% yield); ^{1}H NMR ($CDCl_3$, 700 MHz) δ= 8.00-7.99 (1H, m), 7.93 (dt, 1H, *J* = 7.7, 1.4 Hz), 7.90 (dt, 1H, *J* = 7.7, 1.4 Hz), 7.64 (t, 1H, *J* = 7.7 Hz), 7.50 (d, 1H, *J* = 7.7 Hz), 7.22-7.20 (m, 1H), 7.08-7.06 (m, 1H), 6.92 (d, 1H, *J* = 8.4 Hz), 3.06 (t, 2H, *J* = 7.7 Hz), 2.71 (t, 2H, *J* = 7.7 Hz), 2.37 (s, 3H). ^{13}C NMR (176 MHz, $CDCl_3$) δ= 176.83, 167.48, 137.11, 136.32, 135.93, 133.82, 133.78, 133.28, 129.95, 129.82, 123.66, 123.27, 118.58, 118.42, 117.70, 114.23, 113.55, 33.59, 19.40, 13.39. HRMS (APCI): m/z calculated for $C_{20}H_{17}N_2O_3$ $[M+H]^+$:333.1234, found: 333.1223.

3-(1-(3-Cyanobenzoyl)-5-fluoro-2-methyl-1*H*-indol-3-yl)propanoic acid (51)

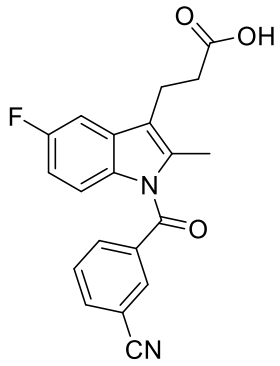

Compound **51** was prepared in accordance with general procedure D, affording the purified product as a white powder (6.23 mg, 14% yield); 1H NMR ($CDCl_3$, 600 MHz) δ = 7.98 (s, 1H), 7.92-7.90 (m, 2H), 7.65 (t, 1H, *J* = 7.8 Hz), 7.15 (dd, 1H, *J* = 8.4, 2.4 Hz), 6.98 (dd, 1H, *J* = 9.0, 4.3 Hz), 6.83-6.80 (m, 1H), 3.00 (t, 2H, *J* = 7.5 Hz), 2.69 (t, 2H, *J* = 7.5 Hz), 2.31 (s, 3H). ^{13}C NMR (151 MHz, $CDCl_3$) δ= 176.72, 167.27, 159.64 (d, *J* = 240.7 Hz), 136.91, 136.02, 135.41, 133.68, 133.20, 132.63, 130.95 (d, *J* = 9.3 Hz), 130.03, 118.48 (d, *J* = 3.8 Hz), 117.61, 115.24 (d, *J* = 9.2 Hz), 113.63, 111.35 (d, *J* = 25.2 Hz), 104.24 (d, *J* = 23.9 Hz), 33.44, 19.37, 13.67. HRMS (APCI): m/z calculated for $C_{20}H_{16}FN_2O_3$ $[M+H]^+$: 351.1140, found: 351.1122.

3-(5-Chloro-1-(3-cyanobenzoyl)-2-methyl-1*H*-indol-3-yl)propanoic acid (52)

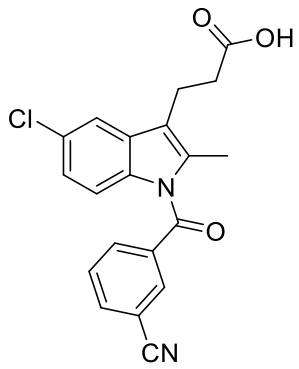

Compound **51** was prepared in accordance with general procedure D, affording the purified product as a white powder (8.33 mg, 18% yield); ^1H NMR ($CDCl_3$, 700 MHz) δ = 7.98-7.97 (m, 1H), 7.92-7.90 (m, 2H), 7.65 (t, 1H, *J* = 7.7 Hz, 1H), 7.46 (d, 1H, *J* = 2.0 Hz), 7.04 (1H, dd, *J* = 9.1, 2.1 Hz), 6.92 (1H, d, *J* = 8.4 Hz), 3.01 (t, *J* = 7.6 Hz, 1H), 2.70 (t, *J* = 7.6 Hz, 1H), 2.33 (s, 3H). ^{13}C NMR (176 MHz, $CDCl_3$) δ= 176.79, 167.24, 136.71, 136.15, 135.25, 134.68, 133.73, 133.25, 131.10, 130.05, 129.05, 123.78, 118.14, 117.97, 117.56, 115.21, 113.68, 33.51, 19.28, 13.54. HRMS (APCI): m/z calculated for $C_{20}H_{16}ClN2O_3$ $[M+H]^+$: 367.0844, found: 367.0849.

3-(1-Benzoyl-2-methyl-1*H*-indol-3-yl)propanoic acid (53):

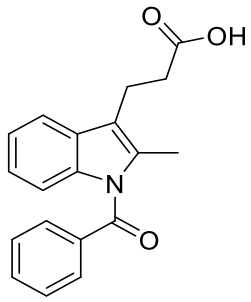

Compound **53** was synthesized following synthetic route B, using ethyl 3-(1-benzoyl-2-methyl-1*H*-indol-3-yl)propanoate (0.30 mmol) and trimethyltinhydroxide (0.83 mmol). The crude product was purified by flash chromatography using ethyl acetate in petroleum ether (25% v/v) as the eluent, affording the target compound as a white powder (90.72 mg, 99% yield); ^{1}H NMR ($CDCl_3$, 500 MHz) δ= 7.72-7.70 (m, 2H), 7.64-7.61 (m, 1H), 7.49 (m, 3H), 7.19-7.16 (m, 1H), 7.06-6.99 (m, 2H) 3.08-3.04 (m, 2H), 2.72-2.69(m, 2H), 2.37 (m, 3H). ^{13}C NMR (126 MHz, $CDCl_3$) δ= 178.13, 169.91, 136.67, 135.82, 134.14, 133.03, 129.92, 129.57, 128.91, 123.15, 122.61, 118.00, 117.44, 114.44, 33.99, 19.46, 13.19. HRMS (ESI): m/z calculated for $C_{19}H_{18}NO_3$ $[M+H]^+$: 308.1281 found:. 308.1281.

3-(1-Benzoyl-5-bromo-2-methyl-1*H*-indol-3-yl)propanoic acid (54):

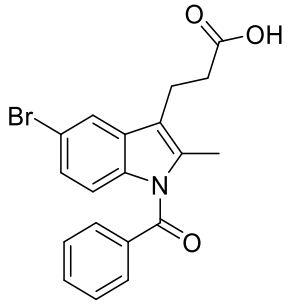

Compound **54** was synthesized following synthetic route B, using ethyl 3-(1-benzoyl-5-bromo-2-methyl-1*H*-indol-3-yl)propanoate (0.20 mmol) and trimethyltin hydroxide (0.40 mmol). The crude product was purified by flash chromatography using ethyl acetate in petroleum ether (22% v/v) as the eluent, affording the target compound as a white powder (76,61 mg, 99% yield); ^{1}H NMR ($CDCl_3$, 500 MHz) δ = 7.69-7.67 (m, 2H), 7.65-7.62 (m, 1H), 7.60 (d, 1H, *J* = 2.0 Hz), 7.51-7.48 (m, 2H), 7.13 (dd, 1H, *J* = 9, *J* = 2.0 Hz,), 6.87 (d, 1H, *J* = 9.0 Hz), 3.01 (t, 2H, *J* = 7.5 Hz), 2.68 (t, 2H, *J* = 7.5 Hz), 2.35 (m, 3H). ^{13}C NMR (126 MHz, $CDCl_3$) δ= 177.98, 169.60, 135.55, 135.36, 135.33, 133.34, 131.34, 129.92, 129.01, 125.90, 120.75, 116.70, 115.97, 115.77, 33.91, 19.32, 13.23. HRMS (ESI): m/z calculated for $C_{19}H_{18}NO_3Br$ $[M+H]^+$:

386.03863 found:. 386.03879, HRMS (ESI): m/z calculated for $C_{19}H_{18}NO_3{}^{81}Br$ $[M+H]^+$: 388.0366 found: 388.0366.

3-(1-Benzoyl-5-isopropyl-2-methyl-1*H*-indol-3-yl)propanoic acid (55)

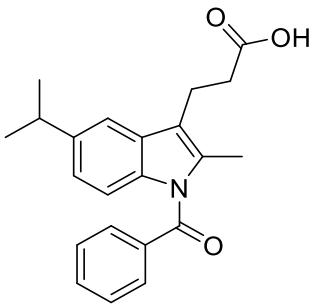

Compound **55** was synthesized following synthetic route B, using ethyl 3-(1-benzoyl-5-isopropyl-2-methyl-1*H*-indol-3-yl)propanoate (0.13 mmol) and trimethyltin hydroxide (0.26 mmol). The crude product was purified by flash chromatography using ethyl acetate in petroleum ether (16% v/v) as the eluent, affording the target compound as a white powder (40 mg, 87% yield); ^{1}H NMR ($CDCl_3$, 600 MHz) δ= 7.71-7.70 (m, 2H), 7.63-7.60 (m, 1H), 7.50-7.47 (m, 2H), 7.29 (m, 1H), 6.93-6.88 (m, 2H) 3.06 (t, 2H, *J* = 7.6 Hz), 2.97 (hep, 1H, *J* =6.9) 2.71 (t, 2H, *J* = 7.8 Hz), 2.36 (s, 3H), 1.28 (d, 6H, *J* = 6.6 Hz). ^{13}C NMR (151 MHz, $CDCl_3$) δ= 178.21, 169.84, 143.57, 136.01, 135.11, 134.26, 132.82, 129.81, 129.74, 128.86, 121.96, 117.62, 115.23, 114.32, 34.23, 34.01, 24.58, 19.42, 13.27. HRMS (ESI): m/z calculated for $C_{22}H_{24}NO_3$ $[M+H]^+$: 350.1751 found: 350.1751.

3-(1-Benzoyl-5-fluoro-2-methyl-1*H*-indol-3-yl)propanoic acid (56)

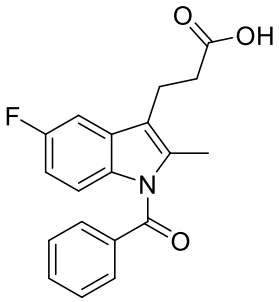

Compound **55** was synthesized following synthetic route B, using ethyl ethyl 3-(1-benzoyl-5-fluoro-2-methyl-1*H*-indol-3-yl)propanoate (0.09 mmol) and trimethyltin hydroxide (0.28 mmol). The crude product was purified by flash chromatography using ethyl acetate in petroleum ether (17% v/v) as the eluent, affording the target compound as a brown powder (21 mg, 67% yield); ^{1}H NMR ($CDCl_3$, 500 MHz) δ= 7.70-7.68 (m, 2H), 7.65-7.62 (m, 1H), 7.51-

7.48 (m, 2H), 7.13 (dd, 1H, *J*=9.0, *J*= 2.5), 6.98 (q, 1H, *J*= 4.5), 6.77 (1H, td, *J* = 9.0, *J*= 2.5 Hz), 3.02-2.99 (m, 2H), 2.69-2.67 (m, 2H), 2.33 (s, 3H). ^{13}C NMR (126 MHz, $CDCl_3$,) δ= 177.75 (d, *J* = 71.7 Hz), 169.70 (s), 159.36 (d, *J* = 239.4 Hz), 135.72 (d, *J* = 35.7 Hz), 133.28 (d, *J*=44.1), 133.15 (s), 131.80 (s), 130.61 (d, *J* = 9.3 Hz), 129.85 (s), 128.97 (s), 117.34 (d, *J* = 3.8 Hz), 115.35 (d, *J* = 9.1 Hz), 110.80 (d, *J* = 25.2 Hz), 109.22 (d, *J* = 26.1 Hz), 103.70 (d, *J* = 23.9 Hz), 103.06 (d, *J* = 23.5 Hz), 34.16 (d, *J* = 103.4 Hz), 19.53 (d, *J* = 23.6 Hz), 12.64 (d, *J* = 190.9 Hz). ^{19}F NMR (470 MHz, $CDCl_3$) δ= -120.73 (td, *J* = 8.9, 4.4 Hz), -124.94 (td, *J* = 9.5, 4.3 Hz). HRMS (ESI): m/z calculated for $C_{19}H_{16}NO_3FNa$ $[M+Na]^+$: 348.1007 found: 348.1004.

3-(1-Benzoyl-5-(furan-3-yl)-2-methyl-1*H*-indol-3-yl)propanoic acid (57)

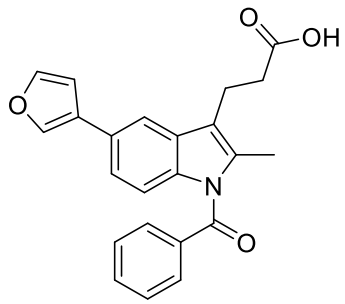

The compound was prepared in accordance with synthetic route C, using ethyl 3-(1-benzoyl-5-(furan-3-yl)-2-methyl-1*H*-indol-3-yl)propanoate (0.08 mmol) and trimethyltin hydroxide (0.32 mmol). The crude product was purified by flash chromatography using ethyl acetate in petroleum ether (25% v/v) as the eluent, affording the target compound as a yellow powder (16 mg, 54%); ^{1}H NMR ($CDCl_3$, 700 MHz) δ= 7.72-7.71 (m, 3H), 7.64-7.62 (m, 1H), 7.55 (d, 1H, *J*= 1.4 Hz), 7.50 (t, 2H, *J* = 7.7 Hz), 7.47 (t, 1H, *J* = 1.4 Hz), 7.17 (dd, 1H, *J* = 8.4, *J*= 1.4 Hz), 6.96 (d, 1H, *J* = 8.4 Hz), 6.72 (m, 1H), 3.07 (t, 2H, *J* = 7.7 Hz), 2.71 (t, 2H, *J* = 7.7 Hz), 2.37 (s, 3H). ^{13}C NMR (176 MHz, $CDCl_3$) δ= 177.56, 169.77, 143.72, 138.30, 135.81, 135.73, 134.86, 133.08, 130.11, 129.91, 128.94, 127.16, 126.87, 121.48, 117.53, 115.13, 114.77, 109.30, 33.98, 19.42, 13.25. HRMS (ESI): m/z calculated for $C_{23}H_{20}NO_4$ $[M+H]^+$: 374.1387 found: 374.1386.

3-(1-Benzoyl-2-methyl-5-(thiophen-2-yl)-1*H*-indol-3-yl)propanoic acid (58):

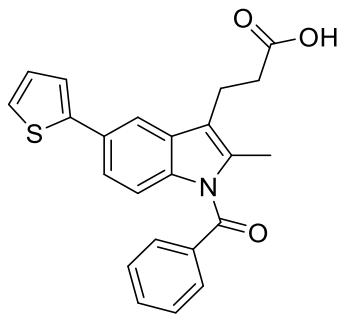

The compound was prepared in accordance with synthetic route C, using ethyl 3-(1-benzoyl-2-methyl-5-(thiophen-2-yl)-1*H*-indol-3-yl)propanoate (0.07 mmol) and trimethyltin hydroxide (0.29 mmol). The crude product was purified by flash chromatography using ethyl acetate in petroleum ether (27% v/v) as the eluent, affording the target compound as a white powder (20 mg, 73%); ^{1}H NMR ($CDCl_3$, 700 MHz) δ= 7.73-7.71 (m, 2H), 7.67 (d, 1H, *J* =2.1), 7.65-7.62 (m, 1H), 7.51-7.49 (m, 2H), 7.30 (dd, 1H, *J* = 8.6, *J* =1.8 Hz,), 7.28 (dd, 1H, *J* = 3.6, *J* = 1.1 Hz), 7.25 (dd, 1H, *J* = 5.1, *J* =1.1 Hz), 7.07 (dd, 1H, *J* = 5.1, *J* = 3.6 Hz), 6.96 (d, 1H, *J* = 8.6 Hz), 3.08 (t, 2H, *J* = 7.7 Hz), 2.72 (t, 2H, 7.7 Hz), 2.38 (s, 3H). ^{13}C NMR (176 MHz, $CDCl_3$) δ= 178.25, 169.72, 145.07, 136.10, 135.63, 135.15, 133.14, 130.11, 129.93, 129.32, 128.96, 128.11, 124.46, 122.89, 121.73, 117.58, 115.34, 114.76, 34.07, 19.38, 13.26. HRMS (ESI): m/z calculated for $C_{23}H_{20}NO_3$ $[M+H]^+$: 390.1159 found: 390.1144.

3-(1-Benzoyl-5-chloro-2-methyl-1*H*-indol-3-yl)propanoic acid (59)

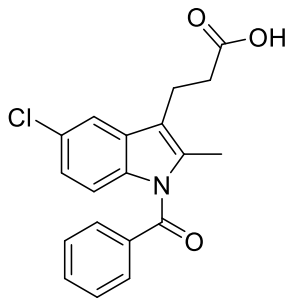

The compound was prepared in accordance with synthetic route B, ethyl 3-(1-benzoyl-5-chloro-2-methyl-1*H*-indol-3-yl)propanoate (0.22 mmol) and trimethyltin hydroxide (0.43 mmol). The crude product was purified by flash chromatography using ethyl acetate in petroleum ether (15% v/v) as the eluent, affording the target compound as colorless crystals (59 mg, 80% yield); ^{1}H NMR ($CDCl_3$, 500 MHz) δ= 7.69-7.66 (m, 2H), 7.65-7.62 (m, 1H), 7.51-7.48 (m, 2H), 7.44 (d, 1H, *J*= 2 Hz), 6.99 (dd, 1H, *J*= 8.8, *J*=2.0), 6.92 (d, 1H, *J*=8.5), 3.01 (t, 2H, *J* = 7.7 Hz), 2.68 (t, 2H, *J* = 7.7 Hz), 2.35 (s, 3H). ^{13}C NMR (126 MHz, $CDCl_3$) δ=

177.52, 169.62, 135.67, 135.38, 135.00, 133.30, 130.84, 129.91, 129.01, 128.34, 123.23, 117.71, 116.84, 115.38, 33.83, 19.35, 13.27. HRMS (ESI): m/z calculated for $C_{19}H_{17}NO_3Cl$ $[M+H]^+$: 342.08915 found: 342.08902; m/z calculated for $C_{19}H_{17}NO_3\,^{37}Cl$ $[M+H]^+$: 344.0862 found: 344.0860.

3-(1-Benzoyl-5-(3,5-dimethylisoxazol-4-yl)-2-methyl-1*H*-indol-3-yl)propanoic acid (60)

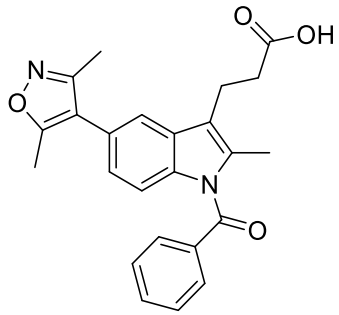

The compound was prepared in accordance with synthetic route C, using ethyl 3-(1-benzoyl-5-(3,5-dimethylisoxazol-4-yl)-2-methyl-1*H*-indol-3-yl)propanoate (0.03 mmol) and trimethyltin hydroxide (0.14 mmol). The crude product was purified by preparative HPLC using acetonitrile and water as eluent, affording the target compound as a white powder (10 mg, 71% yield); ^{1}H NMR ($CDCl_3$, 500 MHz) δ=7.75-7.73 (m, 2H), 7.67-7.64 (m, 1H), 7.52 (t, 2H, *J* = 7.5 Hz), 7.33 (d, 1H, *J* = 1.0 Hz), 7.08 (d, 1H, *J* = 8.5 Hz), 6.92 (dd, 1H, *J* = 8.5, *J* =1.5 Hz), 3.06 (t, 2H, *J* = 7.5 Hz), 2.70 (t, 2H, *J* = 7.7 Hz), 2.41 (s, 3H), 2.38 (s, 3H), 2.28 (s, 3H). ^{13}C NMR (126 MHz, $CDCl_3$) δ= 176.85, 169.82, 165.35, 159.06, 135.98, 135.57, 135.19, 133.27, 130.02, 129.92, 129.03, 124.55, 124.29, 118.62, 117.33, 117.23, 114.69, 33.81, 19.35, 13.30, 11.69, 10.92. HRMS (ESI): m/z calculated for $C_{24}H_{23}N_2O_4$ $[M+H]^+$: 403.1652 found: 403.1650.

3-(1-Benzoyl-5-(2,4-dimethoxypyrimidin-5-yl)-2-methyl-1*H*-indol-3-yl)propanoic acid (61)

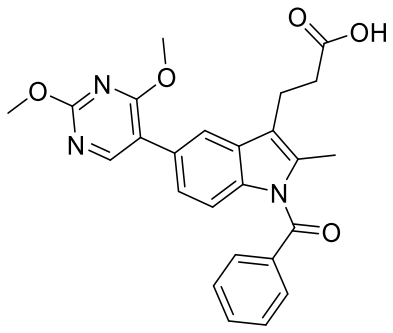

The compound was prepared in accordance with synthetic route C, using ethyl 3-(1-benzoyl-5-(2,4-dimethoxypyrimidin-5-yl)-2-methyl-1*H*-indol-3-yl)propanoate (0.10 mmol) and trimethyltin hydroxide (0.31 mmol). The crude product was purified by flash chromatography using methanol in dichloromethane (2 % v/v) as the eluent, affording the target compound as a white powder (28,5 mg, 62% yield); ^{1}H NMR ($CDCl_3$, 700 MHz) δ= 8.30 (s, 1H), 7.73 (d, 2H, *J* = 7.7 Hz), 7.64 (t, 1H, *J* = 7.7 Hz), 7.57 (d, 1H, *J* = 1.4 Hz), 7.51 (t, 2H, *J* = 7.7 Hz), 7.16 (dd, 1H, *J* = 8.4, *J* =1.4 Hz), 7.02 (d, 1H, *J* = 8.4 Hz), 4.04 (s, 3H), 4.02 (s, 3H), 3.08 (t, 2H, *J* = 7.7 Hz), 2.70 (t, 2H, *J* = 7.7 Hz), 3.07 (s, 3H). ^{13}C NMR (176 MHz, $CDCl_3$) δ= 176.65, 169.78, 168.38, 164.39, 157.60, 136.13, 135.66, 134.93, 133.15, 129.93, 129.88, 128.98, 127.58, 124.08, 118.43, 117.68, 116.70, 114.31, 55.04, 54.35, 33.95, 19.49, 13.23. HRMS (ESI): m/z calculated for $C_{25}H_{24}N_3O_5$ $[M+H]^+$: 446.1711 found: 446.1709.

3-(1-Benzoyl-2-methyl-5-(4-(trifluoromethyl)phenyl)-1*H*-indol-3-yl)propanoic acid (62)

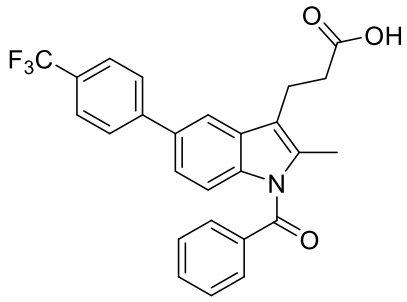

The compound was prepared in accordance with synthetic route C, using ethyl 3-(1-benzoyl-2-methyl-5-(4-(trifluoromethyl)phenyl)-1*H*-indol-3-yl)propanoate (0.10 mmol) and trimethyltin hydroxide (0.42 mmol). The crude product was purified by preparative HPLC using acetonitrile and water as eluent, affording the target compound as a white powder (17 mg, 36% yield); ^{1}H NMR ($CDCl_3$, 500 MHz) δ= 7.84 (m, 1H), 7.78 (m, 1H), 7.74-7-73 (m 2H), 7.67-7.63 (m, 2H), 7.89-7.57 (m, 1H), 7.56-7.50 (m 3H), 7.28 (d, 1H, *J* = 1.5 Hz), 7.05 (d, 1H, *J* = 8.5 Hz), 3.11 (t, 2H, *J* = 7.7 Hz), 2.73 (t, 2H, *J* = 7.7 Hz), 2.40 (s, 3H). ^{13}C NMR (126 MHz, $CDCl_3$) δ= 176.93, 169.78, 142.54, 136.45, 135.59, 135.29, 134.58, 133.23, 131.38, 130.74, 130.24, 129.95, 129.32, 129.00, 123.93 (dd, *J* = 63.3, 3.8 Hz), 122.56, 117.61, 116.59, 114.85, 77.42, 77.16, 76.91, 33.87, 19.38, 13.27. ^{19}F NMR (470 MHz, $CDCl_3$) δ = -62.52. HRMS (ESI): m/z calculated for $C_{26}H_{21}NO_3F_3$ $[M+H]^+$: 452.1468 found: 452.1469.

3-(5-(3-Aminophenyl)-1-benzoyl-2-methyl-1*H*-indol-3-yl)propanoic acid (63)

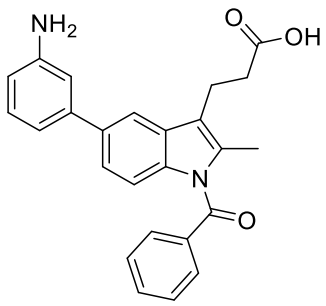

The compound was prepared in accordance with synthetic route C, using ethyl 3-(5-(3-aminophenyl)-1-benzoyl-2-methyl-1*H*-indol-3-yl)propanoate (0.05 mmol) and trimethyltin hydroxide (0.14 mmol). The crude product was purified by preparative HPLC using acetonitrile and water as eluent, affording the target compound as a white powder (9 mg, 48% yield); ^{1}H NMR ($CDCl_3$, 700 MHz) δ= 8.10-8.09 (m, 1H), 7.69-7-67 (m, 2H), 7.64-7.62 (m, 2H), 7.60 (d, 1H, *J*= 1.4 Hz), 7.50-7.46 (m, 4H), 7.13 (m, 1H), 6.88 (d, *J* = 9.0 Hz, 1H), 3.02 (t, 2H, *J* = 7.7 Hz), 2.69 (t, 2H, *J* = 7.7 Hz), 2.34 (s, 3H). ^{13}C NMR (176 MHz, $CDCl_3$) δ= 178.61, 169.63, 135.52, 135.33, 133.32, 131.35, 130.32, 129.91, 129.00, 128.62, 125.89, 123.93, 120.75, 116.76, 115.97, 115.77, 113.92, 112.69, 111.80, 109.85, 34.06, 19.34, 13.24. HRMS (ESI): m/z calculated for $C_{25}H_{23}N_2O_3$ $[M+H]^+$: 399.1703 found: 399.1696.

3-(1-Benzoyl-2,5-dimethyl-1*H*-indol-3-yl)propanoic acid (64)

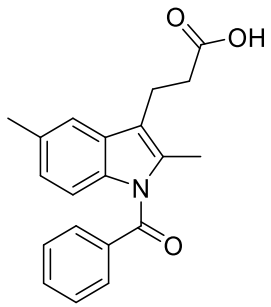

The compound was prepared in accordance with synthetic route B, using ethyl 3-(1-benzoyl-2-methyl-5-(*p*-tolyl)-1*H*-indol-3-yl)propanoate (0.24 mmol) and trimethyltin hydroxide (0.73 mmol). The crude product was purified by flash column chromatography using ethyl acetate in petroleum ether (17 % v/v) as the eluent, affording the target compound as a pale brown powder (77.39 mg, 99% yield); ^{1}H NMR ($CDCl_3$, 500 MHz) δ= 7.71-7.69 (m, 2H), 7.63-7.60 (m, 1H), 7.48 (m, 2H), 7.26 (m, 1H), 6.85 (m, 2H), 3.03 (t, 2H, *J* = 7.8 Hz), 2.70 (t, 2H, *J* = 7.8 Hz), 2.41 (s, 3H), 2.36 (s, 3H). ^{13}C NMR (126 MHz, $CDCl_3$) δ= 179.02, 169.84, 135.93, 134.89,

134.22, 132.85, 132.18, 129.82, 129.81, 128.84, 124.40, 117.96, 117.31, 114.19, 34.14, 21.44, 19.46, 13.23. HRMS (ESI): m/z calculated for $C_{20}H_{20}N_3$ $[M+H]^+$: 322.1438 found: 322.1433.

3-(1-Benzoyl-2-methyl-5-(trifluoromethoxy)-1*H*-indol-3-yl)propanoic acid (65)

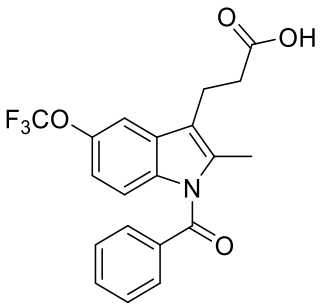

The compound was prepared in accordance with synthetic route B, using ethyl 3-(1-benzoyl-2-methyl-5-(4-(trifluoromethoxy)phenyl)-1*H*-indol-3-yl)propanoate (0.27 mmol) and trimethyltin hydroxide (0.82 mmol). The crude product was purified by flash column chromatography using ethyl acetate in petroleum ether (20 % v/v) as eluent, affording the target compound as an off-white powder (50 mg, 46% yield); ^{1}H NMR ($CDCl_3$, 700 MHz) δ= 7.70-7.69 (m, 2H), 7.65-7-63 (m, 1H), 7.52-7.49 (m, 2H), 7.32 (m, 1H), 7.02 (d, 1H, *J* = 9.0 Hz), 6.98-6.91 (m, 1H), 3.03 (t, 2H, *J* = 7.7 Hz), 2.68 (t, 2H, *J* = 7.7 Hz), 2.35 (s, 3H). ^{13}C NMR (176 MHz, $CDCl_3$) δ= 178.79 (d, *J* = 98.5 Hz), 169.67, 144.95 (d, *J*= 4.7), 136.15, 135.06 (d, *J* = 87.5 Hz), 133.36, 130.34, 129.91, 129.05, 120.78 (q, *J* = 256.2 Hz), 115.05 (d, *J* = 11.4 Hz), 117.29, 116.48, 115.05 (d, J = 11.4 Hz), 110.72 (d, *J* = 34.2 Hz), 110.57 (d, *J* = 7.04 Hz), 34.38 (d, *J* = 143.4 Hz), 19.37 (d, *J* = 32.1 Hz), 12.58 (d, *J* = 262.5 Hz). ^{19}F NMR (470 MHz, $CDCl_3$) δ= -58.02 (d, *J* = 26.0 Hz). HRMS (ESI): m/z calculated for $C_{20}H_{17}F_3NO_4$ $[M+H]^+$: 392.1105 found: 392.1095.

4-(1-Benzoyl-3-(2-carboxyethyl)-2-methyl-1*H*-indol-5-yl)benzoic acid (66)

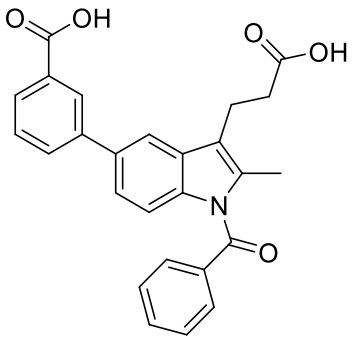

The compound was prepared in accordance with synthetic route C, using 3-(1-benzoyl-3-(3-ethoxy-3-oxopropyl)-2-methyl-1*H*-indol-5-yl)benzoic (0.09 mmol) and trimethyltin hydroxide

(0.26 mmol). The crude product was purified by preparative HPLC using acetonitrile and water as eluent, affording the target compound as a white powder (9.9 mg, 26% yield); ^{1}H NMR ($CDCl_3$, 700 MHz) δ= 8.47 (m, 1H), 8.00 (m, 1H), 7.87 (m, 1H), 7.81 (d, 1H, *J* = 1.6 Hz), 7.76 (dd, 2H, *J*=8.2 Hz, *J*= 1.2 Hz) 7.67-7.65 (m, 1H), 7.54-7.51 (m, 3H), 7.35 (dd, 1H, *J* = 8.6 Hz, 1.8 Hz), 7.04 (d, 1H, *J* = 8.6 Hz), 3.16 (t, 2H, *J*= 8.1 Hz), 2.75-2.72 (t, 2H, *J*= 8.2 Hz), 2.42 (s, 3H). ^{13}C NMR (176 MHz, $CDCl_3$) δ= 179.43, 172.16, 169.77, 141.41, 136.40, 135.63, 135.01, 134.10, 133.19, 132.33, 130.39, 129.95, 129.86, 129.11, 129.00, 128.63, 128.60, 122.01, 117.79, 116.30, 114.87, 34.59, 19.49, 13.24. HRMS (ESI): m/z calculated for $C_{26}H_{22}NO_5$ $[M+H]^+$: 428.1493 found: 428.1493.

3-(1-Benzoyl-5-(4-carbamoylphenyl)-2-methyl-1*H*-indol-3-yl)propanoic acid (67)

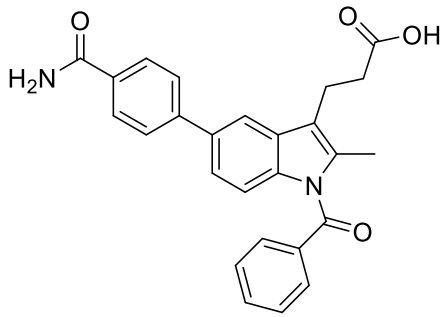

The compound was prepared in accordance with synthetic route C, using ethyl 3-(1-benzoyl-5-(4-carbamoylphenyl)-2-methyl-1*H*-indol-3-yl)propanoate (0.08 mmol) and trimethyltin hydroxide (0.25 mmol). The crude product was purified by HPLC using acetonitrile and water as eluent, affording the target compound as a white powder (30.3 mg, 79% yield, 94% purity); ^{1}H NMR (700 MHz, DMSO-d_6) δ= 12.14 (s, 1H), 8.01 (s, 1H), 7.96-7.95 (2H, m), 7.92 (m, 1H), 7.80 (d, 2H, *J* = 7.7 Hz), 7.75-7.72 (m, 1H), 7.70-7.68 (m, 2H), 7.61-7.59 (m, 2H), 7.44-7.43 (m, 1H), 7.36-7.30 (m, 1H), 7.04 (d, 1H, *J* = 9.1 Hz), 3.00 (t, 2H, *J* = 7.5 Hz), 2.57 (t, 2H, *J* = 7.5 Hz), 2.26 (s, 3H). ^{13}C NMR (176 MHz, DMSO-d_6) δ= 173.95, 169.13, 167.61, 143.25, 135.70, 135.25, 134.21, 133.73, 133.12, 132.53, 129.94, 129.37, 129.01, 128.07, 126.53, 126.19, 122.00, 118.15, 116.73, 114.09, 34.05, 18.97, 12.91. HRMS (ESI): m/z calculated for $C_{26}H_{23}N_2O_4$ $[M+H]^+$: 427.1652 found: 427.1653.

3-(1-Benzoyl-2-methyl-5-(pyridin-4-yl)-1*H*-indol-3-yl)propanoic acid (68)

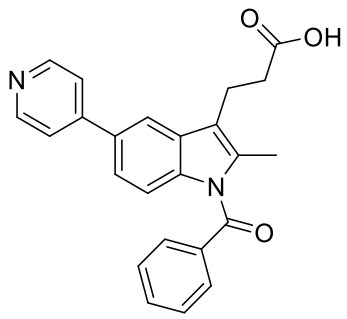

The compound was prepared in accordance with synthetic route C, using ethyl 3-(1-benzoyl-2-methyl-5-(pyridin-4-yl)-1*H*-indol-3-yl)propanoate (0.05 mmol) and trimethyltin hydroxide (0.19 mmol). The crude product was purified by preparative HPLC using acetonitrile and water as eluent, affording the target compound as a white powder (5.03 mg, 27% yield); ^{1}H NMR (CD_3OD, 500 MHz) δ= 8.77-8.76 (m, 2H), 8.36 (dd, 2H, *J*= 5.5 Hz, *J*=1.5 Hz) 8.22 (d, 1H, *J*= 1.8), 7.74-7.72 (m, 3H), 7.66 (dd, 1H, *J* = 8.7 Hz, 2.0 Hz), 7.61-7.57 (m, 2H), 7.24 (d, 1H, *J*= 8.7 Hz), 3.16 (t, 2H, *J*= 7.3 Hz), 2.70 (t, 2H, *J*= 7.5 Hz), 2.37 (s, 3H). ^{13}C NMR (126 MHz, CD_3OD) δ= 176.68, 171.01, 143.48, 139.92, 137.30, 136.53, 134.63, 131.94, 130.89, 130.19, 130.13, 129.46, 124.91, 123.59, 119.59, 119.42, 116.10, 35.22, 20.36, 13.18. HRMS (ESI): m/z calculated for $C_{24}H_{21}N_2O_3$ $[M+H]^+$: 385.1553 found: 385.1547.

3-(1-Benzoyl-2-methyl-5-(1*H*-pyrazol-4-yl)-1*H*-indol-3-yl)propanoic acid (69)

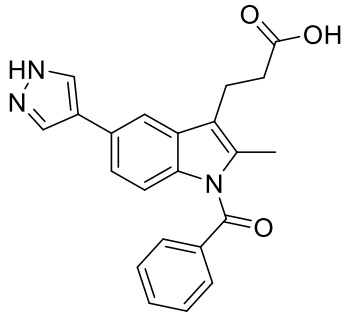

The compound was prepared in accordance with synthetic route C, using ethyl 3-(1-benzoyl-2-methyl-5-(1*H*-pyrazol-4-yl)-1*H*-indol-3-yl)propanoate (0.05 mmol) and trimethyltin hydroxide (0.24 mmol). The crude product was purified by preparative HPLC using acetonitrile and water as eluent, affording the target compound as a white powder (2.5 mg, 14% yield); ^{1}H NMR ($CDCl_3$, 700 MHz) δ= 7.80 (s, 2H), (dd, *J* = 8.4, 1.4 Hz, 2H), 7.65 – 7.63 (m, 2H), 7.50 (t, *J* = 7.7 Hz, 2H), 7.11 (dd, *J* = 8.5, 1.6 Hz, 1H), 6.97 (d, *J* = 8.5 Hz, 1H), 3.14 (t, *J* = 7.2 Hz, 2H), 2.69 (t, *J* = 7.2 Hz, 2H), 2.39 (s, 3H). ^{13}C NMR (176 MHz, $CDCl_3$) δ= 176.80, 169.73,

135.76, 135.69, 135.00, 133.13, 130.53, 129.98, 129.89, 128.97, 125.71, 123.94, 121.09, 118.01, 115.45, 114.84, 34.92, 19.97, 13.24. HRMS (ESI): m/z calculated for $C_{22}H_{20}N_3O_3$ $[M+H]^+$: 374.1499 found:. 374.1499.

3-(1-Benzoyl-5-(2-cyanophenyl)-2-methyl-1*H*-indol-3-yl)propanoic acid (70)

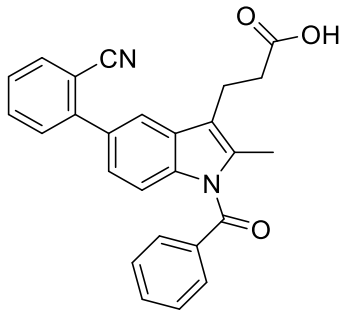

The compound was prepared in accordance with synthetic route C, using ethyl 3-(1-benzoyl-5-(2-cyanophenyl)-2-methyl-1*H*-indol-3-yl)propanoate (0.07 mmol) and trimethyltin hydroxide (0.21 mmol). The crude product was purified by preparative HPLC using acetonitrile and water as eluent, affording the target compound as a white powder (9 mg, 32% yield); ^{1}H NMR ($CDCl_3$, 600 MHz) δ= 7.78-7.77 (m, 2H), 7.75 (d, *J* = 1.3 Hz, 1H), 7.70 (d, *J* = 1.8 Hz, 1H), 7.66-7.63 (m, 2H), 7.55-7.51 (m, 3H), 7.44-7.41 (m, 1H), 7.19 (dd, *J* = 8.6, 1.8 Hz, 1H), 7.10 (d, *J* = 8.5 Hz, 1H), 3.10 (t, *J* = 7.4 Hz, 2H), 2.73 (t, *J* = 7.4 Hz, 2H), 2.40 (s, 3H). ^{13}C NMR (151 MHz, $CDCl_3$) δ= 174.70, 169.81, 146.23, 136.71, 135.56, 135.39, 133.89, 133.26, 132.99, 132.59, 130.46, 129.99, 129.91, 129.03, 127.35, 123.86, 119.40, 118.74, 117.78, 114.62, 111.42, 34.03, 19.78, 13.25. HRMS (ESI): m/z calculated for $C_{26}H_{21}N_2O_3$ $[M+H]^+$: 409.1547 found: 409.1547.

3-(5-(5-Acetylthiophen-2-yl)-1-benzoyl-2-methyl-1*H*-indol-3-yl)propanoic acid (71)

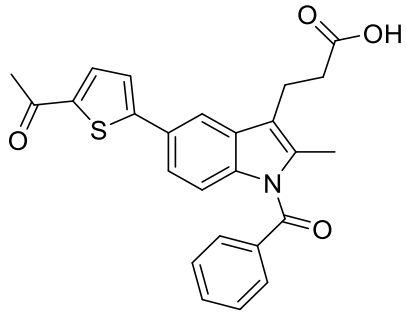

The compound was prepared in accordance with synthetic route C, using ethyl 3-(5-(5-acetylthiophen-2-yl)-1-benzoyl-2-methyl-1*H*-indol-3-yl)propanoate (0.05 mmol) and trimethyltin hydroxide (0.21 mmol). The crude product was purified by preparative HPLC

using acetonitrile and water as eluent, affording the target compound as a brown powder (10 mg, 43% yield), ^{1}H NMR (700 MHz, $CDCl_3$) δ= 7.74 (d, 1H, *J* = 1.6 Hz), 7.72 (dd, 2H, *J* = 8.3, 1.2 Hz), 7.67-7.64 (m, 2H), 7.53-7.50 (m, 2H), 7.33 (m, 1H), 7.30 (d, 1H, *J* = 3.5 Hz), 7.00 (d, 1H, *J* = 8.4 Hz), 3.09 (t, 2H, *J* = 7.7 Hz), 2.72 (t, 2H, *J* = 7.7 Hz), 2.56 (s, 3H), 2.39 (s, 3H). ^{13}C NMR (176 MHz, $CDCl_3$) δ= 190.72, 175.88, 169.64, 153.81, 142.70, 136.96, 135.68, 135.38, 133.74, 133.38, 130.19, 129.98, 129.04, 128.08, 123.62, 121.67, 117.53, 115.93, 114.90, 33.69, 26.67, 19.35, 13.24. HRMS (ESI): m/z calculated for $C_{25}H_{21}NO_4SNa$ $[M+Na]^+$: 454.1084 found: 454.1066.

3-(1-Benzoyl-5-(4-hydroxyphenyl)-2-methyl-1*H*-indol-3-yl)propanoic acid (72)

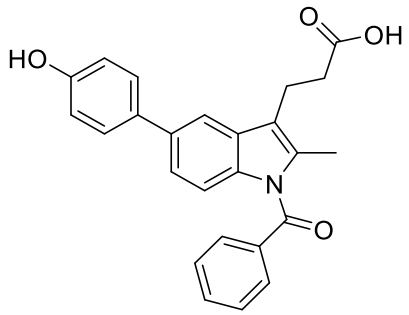

The compound was prepared in accordance with synthetic route C, using ethyl 3-(1-benzoyl-5-(4-hydroxyphenyl)-2-methyl-1*H*-indol-3-yl)propanoate (0.11 mmol) and trimethyltin hydroxide (0.33 mmol). The crude product was purified by flash chromatography using methanol in dichloromethane (4% v/v) as eluent, affording the target compound an off-white powder (34.39 mg, 80% yield); ^{1}H NMR (DMSO, 700 MHz) δ= 12.12 (s, 1H), 9.46 (s, 1H), 7.74-7.72 (m, 2H), 7.69 (d, 2H, *J*=7.7 Hz), 7.60 (t, 1H, *J* = 7.7 Hz), 7.52 (d, 1H, *J* = 9.1 Hz), 7.28 (dd, 1H, *J* = 9.1, *J* = 1.4 Hz), 6.99 (d, 1H, *J* = 8.4 Hz), 6.84 (d, 2H, *J* = 8.4 Hz), 2.98 (t, 2H, *J* = 7.7 Hz), 2.56 (t, 2H, *J* = 7.7 Hz), 2.26 (s, 3H). ^{13}C NMR (176 MHz, DMSO) δ= 173.90, 169.08, 156.70, 135.41, 134.97, 134.80, 133.78, 132.95, 131.42, 129.85, 129.27, 128.95, 127.86, 121.40, 118.10, 115.60, 115.51, 113.93, 34.00, 19.00, 12.91. HRMS (ESI): m/z calculated for $C_{25}H_{22}NO_4$ $[M+H]^+$: 400.1543 found: 400.1542.

3-(1-Benzyl-5-bromo-2-methyl-1*H*-indol-3-yl)propanoic acid (73)

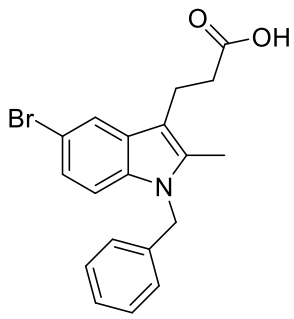

Ethyl 3-(5-bromo-2-methyl-1*H*-indol-3-yl)propanoate (**10b**) (150 mg, 0.48 mmol, 1.0 equiv) was dissolved in 1 mL of DMF in a round-bottom flask and cooled to -20 °C under an inert argon atmosphere. Sodium hydride (NaH, 60% dispersion in mineral oil, 29.01 mg, 0.73 mmol, 1.5 equiv) was carefully added to the solution, and the reaction was stirred for 15 minutes. Benzyl chloride (122.43 mg, 0.97 mmol, 111.29 µL, 2.0 equiv) was then added, and the mixture was allowed to gradually reach room temperature and stirred overnight. Reaction progress was monitored via TLC and LC-MS. Upon completion, methanol was cautiously added to quench the reaction, followed by extraction with ethyl acetate. The organic phases were combined, dried over anhydrous magnesium sulfate, and concentrated under reduced pressure to give the crude intermediate (185 mg, 0.46 mmol, 1.0 equiv), which was dissolved in 1 mL of 1,2-dichloroethane (DCE). To this solution, trimethyltinhydroxide (100.28 mg, 0.56 mmol, 1.2 equiv) was added, and the mixture was heated to reflux. The reaction was monitored by TLC and LC-MS until complete conversion was observed. The solvent was removed under vacuum, and the residue was dissolved in ethyl acetate. The organic phase was sequentially washed three times with 5% aqueous HCl and once with 5 mL of brine. After drying over anhydrous magnesium sulfate, the solution was concentrated and purified by flash chromatography using 2% methanol in dichloromethane (v/v) as the eluent, affording the pure product as a white powder (143 mg, 83% yield); ^{1}H NMR ($CDCl_3$, 500 MHz), δ= 7.65 (d, 1H, *J* = 1.8 Hz), 7.27-7.23 (m, 2H), 7.22-7.21 (m, 1H), 7.17 (dd, 1H, *J* = 8.6, 1.8 Hz), 7.04 (d, 1H, *J* = 8.6 Hz), 6.90 – 6.87 (m, 2H), 5.25 (s, 2H), 3.04 (t, 2H, *J* = 7.6 Hz), 2.66 (t, 2H, *J* = 7.6 Hz), 2.29 (s,3H). ^{13}C NMR (126 MHz, $CDCl_3$) δ= 179.10, 137.57, 135.34, 134.81, 129.34, 128.98, 127.54, 125.93, 123.85, 120.57, 112.66, 110.73, 109.78, 46.80, 35.11, 19.87, 10.40. HRMS (ESI): m/z calculated for $C_{19}H_{19}BrNO_2$ $[M+H]^+$: 372.0594, found: 372.0568.

3-(5-Bromo-1-(cyclohexanecarbonyl)-2-methyl-1*H*-indol-3-yl)propanoic acid (74)

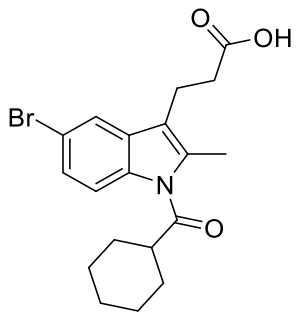

Ethyl 3-(5-bromo-2-methyl-1H-indol-3-yl)propanoate (10b) (150 mg, 0.48 mmol, 1.0 equiv) was dissolved in 1 mL of DMF in a round-bottom flask and cooled to -20 °C under an inert argon atmosphere. Sodium hydride (NaH, 60% dispersion in mineral oil, 29.01 mg, 0.73 mmol, 1.5 equiv) was carefully added to the solution, and the reaction was stirred for 15 minutes. Cyclohexyl carbonyl chloride (2 equiv, 141.8 mg, 0.97 mmol, 129.85 µL was then added, and the mixture was allowed to gradually reach room temperature and stirred overnight. Reaction progress was monitored via TLC and LC-MS. Upon completion, methanol was cautiously added to quench the reaction, followed by extraction with ethyl acetate. The organic phases were combined, dried over anhydrous magnesium sulfate, and concentrated under reduced pressure to give the crude intermediate (1 equiv. 141 mg, 0.34 mmol), which was dissolved in 1 mL of 1,2-dichloroethane (DCE). To this solution, trimethyltinhydroxide trimethyltinhydroxide (2 equiv, 121.48 mg, 0.67 mmol) was added, and the mixture was heated to reflux. The reaction was monitored by TLC and LC-MS until complete conversion was observed. The solvent was removed under vacuum, and the residue was dissolved in ethyl acetate. The organic phase was sequentially washed three times with 5% aqueous HCl and once with 5 mL of brine. After drying over anhydrous magnesium sulfate, the solution was concentrated and purified by flash chromatography using methanol in dichloromethane (1% v/v) as the eluent, affording the pure product as a white powder (120 mg, 91%); ^{1}H NMR ($CDCl_3$, 700 MHz), δ= 7.65 (d, 1H, *J* = 8.8 Hz), 7.58 (d, 1H, *J* = 2.0 Hz), 7.34 (dd, 1H, *J* = 8.8, 2.0 Hz), 3.14 (tt, 1H, *J* = 11.3, 3.3 Hz), 2.98 (t, 2H, *J* = 7.7 Hz), 2.63 (t, 2H, *J* = 7.7 Hz), 2.54 (s, 3H), 1.99-1.97 (m, 2H), 1.88-1.86 (m, 2H), 1.76-1.74 (m, 1H), 1.68-1.62 (m, 2H), 1.39-1.37 (m, 1H), 1.36 – 1.31 (m, 2H). ^{13}C NMR (176 MHz, $CDCl_3$) δ= 177.98, 177.47, 134.76, 134.45, 131.59, 126.48, 120.82, 116.75, 116.02, 115.84, 45.99, 33.96, 29.73, 25.81, 25.72, 19.29, 13.92. HRMS (ESI): m/z calculated for $C_{19}H_{23}BrNO_3$ $[M+H]^+$: 392.0856, found: 392.0848.

Ethyl (*S*)-(6-methyl-5-((3-(2-(piperidin-3-ylamino)pyrimidin-4-yl)pyridin-2-yl)oxy)naphthalen-1-yl)carbamate (G1749)

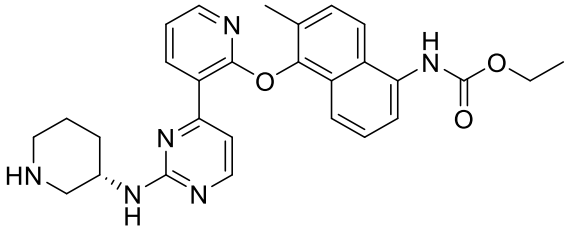

The compound **G1749** was synthesized in accordance with a previously reported method.[133] The product was obtained as an off-white powder in 60% yield; ^{1}H NMR (DMSO-d_6, 600 MHz) δ= 9.57 (s, 1H), 8.48 (d, 1H, *J* = 5.4 Hz), 8.05 (dd, 1H, *J* = 4.8, 1.8 Hz), 7.93 (d, 1H, *J* = 9.0 Hz), 7.58 – 7.55 (m, 2H), 7.51 (d, 1H, *J* = 7.2 Hz), 7.49 (d, 1H, *J* = 9.0 Hz), 7.46 (d, 1H, *J* = 8.4 Hz), 7.41 – 7.37 (m, 1H), 7.26 (dd, 1H, *J* = 7.8, 4.8 Hz), 4.25 (s, 1H), 4.17 (q, *J* = 7.1 Hz, 2H), 3.46 (m, 1H), 3.23-3.21 (m, 1H), 2.89-2.84 (m, 2H), 2.21 (s, 3H), 2.03-1.91 (m, 2H), 1.75-1.61 (m, 2H), 1.28 (t, 3H, *J* = 7.2 Hz). ^{13}C NMR (151 MHz, DMSO-d_6) δ= 161.56, 160.39, 158.22, 157.99, 154.86, 148.74, 146.38, 140.21, 134.23, 128.70, 128.27, 127.89, 126.80, 126.28, 120.46, 120.18, 120.16, 119.02, 117.92, 110.60, 60.41, 46.59, 44.72, 43.14, 28.06, 20.74, 16.14, 14.62.

***(S)*-2-Chloro-*N*-(6-methyl-5-((3-(2-(piperidin-3-ylamino)pyrimidin-4-yl)pyridin-2-yl)oxy)naphthalen-1-yl)benzenesulfonamide (AMG18 or KIRA8)**

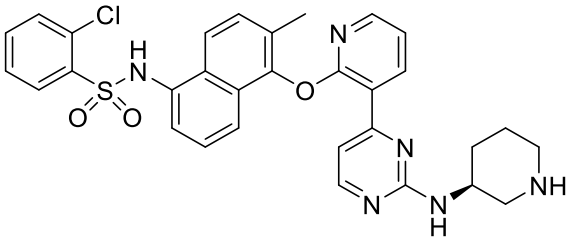

The compound **KIRA8** was synthesized in accordance with a previously reported method.[119] The product was obtained as an off-white powder in 50% yield; ^{1}H NMR (DMSO-d_6, 600 MHz) δ= 10.63 (s, 1H), (d, 1H, *J* = 5.4 Hz), 8.06 (d, 1H, *J* = 8.4 Hz), 8.04 (dd, 1H, *J* = 4.8, 1.8 Hz), 7.85 (dd, 1H, *J* = 7.8, 1.2 Hz), 7.70 (dd, 1H, *J* = 8.4, 1.2 Hz), 7.64-7.61 (m, 1H), 7.54 (d, 1H, *J* = 4.2 Hz), 7.51-7.47 (m, 3H), 7.44 (td, 1H, *J* = 7.8, 1.2 Hz), 7.31-7.28 (m, 1H), 7.26 (dd, 1H, *J* = 7.8, 4.8 Hz), 7.15 (d, 1H, *J* = 7.2 Hz), 4.24 (s, 1H), 3.45-3.43 (m 1H), 3.23-3.20 (m, 1H), 2.91-2.81 (m 2H), 2.17 (s, 3H), 2.02-1.90 (m 2H), 1.74-1.59 (m, 2H). ^{13}C NMR (151

MHz, DMSO-d_6) = 161.54, 160.27, 158.19, 157.96, 148.72, 146.27, 140.23, 137.40, 134.53, 132.24, 131.97, 131.08, 130.89, 129.54, 129.21, 128.44, 127.74, 127.29, 126.19, 122.36, 120.44, 120.18, 119.96, 119.08, 110.63, 46.59, 44.71, 43.13, 28.04, 20.73, 16.12.

5.2.3 IRE1α activators

5.2.3.1 General procedure A for the synthesis of aminopyrimidines 81-84

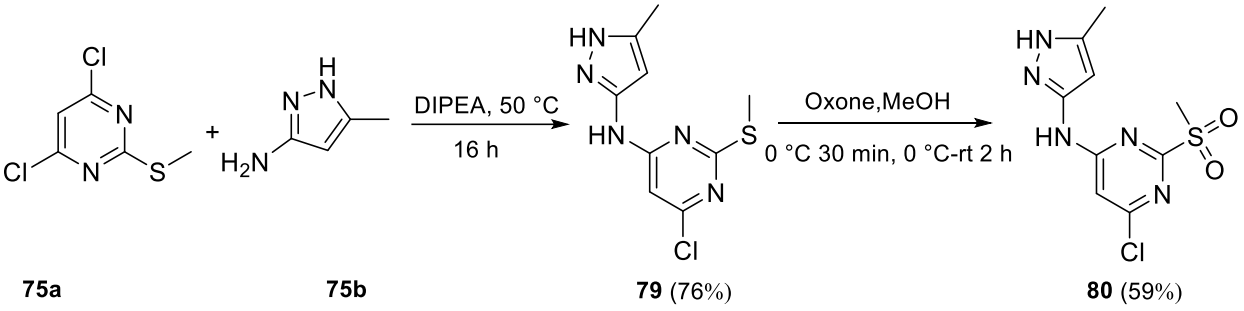

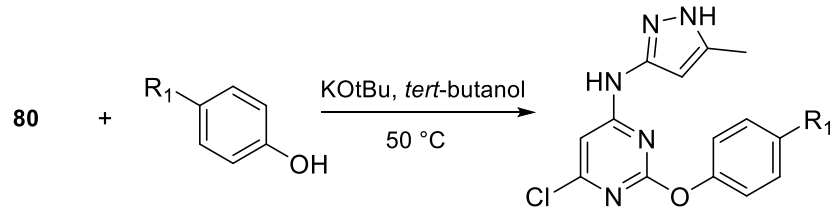

Cpd	R^1	Yield (%)
81	$-CONH_2$	72
82	$-SO_2CH_3$	96
83	$-SO_2NH_2$	87
84	-CHO	quant.

Synthesized using the reported procedure.[142] A stirred solution of 1.0 g (5.12 mmol) of 4,6-dichloro-2-(thiomethyl)pyrimidine, 0.93 g (7.18 mmol) of DIPEA, and 0.70 g (7.18 mmol) of 5-methyl-1*H*-pyrazol-3-amine was heated at 50 °C for 16 hours. After cooling to room temperature, the mixture was poured into 10 mL of water, and the resulting precipitate was filtered off. The solid was then dissolved in 12 mL of EtOAc, filtered again, and finally taken up in 5 mL of MeOH. Drying the product under vacuum produced compound **79**, as a pale-yellow solid with a yield of 76% (1.0 g, 3.91 mmol)

The intermediate compound **79** (1.0 g, 3.91 mmol) produced in the previous step was stirred in 25 mL MeOH and cooled in an ice bath. To it, a slurry of oxone (5.53 g, 9.00 mmol) in water (13 mL) was added portion by portion over 10 minutes. The reaction mixture was stirred by allowing it to come to room temperature for 2 hours. The solid, isolated by filtration, was stirred vigorously in a 1:1 mixture of water and saturated bicarbonate solution. The solid was then filtered and dried in *vacuo* to afford the final product (**80**) as a yellow solid (0.66 g, 2.31 mmol, 59%).

A stirred solution of 6-chloro-N-(5-methyl-1*H*-pyrazol-3-yl)-2-(methylsulfonyl)pyrimidin-4-amine (**80**) (1 eq), potassium *tert*-butoxide (1.15 eq) and the corresponding phenol (1.1 eq) in *tert*- butanol (0.05 M with respect to the pyrimidine) was heated to 50 °C until complete conversion as indicated by LC-MS. The reaction was quenched by the addition of water and EtOAc. The organic layer was separated, and the aqueous layer was extracted with EtOAc (3x). The combined organic layers were dried over magnesium sulfate and concentrated in *vacuo*. The resulting crude was then purified to obtain the desired compound.

_N_-(5-Methyl-1*H*-pyrazol-3-yl)-6-(4-methylpiperazin-1-yl)-2-(4-nitrophenoxy)pyrimidin-4-amine (78)

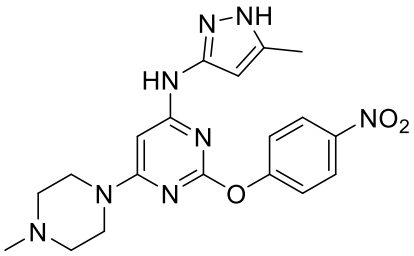

The synthesis was carried out as described in the literature.[135] Product formed as a light-yellow solid. ^{1}H NMR (500 MHz, DMSO-d$_6$) δ= 10.30 (s, 1H), 9.60 (s, 1H), 8.32-8.30 (m, 2H), 7.46-7.43 (m, 2H), 6.33 (s, 1H), 5.66 (s, 1H), 4.19 (m, 2H), 3.48 (m, 2H), 3.22-3.05 (m, 4H), 2.82 (s, 3H), 2.07 (s, 3H). ^{13}C NMR (126 MHz, DMSO-d$_6$) δ 163.75, 163.41, 161.75, 158.62, 148.06, 143.93, 138.65, 125.30, 122.68, 95.22, 80.33, 51.75, 42.18, 41.10, 10.50. HRMS (ESI): m/z calculated for $C_{19}H_{23}N_8O_3$ $[M + H]^+$: 411.1815 , Found: 411.1888.

4-((4-Chloro-6-((5-methyl-1*H*-pyrazol-3-yl)amino)pyrimidin-2-yl)oxy)benzamide (81)

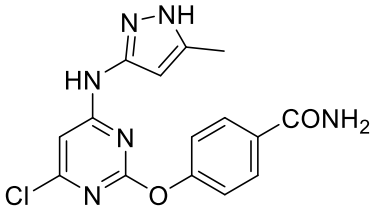

The synthesis was carried out as described in the literature, [142] and pure product **81** formed as 1:1 mixture of rotamers, ^{1}H NMR (400 MHz, DMSO-d$_6$) δ= 11.97 (s, 1H), 10.36 (s, 1H), 8.02, 7.38 (two s, total 2H, two rotamers), 7.99, 7.30 (two m, total 4H, two rotamers), 7.73 (d, *J* = 8.6 Hz, 0.50 H, rotamer 1), 6.77 (d, *J* = 8.6 Hz, 0.50 H, rotamer 2), 6.52 (s, 0.50 H, rotamer 1),

5.52 (s, 0.50 H, rotamer 2), 2.22-1.97 (m, 3H). Spectroscopic data were in accordance with the reported literature.

6-Chloro-*N*-(5-methyl-1*H*-pyrazol-3-yl)-2-(4-(methylsulfonyl)phenoxy)pyrimidin-4-amine (82)

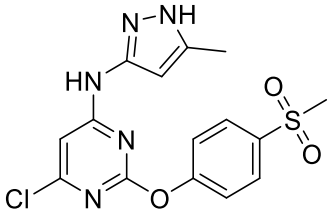

The synthesis was carried out as described in the literature.[142] ^{1}H NMR (500 MHz, DMSO-d_6) δ = 12.15-12.00 (m, 1H), 10.43 – 10.19 (m, 1H), 8.02 (m, 2H), 7.52 (d, *J* = 8.4 Hz, 2H), 6.56 (s, 1H), 5.62(s, 1H), 3.27 (s, 3H), 2.07 (s, 3H). Spectroscopic data were in accordance with the reported literature.

4-((4-Chloro-6-((5-methyl-1*H*-pyrazol-3-yl)amino)pyrimidin-2-yl)oxy)benzenesulfonamide (83)

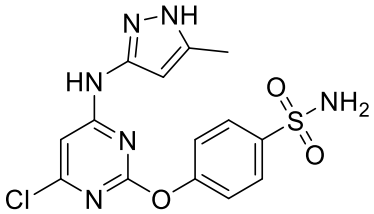

The synthesis was carried out as described in the literature.[142] ^{1}H NMR (500 MHz, DMSO-d_6) δ = 12.00 (s, 1H), 10.41 (s, 1H), 7.90 (d, *J* = 8.0, 2H), 7.44 – 7.42 (m, 4H), 6.55 (s, 1H), 5.69 (s,1H), 2.07 (s, 3H). Spectroscopic data were in accordance with the reported literature.

4-((4-Chloro-6-((5-methyl-1*H*-pyrazol-3-yl)amino)pyrimidin-2-yl)oxy)benzaldehyde (84)

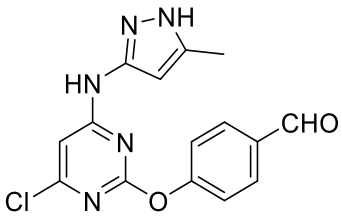

Synthesized by following general procedure A, A stirred solution of 6-chloro-N-(5-methyl-1*H*-pyrazol-3-yl)-2-(methylsulfonyl)pyrimidin-4-amine (**80**) (1 equiv., 50 mg, 0.17 mmol), potassium *tert*-butoxide (1.15 eq, 22.43 mg, 0.20 mmol) and the corresponding phenol (1.1 eq)

in *tert*- butanol (0.05 M with respect to the pyrimidine) was heated to 50 °C until complete conversion as indicated by LCMS. The reaction was quenched by the addition of water and EtOAc. The organic layer was separated, and the aqueous layer was extracted with EtOAc (3x). The combined organic layers were dried over magnesium sulfate and concentrated in *vacuo*. The resulting crude was then purified by preparative HPLC using water and acetonitrile (0-95% gradient) to yield pure product as a white powder (57 mg, quant.). ^{1}H NMR (700 MHz, DMSO-d_6) δ= 12.13-12.00 (m, 1H), 10.42-10.18 (m, 1H), 10.05 (s, 1H), 8.03 (m, 2H), 7.47 (m, 2H), 6.54 (s, 1H), 5.56 (s, 1H), 2.18-1.95 (m, 3H). ^{13}C NMR (176 MHz, DMSO-d_6) δ= 192.08, 176.46, 164.05, 161.22, 158.30, 157.45, 146.95, 138.15, 133.60, 131.35, 123.21, 99.80, 95.80, 10.47. HRMS (ESI): m/z calculated for $C_{15}H_{12}ClN_5O_2$ $[M + H]^+$: 330.0753, Found: 330.0749.

2-(4-Ainophenoxy)-6-chloro-*N*-(5-methyl-1*H*-pyrazol-3-yl)pyrimidin-4-amine (85)

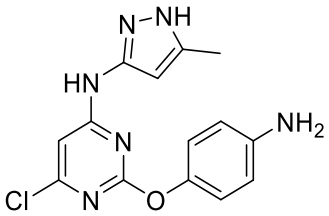

A solution of 4,6-dimethyl-2-(methylsulfonyl)pyrimidine (1 equiv., 100 mg, 0.35 mmol), 4-aminophenol (1 equiv., 37.93 mg, 0.35 mmol) and K_2CO_3 (2 equiv., 96.07 mg 0.70 mmol) in DMF (1.5 mL) was stirred at 100 ˚C for 2 h. The reaction mixture was poured into water and extracted with EtOAc. The organic layer was washed with water and saturated brine, dried over magnesium sulfate, and evaporated. The residue was purified by preparative HPLC using water and acetonitrile (0-95% gradient) to yield pure product as a white powder (53 mg, 48%). ^{1}H NMR (600 MHz, DMSO-d_6) δ = 10.29 (s, 1H), 7.16-1.13 (m, 4H), 6.44 (s, 1H), 5.72 (s, 1H), 2.06 (s, 3H). ^{13}C NMR (151 MHz, DMSO-d_6) δ= 164.40, 161.40, 149.29, 147.14, 138.39, 123.08, 121.40, 99.40, 95.94, 10.59. HRMS (ESI): m/z calculated for $C_{14}H_{14}ClN_6O$ $[M + H]^+$: 317.0913, Found: 317.0915.

5.2.3.2 General procedure B for the synthesis of aminopyrimidines 86-89

Compound **85** (1 equiv.), glyoxylic acid monohydrate (1.2 equiv.), and corresponding boronic acid (1.2 equiv.) were added simultaneously to hexafluoro-2-propanol (HFIP) (0.1 M) with 3Å molecular sieves. The mixture was stirred at room temperature and monitored by LC-MS and

TLC. The solvent then evaporated under reduced pressure. The resulting residue was purified by preparative HPLC using water and acetonitrile (0-95% gradient).

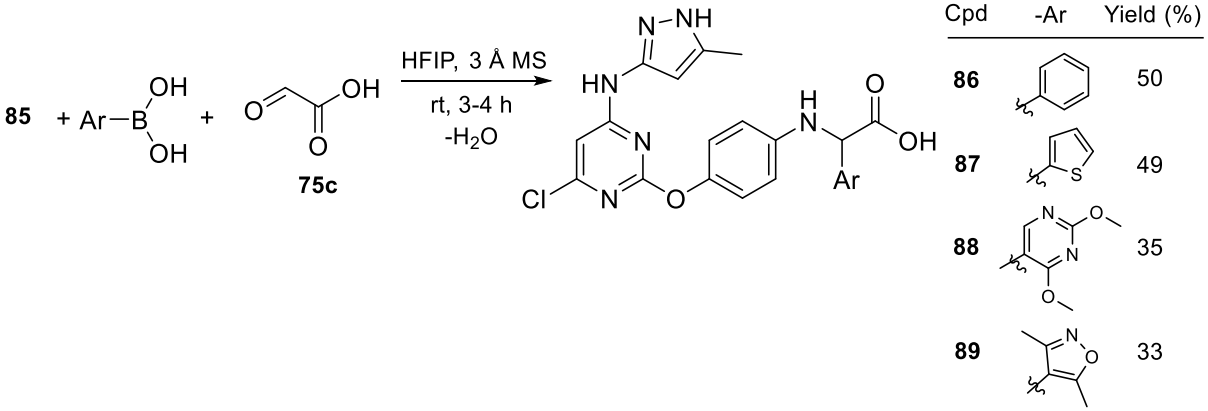

2-((4-((4-Chloro-6-((5-methyl-1*H*-pyrazol-3-yl)amino)pyrimidin-2yl)oxy)phenyl)amino)-2-phenylacetic acid (86)

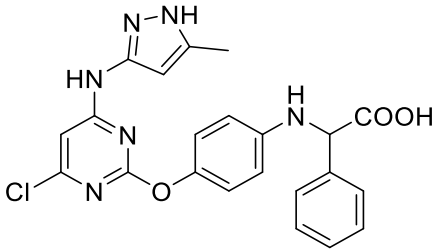

Using the general procedure for the preparation of **86-89**. Compound **86** was obtained from 2-(4-aminophenoxy)-6-chloro-*N*-(5-methyl-1*H*-pyrazol-3-yl)pyrimidin-4-amine, **85** (1 equiv., 42 mg, 0.13 mmol), glyoxylicacid monohydrate (**75c**) (1.2 equiv., 14.7 mg, 0.16 mmol), phenylboronic acid (1.2 equiv., 19.4 mg, 0.16 mmol) in HFIP (2 mL). Purified as a brown powder (29.9 mg, 50% yield). ^{1}H NMR (600 MHz, DMSO-d_6) δ = 10.24 (s, 1H), 7.54 (d, *J* = 7.2 Hz, 2H), 7.37 (m, 2H), 7.31 (m, 1H), 6.89 (d, *J* = 9.0 Hz, 2H), 6.71 (d, *J* = 9.0 Hz, 2H), 5.76 (s, 1H), 5.08 (s, 1H), 3.10-3.05 (m, 1H), 2.09 (s, 3H). ^{13}C NMR (151 MHz, DMSO) δ = 172.95, 164.96, 161.38, 147.12, 144.57, 143.55, 138.56, 128.53, 127.87, 127.54, 124.23, 122.18, 113.42, 98.82, 95.84, 79.21, 60.18, 45.61, 10.50. HRMS (ESI): m/z calculated for $C_{22}H_{20}ClN_6O_3$ $[M + H]^+$: 451.1280, Found: 451.1276.

2-((4-((4-Chloro-6-((5-methyl-1*H*-pyrazol-3-yl)amino)pyrimidin-2yl)oxy)phenyl)amino)-2-(thiophen-2-yl)acetic acid (87)

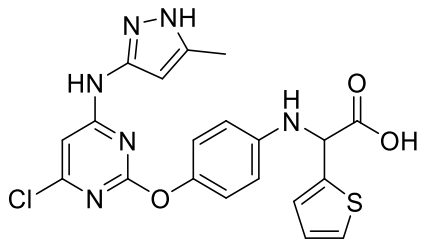

Using the general procedure for the preparation of **86-89**. Compound **87** was obtained from 2-(4-aminophenoxy)-6-chloro-*N*-(5-methyl-1*H*-pyrazol-3-yl)pyrimidin-4-amine (**85**) (50.00 mg, 0.16 mmol), glyoxylic acid monohydrate (**75c**) (17.44 mg, 0.19 mmol), 2-thienylboronic acid (24.24 mg, 0.19 mmol) in HFIP (2 mL). Purified as a white powder (35 mg, 49 % yield). ^{1}H NMR (500 MHz, DMSO-d_6) δ = 7.47 (d, 1H, *J* = 5.0 Hz), 7.21 (m, 1H), 7.03-7.01 (m, 1H), 6.92-6.91 (m, 2H), 6.76 (d, *J* = 7.5 Hz, 2H), 6.46 (s, 1H), 5.76 (s, 1H), 5.35 (s, 1H), 2.08 (s, 3H). HRMS (ESI): m/z calculated for $C_{20}H_{18}ClN_6O_3S$ $[M + H]^+$: 457.0845, Found: 457.0845.

2-((4-((4-Chloro-6-((5-methyl-1*H*-pyrazol-3-yl)amino)pyrimidin-2yl)oxy)phenyl)amino)-2-(2,4-dimethoxypyrimidin-5-yl)acetic acid (88)

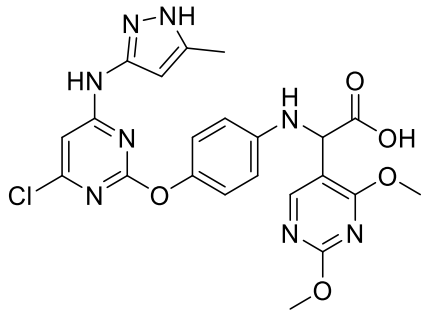

Using general procedure for the preparation of **86-89** was obtained from 2-(4-aminophenoxy)-6-chloro-*N*-(5-methyl-1*H*-pyrazol-3-yl)pyrimidin-4-amine (**85**) (1 equiv. 35.00 mg, 0.11 mmol), glyoxylicacid monohydrate (**75c**) (1.2 equiv., 12.21 mg, 0.13 mmol), 2,4-dimethoxypyrimidin-5-boronsäure (1.2 equiv., 24.39 mg, 0.13 mmol), (1.2 equiv.,16.02 mg, 0.11 mmol) in HFIP (1.5 mL). Purified as a white powder (19 mg, 35 % yield). ^{1}H NMR (500 MHz, CD_3OD) δ = 8.37 (s, 1H), 6.99-6.97 (m, 2H), 6.78-6.77 (m, 2H), 6.65 (s, 1H), 5.81 (s, 1H), 5.30 (s, 1H), 4.13 (s, 3H), 4.04 (s, 3H), 2.16 (s, 3H). ^{13}C NMR (126 MHz, CD_3OD) δ= 173.62, 170.98, 166.66, 165.83, 157.17, 146.36, 145.48, 125.26, 124.96, 123.72, 115.39, 114.08, 100.20, 97.48, 55.94, 55.35, 54.80,10.93. HRMS (ESI): m/z calculated for $C_{22}H_{22}ClN_8O_5$ $[M + H]^+$: 513.1397, Found: 513.1387.

2-((4-((4-Chloro-6-((5-methyl-1*H*-pyrazol-3-yl)amino)pyrimidin-2yl)oxy)phenyl)amino)-2-(3,5-dimethylisoxazol-4-yl)acetic acid (89)

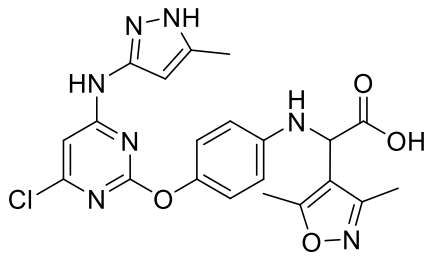

Using general procedure for the preparation of **86-89** was obtained from 2-(4-aminophenoxy)-6-chloro-*N*-(5-methyl-1*H*-pyrazol-3-yl)pyrimidin-4-amine (**85**) (1 equiv. 30.00 mg, 0.095mmol), glyoxylicacid monohydrate (**75c**) (1.2 equiv., 10.46 mg, 0.11 mmol), 3,5-dimethylisoxazol-4-yl-4-boronic acid, (1.2 equiv.,16.02 mg, 0.11 mmol) in HFIP (1.5 mL). Purified as a white powder (15 mg, 34 % yield). ^{1}H NMR (600 MHz, CD_3OD) δ = 7.46-7.45 (m, 1H), 7.39-7.38 (m, 1H), 6.98-6.97 (m, 2H), 6.72-6.70 (m, 2H), 6.66 (s, 1H), 5.37 (s, 1H), 5.03 (s, 1H), 2.47 (s, 3H), 2.31 (s, 3H), 2.16 (s, 3H). ^{13}C NMR (151 MHz, CD_3OD) δ= 173.70, 168.86, 166.82, 160.79, 146.26, 145.91, 142.55, 125.19, 125.07, 123.81, 115.05, 112.89, 100.21, 99.67, 52.83, 11.46, 11.12, 10.62. HRMS (ESI): m/z calculated for $C_{21}H_{21}ClN_7O_4$ [M + H] $^{+}$: 470.1339, Found: 470.1348.

2-(4-(6-((5-Methyl-1*H*-pyrazol-3-yl)amino)-2-(4-sulfamoylphenoxy)pyrimidin-4-yl)piperazin-1-yl)-2-phenylacetic acid (91)

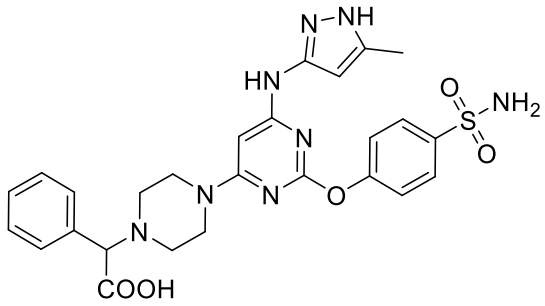

Compound **83** (1 equiv., 0.091 mmol) and piperazine (6.5 equiv., 0.60 mmol) were dissolved in 1,4-dioxane and refluxed at 100 ˚C until complete conversion, monitored by LC-MS. The reaction mixture was then cooled to room temperature, and a saturated solution of sodium bicarbonate was added to the reaction mixture, which was extracted with EtOAc (x3). The combined organic layers were dried over magnesium sulfate and evaporated *in vacuo*. The resultant crude product (**90**) was directly used for the next step without further purification.

90 (1 equiv., 33.00 mg, 0.08 mmol), glyoxylic acid monohydrate (1.2 equiv., 8.47 mg, 0.09 mmol), and phenyl boronic acid (1.2 equiv., 11.22 mg, 0.09 mmol) were added simultaneously to hexafluoro-2-propanol (HFIP) (0.1 M) with 3Å molecular sieves. The mixture was stirred at room temperature and monitored by LC-MS and TLC. The solvent then evaporated under reduced pressure. The resulting residue was purified by preparative HPLC using water and acetonitrile (0-95% gradient) to yield pure product **91** as a white powder (32 mg, 75 %). ^{1}H NMR (500 MHz, CD_3OD) δ = 7.95-7.94 (m, 2H), 7.74-7.72 (m, 1H), 7.57-7.55 (m, 2H), 7.47-7.46 (m, 3H), 7.31 (d, *J* = 8.6 Hz, 2H), 6.88-6.86 (m, 1H), 5.75 (s, 1H), 4.52 (s, 1H), 3.75 (s, 4H), 3.29 (s, 4H), 2.97-2.95 (m, 2H), 2.19 (s, 3H) ^{13}C NMR (126 MHz, CD_3OD) δ= 165.50, 163.66, 162.44, 157.59, 141.49, 134.86, 133.28, 131.03, 130.64, 130.38, 129.35, 128.81, 123.53, 116.31, 96.47, 80.88, 75.64, 51.82, 49.51, 49.34, 49.17, 49.00, 48.83, 48.66, 48.49, 42.78, 11.10. HRMS (APCI): m/z calculated for $C_{26}H_{29}N_8O_5S$ $[M + H]^+$: 565.1977, Found: 565.1986.

6-Chloro-*N*-(5-methyl-1*H*-pyrazol-3-yl)-2-(pyridin-4-ylmethoxy)pyrimidin-4-amine (92)

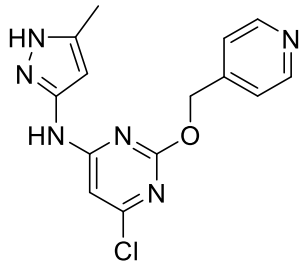

The synthesis was carried out as described in the literature, [142] and the pure product **92** as a white powder (yield 89%)**.** ^{1}H NMR (600 MHz, CD_3OD) δ = 8.80 (d, *J* =6.6 Hz, 2H), 8.06 (d, *J* = 6.6 Hz, 2H), 6.83 (s, 1H), 6.07 (s, 1H), 5.71 (s, 2H), 2.30 (s, 3H). Spectroscopic data were in accordance with the reported literature.[137]

Methyl 1-(4-((3-methyl-1*H*-pyrazol-5-yl)amino)pyrimidin-2-yl)piperidine-4-carboxylate (95)

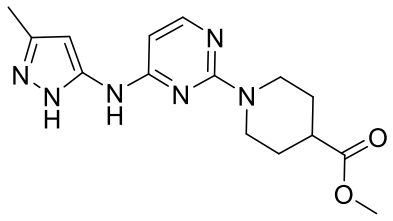

3-Methyl-1*H*-pyrazol-5-amine (1.1 equiv., 717.09 mg, 7.38 mmol) was dissolved in ethanol (15 mL), then 2,4-dichloropyrimidine (1 equiv., 1000.00 mg, 6.71 mmol) was added, followed

by DIPEA (1.7 equiv., 2 mL). The mixture was heated at 50 °C for 24 h, cooled, and evaporated to dryness to give an orange gum Purified by flash silica chromatography, elution gradient 0-10% MeOH in DCM to obtain pure product 2-chloro-*N*-(3-methyl-1*H*-pyrazol-5-yl)pyrimidin-4-amine (**94**) as a yellow powder (Yield 900.58 mg, 64%). Intermediate **94** (374.30 mg, 1.78 mmol) was dissolved in 1,4-dioxane (4 mL), and to it methyl piperidine-4-carboxylate 1.2 equiv, 286. 33 mg, 2 mmol) was added and stirred at 80 °C for 72 h. The solvent then evaporated under reduced pressure. The resulting residue was purified by preparative HPLC using water and acetonitrile (0-95% gradient) to yield the pure product **95** as a white powder (564.85 mg, quant.). ^{1}H NMR (500 MHz, DMSO-d_6) δ = 11.88 (s, 1H), 9.32 (s, 1H), 7.87 (d, 1H, *J* = 6.0 Hz), 6.31 (s, 1H), 6.11 (s, 1H), 2.11 (m, 2H), 3.61 (s, 3H), 2.98 (m, 2H), 2.62 (m, 1H), 2.20 (s, 3H), 1.86 (m, 2H), 1.48 (m, 2H). ^{13}C NMR (126 MHz, DMSO-d_6) δ= 174.70, 172.09, 161.13, 159.78, 156.06, 138.23, 95.89, 95.15, 51.47, 42.78, 40.49, 27.49, 10.81. HRMS (ESI): m/z calculated for $C_{15}H_{21}N_6O_2$ $[M+H]^+$: 317.1721, found: 317.1722.

Ethyl (2-((3-methyl-1*H*-pyrazol-5-yl)amino)pyrimidin-4-yl)carbamate (97)

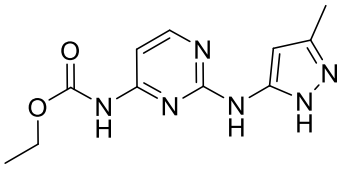

Ethylcarbamate (1 equiv., 100 mg, 1.12 mmol) was dissolved in DMF (1.5 mL), and the mixture was maintained under an argon atmosphere at -20˚C. Then sodium hydride (60%, 1.5 equiv., 67.34 mg, 1.68 mmol) was added carefully to the reaction mixture, which was allowed to stir for 15 min, followed by the addition of 2,4-dichloropyrimidine (1 equiv., 167.22 mg, 1.12 mmol). The resulting mixture was allowed to warm to room temperature and stirred overnight. Once the reaction is completed, as monitored by TLC or LC-MS, the mixture is carefully quenched using methanol and extracted using ethyl acetate. The organic layers were combined, dried over anhydrous magnesium sulphate, and evaporated *in vacuo* to obtain the crude product ethyl (2-chloropyrimidin-4-yl)carbamate (**96**) (203.66 mg, 90%), which was directly used in the next step without further purification. 5-methyl-1*H*-pyrazole-3-amine (1 equiv., 24.09 mg, 0.23 mmol) was added to **96** (2 equiv., 100 mg, 0.496 mmol) dissolved in ethanol (5 ml). To this mixture, *p*-toluenesulfonic acid monohydrate (1 equiv., 94.35 mg, 0.50 mmol) was added and stirred the mixture at 100 °C in reflux for 12 h. Once the reaction is complete, neutralize the mixture with a saturated aqueous solution. of $NaHCO_3$. Extract the resulting mixture with EtOAc (x 3). Dry over magnesium sulphate and purified by preparative

HPLC using water and acetonitrile (0-95% gradient) to yield the pure product **97** as a white powder (81 mg, 62 %). ^{1}H NMR (500 MHz, $CDCl_3$) δ = 10.57 (s, 1H), 8.23 (d, 1H, *J* = 6.5 Hz), 7.77 (d, 1H, *J* = 6.5 Hz), 6.02 (s, 1H), 4.29 (q, 2H, *J*= 7.5 Hz), 2.42 (s, 3H), 1.36 (t, 3H, *J* = 7.5 Hz). ^{13}C NMR (126 MHz, $CDCl_3$) δ= 164.23, 161.49, 154.42, 153.13, 143.21, 141.28, 102.14, 94.66, 62.76, 14.07, 11.70. HRMS (ESI): m/z calculated for $C_{11}H_{15}N_6O_2$ $[M+H]^+$: 263.1251, found: 263.1250.

(*S*)-*N*-(6-Methyl-5-((3-(2-(piperidin-3-ylamino)pyrimidin-4-yl)pyridin-2-yl)oxy)naphthalen-1-yl)but-2-ynamide (G7658)

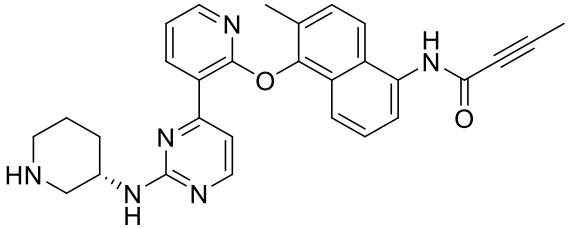

The reference compound **G7658** was synthesized in accordance with a previously reported method.[133] The product was obtained as a yellow powder. Spectroscopic data were consistent with those reported in the literature.[133] ^{1}H NMR (600 MHz, MeOD) δ = 8.64 (d, *J*= 7.2 Hz, 1H), 8.45 (d, *J*= 5.4 Hz, 1H), 7.98 (dd, *J*= 1.8 Hz, 4.8 Hz, 1H), 7.86 (d, *J*= 8.4, 1H), 7.69 (d, *J*=5.4, 1H), 7.62 (d, *J*=8.4, 1H), 7.57 (d, *J*=7.2, 1H), 7.52 (d, *J*=8.4, 1H), 7.39 (m, 1H), 7.22 (dd, *J*=4.8 Hz, 7.8 Hz, 1H), 4.36 (m, 1H), 3. 61 (dd, *J*= 3 Hz, 12 Hz, 1H), 3.35-3.33 (m, 1H), 3.09-3.03 (m 2H), 2.27 (s, 3H), 2.22-2.12 (m, 2H), 2.10 (s, 3H), 1.92-1.77 (m, 2H).

5.3 X-Ray crystallography

5.3.1 X-Ray diffraction parameters and data for 5a

Compound **5a** was crystallized from a solvent mixture of dichloromethane and diethyl ether at room temperature, yielding single crystals. The asymmetric unit comprises two distinct molecules. Structural analysis of **5a** revealed disorder in the thiophene substituent, which was resolved during refinement.

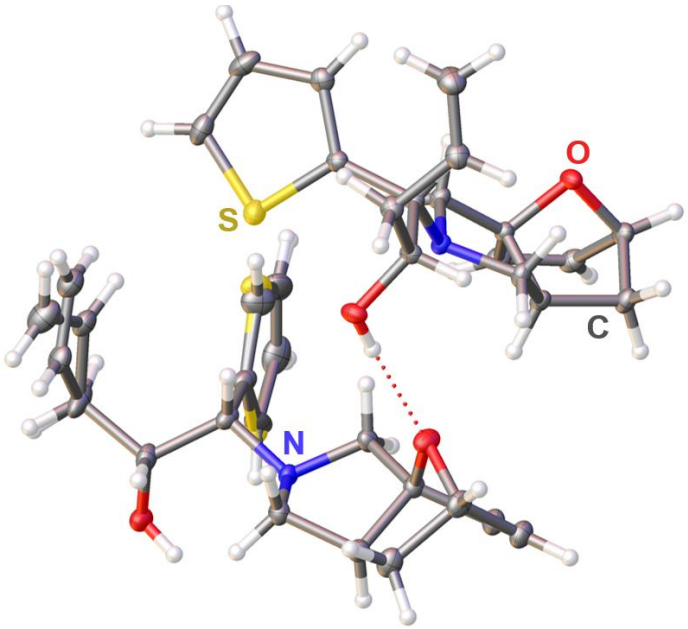

Figure S1. Single Crystal X-ray structure of **5a** (CCDC number: 2191710)

Compound ID	**mo_B2684**
Formula	$C_{17}H_{21}NO_2S$
$D_{calc.}$/ g cm^{-3}	1.327
m/mm^{-1}	0.217
Formula Weight	303.41
Colour	colourless
Shape	plate
Size/mm^3	0.66×0.28×0.12
T/K	100.00
Crystal System	monoclinic

Space Group	$P2_1/c$
a/Å	9.9071(4)
b/Å	15.6821(5)
c/Å	19.5899(7)
a/°	90
b/°	93.5510(10)
g/°	90
V/Å^3	3037.72(19)
Z	8
Z'	2
Wavelength/Å	0.71073
Radiation type	MoK$_a$
Q_{min}/°	2.060
Q_{max}/°	31.610
Measured Refl.	202138
Independent Refl.	10174
Reflections with I > 2(I)	8849
R_{int}	0.0560
Parameters	419
Restraints	0
Largest Peak	0.811
Deepest Hole	-0.502
GooF	1.057
wR_2 (all data)	0.1137
wR_2	0.1082
R_1 (all data)	0.0486
R_1	0.412

5.3.2 X-Ray diffraction parameters and data for 9a

Compound **9a** was crystallized from a solvent mixture of dichloromethane and acetonitrile at room temperature, yielding single crystals. Disorder at the thiophene substituent in the structure of **9a** was resolved in refinement.

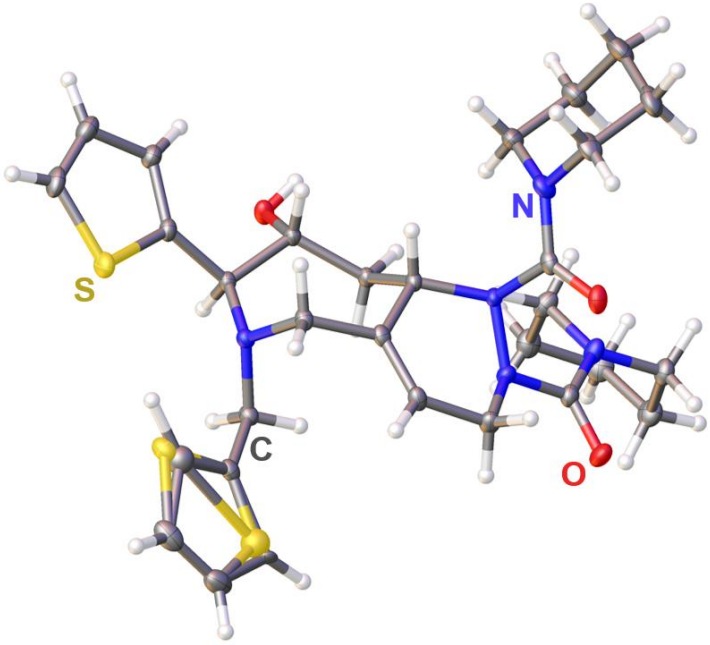

Figure S2. Single Crystal X-ray structure of **9a** (CCDC number: 2191711)

Compound ID	**mo_B2666_0m**
Empirical formula	$C_{29}H_{39}N_5O_3S_2$
Formula weight	569.77
Temperature/K	100.00
Crystal system	monoclinic
Space group	$P2_1/n$
a/Å	9.725(2)
b/Å	13.562(3)
c/Å	22.111(5)
α/°	90
β/°	98.704(10)
γ/°	90

Volume/Å^3	2882.7(11)
Z	4
ρ_{calc}g/cm^3	1.313
μ/mm^{-1}	0.224
F(000)	1216.0
Crystal size/mm^3	0.216 × 0.192 × 0.061
Radiation	MoKα (λ = 0.71073)
2Θ range for data collection/°	3.728 to 60.192
Index ranges	$-13 \leq h \leq 13$, $-18 \leq k \leq 19$, $-31 \leq l \leq 31$
Reflections collected	62861
Independent reflections	8474 [R_{int} = 0.0458, R_{sigma} = 0.0296]
Data/restraints/parameters	8474/0/377
Goodness-of-fit on F^2	1.062
Final R indexes [I>=2σ (I)]	R_1 = 0.0417, wR_2 = 0.0920
Final R indexes [all data]	R_1 = 0.0578, wR_2 = 0.1013
Largest diff. peak/hole / e Å^{-3}	0.31/-0.47

5.3.3 X-Ray diffraction parameters and data for 9j

Compound **9j** was crystallized from a solvent mixture of dichloromethane and acetonitrile at room temperature, yielding single crystals. Structural analysis of **9j** revealed disorder in the thiophene substituent, which was resolved during refinement.

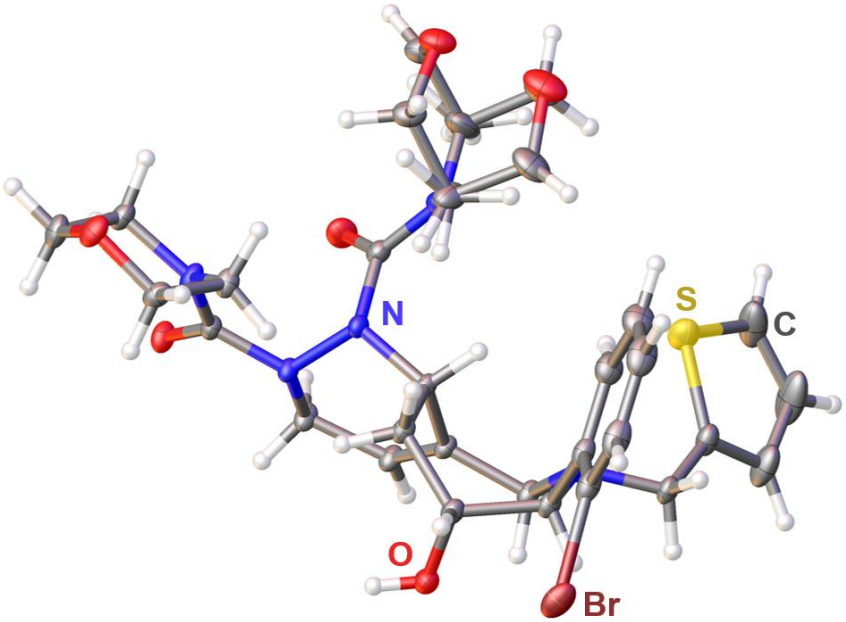

Figure S3. Single Crystal X-ray structure of **9j** (CCDC number: 2191712)

Compound ID	**mo_B2498_0m**
Empirical formula	$C_{29}H_{35}BrN_5O_5S$
Formula weight	645.59
Temperature/K	100.00
Crystal system	triclinic
Space group	P-1
a/Å	10.1270(3)
b/Å	12.4110(5)
c/Å	12.9814(5)
α/°	94.3570(10)
β/°	105.8450(10)
γ/°	109.4430(10)

Volume/Å^3	1454.83(9)
Z	2
ρ_{calc}g/cm^3	1.474
μ/mm^{-1}	1.533
F(000)	670.0
Crystal size/mm^3	0.264 × 0.193 × 0.125
Radiation	MoKα (λ = 0.71073)
2Θ range for data collection/°	3.54 to 66.552
Index ranges	$-15 \leq h \leq 14$, $-19 \leq k \leq 19$, $-19 \leq l \leq 19$
Reflections collected	79554
Independent reflections	10929 [R_{int} = 0.0447, R_{sigma} = 0.0304]
Data/restraints/parameters	10929/0/399
Goodness-of-fit on F^2	1.025
Final R indexes [I>=2σ (I)]	R_1 = 0.0400, wR_2 = 0.1019
Final R indexes [all data]	R_1 = 0.0529, wR_2 = 0.1088
Largest diff. peak/hole / e Å^{-3}	1.27/-0.87

5.4 Biological Evaluation

5.4.1 Methods for evaluation of Petasis-sequence reaction products

Antiproliferative MTT assay in cancer cells

To assess the anti-proliferative effects of the synthesized compounds, an MTT assay was conducted. MOLM13 and JAR cancer cell lines (from DSMZ – German Collection of Microorganisms and Cell Cultures, Braunschweig) were plated at a density of 4,000 cells per well in 96-well plates and allowed to adhere and grow for 24 hours. Following incubation, the existing medium was removed and replaced with fresh medium containing the test compounds. A vehicle control consisting of medium with 1% DMSO was used for normalization. After 72 hours of treatment, 20 µL of MTT solution (5 mg/mL) was added to each well under light-protected conditions, and the cells were incubated for an additional 4 hours. Subsequently, the medium containing MTT was discarded, and 150 µL of DMSO was added to each well to solubilize the formazan crystals. Absorbance was measured at 492 nm using a TECAN plate reader.

5.4.2 Methods for the identification and evaluation of IRE1α modulators

IRE1α expression and purification

The purification of protein was carried out by following the reported procedures.[133] The gene segment encoding the human IRE1α kinase and RNase domains (residues 547–977) was cloned into a pLIB vector featuring a His-tag and a TEV protease cleavage site. Expression was carried out using the Bac-to-Bac baculovirus system. For protein expression, SF9 insect cells were infected with recombinant baculovirus and incubated for 72 h at 27 °C, with shaking at 110 rpm. After harvesting by centrifugation at 4,000 rpm for 15 minutes, the cell pellets were resuspended in lysis buffer (300 mM Sodium Chloride, 50 mM HEPES pH 7.5, 10% glycerol, 1 mM $MgCl_2$, 1 mM TCEP, 5 mM imidazole). The buffer was enriched with benzonase (1:10,000 dilution; Sigma E1014), one SIGMAFAST™ protease inhibitor tablet per 25 mL (Sigma S8830), and 1 mM PMSF. Lysis was achieved via sonication on ice. The lysate was clarified by centrifugation at 20,000 rpm for 45 minutes, and the supernatant was filtered before loading onto a pre-equilibrated Ni^{2+}-affinity column (Ni Sepharose™ 6 Fast Flow, GE Healthcare). After washing with lysis buffer containing 30 mM imidazole, the target protein was eluted with lysis buffer with 300 mM imidazole. The eluted protein was incubated overnight at 4 °C with TEV protease to remove the His-tag. The resulting sample was diluted sixfold in buffer (5% glycerol, 50 mM HEPES pH 7.5, 1 mM TCEP,) and loaded onto a 5 mL

HiTrap Q HP anion exchange column (Cytiva) equilibrated in QA buffer (50 mM Sodium chloride, 50 mM HEPES pH 7.5, 1 mM TCEP, 5% glycerol). A linear gradient elution (0–30%) of QB buffer (1M NaCl, 5% glycerol, 50 mM HEPES (pH 7.5), 1 mM TCEP) was used to separate phosphorylated and unphosphorylated protein species. Fractions were analyzed by LC-MS to confirm phosphorylation states. The phosphorylated IRE1α fraction was further purified using size-exclusion chromatography (HiLoad 16/600 Superdex 200 pg column, Cytiva) in SEC buffer (10% glycerol, 25 mM HEPES (pH 7.5), 1 mM TCEP, 250 mM NaCl), and monomeric fractions were collected. Remaining fractions from the anion exchange step were treated overnight with Lambda protein phosphatase (New England BioLabs, P0753S) at 4 °C. Dephosphorylation was verified by LC-MS, followed by another round of size-exclusion chromatography in the same SEC buffer. Final purified proteins were frozen and stored at −80 °C.

Small-molecule screening

An RNase activity-based small-molecule screen aimed at identifying novel modulators of RNase activity was conducted using an in-house library of approximately 10000 compounds, sourced from COMAS, MPI Dortmund. The FRET assay described below was used to assess the compound's activity. Each compound was tested at a concentration of 5 μM in a 384-well black plate with 40 nM IRE1α protein and 100 nM dual-labeled RNA substrate.

FRET assay

RNA substrate bearing a 5′ FAM fluorophore and a 3′ BHQ-1 quencher, corresponding to the *XBP1* cleavage sequence (5′FAM-CAUGUCCGCAGCGCAUG-3′BHQ1), was obtained from Integrated DNA Technologies (IDT). The assay was performed in a reaction buffer (50 mM potassium acetate, 20 mM HEPES (pH 7.5), 1 mM magnesium acetate, 1 mM DTT, and 0.05% Triton X-100), with a final volume of 20 μL per well using black 384-well plates. For experiments involving unphosphorylated IRE1α, final concentrations of 40 nM IRE1α protein and 100 nM RNA substrate were used. In contrast, reactions with phosphorylated IRE1α (p-IRE1α) employed 4 nM protein and 200 nM substrate. The protein and compounds were pre-incubated at room temperature for 30 minutes before initiating the reaction with the RNA substrate. Fluorescence signals were monitored kinetically for one hour using a TECAN Spark plate reader with excitation at 485 nm and emission at 535 nm (both with 10 nm bandwidths), in top-read mode. The initial linear portion of each fluorescence-time curve was fitted using

linear regression to calculate the slope, representing reaction velocity. Percent inhibition was calculated using the following formula:

Inhibition (%) = 100 × [(slope of DMSO control – slope of sample) / (slope of DMSO control – slope of blank)],

where the DMSO control contained both protein and substrate, and the blank contained only substrate in DMSO. The dose-response model in GraphPad Prism 9 software was used to determine the IC_{50} values.

Gel-based cleavage assay

To assess cleavage activity, p-IRE1α (10 nM) was incubated with test compounds for 30 min at ambient temperature. Following incubation, FAM and BHQ-labeled *XBP1* (50 nM) RNA substrate was introduced and let it incubated for another 45 min at room temperature. Reactions were terminated by mixing with 6× TBE loading dye containing 40% glycerol, 45% water, 15% 10× TBE, and 0.1% of bromophenol blue. A 5 μL aliquot of each reaction mixture was loaded onto a 15% denaturing urea-PAGE gel that had been pre-run in 1× TBE buffer at approximately 60 °C. Gel electrophoresis was conducted in the dark to preserve fluorophore integrity. After separation, fluorescence signals were captured using the ChemiDoc MP system (Bio-Rad) to detect cleaved RNA fragments.

LanthaScreen™ Eu-based kinase assay and kinase profiling.

Kinase binding interactions were evaluated using the LanthaScreen™ Eu binding assay, conducted by Thermo Fisher's SelectScreen Kinase Profiling Services. For the IRE1α (ERN1) assay, reaction mixtures contained 5 nM of ERN1, 2 nM of Eu-labeled anti-GST antibody, and 100 nM of tracer 236 (K_D= 160 nM). In the IRE1β (ERN2) assay, the same concentrations were used, with tracer 236 having a K_D of 108 nM. Changes in FRET signal were used to assess compound binding affinity.

Broad-spectrum kinase profiling was carried out by Thermo Fisher's SelectScreen Kinase Profiling Services using a combination of assay platforms, including Z′-LYTE™, Adapta™, and LanthaScreen™ Eu kinase binding assays, depending on the target kinase.

DSS-crosslinking assay

To probe protein-compound interactions, phosphorylated IRE1α (2 μM) was incubated in a buffer (50 mM KOAc, 1 mM $MgOAc_2$, 20 mM HEPES, pH 7.5, 1 mM DTT, 0.05% v/v TritonX-100) with selected compounds (100 μM) for 30 minutes at room temperature. Following incubation, disuccinimidyl suberate was added to a final concentration of 250 μM to initiate crosslinking, which proceeded for 1 hour at room temperature. The reaction was quenched by adding Tris buffer (pH 7.5) to a final concentration of 50 mM. Crosslinked samples were analyzed by mass photometry using an instrument from Refeyn Ltd. Prior to measurement, samples were diluted to 100 nM protein concentration in PBS buffer. Results from three replicates were combined and analyzed by Discover MP software.

Differential scanning fluorimetry

Reactions were prepared in PBS buffer supplemented with 2 mM DTT, with a total volume of 20 μL per well. Each mixture contained 1 μM of dephosphorylated IRE1α protein, 5× SYPRO Orange dye (from a 5000X stock in DMSO; Sigma S5692), and test compounds at a final DMSO concentration of 1%. Thermal unfolding was monitored using a Bio-Rad CFX96 Real-Time PCR detection system in FRET scan mode. The temperature was increased from 25 °C to 95 °C in 1 °C increments, with each step lasting 30 seconds. The melting temperature (T_m) was derived by fitting the fluorescence data to a Boltzmann sigmoidal curve using GraphPad Prism software. The thermal shift (ΔT_m) was calculated using the following formula: $\Delta T_m = T_m$ (compound) – T_m (DMSO control).

Isothermal titration calorimetry assay

All ITC measurements were performed at 25 °C using a MicroCal PEAQ-ITC system (Malvern) in buffer (250 mM NaCl, 25 mM HEPES (pH 7.5), 1 mM TCEP, 5% glycerol, 1% DMSO). Pure IRE1α protein and compound samples were degassed before loading. 200 μM of compound was loaded into the syringe, while 10 μM of IRE1α protein was added to the calorimeter cell. For competitive binding assays, the protein was pre-incubated with a compound at a final DMSO concentration of 1% prior to loading. Experimental parameters included a reference power of 10 μcal/s, high feedback mode, and stirring at 750 rpm. After an initial delay of 60 seconds, 18 (or 15) injections of 2 μL each were performed following a 0.4 μL initial injection, with 150-second spacing between injections and 4-second durations. Data analysis was carried out using the MicroCal PEAQ-ITC software.

Microscale thermophoresis

Binding interactions between dephosphorylated IRE1α and small molecules were assessed using microscale thermophoresis. The protein was fluorescently labeled using the RED-NHS 2nd Generation Protein Labeling Kit (NanoTemper, MO-L011) following the manufacturer's protocol. Labeling was performed in a buffer consisting of 200 mM NaCl, 2% glycerol, 50 mM HEPES (pH 7.5), 0.5 mM TCEP, and 0.05% Tween-20. MST measurements were performed on a Monolith NT. 115 instrument (NanoTemper). Labeled protein was used at a final concentration of 20 nM. Compounds were prepared as a serial 2-fold dilution and incubated with the labeled protein. The highest tested concentration was 250 μM, with a final DMSO content of 2.5%. Measurements were taken using the red channel detector and 60% LED excitation power. Binding curves were generated, and data were processed using NanoTemper's analysis software. Measurements were done in three independent replicates.

Cell culture

The human cancer cell lines A549, HCT 116, HT-29, and MDA-MB-468 were procured from the American Type Culture Collection (ATCC) and cultured in high-glucose Dulbecco's Modified Eagle Medium (DMEM; Gibco, 61965026) supplemented with 1% penicillin-streptomycin (Gibco, 15140122) and 10% fetal bovine serum (FBS; Gibco, 10500064) and at 37 °C in a humidified incubator with 5% CO_2.

RT-qPCR

A549 cells (obtained from ATCC) were plated in 6-well plates at a density of 5 x 10^5 cells per well in 6-well plates and allowed to adhere overnight. The following day, cells were treated with either test compounds or DMSO control for 2 hours. Subsequently, tunicamycin (Tm) was introduced to achieve a final concentration of 0.5 μg/mL to induce endoplasmic reticulum (ER) stress, and cells were incubated for an additional 2 hours. Total RNA was extracted using the RNeasy Mini Kit (Qiagen, 74106), and 500 ng of RNA was used for cDNA synthesis using the High-Capacity cDNA Reverse Transcription Kit (Thermo Fisher, 4368814). The resulting cDNA was diluted 1:5 with RNase-free water, and 1 μL was used per qPCR reaction. Reactions were performed using PowerUp™ SYBR™ Green Master Mix (Thermo Fisher, A25742) in a total volume of 10 μL on a Bio-Rad CFX96 Real-Time PCR Detection System. Thermal cycling conditions followed the manufacturer's standard protocol for primers with annealing temperatures ≥60 °C. Gene expression data were analyzed using the $2^{-\Delta\Delta Ct}$ method. Inhibition percentages were determined using the following equation:

Inhibition (%) = 100 x (normalized Tm control − normalized sample) / (normalized Tm control − normalized DMSO control), where the Tm control refers to tunicamycin-treated cells and the DMSO control to vehicle-only treated cells.

Cell colony formation assay

HT-29 and MDA-MB-468 cell lines were purchased from ATCC, and MCF-7 was purchased from DMSZ (Deutsche Sammlung von Mikroorganismen und Zellkulturen). The cell lines were cultured as per the previously mentioned protocol under cell culture conditions. Each cell line was plated at a density of 1000 cells/well in 24-well plates and incubated overnight. Test compounds were diluted using medium, whereby a 2-times dilution was done with a total of 7 concentrations. Every three days, the medium was discarded, and the cells were treated with compounds that were dissolved in the medium. After 9 days, the medium was discarded, and cells were washed 2 times with 500 µL phosphate-buffered saline (PBS) and fixed with 4 % paraformaldehyde (500 µL) for 15 minutes. Following fixation, wells were washed again with PBS and stained using 0.1% (w/v) crystal violet solution for 15 minutes. Excess stain was removed by repeated PBS washes, and plates were left to dry overnight before imaging the resulting colonies.

6 References

(1) Nielsen, T. E.; Schreiber, S. L., Towards the optimal screening collection: a synthesis strategy. *Angew. Chem., Int. Ed. Engl.*, **2008,** *47*, 48.

(2) Dobson, C. M., Chemical space and biology. *Nature*, **2004,** *432*, 824.

(3) Thanh Le, G.; Abbenante, G.; Becker, B.; Grathwohl, M.; Halliday, J.; Tometzki, G.; Zuegg, J.; Meutermans, W., Molecular diversity through sugar scaffolds. *Drug Discov. Today*, **2003,** *8*, 701.

(4) Wetzel, S.; Bon, R. S.; Kumar, K.; Waldmann, H., Biology-Oriented Synthesis. *Angew. Chem. Int. Ed.*, **2011,** *50*, 10800.

(5) Wetzel, S.; Klein, K.; Renner, S.; Rauh, D.; Oprea, T. I.; Mutzel, P.; Waldmann, H., Interactive exploration of chemical space with Scaffold Hunter. *Nat. Chem. Biol.*, **2009,** *5*, 581.

(6) Gromski, P. S.; Henson, A.; Granda, J. M.; Cronin, L., How to explore chemical space using algorithms and automation. *Nat. Rev. Chem.*, **2019,** *3*, 119.

(7) Galloway, W. R. J. D.; Spring, D. R., Is synthesis the main hurdle for the generation of diversity in compound libraries for screening? *Expert Opin. Drug Discov.*, **2009,** *4*, 467.

(8) Ostresh, J. M.; Husar, G. M.; Blondelle, S. E.; Dörner, B.; Weber, P. A.; Houghten, R. A., "Libraries from libraries": chemical transformation of combinatorial libraries to extend the range and repertoire of chemical diversity. *Proc. Natl. Acad. Sci.*, **1994,** *91*, 11138.

(9) Galloway, W. R. J. D.; Isidro-Llobet, A.; Spring, D. R., Diversity-oriented synthesis as a tool for the discovery of novel biologically active small molecules. *Nat. Commun.*, **2010,** *1*, 80.

(10) Wetzel, S.; Bon, R. S.; Kumar, K.; Waldmann, H., Biology-oriented synthesis. *Angew. Chem., Int. Ed. Engl.*, **2011,** *50*, 10800.

(11) Gerry, C. J.; Schreiber, S. L., Chemical probes and drug leads from advances in synthetic planning and methodology. *Nat. Rev. Drug Discov.*, **2018,** *17*, 333.

(12) Wu, P.; Nielsen, T. E., Petasis three-component reactions for the synthesis of diverse heterocyclic scaffolds. *Drug Discov. Today Technol.*, **2018,** *29*, 27.

(13) Ruijter, E.; Scheffelaar, R.; Orru, R. V., Multicomponent reaction design in the quest for molecular complexity and diversity. *Angew. Chem., Int. Ed. Engl.*, **2011,** *50*, 6234.

(14) Sutanto, F.; Shaabani, S.; Neochoritis, C. G.; Zarganes-Tzitzikas, T.; Patil, P.; Ghonchepour, E.; Dömling, A., Multicomponent reaction–derived covalent inhibitor space. *Sci. Adv.,* **2021,** *7*, eabd9307.

(15) Dömling, A.; Wang, W.; Wang, K., Chemistry and Biology Of Multicomponent Reactions. *Chem. Rev.,* **2012,** *112*, 3083.

(16) Cioc, R. C.; Ruijter, E.; Orru, R. V. A., Multicomponent reactions: advanced tools for sustainable organic synthesis. *Green Chem.,* **2014,** *16*, 2958.

(17) Petasis, N. A.; Akritopoulou, I., The boronic acid mannich reaction: A new method for the synthesis of geometrically pure allylamines. *Tetrahedron Lett.,* **1993,** *34*, 583.

(18) Candeias, N. R.; Montalbano, F.; Cal, P. M. S. D.; Gois, P. M. P., Boronic Acids and Esters in the Petasis-Borono Mannich Multicomponent Reaction. *Chem. Rev.,* **2010,** *110*, 6169.

(19) Wu, P.; Givskov, M.; Nielsen, T. E., Reactivity and Synthetic Applications of Multicomponent Petasis Reactions. *Chem. Rev.,* **2019,** *119*, 11245.

(20) Cannillo, A.; Norsikian, S.; Retailleau, P.; Dau, M. E.; Iorga, B. I.; Beau, J. M., Fast synthesis of complex enantiopure heterocyclic scaffolds by a tandem sequence of simple transformations on α-hydroxyaldehydes. *Chemistry,* **2013,** *19*, 9127.

(21) Cannillo, A.; Norsikian, S.; Tran Huu Dau, M.-E.; Retailleau, P.; Iorga, B. I.; Beau , J.-M., From Enantiopure Hydroxyaldehydes to Complex Heterocyclic Scaffolds: Development of Domino Petasis/Diels–Alder and Cross-Metathesis/Michael Addition Reactions. *Chem. Eur. J.,* **2014,** *20*, 12133.

(22) Davis, A. S.; Pyne, S. G.; Skelton, B. W.; White, A. H., Synthesis of putative uniflorine A. *J. Org. Chem.,* **2004,** *69*, 3139.

(23) Marques, C.; Brandão, P., The Asymmetric Petasis Borono-Mannich Reaction: Insights on the Last 15 Years. *Catalysts,* **2023,** *13*, 1022.

(24) Wang, G.-B.; Wang, Y.-J.; Kan, J.-L.; Xie, K.-H.; Xu, H.-P.; Zhao, F.; Wang, M.-C.; Geng, Y.; Dong, Y.-B., Construction of Covalent Organic Frameworks via a Visible-Light-Activated Photocatalytic Multicomponent Reaction. *J. Am. Chem. Soc.,* **2023,** *145*, 4951.

(25) Rafiee, F.; Hosseinvand, S., CuII Immobolized on the Amidinoglycine Functionalized Magnetic Graphene Oxide Promoted the Alkyl Aminophenols Synthesis. *Iran. J. Sci. Technol. Trans. A: Sci.,* **2021,** *45*, 503.

(26) Ricardo, M. G.; Llanes, D.; Wessjohann, L. A.; Rivera, D. G., Introducing the Petasis Reaction for Late-Stage Multicomponent Diversification, Labeling, and Stapling of Peptides. *Angew. Chem. Int. Ed.,* **2019,** *58*, 2700.

(27) Vytla, D.; Emmadi, J.; Velayuthaperumal, R.; Shaw, P.; Cavallaro, C. L.; Mathur, A.; Roy, A., Visible-light enabled one-pot three-component Petasis reaction for synthesis of α-substituted secondary sulfonamides/amides/hydrazides. *Tetrahedron Lett.,* **2022,** *106*, 154055.

(28) Avathan Veettil, A. K.; Kirchhoff, J.-L.; Brieger, L.; Strohmann, C.; Wu, P., Petasis Sequence Reactions for the Scaffold-Diverse Synthesis of Bioactive Polycyclic Small Molecules. *ACS Omega,* **2023,** *8*, 1168.

(29) Ascic, E.; Le Quement, S. T.; Ishoey, M.; Daugaard, M.; Nielsen, T. E., Build/couple/pair strategy combining the Petasis 3-component reaction with Ru-catalyzed ring-closing metathesis and isomerization. *ACS Comb. Sci.,* **2012,** *14*, 253.

(30) Flagstad, T.; Hansen, M. R.; Le Quement, S. T.; Givskov, M.; Nielsen, T. E., Combining the Petasis 3-Component Reaction with Multiple Modes of Cyclization: A Build/Couple/Pair Strategy for the Synthesis of Densely Functionalized Small Molecules. *ACS Comb. Sci.,* **2015,** *17*, 19.

(31) Ishoey, M.; Petersen, R. G.; Petersen, M. Å.; Wu, P.; Clausen, M. H.; Nielsen, T. E., Diastereoselective synthesis of novel heterocyclic scaffolds through tandem Petasis 3-component/intramolecular Diels–Alder and ROM–RCM reactions. *Chemical Commun.,* **2017,** *53*, 9410.

(32) Flagstad, T.; Azevedo, C. M. G.; Min, G.; Willaume, A.; Morgentin, R.; Nielsen, T. E.; Clausen, M. H., Petasis/Diels–Alder/Cyclization Cascade Reactions for the Generation of Scaffolds with Multiple Stereogenic Centers and Orthogonal Handles for Library Production. *Eur. J. Org. Chem.,* **2018,** *2018*, 6596.

(33) Crick, F., Central dogma of molecular biology. *Nature,* **1970,** *227*, 561.

(34) Caprara, M. G.; Nilsen, T. W., RNA: Versatility in form and function. *Nat. Struct. Biol.,* **2000,** *7*, 831.

(35) Djebali, S.; Davis, C. A.; Merkel, A.; Dobin, A.; Lassmann, T.; Mortazavi, A.; Tanzer, A.; Lagarde, J.; Lin, W.; Schlesinger, F.; Xue, C.; Marinov, G. K.; Khatun, J.; Williams, B. A.; Zaleski, C.; Rozowsky, J.; Röder, M.; Kokocinski, F.; Abdelhamid, R. F.; Alioto, T.; Antoshechkin, I.; Baer, M. T.; Bar, N. S.; Batut, P.; Bell, K.; Bell, I.; Chakrabortty, S.; Chen, X.; Chrast, J.; Curado, J.; Derrien, T.; Drenkow, J.; Dumais, E.; Dumais, J.; Duttagupta, R.; Falconnet, E.; Fastuca, M.;

Fejes-Toth, K.; Ferreira, P.; Foissac, S.; Fullwood, M. J.; Gao, H.; Gonzalez, D.; Gordon, A.; Gunawardena, H.; Howald, C.; Jha, S.; Johnson, R.; Kapranov, P.; King, B.; Kingswood, C.; Luo, O. J.; Park, E.; Persaud, K.; Preall, J. B.; Ribeca, P.; Risk, B.; Robyr, D.; Sammeth, M.; Schaffer, L.; See, L.-H.; Shahab, A.; Skancke, J.; Suzuki, A. M.; Takahashi, H.; Tilgner, H.; Trout, D.; Walters, N.; Wang, H.; Wrobel, J.; Yu, Y.; Ruan, X.; Hayashizaki, Y.; Harrow, J.; Gerstein, M.; Hubbard, T.; Reymond, A.; Antonarakis, S. E.; Hannon, G.; Giddings, M. C.; Ruan, Y.; Wold, B.; Carninci, P.; Guigó, R.; Gingeras, T. R., Landscape of transcription in human cells. *Nature*, **2012,** *489*, 101.

(36) Lander, E. S.; Linton, L. M.; Birren, B.; Nusbaum, C.; Zody, M. C.; Baldwin, J.; Devon, K.; Dewar, K.; Doyle, M.; FitzHugh, W.; Funke, R.; Gage, D.; Harris, K.; Heaford, A.; Howland, J.; Kann, L.; Lehoczky, J.; LeVine, R.; McEwan, P.; McKernan, K.; Meldrim, J.; Mesirov, J. P.; Miranda, C.; Morris, W.; Naylor, J.; Raymond, C.; Rosetti, M.; Santos, R.; Sheridan, A.; Sougnez, C.; Stange-Thomann, N.; Stojanovic, N.; Subramanian, A.; Wyman, D.; Rogers, J.; Sulston, J.; Ainscough, R.; Beck, S.; Bentley, D.; Burton, J.; Clee, C.; Carter, N.; Coulson, A.; Deadman, R.; Deloukas, P.; Dunham, A.; Dunham, I.; Durbin, R.; French, L.; Grafham, D.; Gregory, S.; Hubbard, T.; Humphray, S.; Hunt, A.; Jones, M.; Lloyd, C.; McMurray, A.; Matthews, L.; Mercer, S.; Milne, S.; Mullikin, J. C.; Mungall, A.; Plumb, R.; Ross, M.; Shownkeen, R.; Sims, S.; Waterston, R. H.; Wilson, R. K.; Hillier, L. W.; McPherson, J. D.; Marra, M. A.; Mardis, E. R.; Fulton, L. A.; Chinwalla, A. T.; Pepin, K. H.; Gish, W. R.; Chissoe, S. L.; Wendl, M. C.; Delehaunty, K. D.; Miner, T. L.; Delehaunty, A.; Kramer, J. B.; Cook, L. L.; Fulton, R. S.; Johnson, D. L.; Minx, P. J.; Clifton, S. W.; Hawkins, T.; Branscomb, E.; Predki, P.; Richardson, P.; Wenning, S.; Slezak, T.; Doggett, N.; Cheng, J.-F.; Olsen, A.; Lucas, S.; Elkin, C.; Uberbacher, E.; Frazier, M.; Gibbs, R. A.; Muzny, D. M.; Scherer, S. E.; Bouck, J. B.; Sodergren, E. J.; Worley, K. C.; Rives, C. M.; Gorrell, J. H.; Metzker, M. L.; Naylor, S. L.; Kucherlapati, R. S.; Nelson, D. L.; Weinstock, G. M.; Sakaki, Y.; Fujiyama, A.; Hattori, M.; Yada, T.; Toyoda, A.; Itoh, T.; Kawagoe, C.; Watanabe, H.; Totoki, Y.; Taylor, T.; Weissenbach, J.; Heilig, R.; Saurin, W.; Artiguenave, F.; Brottier, P.; Bruls, T.; Pelletier, E.; Robert, C.; Wincker, P.; Rosenthal, A.; Platzer, M.; Nyakatura, G.; Taudien, S.; Rump, A.; Smith, D. R.; Doucette-Stamm, L.; Rubenfield, M.; Weinstock, K.; Lee, H. M.; Dubois, J.; Yang, H.; Yu, J.; Wang, J.; Huang, G.; Gu, J.; Hood, L.; Rowen, L.; Madan, A.; Qin, S.; Davis, R. W.;

Federspiel, N. A.; Abola, A. P.; Proctor, M. J.; Roe, B. A.; Chen, F.; Pan, H.; Ramser, J.; Lehrach, H.; Reinhardt, R.; McCombie, W. R.; de la Bastide, M.; Dedhia, N.; Blöcker, H.; Hornischer, K.; Nordsiek, G.; Agarwala, R.; Aravind, L.; Bailey, J. A.; Bateman, A.; Batzoglou, S.; Birney, E.; Bork, P.; Brown, D. G.; Burge, C. B.; Cerutti, L.; Chen, H.-C.; Church, D.; Clamp, M.; Copley, R. R.; Doerks, T.; Eddy, S. R.; Eichler, E. E.; Furey, T. S.; Galagan, J.; Gilbert, J. G. R.; Harmon, C.; Hayashizaki, Y.; Haussler, D.; Hermjakob, H.; Hokamp, K.; Jang, W.; Johnson, L. S.; Jones, T. A.; Kasif, S.; Kaspryzk, A.; Kennedy, S.; Kent, W. J.; Kitts, P.; Koonin, E. V.; Korf, I.; Kulp, D.; Lancet, D.; Lowe, T. M.; McLysaght, A.; Mikkelsen, T.; Moran, J. V.; Mulder, N.; Pollara, V. J.; Ponting, C. P.; Schuler, G.; Schultz, J.; Slater, G.; Smit, A. F. A.; Stupka, E.; Szustakowki, J.; Thierry-Mieg, D.; Thierry-Mieg, J.; Wagner, L.; Wallis, J.; Wheeler, R.; Williams, A.; Wolf, Y. I.; Wolfe, K. H.; Yang, S.-P.; Yeh, R.-F.; Collins, F.; Guyer, M. S.; Peterson, J.; Felsenfeld, A.; Wetterstrand, K. A.; Myers, R. M.; Schmutz, J.; Dickson, M.; Grimwood, J.; Cox, D. R.; Olson, M. V.; Kaul, R.; Raymond, C.; Shimizu, N.; Kawasaki, K.; Minoshima, S.; Evans, G. A.; Athanasiou, M.; Schultz, R.; Patrinos, A.; Morgan, M. J.; International Human Genome Sequencing, C.; Whitehead Institute for Biomedical Research, C. f. G. R.; The Sanger, C.; Washington University Genome Sequencing, C.; Institute, U. D. J. G.; Baylor College of Medicine Human Genome Sequencing, C.; Center, R. G. S.; Genoscope; Cnrs, U. M. R.; Department of Genome Analysis, I. o. M. B.; Center, G. T. C. S.; Beijing Genomics Institute/Human Genome, C.; Multimegabase Sequencing Center, T. I. f. S. B.; Stanford Genome Technology, C.; University of Oklahoma's Advanced Center for Genome, T.; Max Planck Institute for Molecular, G.; Cold Spring Harbor Laboratory, L. A. H. G. C.; Biotechnology, G. B. G. R. C. f.; *Genome Analysis, G.; Scientific management: National Human Genome Research Institute, U. S. N. I. o. H.; Stanford Human Genome, C.; University of Washington Genome, C.; Department of Molecular Biology, K. U. S. o. M.; University of Texas Southwestern Medical Center at, D.; Office of Science, U. S. D. o. E.; The Wellcome, T., Initial sequencing and analysis of the human genome. *Nature*, **2001,** *409*, 860.

(37) An integrated encyclopedia of DNA elements in the human genome. *Nature*, **2012,** *489*, 57.

(38) Nemeth, K.; Bayraktar, R.; Ferracin, M.; Calin, G. A., Non-coding RNAs in disease: from mechanisms to therapeutics. *Nat. Rev. Genet.*, **2024,** *25*, 211.

(39) Zhu, Y.; Zhu, L.; Wang, X.; Jin, H., RNA-based therapeutics: an overview and prospectus. *Cell Death Dis.*, **2022,** *13*, 644.

(40) Wang, F.; Zuroske, T.; Watts, J. K., RNA therapeutics on the rise. *Nat. Rev. Drug Discov.*, **2020,** *19*, 441.

(41) Chiriboga, C. A.; Swoboda, K. J.; Darras, B. T.; Iannaccone, S. T.; Montes, J.; De Vivo, D. C.; Norris, D. A.; Bennett, C. F.; Bishop, K. M., Results from a phase 1 study of nusinersen (ISIS-SMN_{Rx}) in children with spinal muscular atrophy. *Neurology*, **2016,** *86*, 890.

(42) Carroll, D., RNA in Therapeutics: CRISPR in the Clinic. *Mol. Cells*, **2023,** *46*, 4.

(43) Adachi, T.; Nakamura, Y., Aptamers: A Review of Their Chemical Properties and Modifications for Therapeutic Application. *Molecules*, **2019,** *24*.

(44) Zhou, J.; Rossi, J., Aptamers as targeted therapeutics: current potential and challenges. *Nat. Rev. Drug Discov.*, **2017,** *16*, 181.

(45) Lamb, Y. N., BNT162b2 mRNA COVID-19 Vaccine: First Approval. *Drugs*, **2021,** *81*, 495.

(46) Baden, L. R.; El Sahly, H. M.; Essink, B.; Kotloff, K.; Frey, S.; Novak, R.; Diemert, D.; Spector, S. A.; Rouphael, N.; Creech, C. B., Efficacy and safety of the mRNA-1273 SARS-CoV-2 vaccine. *N. Engl. J. Med.*, **2021,** *384*, 403.

(47) Falese, J. P.; Donlic, A.; Hargrove, A. E., Targeting RNA with small molecules: from fundamental principles towards the clinic. *Chem. Soc. Rev.*, **2021,** *50*, 2224.

(48) Kovachka, S.; Panosetti, M.; Grimaldi, B.; Azoulay, S.; Di Giorgio, A.; Duca, M., Small molecule approaches to targeting RNA. *Nat. Rev. Chem.*, **2024,** *8*, 120.

(49) Chen, S.; Mao, Q.; Cheng, H.; Tai, W., RNA-Binding Small Molecules in Drug Discovery and Delivery: An Overview from Fundamentals. *J. Med. Chem.*, **2024,** *67*, 16002.

(50) Warner, K. D.; Hajdin, C. E.; Weeks, K. M., Principles for targeting RNA with drug-like small molecules. *Nat. Rev. Drug Discov.*, **2018,** *17*, 547.

(51) Magnet, S.; Blanchard, J. S., Molecular insights into aminoglycoside action and resistance. *Chem. Rev.*, **2005,** *105*, 477.

(52) Wilson, D. N., Ribosome-targeting antibiotics and mechanisms of bacterial resistance. *Nat. Rev. Microbiol.*, **2014,** *12*, 35.

(53) Ratni, H.; Scalco, R. S.; Stephan, A. H., Risdiplam, the First Approved Small Molecule Splicing Modifier Drug as a Blueprint for Future Transformative Medicines. *ACS Med. Chem. Lett.*, **2021,** *12*, 874.

(54) Donlic, A.; Swanson, E. G.; Chiu, L. Y.; Wicks, S. L.; Juru, A. U.; Cai, Z.; Kassam, K.; Laudeman, C.; Sanaba, B. G.; Sugarman, A.; Han, E.; Tolbert, B. S.; Hargrove, A. E., R-BIND 2.0: An Updated Database of Bioactive RNA-Targeting Small Molecules and Associated RNA Secondary Structures. *ACS Chem. Biol.,* **2022,** *17*, 1556.

(55) Childs-Disney, J. L.; Yang, X.; Gibaut, Q. M. R.; Tong, Y.; Batey, R. T.; Disney, M. D., Targeting RNA structures with small molecules. *Nat. Rev. Drug Discov.,* **2022,** *21*, 736.

(56) Liu, X.; Haniff, H. S.; Childs-Disney, J. L.; Shuster, A.; Aikawa, H.; Adibekian, A.; Disney, M. D., Targeted Degradation of the Oncogenic MicroRNA 17-92 Cluster by Structure-Targeting Ligands. *J. Am. Chem. Soc.,* **2020,** *142*, 6970.

(57) Bechhofer, D. H.; Deutscher, M. P., Bacterial ribonucleases and their roles in RNA metabolism. *Crit. Rev. Biochem. Mol. Biol.,* **2019,** *54*, 242.

(58) Canestrari, E.; Paroo, Z., Ribonucleases as Drug Targets. *Trends Pharmacol. Sci.,* **2018,** *39*, 855.

(59) Hameş, E. E.; Demir, T., Microbial ribonucleases (RNases): production and application potential. *World J. Microbiol. Biotechnol.,* **2015,** *31*, 1853.

(60) Cho, S.; Beintema, J. J.; Zhang, J., The ribonuclease A superfamily of mammals and birds: identifying new members and tracing evolutionary histories. *Genomics,* **2005,** *85*, 208.

(61) Zhang, J.; Dyer, K. D.; Rosenberg, H. F., RNase 8, a novel RNase A superfamily ribonuclease expressed uniquely in placenta. *Nucleic Acids Res.,* **2002,** *30*, 1169.

(62) Kuehbacher, A.; Urbich, C.; Zeiher, A. M.; Dimmeler, S., Role of Dicer and Drosha for Endothelial MicroRNA Expression and Angiogenesis. *Circ. Res.,* **2007,** *101*, 59.

(63) Kim, W. C.; Lee, C. H., The role of mammalian ribonucleases (RNases) in cancer. *Biochim. Biophys. Acta,* **2009,** *1796*, 99.

(64) Muralidhar, B.; Goldstein, L. D.; Ng, G.; Winder, D. M.; Palmer, R. D.; Gooding, E. L.; Barbosa-Morais, N. L.; Mukherjee, G.; Thorne, N. P.; Roberts, I.; Pett, M. R.; Coleman, N., Global microRNA profiles in cervical squamous cell carcinoma depend on Drosha expression levels. *J. Pathol.,* **2007,** *212*, 368.

(65) Suswam, E.; Li, Y.; Zhang, X.; Gillespie, G. Y.; Li, X.; Shacka, J. J.; Lu, L.; Zheng, L.; King, P. H., Tristetraprolin down-regulates interleukin-8 and vascular endothelial growth factor in malignant glioma cells. *Cancer Res.,* **2008,** *68*, 674.

(66) Shukla, S.; Bjerke, G. A.; Muhlrad, D.; Yi, R.; Parker, R., The RNase PARN Controls the Levels of Specific miRNAs that Contribute to p53 Regulation. *Mol. Cell*, **2019,** *73*, 1204.

(67) Al-Ahmadi, W.; al-Haj, L.; Al-Mohanna, F. A.; Silverman, R. H.; Khabar, K. S. A., RNase L downmodulation of the RNA-binding protein, HuR, and cellular growth. *Oncogene*, **2009,** *28*, 1782.

(68) Casey, G.; Neville, P. J.; Plummer, S. J.; Xiang, Y.; Krumroy, L. M.; Klein, E. A.; Catalona, W. J.; Nupponen, N.; Carpten, J. D.; Trent, J. M.; Silverman, R. H.; Witte, J. S., RNASEL Arg462Gln variant is implicated in up to 13% of prostate cancer cases. *Nat. Genet.*, **2002,** *32*, 581.

(69) Xiang, Y.; Wang, Z.; Murakami, J.; Plummer, S.; Klein, E. A.; Carpten, J. D.; Trent, J. M.; Isaacs, W. B.; Casey, G.; Silverman, R. H., Effects of RNase L mutations associated with prostate cancer on apoptosis induced by 2',5'-oligoadenylates. *Cancer Res.*, **2003,** *63*, 6795.

(70) Drogat, B.; Auguste, P.; Nguyen, D. T.; Bouchecareilh, M.; Pineau, R.; Nalbantoglu, J.; Kaufman, R. J.; Chevet, E.; Bikfalvi, A.; Moenner, M., IRE1 signaling is essential for ischemia-induced vascular endothelial growth factor-A expression and contributes to angiogenesis and tumor growth in vivo. *Cancer Res.*, **2007,** *67*, 6700.

(71) Guichard, C.; Pedruzzi, E.; Fay, M.; Marie, J. C.; Braut-Boucher, F.; Daniel, F.; Grodet, A.; Gougerot-Pocidalo, M. A.; Chastre, E.; Kotelevets, L.; Lizard, G.; Vandewalle, A.; Driss, F.; Ogier-Denis, E., Dihydroxyphenylethanol induces apoptosis by activating serine/threonine protein phosphatase PP2A and promotes the endoplasmic reticulum stress response in human colon carcinoma cells. *Carcinogenesis*, **2006,** *27*, 1812.

(72) Joo, J. H.; Liao, G.; Collins, J. B.; Grissom, S. F.; Jetten, A. M., Farnesol-induced apoptosis in human lung carcinoma cells is coupled to the endoplasmic reticulum stress response. *Cancer Res.*, **2007,** *67*, 7929.

(73) Holcik, M.; Sonenberg, N., Translational control in stress and apoptosis. *Nat. Rev. Mol. Cell Biol.*, **2005,** *6*, 318.

(74) Huang, S.; Xing, Y.; Liu, Y., Emerging roles for the ER stress sensor IRE1α in metabolic regulation and disease. *J. Biol. Chem.*, **2019,** *294*, 18726.

(75) Bernales, S.; Papa, F. R.; Walter, P., Intracellular signaling by the unfolded protein response. *Annu. Rev. Cell Dev. Biol.*, **2006,** *22*, 487.

(76) Walter, P.; Ron, D., The Unfolded Protein Response: From Stress Pathway to Homeostatic Regulation. *Science*, **2011,** *334*, 1081.

(77) Kimata, Y.; Kohno, K., Endoplasmic reticulum stress-sensing mechanisms in yeast and mammalian cells. *Curr. Opin. Cell Biol.*, **2011,** *23*, 135.

(78) Kozutsumi, Y.; Segal, M.; Normington, K.; Gething, M.-J.; Sambrook, J., The presence of malfolded proteins in the endoplasmic reticulum signals the induction of glucose-regulated proteins. *Nature*, **1988,** *332*, 462.

(79) Tirasophon, W.; Welihinda, A. A.; Kaufman, R. J., A stress response pathway from the endoplasmic reticulum to the nucleus requires a novel bifunctional protein kinase/endoribonuclease (Ire1p) in mammalian cells. *Genes Dev*, **1998,** *12*, 1812.

(80) Janssens, S.; Pulendran, B.; Lambrecht, B. N., Emerging functions of the unfolded protein response in immunity. *Nat. Immunol.*, **2014,** *15*, 910.

(81) Logue, S. E.; McGrath, E. P.; Cleary, P.; Greene, S.; Mnich, K.; Almanza, A.; Chevet, E.; Dwyer, R. M.; Oommen, A.; Legembre, P.; Godey, F.; Madden, E. C.; Leuzzi, B.; Obacz, J.; Zeng, Q.; Patterson, J. B.; Jäger, R.; Gorman, A. M.; Samali, A., Inhibition of IRE1 RNase activity modulates the tumor cell secretome and enhances response to chemotherapy. *Nat. Commun.*, **2018,** *9*, 3267.

(82) Chen, X.; Iliopoulos, D.; Zhang, Q.; Tang, Q.; Greenblatt, M. B.; Hatziapostolou, M.; Lim, E.; Tam, W. L.; Ni, M.; Chen, Y.; Mai, J.; Shen, H.; Hu, D. Z.; Adoro, S.; Hu, B.; Song, M.; Tan, C.; Landis, M. D.; Ferrari, M.; Shin, S. J.; Brown, M.; Chang, J. C.; Liu, X. S.; Glimcher, L. H., XBP1 promotes triple-negative breast cancer by controlling the HIF1α pathway. *Nature*, **2014,** *508*, 103.

(83) Raymundo, D. P.; Doultsinos, D.; Guillory, X.; Carlesso, A.; Eriksson, L. A.; Chevet, E., Pharmacological Targeting of IRE1 in Cancer. *Trends Cancer*, **2020,** *6*, 1018.

(84) Duran-Aniotz, C.; Cornejo, V. H.; Espinoza, S.; Ardiles, Á. O.; Medinas, D. B.; Salazar, C.; Foley, A.; Gajardo, I.; Thielen, P.; Iwawaki, T.; Scheper, W.; Soto, C.; Palacios, A. G.; Hoozemans, J. J. M.; Hetz, C., IRE1 signaling exacerbates Alzheimer's disease pathogenesis. *Acta Neuropathol.*, **2017,** *134*, 489.

(85) Zhou, J.; Liu, C. Y.; Back, S. H.; Clark, R. L.; Peisach, D.; Xu, Z.; Kaufman, R. J., The crystal structure of human IRE1 luminal domain reveals a conserved dimerization interface required for activation of the unfolded protein response. *Proc. Natl. Acad. Sci.*, **2006,** *103*, 14343.

(86) Yoshida, H.; Matsui, T.; Yamamoto, A.; Okada, T.; Mori, K., XBP1 mRNA is induced by ATF6 and spliced by IRE1 in response to ER stress to produce a highly active transcription factor. *Cell*, **2001,** *107*, 881.

(87) Hetz, C.; Chevet, E.; Oakes, S. A., Proteostasis control by the unfolded protein response. *Nat. Cell Biol.*, **2015,** *17*, 829.

(88) Maurel, M.; Chevet, E.; Tavernier, J.; Gerlo, S., Getting RIDD of RNA: IRE1 in cell fate regulation. *Trends Biochem. Sci.*, **2014,** *39*, 245.

(89) Bertolotti, A.; Zhang, Y.; Hendershot, L. M.; Harding, H. P.; Ron, D., Dynamic interaction of BiP and ER stress transducers in the unfolded-protein response. *Nat. Cell Biol.*, **2000,** *2*, 326.

(90) Tsuru, A.; Fujimoto, N.; Takahashi, S.; Saito, M.; Nakamura, D.; Iwano, M.; Iwawaki, T.; Kadokura, H.; Ron, D.; Kohno, K., Negative feedback by IRE1β optimizes mucin production in goblet cells. *Proc. Natl. Acad. Sci.*, **2013,** *110*, 2864.

(91) Siwecka, N.; Rozpędek-Kamińska, W.; Wawrzynkiewicz, A.; Pytel, D.; Diehl, J. A.; Majsterek, I., The Structure, Activation and Signaling of IRE1 and Its Role in Determining Cell Fate. *Biomedicines*, **2021,** *9*, 156.

(92) Halbleib, K.; Pesek, K.; Covino, R.; Hofbauer, H. F.; Wunnicke, D.; Hänelt, I.; Hummer, G.; Ernst, R., Activation of the unfolded protein response by lipid bilayer stress. *Mol. Cell*, **2017,** *67*, 673.

(93) Ali, M. M.; Bagratuni, T.; Davenport, E. L.; Nowak, P. R.; Silva-Santisteban, M. C.; Hardcastle, A.; McAndrews, C.; Rowlands, M. G.; Morgan, G. J.; Aherne, W.; Collins, I.; Davies, F. E.; Pearl, L. H., Structure of the Ire1 autophosphorylation complex and implications for the unfolded protein response. *EMBO J.*, **2011,** *30*, 894.

(94) Sidrauski, C.; Walter, P., The transmembrane kinase Ire1p is a site-specific endonuclease that initiates mRNA splicing in the unfolded protein response. *Cell*, **1997,** *90*, 1031.

(95) Tirasophon, W.; Lee, K.; Callaghan, B.; Welihinda, A.; Kaufman, R. J., The endoribonuclease activity of mammalian IRE1 autoregulates its mRNA and is required for the unfolded protein response. *Gene Dev.*, **2000,** *14*, 2725.

(96) Sanches, M.; Duffy, N. M.; Talukdar, M.; Thevakumaran, N.; Chiovitti, D.; Canny, M. D.; Lee, K.; Kurinov, I.; Uehling, D.; Al-awar, R.; Poda, G.; Prakesch, M.; Wilson, B.; Tam, V.; Schweitzer, C.; Toro, A.; Lucas, J. L.; Vuga, D.; Lehmann, L.; Durocher, D.; Zeng, Q.; Patterson, J. B.; Sicheri, F., Structure and mechanism of

action of the hydroxy–aryl–aldehyde class of IRE1 endoribonuclease inhibitors. *Nat. Commun.,* **2014,** *5*, 4202.

(97) Hetz, C.; Papa, F. R., The Unfolded Protein Response and Cell Fate Control. *Mol. Cell,* **2018,** *69*, 169.

(98) Hetz, C.; Axten, J. M.; Patterson, J. B., Pharmacological targeting of the unfolded protein response for disease intervention. *Nat. Chem. Biol.,* **2019,** *15*, 764.

(99) Sheng, X.; Nenseth, H. Z.; Qu, S.; Kuzu, O. F.; Frahnow, T.; Simon, L.; Greene, S.; Zeng, Q.; Fazli, L.; Rennie, P. S.; Mills, I. G.; Danielsen, H.; Theis, F.; Patterson, J. B.; Jin, Y.; Saatcioglu, F., Correction to: IRE1α-XBP1s pathway promotes prostate cancer by activating c-MYC signaling (Nature Communications, (2019), 10, 1, (323), 10.1038/s41467-018-08152-3). *Nat. Commun.,* **2024,** *15*.

(100) Zhao, N.; Cao, J.; Xu, L.; Tang, Q.; Dobrolecki, L. E.; Lv, X.; Talukdar, M.; Lu, Y.; Wang, X.; Hu, D. Z.; Shi, Q.; Xiang, Y.; Wang, Y.; Liu, X.; Bu, W.; Jiang, Y.; Li, M.; Gong, Y.; Sun, Z.; Ying, H.; Yuan, B.; Lin, X.; Feng, X.-H.; Hartig, S. M.; Li, F.; Shen, H.; Chen, Y.; Han, L.; Zeng, Q.; Patterson, J. B.; Kaipparettu, B. A.; Putluri, N.; Sicheri, F.; Rosen, J. M.; Lewis, M. T.; Chen, X., Pharmacological targeting of MYC-regulated IRE1/XBP1 pathway suppresses MYC-driven breast cancer. *J. Clin. Invest.,* **2018,** *128*, 1283.

(101) Logue, S. E.; McGrath, E. P.; Cleary, P.; Greene, S.; Mnich, K.; Almanza, A.; Chevet, E.; Dwyer, R. M.; Oommen, A.; Legembre, P., Inhibition of IRE1 RNase activity modulates the tumor cell secretome and enhances response to chemotherapy. *Nat. Commun.,* **2018,** *9*, 3267.

(102) Lhomond, S.; Avril, T.; Dejeans, N.; Voutetakis, K.; Doultsinos, D.; McMahon, M.; Pineau, R.; Obacz, J.; Papadodima, O.; Jouan, F., Dual IRE 1 RN ase functions dictate glioblastoma development. *EMBO Mol. Med.,* **2018,** *10*, e7929.

(103) Koong, A. C.; Chauhan, V.; Romero-Ramirez, L., Targeting XBP-1 as a novel anti-cancer strategy. *Cancer Biol. Ther.,* **2006,** *5*, 756.

(104) Shi, W.; Chen, Z.; Li, L.; Liu, H.; Zhang, R.; Cheng, Q.; Xu, D.; Wu, L., Unravel the molecular mechanism of XBP1 in regulating the biology of cancer cells. *J. Cancer.,* **2019,** *10*, 2035.

(105) Chen, C.; Zhang, X., IRE1α-XBP1 pathway promotes melanoma progression by regulating IL-6/STAT3 signaling. *J. Transl. Med.,* **2017,** *15*, 42.

(106) Cross, B. C.; Bond, P. J.; Sadowski, P. G.; Jha, B. K.; Zak, J.; Goodman, J. M.; Silverman, R. H.; Neubert, T. A.; Baxendale, I. R.; Ron, D.; Harding, H. P., The

molecular basis for selective inhibition of unconventional mRNA splicing by an IRE1-binding small molecule. *Proc. Natl. Acad. Sci. U S A*, **2012,** *109*, E869.

(107) Mimura, N.; Fulciniti, M.; Gorgun, G.; Tai, Y. T.; Cirstea, D.; Santo, L.; Hu, Y.; Fabre, C.; Minami, J.; Ohguchi, H.; Kiziltepe, T.; Ikeda, H.; Kawano, Y.; French, M.; Blumenthal, M.; Tam, V.; Kertesz, N. L.; Malyankar, U. M.; Hokenson, M.; Pham, T.; Zeng, Q.; Patterson, J. B.; Richardson, P. G.; Munshi, N. C.; Anderson, K. C., Blockade of XBP1 splicing by inhibition of IRE1α is a promising therapeutic option in multiple myeloma. *Blood*, **2012,** *119*, 5772.

(108) Sanches, M.; Duffy, N. M.; Talukdar, M.; Thevakumaran, N.; Chiovitti, D.; Canny, M. D.; Lee, K.; Kurinov, I.; Uehling, D.; Al-Awar, R., Structure and mechanism of action of the hydroxy–aryl–aldehyde class of IRE1 endoribonuclease inhibitors. *Nat. Commun.*, **2014,** *5*, 4202.

(109) Tang, C. H. A.; Ranatunga, S.; Kriss, C. L.; Cubitt, C. L.; Tao, J.; Pinilla-Ibarz, J. A.; Del Valle, J. R.; Hu, C. C. A., Inhibition of ER stress-associated IRE-1/XBP-1 pathway reduces leukemic cell survival. *J Clin. Invest.*, **2014,** *124*, 2585.

(110) Papandreou, I.; Denko, N. C.; Olson, M.; Van Melckebeke, H.; Lust, S.; Tam, A.; Solow-Cordero, D. E.; Bouley, D. M.; Offner, F.; Niwa, M.; Koong, A. C., Identification of an Ire1alpha endonuclease specific inhibitor with cytotoxic activity against human multiple myeloma. *Blood*, **2011,** *117*, 1311.

(111) Sanches, M.; Duffy, N. M.; Talukdar, M.; Thevakumaran, N.; Chiovitti, D.; Canny, M. D.; Lee, K.; Kurinov, I.; Uehling, D.; Al-Awar, R.; Poda, G.; Prakesch, M.; Wilson, B.; Tam, V.; Schweitzer, C.; Toro, A.; Lucas, J. L.; Vuga, D.; Lehmann, L.; Durocher, D.; Zeng, Q.; Patterson, J. B.; Sicheri, F., Structure and mechanism of action of the hydroxy-aryl-aldehyde class of IRE1 endoribonuclease inhibitors. *Nat. Commun.*, **2014,** *5*.

(112) Chan, S. M. H.; Lowe, M. P.; Bernard, A.; Miller, A. A.; Herbert, T. P., The inositol-requiring enzyme 1 (IRE1α) RNAse inhibitor, 4μ8C, is also a potent cellular antioxidant. *Biochem. J.*, **2018,** *475*, 923.

(113) Tang, C. H.; Ranatunga, S.; Kriss, C. L.; Cubitt, C. L.; Tao, J.; Pinilla-Ibarz, J. A.; Del Valle, J. R.; Hu, C. C., Inhibition of ER stress-associated IRE-1/XBP-1 pathway reduces leukemic cell survival. *J. Clin. Invest.*, **2014,** *124*, 2585.

(114) Feldman, H. C.; Tong, M.; Wang, L.; Meza-Acevedo, R.; Gobillot, T. A.; Lebedev, I.; Gliedt, M. J.; Hari, S. B.; Mitra, A. K.; Backes, B. J.; Papa, F. R.; Seeliger, M.

A.; Maly, D. J., Structural and Functional Analysis of the Allosteric Inhibition of IRE1α with ATP-Competitive Ligands. *ACS Chemical Biology*, **2016,** *11*, 2195.

(115) Wang, L.; Perera, B. G.; Hari, S. B.; Bhhatarai, B.; Backes, B. J.; Seeliger, M. A.; Schürer, S. C.; Oakes, S. A.; Papa, F. R.; Maly, D. J., Divergent allosteric control of the IRE1α endoribonuclease using kinase inhibitors. *Nat Chem Biol*, **2012,** *8*, 982.

(116) Thamsen, M.; Ghosh, R.; Auyeung, V. C.; Brumwell, A.; Chapman, H. A.; Backes, B. J.; Perara, G.; Maly, D. J.; Sheppard, D.; Papa, F. R., Small molecule inhibition of IRE1α kinase/RNase has anti-fibrotic effects in the lung. *PLOS ONE*, **2019,** *14*, e0209824.

(117) Ghosh, R.; Wang, L.; Wang, Eric S.; Perera, B. Gayani K.; Igbaria, A.; Morita, S.; Prado, K.; Thamsen, M.; Caswell, D.; Macias, H.; Weiberth, Kurt F.; Gliedt, Micah J.; Alavi, Marcel V.; Hari, Sanjay B.; Mitra, Arinjay K.; Bhhatarai, B.; Schürer, Stephan C.; Snapp, Erik L.; Gould, Douglas B.; German, Michael S.; Backes, Bradley J.; Maly, Dustin J.; Oakes, Scott A.; Papa, Feroz R., Allosteric Inhibition of the IRE1α RNase Preserves Cell Viability and Function during Endoplasmic Reticulum Stress. *Cell*, **2014,** *158*, 534.

(118) Colombano, G.; Caldwell, J. J.; Matthews, T. P.; Bhatia, C.; Joshi, A.; McHardy, T.; Mok, N. Y.; Newbatt, Y.; Pickard, L.; Strover, J.; Hedayat, S.; Walton, M. I.; Myers, S. M.; Jones, A. M.; Saville, H.; McAndrew, C.; Burke, R.; Eccles, S. A.; Davies, F. E.; Bayliss, R.; Collins, I., Binding to an Unusual Inactive Kinase Conformation by Highly Selective Inhibitors of Inositol-Requiring Enzyme 1alpha Kinase-Endoribonuclease. *J. Med. Chem.*, **2019,** *62*, 2447.

(119) Harrington, P. E.; Biswas, K.; Malwitz, D.; Tasker, A. S.; Mohr, C.; Andrews, K. L.; Dellamaggiore, K.; Kendall, R.; Beckmann, H.; Jaeckel, P.; Materna-Reichelt, S.; Allen, J. R.; Lipford, J. R., Unfolded Protein Response in Cancer: IRE1α Inhibition by Selective Kinase Ligands Does Not Impair Tumor Cell Viability. *ACS Med. Chem. Lett.*, **2015,** *6*, 68.

(120) Harnoss, J. M.; Le Thomas, A.; Shemorry, A.; Marsters, S. A.; Lawrence, D. A.; Lu, M.; Chen, Y.-C. A.; Qing, J.; Totpal, K.; Kan, D.; Segal, E.; Merchant, M.; Reichelt, M.; Ackerly Wallweber, H.; Wang, W.; Clark, K.; Kaufman, S.; Beresini, M. H.; Laing, S. T.; Sandoval, W.; Lorenzo, M.; Wu, J.; Ly, J.; De Bruyn, T.; Heidersbach, A.; Haley, B.; Gogineni, A.; Weimer, R. M.; Lee, D.; Braun, M.-G.; Rudolph, J.; VanWyngarden, M. J.; Sherbenou, D. W.; Gomez-Bougie, P.; Amiot, M.; Acosta-

Alvear, D.; Walter, P.; Ashkenazi, A., Disruption of IRE1α through its kinase domain attenuates multiple myeloma. *Proc. Natl. Acad. Sci.,* **2019,** *116*, 16420.

(121) Korennykh, A. V.; Egea, P. F.; Korostelev, A. A.; Finer-Moore, J.; Zhang, C.; Shokat, K. M.; Stroud, R. M.; Walter, P., The unfolded protein response signals through high-order assembly of Ire1. *Nature,* **2009,** *457*, 687.

(122) Joshi, A.; Newbatt, Y.; McAndrew, P. C.; Stubbs, M.; Burke, R.; Richards, M. W.; Bhatia, C.; Caldwell, J. J.; McHardy, T.; Collins, I.; Bayliss, R., Molecular mechanisms of human IRE1 activation through dimerization and ligand binding. *Oncotarget,* **2015,** *6*, 13019.

(123) Chen, X. L.; Fu, J. P.; Shi, J.; Wan, P.; Cao, H.; Tang, Z. M., CXC195 induces apoptosis and endoplastic reticulum stress in human hepatocellular carcinoma cells by inhibiting the PI3K/Akt/mTOR signaling pathway. *Mol. Med. Rep.,* **2015,** *12*, 8229.

(124) Flagstad, T.; Azevedo, C. M. G.; Troelsen, N. S.; Min, G. K.; Macé, Y.; Willaume, A.; Guilleux, R.; Velay, M.; Bonnet, K.; Morgentin, R.; Nielsen, T. E.; Clausen, M. H., Generation of a Heteropolycyclic and sp3-Rich Scaffold for Library Synthesis from a Highly Diastereoselective Petasis/Diels–Alder and ROM–RCM Reaction Sequence. *Eur. J. Org. Chem.,* **2019,** *2019*, 1061.

(125) Flagstad, T.; Hansen, M. R.; Le Quement, S. T.; Givskov, M.; Nielsen, T. E., Combining the Petasis 3-component reaction with multiple modes of cyclization: a build/couple/pair strategy for the synthesis of densely functionalized small molecules. *ACS Comb. Sci.,* **2015,** *17*, 19.

(126) Firth, J. D.; Craven, P. G. E.; Lilburn, M.; Pahl, A.; Marsden, S. P.; Nelson, A., A biosynthesis-inspired approach to over twenty diverse natural product-like scaffolds. *Chemical Commun.,* **2016,** *52*, 9837.

(127) Motiwala, H. F.; Armaly, A. M.; Cacioppo, J. G.; Coombs, T. C.; Koehn, K. R. K.; Norwood, V. M. I. V.; Aubé, J., HFIP in Organic Synthesis. *Chem. Rev.,* **2022,** *122*, 12544.

(128) Hwang, J.; Borgelt, L.; Wu, P., Multicomponent Petasis Reaction for the Synthesis of Functionalized 2-Aminothiophenes and Thienodiazepines. *ACS Comb. Sci.,* **2020,** *22*, 495.

(129) Molavipordanjani, S.; Emami, S.; Mardanshahi, A.; Talebpour Amiri, F.; Noaparast, Z.; Hosseinimehr, S. J., Novel 99mTc-2-arylimidazo[2,1-b]benzothiazole derivatives as SPECT imaging agents for amyloid-β plaques. *Eur. J. Med. Chem.,* **2019,** *175*, 149.

(130) Pires, D. E. V.; Blundell, T. L.; Ascher, D. B., pkCSM: Predicting Small-Molecule Pharmacokinetic and Toxicity Properties Using Graph-Based Signatures. *J. Med. Chem.,* **2015,** *58,* 4066.

(131) Rosenbaum, C.; Röhrs, S.; Müller, O.; Waldmann, H., Modulation of MRP-1-mediated multidrug resistance by indomethacin analogues. *J Med Chem,* **2005,** *48,* 1179.

(132) Yoshida, H.; Matsui, T.; Yamamoto, A.; Okada, T.; Mori, K., XBP1 mRNA is induced by ATF6 and spliced by IRE1 in response to ER stress to produce a highly active transcription factor. *Cell,* **2001,** *107,* 881.

(133) Ferri, E.; Le Thomas, A.; Wallweber, H. A.; Day, E. S.; Walters, B. T.; Kaufman, S. E.; Braun, M.-G.; Clark, K. R.; Beresini, M. H.; Mortara, K.; Chen, Y.-C. A.; Canter, B.; Phung, W.; Liu, P. S.; Lammens, A.; Ashkenazi, A.; Rudolph, J.; Wang, W., Activation of the IRE1 RNase through remodeling of the kinase front pocket by ATP-competitive ligands. *Nat. Commun.,* **2020,** *11,* 6387.

(134) Iwawaki, T.; Hosoda, A.; Okuda, T.; Kamigori, Y.; Nomura-Furuwatari, C.; Kimata, Y.; Tsuru, A.; Kohno, K., Translational control by the ER transmembrane kinase/ribonuclease IRE1 under ER stress. *Nat. Cell Biol.,* **2001,** *3,* 158.

(135) Richters, A.; Basu, D.; Engel, J.; Ercanoglu, M. S.; Balke-Want, H.; Tesch, R.; Thomas, R. K.; Rauh, D., Identification and further development of potent TBK1 inhibitors. *ACS Chem. Biol.,* **2015,** *10,* 289.

(136) Korennykh, A. V.; Egea, P. F.; Korostelev, A. A.; Finer-Moore, J.; Zhang, C.; Shokat, K. M.; Stroud, R. M.; Walter, P., The unfolded protein response signals through high-order assembly of Ire1. *Nature,* **2009,** *457,* 687.

(137) Robke, L.; Laraia, L.; Carnero Corrales, M. A.; Konstantinidis, G.; Muroi, M.; Richters, A.; Winzker, M.; Engbring, T.; Tomassi, S.; Watanabe, N.; Osada, H.; Rauh, D.; Waldmann, H.; Wu, Y.-W.; Engel, J., Phenotypic Identification of a Novel Autophagy Inhibitor Chemotype Targeting Lipid Kinase VPS34. *Angew. Chem. Int. Ed.,* **2017,** *56,* 8153.

(138) Ghelfi, F.; Parsons, Andrew F.; Tommasini, D.; Mucci, A., Intramolecular Diels−Alder Cycloaddition of N-Allyl-N-(2-furylmethyl)amides − First Step of a New Route Towards the Synthesis of a Densely Functionalized Pyrrolizidine Ring. *Eur. J. Org. Chem.,* **2001,** *2001,* 1845.

(139) Molavipordanjani, S.; Emami, S.; Mardanshahi, A.; Amiri, F. T.; Noaparast, Z.; Hosseinimehr, S. J., Novel 99mTc-2-arylimidazo [2, 1-b] benzothiazole derivatives as SPECT imaging agents for amyloid-β plaques. *Eur. J. Med. Chem.*, **2019,** *175*, 149.

(140) Wey, S. J.; Augustyniak, M. E.; Cochran, E. D.; Ellis, J. L.; Fang, X.; Garvey, D. S.; Janero, D. R.; Letts, L. G.; Martino, A. M.; Melim, T. L.; Murty, M. G.; Richardson, S. K.; Schroeder, J. D.; Selig, W. M.; Trocha, A. M.; Wexler, R. S.; Young, D. V.; Zemtseva, I. S.; Zifcak, B. M., Structure-based design, synthesis, and biological evaluation of indomethacin derivatives as cyclooxygenase-2 inhibiting nitric oxide donors. *J. Med. Chem.*, **2007,** *50*, 6367.

(141) Chambers, S. J.; Coulthard, G.; Unsworth, W. P.; O'Brien, P.; Taylor, R. J. K., From Heteroaromatic Acids and Imines to Azaspirocycles: Stereoselective Synthesis and 3D Shape Analysis. *Chem. Eur. J.*, **2016,** *22*, 6496.

(142) Robke, L.; Laraia, L.; Carnero Corrales, M. A.; Konstantinidis, G.; Muroi, M.; Richters, A.; Winzker, M.; Engbring, T.; Tomassi, S.; Watanabe, N.; Osada, H.; Rauh, D.; Waldmann, H.; Wu, Y. W.; Engel, J., Phenotypic Identification of a Novel Autophagy Inhibitor Chemotype Targeting Lipid Kinase VPS34. *Angew. Chem., Int. Ed. Engl.*, **2017,** *56*, 8153.

7 Abbreviations

ATP	Adenosine Triphosphate
BHQ	Black Hole Quencher
BIOS	Biology-oriented synthesis
Boc	tert-butyloxycarbonyl
CCDC	Cambridge Crystallographic Data Centre
$CDCl_3$	Deuterated chloroform
circRNA	Circular RNA
Cpd	Compound
3C-PR	3 Component Petasis Reaction
DCE	1,2-Dichloroethane
DCM	Dichloromethane
DFT	Density Functional Theory
DOS	Diveraity-oriented synthesis
DIPEA	*N*,*N*-Diisopropylethylamine
DMSO	Dimethylsulphoxide
DNA	Deoxyribonucleic acid
DMF	Dimethylformamide
DSF	Differential Scanning Fluorimetry
DSS	Disuccinimidyl suberate
d.r.	Diastereomeric ratio
EC_{50}	Half maximal effective Concentration
Et	Ethyl
EtOAc / EA	Ethyl acetate
ER	Endoplasmic Reticulum
FAM	Fluorescein amidites
JNK	c-Jun N-terminal Kinases
h	Hours
HRMS	High-Resolution Mass Spectrometry
IC_{50}	Half maximal inhibitory concentration
IRE1α	Inositol Requiring Enzyme 1 Alpha
ITC	Isothermal Titration Calorimetry

LC-MS	Liquid chromatography-mass spectrometry
LD	Luminal Domain
lncRNA	Long Non-Coding RNA
mCPBA	*meta*-Chloroperoxybenzoic acid
MCRs	Multicomponent Reactions
MeOD	Deuterated methanol
mRNA	Messenger RNA
MST	Microscale Thermophoresis
MTT	3-(4,5-Dimethylthiazol-2-yl)-2,5-diphenyltetrazolium bromide
NMR	Nuclear Magnetic Resonance
PARN	Poly(A)-specific ribonuclease
PBS	Phosphate Buffered Saline
piRNA	PIWI-interacting RNA
PR	Petasis Reaction
PTSA	*para*-toluene sulfonic acid
RCM	Ring opening metathesis
ROM	Ring closing metathesis
RIDD	Regulated IRE1-Dependent Decay
RNA	Ribonucleic acid
rRNA	Ribosomal RNA
rt	Room Temperature
RT-qPCR	Reverse Transcription quantitative PCR
scRNA	Small Cytoplasmic RNA
snRNA	Small Nuclear RNA
TLC	Thin-layer chromatography
tRNA	Transfer RNA
UPR	Unfolded protein response
RIBOTACs	Ribonuclease Targeting Chimeras

8 Appendix

8.1 Affidavit

Eidesstattliche Versicherung (Affidavit)

Name, Vorname
(Surname, first name)

Matrikel-Nr.
(Enrolment number)

Belehrung:

Wer vorsätzlich gegen eine die Täuschung über Prüfungsleistungen betreffende Regelung einer Hochschulprüfungsordnung verstößt, handelt ordnungswidrig. Die Ordnungswidrigkeit kann mit einer Geldbuße von bis zu 50.000,00 € geahndet werden. Zuständige Verwaltungsbehörde für die Verfolgung und Ahndung von Ordnungswidrigkeiten ist der Kanzler/die Kanzlerin der Technischen Universität Dortmund. Im Falle eines mehrfachen oder sonstigen schwerwiegenden Täuschungsversuches kann der Prüfling zudem exmatrikuliert werden, § 63 Abs. 5 Hochschulgesetz NRW.

Die Abgabe einer falschen Versicherung an Eides statt ist strafbar.

Wer vorsätzlich eine falsche Versicherung an Eides statt abgibt, kann mit einer Freiheitsstrafe bis zu drei Jahren oder mit Geldstrafe bestraft werden, § 156 StGB. Die fahrlässige Abgabe einer falschen Versicherung an Eides statt kann mit einer Freiheitsstrafe bis zu einem Jahr oder Geldstrafe bestraft werden, § 161 StGB.

Die oben stehende Belehrung habe ich zur Kenntnis genommen:

Official notification:

Any person who intentionally breaches any regulation of university examination regulations relating to deception in examination performance is acting improperly. This offence can be punished with a fine of up to EUR 50,000.00. The competent administrative authority for the pursuit and prosecution of offences of this type is the chancellor of the TU Dortmund University. In the case of multiple or other serious attempts at deception, the candidate can also be unenrolled, Section 63, paragraph 5 of the Universities Act of North Rhine-Westphalia.

The submission of a false affidavit is punishable.

Any person who intentionally submits a false affidavit can be punished with a prison sentence of up to three years or a fine, Section 156 of the Criminal Code. The negligent submission of a false affidavit can be punished with a prison sentence of up to one year or a fine, Section 161 of the Criminal Code.

I have taken note of the above official notification.

Ort, Datum
(Place, date)

Unterschrift
(Signature)

Titel der Dissertation:
(Title of the thesis):

Ich versichere hiermit an Eides statt, dass ich die vorliegende Dissertation mit dem Titel selbstständig und ohne unzulässige fremde Hilfe angefertigt habe. Ich habe keine anderen als die angegebenen Quellen und Hilfsmittel benutzt sowie wörtliche und sinngemäße Zitate kenntlich gemacht.
Die Arbeit hat in gegenwärtiger oder in einer anderen Fassung weder der TU Dortmund noch einer anderen Hochschule im Zusammenhang mit einer staatlichen oder akademischen Prüfung vorgelegen.

I hereby swear that I have completed the present dissertation independently and without inadmissible external support. I have not used any sources or tools other than those indicated and have identified literal and analogous quotations.

The thesis in its current version or another version has not been presented to the TU Dortmund University or another university in connection with a state or academic examination.*

*Please be aware that solely the German version of the affidavit ("Eidesstattliche Versicherung") for the PhD thesis is the official and legally binding version.

Ort, Datum
(Place, date)

Unterschrift
(Signature)